MODELING MULTIPHASE FLOW IN HETEROGENEOUS MEDIA USING STREAMTUBES

A DISSERTATION
SUBMITTED TO THE DEPARTMENT OF PETROLEUM ENGINEERING
AND THE COMMITTEE ON GRADUATE STUDIES
OF STANFORD UNIVERSITY
IN PARTIAL FULFILLMENT OF THE REQUIREMENTS
FOR THE DEGREE OF
DOCTOR OF PHILOSOPHY

By
Marco Roberto Thiele
December 1994

Nothing enters the mind more readily than geometric figures.

Descartes, 1596–1650

Dedicated with love to
Nicola and Valentina.

I certify that I have read this dissertation and that in my opinion it is fully adequate, in scope and quality, as a dissertation for the degree of Doctor of Philosophy.

Dr. Franklin M. Orr (Principal Adviser)

I certify that I have read this dissertation and that in my opinion it is fully adequate, in scope and quality, as a dissertation for the degree of Doctor of Philosophy.

Dr. Martin Blunt (co-Adviser)

I certify that I have read this dissertation and that in my opinion it is fully adequate, in scope and quality, as a dissertation for the degree of Doctor of Philosophy.

Dr. Thomas A. Hewett

I certify that I have read this dissertation and that in my opinion it is fully adequate, in scope and quality, as a dissertation for the degree of Doctor of Philosophy.

Dr. Khalid Aziz

Approved for the University Committee on Graduate Studies:

Abstract

Streamtubes are used to determine fast and accurate solutions to multiphase, multicomponent displacements through heterogeneous, cross-sectional systems. Solutions are constructed by treating each streamtube as a one-dimensional system along which mass conservations equations are solved, either analytically or numerically. The nonlinearity of the underlying flow field is resolved by periodically updating the streamtubes and remapping the one-dimensional solution(s) as an integration from $t_D = 0$ to $t_D = t_D + \Delta t_D$. Examples for (1) tracer flow, (2) two-phase immiscible flow, (3) first contact miscible flow, and (4) two-phase, compositional flow demonstrate that recoveries and large-scale displacements characteristics dictated by reservoir heterogeneity can be predicted accurately using two to five orders of magnitude less computation time than traditional simulation approaches. Mapping analytical solutions along streamtubes allows diffusion-free, two-dimensional solutions to be found. By comparing streamtube solutions to traditional finite difference solutions, numerical diffusion is shown to reduce substantially and in some cases even to eliminate completely the mobility contrast in compositional displacements. The coupling of phase behavior and numerical diffusion is found to be so dominant as to force only very slow convergence of the solution by progressive grid refinement. The speed of the streamtube method is used to quantify the uncertainty in recovery arising from the statistical description of reservoir heterogeneity interacting with the inherent nonlinearity of the problem formulation. The uncertainty is shown to be significant and characterized by a large spread in overall recovery.

Acknowledgments

My years at Stanford as a PhD student have been wonderful ones. I owe this to many people who, in their own way, have helped me complete this work successfully and have made my stay on the Farm so rewarding.

I am deeply indebted to my supervisor, Lynn Orr, for taking me into his research group and for supporting me all these years. I am grateful for the freedom he has allowed me in exploring the vast academic resources available at Stanford and for the opportunity to teach PE251 – Thermodynamics of Phase Equilibria. My co-advisor, Martin Blunt, has been a source of enthusiasm and support for this work, and his untiring push and criticism were determining factors in shaping this dissertation. I thank Tom Hewett and Khalid Aziz for their careful reading and constructive suggestions. I must acknowledge Roland Horne for his incredible stamina in computer matters, which has aided this research significantly, and Christina and Yolanda for helping me find my way through Stanford's administrative maze. John and Rafael have been a formidable duo to share an office with, and Chick's GPS program has been invaluable for presenting my work. An encompassing thank you to all who have contributed in making the department such an enjoyable and productive environment to work in. The financial support of all SUPRI-C affiliates and DOE is also gratefully acknowledged.

I thank the Bourke family for a memorable first year and warm embrace, and Paula and Phillip Kirkeby for their sincere friendship. Although far away, the loving support of my parents, Maria-Gloria and Roberto, my sister, Alessandra, and my grandmother, Valentina, could not have been felt closer. Finally, I thank Nicola for riding with me on the inevitable rollercoaster of euphoria and depression that is inherent in getting a PhD, and paralleled in life and love.

Contents

List of Tables

List of Figures

Chapter 1

Introduction

This chapter presents the main objective of the streamtube approach and the motivations that led to this research. The principal idea of using streamtubes as one-dimensional systems, the Riemann approach for mapping solutions along streamtubes, and the issue of nonlinearity in the problem formulation are briefly reviewed. The class of problems for which the streamtube technique is applicable and its limitations are discussed, and a brief overview of each chapter is given.

The primary objective of the streamtube approach is to enable fast and accurate numerical solutions to displacements through strongly heterogeneous systems while retaining the details of the underlying physical models seen in one-dimensional solutions. The fundamental assumption in using the streamtube approach rests on the belief that field scale displacements are dominated by reservoir heterogeneity: by capturing flow paths and their relative importance as one-dimensional transport conduits between wells while honoring the physical displacement mechanism along these conduits allows difficult enhanced oil recovery displacements to be modeled successfully.

Fast and slow flow regions in the reservoir can be represented using quasi one-dimensional streamtubes. Streamtubes can be visualized as an array of pipes, having variable geometries and connecting the injector and producer wells. The shape of each pipe (streamtube) is dictated by the reservoir geology and, most importantly, each pipe is assumed to conserve mass: what goes in a pipe must come out.

The motivation for this research originated from recent advances in the one-dimensional theory of multicomponent, two-phase, compositional displacements (*Johns et al. 1992, Dindoruk et al. 1992, Orr et al. 1991*) and a desire to extend the sophisticated physical models to two-dimensional heterogeneous systems. Traditional numerical solutions to two- and three-dimensional compositional problems are prohibitively expensive, while returning less than satisfactory solutions due to substantial numerical errors. Motivation for a fast numerical technique was also sparked by the now established statistical methods used in reservoir description. Many equiprobable realizations of a particular reservoir, conditioned possibly on log data, core analysis, and seismic data, allow probabilities to be attached to cumulative oil recoveries. Yet processing the hundreds of geostatistical realizations using traditional reservoir simulation techniques remains numerically expensive, if not impossible.

1.1 Streamtubes and The Riemann Approach

The method used for modeling the four different displacement mechanisms discussed in this dissertation — (1) tracer flow, (2) two-phase immiscible flow, (3) first contact miscible flow[1], and (4) compositional flow — centers on the idea of a streamtube as a quasi one-dimensional object. Two-dimensional solutions are then constructed by mapping one-dimensional solutions to the appropriate mass conservation equations along each streamtube. Because the streamtubes are treated as one-dimensional objects, the conservation equations are solved using Riemann boundary conditions (for which analytical solutions can be found) and mapped along streamtubes as Riemann solutions. For any new time step, the solution along a streamtube is always found by integrating from 0 to $t_D + \Delta t_D$ rather than from t_D to $t_D + \Delta t_D$. Mapping the one-dimensional solution in this manner along the streamtubes is referred to as the 'Riemann approach' throughout the text. The Riemann approach is introduced to circumvent the difficulties associated with general type initial conditions that arise along periodically updated streamtubes.

[1]Sometimes also referred to as ideal miscible flow.

1.2 Nonlinearity

The fundamental difficulty in solving the partial differential equations (PDE's) governing the flow through porous media is their nonlinear formulation. In other words, in order to account for the relevant physics of fluid flow, the coefficients that appear in the governing equations (relative permeabilities, viscosities, densities, etc...) become functions of the independent variables of the problem, usually phase saturations and/or overall compositions. A special case occurs when the coefficients are assumed constant with respect to the independent variables[2], as is done in unit mobility ratio (M=1) flow. In that case the streamtubes are fixed with time and the flow is said to be linear.

To account for the inherent nonlinearity of all other displacements, the streamtube approach periodically updates the streamtubes (i.e. solves the elliptic PDE for the streamfunction) and maps the one-dimensional solution to the particular transport problem onto the new streamtubes using the Riemann approach. Thus, the term 'nonlinearity' is used in this dissertation to describe the changing velocity field with time, as reflected by the dependence of the total mobility on saturation and/or compositions in the elliptic PDE for the streamfunction.

1.3 Class of Problems

The streamtube approach is meant to solve problems that are dominated by reservoir heterogeneity and convective forces. Only cross-sectional problems are discussed here, although there are no dimensional limitations and the method can be used in areal, multiwell configurations as well as in three dimensions[3]. Solutions by the streamtube approach discussed in this dissertation are restricted to problems with constant initial and injected conditions (Riemann boundary conditions) and no gravity-driven

[2] Although the coefficients (like permeability) may still vary spatially.

[3] Although not as easily derived as in two-dimensions, three dimensional streamtubes arise by considering the intersection of stream surfaces (*Bear 1972, p.226*). Once a three-dimensional streamtube is defined, all the arguments with regard to mapping one-dimensional solutions along a streamtube in two dimensions can be applied directly to a streamtube in three dimensions.

flow. Finally, the one-dimensional nature of the streamtubes requires transverse flow mechanisms (normal to the streamtube boundaries) to be of negligible importance.

1.4 Outline

Chapter 2 outlines the relevant literature on streamlines and streamtubes. The primary emphasis is on the petroleum literature, which has seen repeated applications of streamline and streamtube methods, beginning with *Muskat and Wyckoff* (1934) who were among the first to use streamlines to study how well patterns would affect oil recovery. The groundwater literature is briefly reviewed as well, although a comprehensive coverage is traded for key publications that may serve as anchor points to the vast body of literature dealing with the subject. The boundary element method is reviewed as an alternative and efficient method to generate streamlines, and front tracking is presented as a related method to the streamtube approach in moving discontinuous solutions along streamlines.

Chapter 3 introduces the mathematical model for simulating fluid flow through porous media using streamtubes. The governing PDE for the streamfunction in heterogeneous media is discussed, and the resulting streamtubes are presented as pseudo one-dimensional systems. The key issue of mapping one-dimensional solutions along streamtubes is discussed.

Chapter 4 applies the streamtube approach to unit mobility (tracer) displacements. A piston-like, one-dimensional solution is mapped along streamtubes to give a numerical-diffusion-free, two-dimensional solution for a heterogeneous domain. Physical longitudinal diffusion is added to the solution by mapping the convection-diffusion equation along streamtubes. The error caused by numerical diffusion in traditional finite difference approaches is quantified using the diffusion-free streamtube solution as reference solution.

Chapter 5 solves the two-phase immiscible problem by mapping the well-known Buckley-Leverett solution along streamtubes. The issue of the inherent nonlinearity in the velocity field is solved by periodically updating the streamtubes and remapping the Buckley-Leverett solution using the Riemann approach. The Riemann approach

is validated and shown to introduce smaller errors than numerical diffusion in traditional finite difference simulators. It is also compared to the Higgins and Leighton method in which the streamtubes are fixed throughout the displacement and rates are allocated according to the total flow resistance of each streamtube. The key result of this chapter is the demonstration that two-phase immiscible displacements can be successfully modeled using two-orders of magnitude fewer matrix inversions than traditional finite difference simulators. The superior speed is then put to use to assess the interaction of nonlinearity and reservoir heterogeneity in defining the uncertainty in cumulative recovery.

Chapter 6 looks at solving first contact miscible displacements (FCM) by mapping three possible one-dimensional solutions along streamtubes: (1) a piston-like solution, (2) a convection-diffusion solution, and (3) a viscous fingering solution. The important issue of scale is discussed given that viscous fingering cannot be represented explicitly and is captured at the sub-streamtube scale by using a Todd–Longstaff model. Streamtubes are assumed to be on a field scale, attaining a Fickian limit within each streamtube for $M = 1$ flow while giving rise to viscous fingering for $M > 1$. The streamtube approach is shown to match overall recoveries obtained using Mistress, a finite difference code with a flux-corrected-transport formulation (*Christie and Bond 1985*), with a speed-up by two to three orders of magnitude. Ninety geostatistical realizations with different heterogeneity indices ($HI = 0.077, 0.18, 0.86$ —30 realizations per HI) are used in 180 displacements ($M = 5$ and $M = 10$) to demonstrate that increasing heterogeneity and increasing nonlinearity combine to increase substantially the uncertainty in recovery.

Chapter 7 applies the streamtube approach to compositional displacements through heterogeneous systems. One-dimensional as well as two-dimensional reference solutions are found numerically using a finite difference compositional simulator (UTCOMP). By comparing the diffusion-free streamtube solutions to the UTCOMP solutions, numerical diffusion is shown to reduce substantially the original instability of the displacement. Streamtube solutions are made to match the UTCOMP solutions by completely eliminating the mobility contrast, i.e. setting $M = 1$. The resulting speed-up is by four to five orders of magnitude. Crossflow is not found to be a

dominant factor in mitigating the displacements for the heterogeneous systems investigated here, and the effect of crossflow is argued to be on the order of transverse diffusion.

Finally, Chapter 8 gives a brief summary of the dissertation, points out the limitations of the streamtube approach, and identifies the main conclusions of this research.

Chapter 2

Literature Review

This chapter reviews the relevant literature on streamlines and streamtubes, with particular emphasis on the petroleum literature. Brief reviews of the groundwater literature, the boundary element method (an alternative approach for generating streamlines), and the front-tracking method are presented as well.

2.1 Introduction

Streamlines and streamtubes are well established in computational fluid dynamics and have given rise to a very large body of literature. This chapter reviews ideas and concepts in the published literature involving streamlines/streamtubes which are directly related to modeling of subsurface fluid flow.

Unfortunately, the groundwater and petroleum literatures have evolved quite independently from each other and little cross referencing has taken place on the general subject of streamlines and streamtubes. In part, this is due to the difference in the fundamental problem the two fields are concerned with: regional, single-phase flow with emphasis on aquatic chemistry in groundwater mechanics versus confined, multiphase, multicomponent flow in petroleum engineering. This chapter is biased towards the petroleum literature, although it is fair to say that the concepts of streamlines/streamtubes are probably better established in the groundwater literature. Textbooks on groundwater flow (*e.g. Bear 1972, Strack 1989*) usually include a discussion on streamlines and streamtubes as a modeling technique, whereas it is

rare to find these ideas discussed in petroleum engineering text books[1].

Two main issues arise in modeling multiphase displacements in porous media streamtubes: (1) generating streamlines/streamtubes for a particular geometry and reservoir heterogeneity and (2) accounting for the inherent nonlinearity in the flow field. Streamtubes are generally found by solving for the pressure field and then tracing streamlines using the derived velocity field. An alternative is given by the boundary element method (BEM), which has a high degree of accuracy and leads to a smaller system of algebraic equations, although it has difficulties in handling heterogeneous domains. The nonlinearity in the velocity field is usually accounted for by fixing the streamtubes in time (i.e. solving the velocity field only once) and then modifying the flow rate associated with each streamtube according to the total resistance of the system as a function of time. A more rigorous, but somewhat involved approach, is the front-tracking method; the velocity field is recalculated periodically and the saturation/concentration fronts are moved according to their characteristic velocities.

In reviewing the relevant literature, a chronological order is used to highlight original contributions by the authors as well as to maintain the natural succession of ideas. Brief summaries of some of the papers discussed here can be found in Appendix B.

2.2 Petroleum Literature

As with many subjects in reservoir engineering, Muskat was one of the first to apply streamlines to study how well patterns would affect recovery (*Muskat and Wyckoff, 1934*). Using electrical conduction models, Muskat and Wyckoff compare the recovery efficiency of a staggered line drive, a direct line drive, a five-spot pattern, and a seven-spot pattern, finding the staggered line drive as having 'the most favorable physical features'. They discuss their results in terms of two-phase flow, although tracer-flow assumptions are used for all calculations. Thus, the streamlines are assumed fixed in time. An interesting note is that Muskat and Wyckoff conclude their discussion by

[1] An exception is the book by *Muskat* (1937): *The Flow of Homogeneous Fluids.*

suggesting that, all things considered, well spacing and arrangement may be of minor importance compared to the channeling caused by 'high permeability zones within the main body of sand', an idea that is clearly in line with current beliefs on the importance of reservoir heterogeneity in determining recovery.

Muskat devotes an entire chapter in his famous textbook, *Flow of Homogeneous Fluids* (*Muskat 1937*), to two-dimensional problems that can be analyzed using potential-theory methods. These methods rely on the analogy between the equations describing steady state current flow in an electrolytic medium and the equations describing steady-state fluid flow in porous media and are used to capture the streamlines resulting from the geometrical constraints imposed by the boundaries and wells (*Lee 1948*). Muskat (*Muskat 1948*) extends the potentiometric approach to account for reservoir heterogeneity by demonstrating that varying the electrolyte layer thickness is equivalent to specifying a spatial kh distribution.

Higgins and Leighton are credited with being the first to apply the streamtube technique to model nonlinear displacements in homogeneous, areal domains for several regular well patterns. Their work is discussed in three publications: *Higgins and Leighton* (1962a) discusses two-phase flow, *Higgins and Leighton* (1962b) considers three-phase flow, and *Higgins et al.* (1964) studies the influence of several different well patterns. In their first paper, Higgins and Leighton consider a homogeneous quarter five-spot pattern in which ten streamtubes are divided into 'sand elements' of equal volume. By determining the average mobility (actually referred to as average permeability in the paper) and a 'geometric shape factor' for each sand element at the end of each time step, Higgins and Leighton find the total resistance of each streamtube ('channel'). The amount of fluid injected into each streamtube is then allocated proportionally to the ratio of the resistance of each streamtube to the total resistance of the system. Although the streamtubes are fixed throughout the displacement, Higgins and Leighton show excellent agreement with laboratory waterflood data reported by *Douglas et al.* (1959) for end-point viscosity ratios ranging from 0.083 to 754. It is important to note however, that in all cases the relative permeability curves ('permeability-saturation curves') used by Higgins and Leighton in their simulations give rise to rarefaction waves only. In other words, although the end-point mobility

ratio is very high, the instability is mitigated across a very long rarefaction wave. *Higgins and Leighton* (9/1962b) then extend their approach to three-phase flow by using the water-oil fractional flow to find the two-phase mixed-wave solution and assuming that the gas has infinite mobility such that it will always travel ahead of the water-oil region. Although the one-dimensional three-phase flow assumptions are questionable, Higgins and Leighton show a good match with a layered system. Finally, *Higgins et al.* (1964) extend the Higgins and Leighton method to several production patterns, including a seven-spot, a direct line-drive, and a staggered line-drive and provide the reader with a table of shape factors for the various cases.

Hauber (1964) derives analytical expressions for calculating injectivity, time, and cumulative water injected when the water-oil interface has moved a given distance along a streamtube and introduces a distortion factor for non-unit mobility ratio displacements to account for changing streamtube geometries as the flood progresses. Hauber applies his method to a five spot and direct line drive. He then compares his results to experimental data obtained from an electrolytic model and X-ray shadowgraph model, as well as a moving interface algorithm proposed by *Sheldon and Dougherty* (1964). Reasonable agreement with experimental data and the moving interface algorithm is shown.

An important extension to the Higgins and Leighton method is presented by *Doyle and Wurl* (1971). Doyle and Wurl apply the streamtube approach to fields that have asymmetrical well patterns and irregular boundaries. They use superposition to find the streamlines and proceed to find the geometrical shape factors for each streamtube allowing them to apply the Higgins and Leighton method. Unfortunately, Doyle and Wurl never actually discuss the algorithm they use to introduce the field boundaries in their streamline generation. The contribution by Doyle and Wurl is to extend the streamtube method to real field geometries and to set the stage for a number of papers to follow by other authors, which use streamtubes to model real field cases.

LeBlanc and Caudle (1971) also use superposition of line sources and sinks to generate streamlines for a homogeneous domain, but do away with the geometrical shape factors necessary in the Higgins and Leighton method by noting that the total fluid velocity along the dividing streamline is known if each streamtube is assumed

to carry the same injection rate. Instead of using a geometrical approach, LeBlanc and Caudle integrate along each streamline to capture the variation in total velocity.

Parsons (1972) was the first to consider permeability anisotropy. He shows how flow patterns can be substantially altered leading to much lower recoveries than in the isotropic cases. It is interesting to note that Parsons uses a time-of-flight coordinate along streamlines, thereby defining a flood front as points having an equal time-of-flight value. In fact, a similar variable was used by Muskat (*Muskat 1948*) to define 'constant time surfaces'.

An important note was published by *Martin et al.* (1973) on why the streamtube method successfully models unfavorable mobility ratios, but fails for favorable mobility ratios. In particular, they show an interesting comparison of recovery curves for a five spot, obtained by using streamtubes and a moving interface algorithm (*Sheldon and Dougherty 1964, Dougherty and Sheldon 1964, Morel-Seytoux 1965*) for mobility ratios of 0.1, 1, 10, and 100. A considerable difference in the recovery curves occurs for $M = 0.1$. Martin et al. argue that for favorable mobility ratios the streamtube approach underestimates recovery due to the fact that the streamlines in the watered-out region are almost independent of the high-mobility region ahead of the water bank and show that a better solution is obtained by updating the tubes several times as the flood progresses. A interesting plot is presented which compares the tracer streamlines to streamlines updated at some later time. Using a 'revised streamtube model' Martin et al. recalculate the streamtubes, locate the old saturations onto the new streamtubes, and continue the displacement calculations. Unfortunately, they never discuss how the old saturation points are advanced along the new streamtubes. This is an important, because the old saturation points along a new streamtube will give rise to nonuniform initial conditions, for which there is no analytical solution. It is probable that a moving interface algorithm was used for each streamtube.

A more extensive investigation of the error caused by the fixed streamtube assumption is given by *Martin and Wegner* (1979). By considering mobility ratios ranging from 0.1 to 1000, they conclude that the fixed streamtube approach is satisfactory for most two-phase problems. As in the note by *Martin et al.* (1973), Martin and Wegner show that the largest error occurs for favorable mobility ratios. It is important to

mention that in all unfavorable mobility ratio cases, the relative permeability curves used by Martin and Wegner give rise to rarefaction waves only (as in the case for Higgins and Leighton), which also explains why their $M = 1000$ comparison on p. 314 shows such good agreement. Martin and Wegner also mention how the problem of numerical diffusion is overcome by using streamtubes, but do not attempt to quantify this advantage.

An interesting application of streamtubes to modeling in-situ uranium leaching is presented by *Bommer and Schechter* (1979). For this particular case, the unit mobility displacement involved justifies the constant streamtube assumption. The original contribution by Bommer and Schechter is to solve the conservation equations using a one-dimensional finite difference formulation along each streamtube. Using this approach, they are able to account for chemical reactions and physical diffusion in the main direction of flow, thereby modeling the relevant physics of the leaching process. The streamlines are found analytically using superposition, with the no-flow field boundary defined by image wells placed accordingly. A very similar application for a micellar/polymer flood is presented by *Wang et al.* (1981). A streamline generator sets up the flow field and then the concentration balance is solved by finite difference along each fixed streamline.

An important step forward in the attempt to include heterogeneity in the displacement calculations is due to *Lake et al.* (1981). Using physical data from laboratory experiments along with a layered geological model, Lake et al. generate a detailed, vertical cross-sectional finite difference solution for a polymer flood, which is then collapsed into an average one-dimensional solution and mapped onto areal streamtubes to obtain a three-dimensional field response. The importance of this paper lies in the novel idea of introducing the interaction of heterogeneity with the physics of the surfactant/polymer displacement by decoupling the vertical response from the areal one. The main assumption in the method proposed by Lake et al. is that the areal flow field is primarily influenced by well placement, whereas the vertical response is a strong function of geology and type of displacement. Lake et al. assume constant streamtube injectivities in their calculations.

Abbaszadeh-Dehghani (1982) applies the streamtube approach to solve the inverse

problem. From breakthrough curves of tracer slug injections, Abbaszadeh-Dehghani is able to reconstruct layered kh models that will honor the field data. He maps a convection-diffusion solution onto the pattern of streamtubes and uses a nonlinear optimization technique to converge onto the best layered model.

Emanuel et al. (1989) apply the powerful, hybrid streamtube technique proposed by *Lake et al.* (1981) to determine the field performance of three CO_2 floods and one mature waterflood. The cross-sectional response function is found by detailed finite-difference simulation using a fractal description of the porosity/permeability distribution and coreflood data. In determining the areal solution, Emanuel et al. account for nonunit mobility ratios, permeability/thickness values, and no-flow boundaries. For all cases, Emanuel et al. show excellent agreement with total field response data.

Other examples of the hybrid streamtube technique are given by *Mathews et al.* (1989) (miscible-hydrocarbon WAG flood) and *Tang et al.* (1989) (a waterflood and a CO_2 flood). The examples by Tang et al. are particularly interesting because in determining the average cross-sectional response function, they varied the width of the cross-section in the finite difference simulation in order to capture the transition from radial flow near the wells to linear flow away from the wells, thus including gravity effects. Furthermore, Tang et al. generate ten different fractional flow curves to account for varying CO_2 slug sizes, which results from updating the flow rates for each streamtube as the flood progresses.

Motivated by the success of the hybrid streamtube approach, *Hewett and Behrens* (1991) give a detailed discussion on scaling properties of hyperbolic conservation problems and on determining average response functions (pseudofunctions) for heterogeneous cross sections. In particular, Hewett and Behrens show that for single slug injections the solution is scalable by x_D/t_{Ds} and t_D/t_{Ds}, where t_{Ds} is the dimensionless slug volume. Since the hybrid streamtube method requires an averaged cross-sectional response, Hewett and Behrens study the influence of heterogeneity on the scaling properties of a pseudo one-dimensional solution. They conclude that, in general, heterogeneity does not allow a two-dimensional solution to be collapsed into a one-dimensional solution that can be scaled by x_D/t_D, although in some special cases the permeability correlation length may be used as an additional parameter to

give reasonably scaled solutions.

Renard (1990) departs from the assumption of constant streamtubes and allocation of rates according to total resistance. Instead, he periodically updates the streamtubes and maps the old saturations/concentrations onto the new streamtubes. Renard presents a micellar/polymer example in which he compares field data with fixed and updated streamtube solutions. The solution with updated streamtubes is closer to the field data than the one using fixed streamtubes. Unfortunataly Renard does not indicate how he actually moves the old saturations/concentrations along the new streamtubes.

King et al. (1993) present a modified streamline approach as a rapid technique to evaluate the impact of heterogeneity on miscible displacements. A time-of-flight coordinate is used to map the Todd–Longstaff model along each streamline, much in the same way as *Parsons* (1972) does to locate the position of a tracer front. To account for unfavorable mobility ratios, King et al. use a 'boost' factor by integrating Darcy's law along each streamline up to the isobar coinciding with the fastest finger, a slightly different approach than that used by previous authors, who integrate over the entire streamline.

2.3 Groundwater Literature

It is fair to say that the concepts of streamlines and streamtubes for modeling subsurface fluid flow are well established in the groundwater literature. A testimony to this fact is the considerable number of publications that deal directly or indirectly with the streamfunction as well as the many textbooks that give a complete presentation of the method (*Bear 1972, Strack 1989*). It would therefore be difficult to give a formal review of the subject without the danger of not citing many important contributions. This section is principally an acknowledgment of the vast body of literature dealing with streamlines and streamtubes in the groundwater literature. Its purpose is to identify some key publications that will serve as a reference for a more comprehensive coverage.

Streamlines and streamtubes are particularly suitable as a modeling technique for

groundwater flow given the steady state nature of many problems of concern to the hydrogeologists. For example, the transport of contaminants by a regional flow field is a steady-state problem that is probably best captured by a streamtube approach as demonstrated by *Nelson* (1978) and *Frind et al.* (1985). A nice review of the theory related to the streamtube approach is presented by *Frind and Matanga* (1985). *Frind et al.* (1988) use the streamtube approach ('dual potential-streamfunction formulation') to capture dispersive processes at different scales that can influence the evolution of a plume as it migrates downstream in heterogeneous media. Local scale diffusive processes are captured by using a local Peclet number in the convection-diffusion equation, while larger-scale diffusion is represented through the resolution of the flow field (streamtubes) and diffusive exchange between streamtubes. A variable density formulation of the streamfunction is presented by *Evans and Raffensperger* (1992), which they use to model flow near a salt dome. They show that in the case of gravity driven, single-phase flow the streamfunction should be derived in terms of mass flux rather than volume flux. Finally, several authors present extension of the streamtube method to three-dimensions (*Matanga 1993, Zijl 1986, Bear 1972, and Yih 1957*).

2.4 Boundary Element Methods

The use of streamtubes to generate solutions for particular displacement processes rests on the ability to generate streamlines for a particular reservoir geometry and configuration of wells. Streamlines can be found by either solving for the pressure distribution and then using Darcy's law to find the flow field and the resulting streamlines by tracing a particle from a source to sink, or by solving for the streamfunction directly. If the reservoir is homogeneous and the well pattern is symmetric and repeatable to infinity, superposition can be used to find explicit expressions for the velocity vector anywhere in the reservoir (*Muskat 1937, LeBlanc and Caudle 1971, Wang et al. 1981*). On the other hand, if the reservoir has an irregular boundary placing image wells so as to honor the reservoir boundary becomes difficult and a trial-and-error solution is necessary (*Lin 1972*).

An interesting and efficient alternative to generate streamlines, particularly for domains with an arbitrary boundary, is provided by the boundary element method (BEM). The BEM rests on Green's second identity and features a number of advantages over the conventional finite difference method (*Masukawa and Horne, 1988*): (a) discretization errors occur on the boundary only, thereby reducing numerical diffusion and grid orientation effects, (b) there are few restrictions on field geometries, (c) a reduction of the problem dimensionality by one (3D problems are reduced to 2D, 2D problems to 1D), and (d) the flow potential and velocity can be determined for any point in the domain. A number of authors have presented applications of the BEM method to solve subsurface fluid flow problems. *Liu et al.* (1981) solves a moving interface problem and present numerical and experimental results for the tilting of a vertical interface in a Hele-Shaw cell. *Lafe et al.* (1981) extend the BEM method to solve nonlinear equations and equations that have nonconstant coefficients. Both, *Cheng* (1984) and *Lafe and Cheng* (1987) develop the BEM method for heterogeneous domains.

Applications of the BEM to reservoir engineering are also presented by *Masukawa and Horne* (1988) who apply it to immiscible displacement problems. *Numbere and Tiab* (1988) present the BEM methods as an improved streamline generating technique, while *Sato* (1992), and *Sato and Horne* (1993) use a perturbation approach to solve steady-state and transient flow problems in heterogeneous domains. An elegant application of the BEM to track streamlines across fractures is presented by *Sato and Abbaszadeh* (1994).

Although powerful, the BEM method has been slow to gain acceptance in petroleum engineering research, probably due to its involved mathematical formulation and its limitations in handling heterogeneous domains. *Sato and Horne* (1993) use regular perturbation methods to decompose the underlying equations for the heterogeneous case and are able to obtain streamlines. Nevertheless, they caution against slow convergence and divergence of the perturbation series as the magnitude of spatial variability increases.

2.5 Front Tracking

A related method to the streamtube approach is the front tracking method. The central idea of the front tracking method is to move fronts with their characteristic velocities along streamlines, thereby retaining saturation discontinuities (shocks) that arise in the solutions of hyperbolic conservation equations.

Sheldon and Dougherty (1964), *Dougherty and Sheldon* (1964), and *Morel-Seytoux* (1965) introduced the idea of front-tracking (sometimes referred to as moving interface method) to the petroleum literature. Sheldon and Dougherty discuss the general idea of moving a single fluid interface with time and Dougherty and Sheldon then apply these ideas to a waterflood in which the 1D saturation profile is treated as a series of fronts. Morel-Seytoux introduces an 'analytical-numerical' method in which the streamlines are found analytically for the unit mobility ratio case and then used to find a scale-factor in the frontal advance equations.

More recent applications of the front tracking approach are due to *Glimm et al.* (1983), *Ewing et al.* (1983), and *Bratvedt et al.* (1989). The approach presented by Bratvedt et al. is particularly interesting because it directly relates to the idea of updating streamtubes in nonlinear displacements (*Martin et al. 1973, Renard 1990*) and moving saturation along new streamtubes. In particular, Bratvedt et al. use a piecewise linear approximation of the fractional flow function, which leads to a saturation profile that is piecewise constant, in the same manner as assumed by *Dougherty and Sheldon* (1964). Each saturation front is then considered as a local Riemann problem and can be moved forward in time by using its characteristic velocity. Bratvedt et al. are able to account for colliding fronts and apply their method to field scale problems with good results.

2.6 Concluding Remarks

A substantial amount of work has been done in trying to use streamlines and streamtubes as a predictive tool for field scale displacements. Nevertheless, much room for improvement remains, particularly in trying to account for reservoir heterogeneity

and the inherent nonlinearity in the velocity field for unstable displacements. This work extends the streamtube method to consider these issues. Cross-sectional domains are used emphasizing reservoir heterogeneity, and streamtubes are updated periodically to account for nonlinear behavior. Solutions for various displacement mechanisms are then constructed by treating streamtubes as true one-dimensional systems along which mass conservation solution(s) can be mapped, thus retaining the essential physics of flow. A 'Riemann approach' is used to map one-dimensional solutions along periodically updated streamtubes; this is different from any previous streamtube/streamline methods and is introduced to allow the use of one-dimensional Riemann solutions along changing streamtubes. As a result, the streamtube method becomes particularly powerful in the case of compositional solutions, where one-dimensional solutions containing all the relevant physics are combined with streamtubes to produce very fast and accurate displacement predictions for heterogeneous systems.

Chapter 3

Mathematical Model

This chapter introduces the mathematical model for simulating fluid flow through porous media using streamtubes. The streamfunction for two-dimensional, heterogeneous media is derived and the appropriate boundary conditions presented. The concept of a streamtube as a pseudo one-dimensional system is introduced, and the mapping of a one-dimensional solution onto streamtubes to construct a two-dimensional solution is discussed.

3.1 Introduction

The streamtube approach rests on two key ideas: (a) generating streamlines and streamtubes for the particular domain of interest and (b) mapping of a one-dimensional solution along each streamtube. These central ideas, and the key assumptions associated with them, are developed in this chapter.

The streamfunction is discussed in several textbooks (*Muskat 1937, Bear 1972, Strack 1989*), and for a general discussion the reader is referred to these sources. In this chapter, the governing partial differential equation for the streamfunction and the appropriate boundary conditions are derived for a cross-sectional heterogeneous domain. Injection is assumed to occur over the entire left face of the domain and production over the entire right face. The top and bottom boundaries are treated as no-flow boundaries.

The choice of a cross-sectional domain is motivated by the interest to understand

the effects of heterogeneity on nonlinear displacement processes. Furthermore, in a cross-sectional domain the streamlines can be solved for directly and very easily. In the case of areal problems with multiple wells, the streamfunction can still be used although it becomes multivalued and branch cuts (bounding streamlines) must be found (*Emmanuel et al. 1989*). For these cases it may be easier to determine the pressure distribution and combine it with Darcy's Law to find the underlying total velocity field and trace streamlines by launching particles.

3.2 The Streamfunction - Constant Coefficients

By definition, a streamline is a line everywhere tangent to the velocity vector (*Muskat 1937, Bear 1972, Strack 1989*) at any instant in time. In parametric form, a streamline can be written as

$$x = x(s) \; ; \qquad y = y(s) \quad .^{1} \tag{3.1}$$

The slope of a velocity vector anywhere along a streamline is given by

$$\frac{dy/ds}{dx/ds} = \frac{u_y}{u_x} \quad ,$$

which can be rearranged as

$$u_y \frac{dx}{ds} - u_x \frac{dy}{ds} = 0 \quad . \tag{3.2}$$

u_x and u_y are the Darcy velocity components in the x and y direction respectively. Consider now a function Ψ, called the streamfunction. If the streamfunction Ψ is required to be constant along a streamline, then it must hold that

$$d\Psi = \frac{\partial \Psi}{\partial x}\frac{dx}{ds} + \frac{\partial \Psi}{\partial y}\frac{dy}{ds} = 0 \quad . \tag{3.3}$$

[1]Streamlines, of course, exist in unsteady flow as well: $x = x(s,t)$, $y = y(s,t)$. In this case one distinguishes between pathlines, streamlines, and streaklines. The pathline is the locus of a particle in space as time passes; a streamline is a line everywhere tangent to the velocity vector; and a streakline is the locus of all points seen by a fluid particle that passed through a fixed point space at some earlier time (*Bear 1972*). In steady state flow pathlines, streamlines, and streaklines coincide, whereas in unsteady state flow they do not.

Comparisons of terms with Eq. 3.2 gives

$$\frac{\partial \Psi}{\partial x} = u_y \quad , \quad \frac{\partial \Psi}{\partial y} = -u_x \quad , \tag{3.4}$$

and substituting for u_x and u_y using Darcy's law returns

$$\frac{\partial \Psi}{\partial x} = \lambda \frac{\partial P}{\partial y} \quad , \quad \frac{\partial \Psi}{\partial y} = -\lambda \frac{\partial P}{\partial x} \quad ,$$

where λ is the mobility of the fluid. Assuming that λ is spatially constant (homogeneous fluid and rock properties) it can be taken into the partial derivatives such that

$$\frac{\partial \Psi}{\partial x} = \frac{\partial (\lambda P)}{\partial y} \quad , \quad \frac{\partial \Psi}{\partial y} = -\frac{\partial (\lambda P)}{\partial x}$$

and setting $\Phi = \lambda P$ gives

$$\frac{\partial \Psi}{\partial x} = \frac{\partial \Phi}{\partial y} \quad , \quad \frac{\partial \Psi}{\partial y} = -\frac{\partial \Phi}{\partial x} \quad . \tag{3.5}$$

Equations 3.5 are the well known Cauchy-Riemann equations[2] that arise in the study of functions of a complex variable (*Churchill and Brown 1990*).

In particular, if a function $f(z) = u(x,y) + iv(x,y)$ of a complex variable $z = x + iy$ is said to be analytic, then the Cauchy-Riemann equations will hold for the functions u and v:[3] $u_x = v_y$ and $u_y = -v_x$. The function $f(z)$ is analytic if its derivative, $f'(z)$, exists everywhere in the domain D. The importance of analytic functions for modeling fluid flow hinges on the fact that if $f(z)$ is analytic in D, then its component functions u and v are harmonic in D. Harmonic functions are functions that satisfy Laplace's equation. Thus, if $f(z) = u(x,y) + iv(x,y)$ is analytic, then u and v will satisfy the Cauchy-Riemann equations as well as

$$u_{xx} + u_{yy} = 0 \;\; ; \;\; v_{xx} + v_{yy} = 0.$$

In fluid flow through porous media an analytic function is referred to as the complex

[2]The Cauchy-Riemann equations are named after the French mathematician A.L. Cauchy (1789-1857) who discovered and used them, and after the German mathematician G.F.B. Riemann (1826-1866), who used them in the development of the theory of functions of a complex variable.

[3]Here u is simply used as a function name and is not to be confused with the Darcy's velocity.

potential (*Muskat 1937, Bear 1972, Strack 1989*) and written as

$$\Omega(x,y) = \Phi(x,y) + i\Psi(x,y) \quad , \tag{3.6}$$

where Φ is the potential function and Ψ is the streamfunction. Thus, a complex potential Ω that is analytic in D will give the governing partial differential equation for the streamfunction as simply

$$\frac{\partial^2 \Psi}{\partial x^2} + \frac{\partial^2 \Psi}{\partial y^2} = 0 \quad . \tag{3.7}$$

For some homogeneous domains Ω can be found analytically using conformal mapping. Φ and Ψ, of course, give rise to the well known orthogonal flow nets that are widely used in hydrology.

3.3 The Streamfunction - Variable Coefficients

For this work, the interest lies in deriving the governing partial differential equation for the streamfunction which accounts for reservoir heterogeneity and spatially varying fluid properties (relative permeabilities and viscosities). Substituting for Darcy's law in Eq. 3.4, gives

$$\frac{\partial \Psi}{\partial x} = -\lambda_y \frac{\partial P}{\partial y} \quad , \quad \frac{\partial \Psi}{\partial y} = \lambda_x \frac{\partial P}{\partial x} \quad , \tag{3.8}$$

where λ_x and λ_y now are the total fluid mobilities in the x and y direction and given by

$$\lambda_x = \sum_{j=1}^{N_p} \frac{k_x k_{rj}}{\mu_j} \quad , \quad \lambda_y = \sum_{j=1}^{N_p} \frac{k_y k_{rj}}{\mu_j} \quad . \tag{3.9}$$

j is the phase index, N_p is the total number of phases present, k_x and k_y are the absolute permeabilities in the x and y direction respectively, k_{rj} is the relative permeability of phase j, and μ_j is the viscosity of phase j. The phase relative permeabilities k_{rj} and phase viscosities μ_j are indirect functions of x and y since they depend on phase saturations/compositions which in turn are functions of x and y.

Eqs. 3.8 are still Cauchy-Riemann equations and can be expressed as

$$\frac{1}{\lambda_y}\frac{\partial \Psi}{\partial x} = -\frac{\partial P}{\partial y} \quad , \quad \frac{1}{\lambda_x}\frac{\partial \Psi}{\partial y} = \frac{\partial P}{\partial x} \quad . \tag{3.10}$$

It is important to note that the Cauchy-Riemann equations alone are not a sufficient condition for the existence of an analytical function. Rather,a function $f(z) = u(x,y) + iv(x,y)$ is analytic in a domain D if and only if v is a harmonic conjugate of u in D. In other words, to find the complex potential $\Omega = P + i\bar{\Psi}$, where the bar indicates that $\bar{\Psi}$ is now related to Ψ by

$$\frac{\partial \bar{\Psi}}{\partial x} = \frac{1}{\lambda_y}\frac{\partial \Psi}{\partial x} \quad , \quad \frac{\partial \bar{\Psi}}{\partial y} = \frac{1}{\lambda_x}\frac{\partial \Psi}{\partial y} \quad .$$

it must hold that

$$\frac{\partial}{\partial x}\left(\frac{1}{\lambda_y}\frac{\partial \Psi}{\partial x}\right) + \frac{\partial}{\partial y}\left(\frac{1}{\lambda_x}\frac{\partial \Psi}{\partial y}\right) = 0 \quad . \tag{3.11}$$

and $\bar{\Psi}$ must be a harmonic conjugate of P (*Bear 1972*).

Eq. 3.11 is the governing pde for the streamfunction Ψ and accounts for reservoir heterogeneity through its nonconstant spatial coefficients. In practice the complex potential Ω is never found and usually only one of the component functions is used for displacement calculations[4]. In this work, the streamfunction Ψ is the function of interest and solved by applying Eq. 3.11 to a particular domain D.

A second, very simple derivation leading to Eq. 3.11 as well, begins by stating that P is a single-valued function in D (*Martin and Wegner 1979*). Then the mixed partials of P must be equal leading to

$$\frac{\partial}{\partial x}\left(\frac{\partial P}{\partial y}\right) = \frac{\partial}{\partial y}\left(\frac{\partial P}{\partial x}\right) \quad , \tag{3.12}$$

and substituting for the pressure gradients from the Cauchy-Riemann equations (Eqs. 3.8) gives

$$\frac{\partial}{\partial x}\left(-\frac{1}{\lambda_y}\frac{\partial \Psi}{\partial x}\right) = \frac{\partial}{\partial y}\left(\frac{1}{\lambda_x}\frac{\partial \Psi}{\partial y}\right) \quad , \tag{3.13}$$

[4]The same argument used to find Ψ can be used to find P. In this case, the Cauchy-Riemann equations are written as

$$\frac{\partial \Psi}{\partial x} = -\lambda_y \frac{\partial P}{\partial y} \quad , \quad \frac{\partial \Psi}{\partial y} = \lambda_x \frac{\partial P}{\partial x} \quad ,$$

the complex potential is given by $\Omega = \bar{P} + i\Psi$ and the governing pde for P is

$$\frac{\partial}{\partial x}\left(\lambda_x \frac{\partial P}{\partial x}\right) + \frac{\partial}{\partial y}\left(\lambda_y \frac{\partial P}{\partial y}\right) = 0 \quad .$$

which returns the same governing equation for the streamfunction Ψ as Eq. 3.11

$$\frac{\partial}{\partial x}\left(\frac{1}{\lambda_y}\frac{\partial \Psi}{\partial x}\right) + \frac{\partial}{\partial y}\left(\frac{1}{\lambda_x}\frac{\partial \Psi}{\partial y}\right) = 0 \quad .$$

3.4 Boundary Conditions

Equation 3.11 is an elliptic partial differential equation, which requires either Neumann or Dirichlet type boundary conditions. Only cross-sectional domains are considered in this work, and therefore the boundary conditions to be considered are no-flow at the top and bottom of the domain and constant pressure or uniform rate at either end. The boundary conditions for the streamfunction are particularly easy to formulate, once a physical interpretation is given to the streamfunction Ψ.

The volumetric flowrate at any point in the domain can be written in differential form as

$$dQ = \vec{u} \cdot d\vec{A} \quad , \tag{3.14}$$

where $d\vec{A}$ is an arbitrary area between two adjacent streamlines defined as $d\vec{A} = \vec{e}_z \times d\vec{s}$. $\vec{e}_z$ is the unit vector perpendicular to the xy plane and ds is the length of $d\vec{A}$. The total volumetric flow rate across an arbitrary area A, between two streamlines $\mathcal{A}$ and $\mathcal{B}$, is then simply given by (*Bear 1972, p.226*)

$$\begin{aligned} \int_{\mathcal{A}}^{\mathcal{B}} \vec{u} \cdot d\vec{A} = \Delta Q_{\mathcal{AB}} &= \int_{\mathcal{A}}^{\mathcal{B}} \vec{u} \cdot (\vec{e}_z \times d\vec{s}) \\ &= \int_{\mathcal{A}}^{\mathcal{B}} u_x dy - u_y dx \\ &= \int_{\mathcal{A}}^{\mathcal{B}} d\Psi = \Psi_{\mathcal{B}} - \Psi_{\mathcal{A}} \end{aligned} \tag{3.15}$$

In other words, the total flow rate between two streamlines is simply given by the difference in value of the streamfunction associated with each streamline.

Using this fact, the boundary conditions for the cross sectional domain are indeed easy to find. Since the top and bottom no flow boundaries and are themselves streamlines, the difference in the value of the streamfunction between the two must equal to the total flowrate. An obvious choice then is to set the bottom boundary to

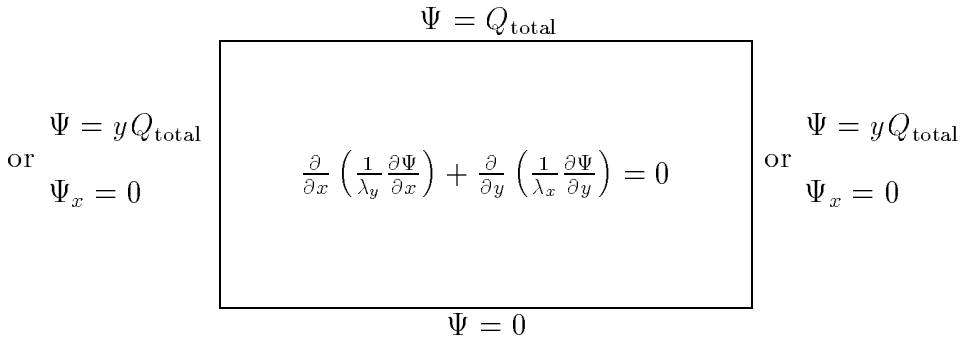

Figure 3.1: *Possible boundary conditions of the streamfunction* Ψ.

$\Psi = 0$ and the top boundary to $\Psi = Q_{\text{total}}$[5]. Similarly, a uniform rate distribution along the inlet or outlet face must be given by a linear distribution of Ψ from 0 to Q_{total}. Thus,

$$\Psi_{\text{in/out}} = yQ_{\text{total}} \;\; ; \;\; 0 \leq y \leq 1 \;\; . \tag{3.16}$$

To find the equivalent of a constant pressure/total rate boundary condition in terms of the streamfunction it is necessary to consider the Cauchy-Riemann equation

$$\frac{1}{\lambda_y}\frac{\partial \Psi}{\partial x} = -\frac{\partial P}{\partial y} \;\; .$$

A constant pressure boundary states that gradient in the y direction must be zero. For a nonzero coefficient λ_y^{-1} it follows that

$$\frac{\partial P}{\partial y} = 0 \quad \Longrightarrow \quad \frac{\partial \Psi}{\partial x} = 0 \;\; . \tag{3.17}$$

Total flow is automatically honored by the value associated with the top and bottom limiting streamlines. The two possible boundary conditions for the the inlet and outlet end are summarized in Fig. 3.1.

[5]Clearly, the opposite choice is just as good.

3.5 Numerical Solution

The numerical solution of Eq. 3.11 in a heterogeneous domain with any of the boundary conditions specified in Fig. 3.1 is straightforward and well documented in the literature (*Aziz and Settari 1979*). A standard five-point finite difference formulation is used to discretize Eq. 3.11 resulting in

$$A\Psi_{i+1,j} + B\Psi_{i-1,j} + C\Psi_{i,j+1} + D\Psi_{i,j-1} - (A+B+C+D)\Psi_{i+1,j} = 0 \quad , \tag{3.18}$$

where the coefficients A,B,C, and D are given by

$$A = \frac{1}{\Delta x^2}\left(\frac{1}{\lambda_y}\right)_{i+1/2,j} \quad , \tag{3.19}$$

$$B = \frac{1}{\Delta x^2}\left(\frac{1}{\lambda_y}\right)_{i-1/2,j} \quad , \tag{3.20}$$

$$C = \frac{1}{\Delta y^2}\left(\frac{1}{\lambda_x}\right)_{i,j+1/2} \quad , \tag{3.21}$$

$$D = \frac{1}{\Delta y^2}\left(\frac{1}{\lambda_x}\right)_{i,j+1/2} \quad . \tag{3.22}$$

In solving for the streamfunction using Eq. 3.18, it is important to notice that the gradient of Ψ in the x-direction is associated with the reciprocal of the mobility in the y-direction. This is different, of course, from solving for pressure, where the gradient of P in the x-direction is associated with the mobility in the x-direction. λ in Eq. 3.19 - 3.22 is the total mobility and can never be equal to zero unless the block absolute permeability is zero. The harmonic average is used to find the value at the internodal points $(i \pm 1/2, j \pm 1/2)$. As an example, the coefficient A would be given by

$$A = \frac{1}{\Delta x^2}\left(\frac{\lambda_{y_{i,j}} + \lambda_{y_{i+1,j}}}{2\lambda_{y_{i,j}}\lambda_{y_{i+1,j}}}\right) \quad . \tag{3.23}$$

Because of the Cauchy-Riemann equations, the streamfunction grid is shifted with respect to the traditional pressure/permeability grid as shown in Fig. 3.2. A grid with $NX \times NY$ permeability values will give rise to a $(NX+1)\times(NY+1)$ streamfunction grid, which in turn results in a system of $(NX-1)\times(NY-1)$ linear equations.

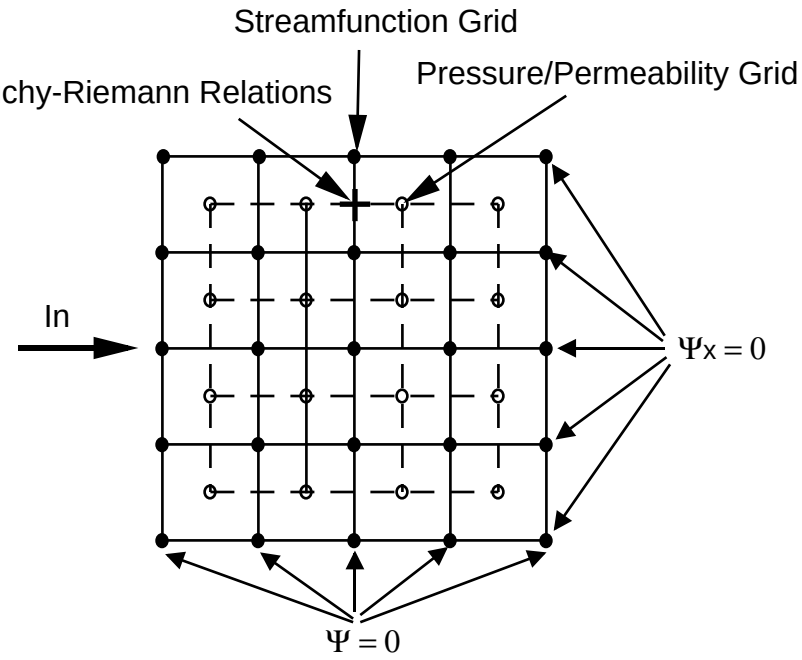

Figure 3.2: *Numerical grid for streamfunction in relation to the traditional block-centered pressure/permeability grid.*

3.6 Streamtubes

Once the streamfunction has been solved for the particular heterogeneous domain of interest, streamtubes are defined by considering two adjacent streamlines: N streamlines will define $N-1$ streamtubes.

The advantage of using streamtubes versus streamlines as the fundamental object on which to map a one dimensional solution is that streamtubes offer a visual interpretation of the local flow velocity whereas streamlines do not. Tracing a single streamline from inlet to outlet yields no information about how fast a particle moves along that streamline. A streamtube on the other hand, allows identification of slow and fast flow regions: thick sections of a streamtube correspond to slow flow regions, thin sections to fast flow regions. The geometry of the streamtubes therefore captures the distribution of the flow velocity imposed by the underlying permeability field as demonstrated in Fig. 3.3. An additional advantage of the streamtube versus the streamline approach has to do with mapping the one-dimensional solution

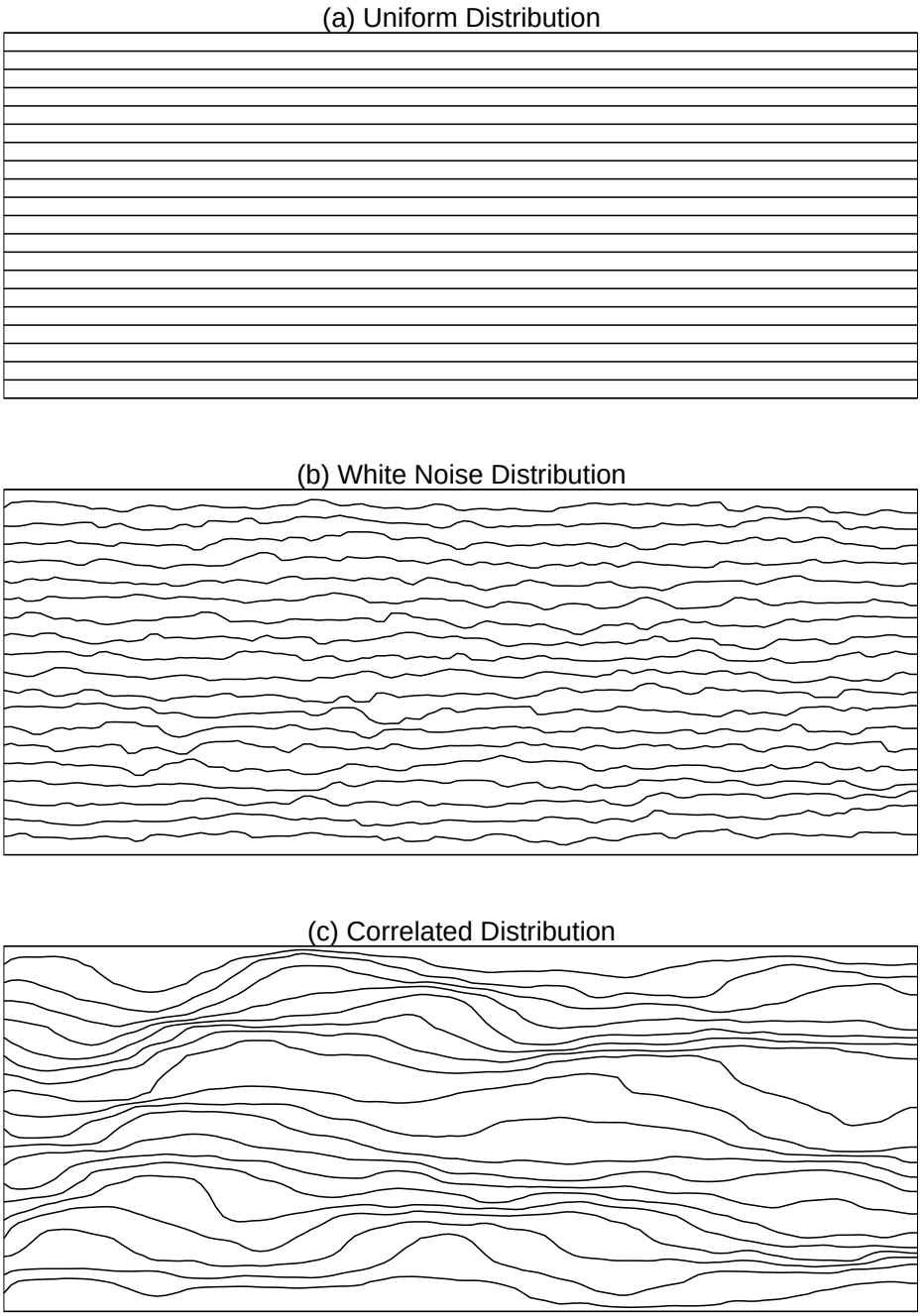

Figure 3.3: *Streamtube geometries as a function of permeability correlation. From top to bottom: (a) homogeneous distribution , (b) white noise (no correlation), and (c) correlated permeability field.*

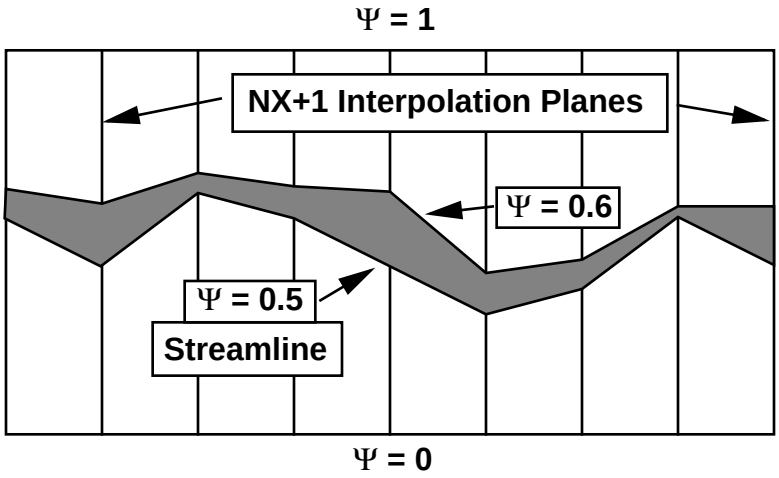

Figure 3.4: *Simple interpolation algorithm used to determine streamlines/streamtubes for the cross-sectional problem.*

back onto the two-dimensional cartesian grid, which is necessary for updating the total mobility in nonlinear displacements and plotting of the concentration/saturation distributions[6].

Once the streamfunction has been solved on the discretized domain, constructing the streamtubes becomes a contouring problem. A very simple approach was used here, motivated mainly by the geometry of the cross-sectional problem: the streamfunction was interpolated along vertical lines corresponding to the $NX + 1$ Ψ-nodes as shown in Fig. 3.4. This simple interpolation approach produces a good approximation of the actual streamlines/streamtubes because the main direction of flow is in the x-direction and because the number of blocks in the x-direction is usually taken to be larger than in the y-direction. A particular appealing feature of this simple contouring approach is that each streamtube will have the same number of (x, y) points defining its location in space, thereby making it very easy to treat the streamtubes as geometrical objects for integration and mapping purposes.

[6]Mathematically integrating along a streamline to obtain a time-of-flight coordinate (*Parsons 1972, King et al. 1993*) or along a streamtube to obtain cumulative volume injected leads to identical solutions.

3.7 Streamtubes as 1D Systems

The key idea in using streamtubes to model two-dimensional displacements is to treat each streamtube as a one-dimensional system. *Higgins and Leighton* (1962a, 1962b) showed that in order to map a one-dimensional solution along streamtubes, the solution must scale volumetrically. *Hewett and Behrens* (1991) present a nice review on scaling of one-dimensional, hyperbolic solutions along streamtubes.

Treating each streamtube as a one-dimensional system automatically associates a pore volume with it, which must be a fraction of the total pore volume of the system. By definition, a streamtube will see a volumetric flowrate which is given by the difference of the streamfunction associated with the bounding streamlines (Eq. 3.15). Therefore, for each streamtube it is possible to use the common form of dimensionless time given by

$$t_{Di} = \frac{\int q_i dt}{\overline{V}_P} \quad , \tag{3.24}$$

where q_i is the flowrate of streamtube i given by $\Psi_{\mathcal{B}} - \Psi_{\mathcal{A}}$, with the subscripts $\mathcal{A}$ and $\mathcal{B}$ referring to the bounding streamlines, and $\overline{V}_P$ is an arbitrary pore volume used for scaling. If all streamtubes see the same $\Delta\Psi$ (i.e, the streamlines are found by interpolating using a constant $\Delta\Psi$), then

$$Q = \sum_i^N q_i = q \sum_i^N = qN \quad , \tag{3.25}$$

where N is the number of streamtubes, and the dimensionless time for each streamtube can be written as

$$t_{Di} = \frac{\int q_i dt}{\overline{V}_P} = \frac{\int q dt}{\overline{V}_P} = \frac{\int Q dt}{N\,\overline{V}_P} \quad . \tag{3.26}$$

Similarly, a dimensionless length can be associated with each streamtube given by

$$x_{Di} = \frac{\int \phi A_i(\zeta) d\zeta}{\overline{V}_P} \quad , \tag{3.27}$$

where A_i is the area of the streamtube as a function of a one-dimensional coordinate, ζ, along a streamtube. The 'best' choice for $\overline{V}_P$ is clearly

$$\overline{V}_P = \frac{V_{P_T}}{N} \quad , \tag{3.28}$$

where V_{P_T} is the total system pore volume and N is the number of streamtubes. In the limit of a homogeneous system each streamtube will have a dimensionless 'length' of $x_D = 1$.

With dimensionless time and dimensionless distance defined for each streamtube any one-dimensional solutions to conservation equations that scale volumetrically can be mapped onto a streamtube. For example, the conservation equation along a general, one-dimensional path ζ for a tracer with no diffusion is given by

$$\phi \frac{\partial (AC)}{\partial t} + q \frac{\partial C}{\partial \zeta} = 0 \quad . \tag{3.29}$$

If the system has a constant cross section, then $\zeta = x$, $A =$ constant, and the well known expression

$$\phi \frac{\partial C}{\partial t} + u \frac{\partial C}{\partial x} = 0 \tag{3.30}$$

results, where $u = q/A$ is the Darcy flow velocity. On the other hand, if the system is along some general coordinate ζ, and the area is a function of ζ such that $A = A(\zeta)$, then Eq. 3.29 can be written as

$$\frac{1}{q} \frac{\partial C}{\partial t} + \frac{1}{\phi A(\zeta)} \frac{\partial C}{\partial \zeta} = 0 \quad . \tag{3.31}$$

Multiplying by the pore volume, $\overline{V}_P$, gives

$$\frac{\partial C}{(q \partial t)/\overline{V}_P} + \frac{\partial C}{(\phi A(\zeta) \partial \zeta)/\overline{V}_P} = 0 \quad , \tag{3.32}$$

which defines the dimensionless variables

$$t_D = \frac{\int q dt}{\overline{V}_P} \quad , \quad x_D = \frac{\int \phi A(\zeta) d\zeta}{\overline{V}_P} \quad .$$

With dimensionless time and distance defined along each streamtube, it is also possible to define a dimensionless velocity as

$$v_{Di} = \frac{x_{Di}}{t_{Di}} = \left(\frac{\int \phi A_i(\zeta) d\zeta}{\overline{V}_P} \right) \left(\frac{N \ \overline{V}_P}{\int Q dt} \right) = \frac{N \int \phi A_i(\zeta) d\zeta}{\int Q dt} \quad . \tag{3.33}$$

The importance of Eq. 3.33 lies in the fact that solutions that scale as x_D/t_D can now be mapped directly onto a streamtube by simply evaluating Eq. 3.33. It is worth noting that the $\overline{V}_P$ cancels out in Eq. 3.33, which says that the dimensionless velocity does not depend on the choice of $\overline{V}_P$, as *Hewett and Behrens* (1991) point

out. However, it is also true that to define the dimensionless variables x_D and t_D explicitly, a choice for $\overline{V}_P$ must be made.

3.7.1 Mapping of a 1D Solution - Method A

With the geometry of the streamtube determined, finding either the dimensionless distance or dimensionless velocity is a simple matter of evaluating the integral

$$\int \phi A_i(\zeta) d\zeta \tag{3.34}$$

along each streamtube. A first approximation to Eq. 3.34 can be found by setting the area A as the difference in the y coordinate of two streamlines defining a streamtube at a particular value of x. Since the streamlines are piecewise linear functions of x, with values known at the $N+1$ nodes in the x-direction, the pore volume as a function of x may be approximated as

$$\begin{aligned} \int_0^{\chi} \phi A_i(\zeta) d\zeta &\approx \int_0^{X} \phi(y_A - y_B) dx \\ &\approx \frac{\Delta x \phi}{2} \sum_{i=1}^{I} \left(y_{Ai} + y_{Ai+1} - y_{Bi} - y_{Bi+1} \right) \quad . \end{aligned} \tag{3.35}$$

where y_A and y_B are the y-coordinates of the piecewise linear streamlines, I is a node such that $I \leq (N+1)$, and ϕ is assumed constant. The interpretation of Eq. 3.35 is shown graphically in Fig. 3.5. Ideally, the cross sectional area A should coincide with the isobar at the particular point at which the integration is desired. On the other hand, it can be argued that the error is small, since the flow is mainly in the x-direction, and the resulting pressure contours will be 'fairly' vertical. Furthermore, by increasing the number of streamtubes the error is reduced further, since the integration that would have taken place along a single streamtube is now split up among several streamtubes, which can better approximate the cross-sectional area. But most importantly, the error is not cumulative. Instead it is a function only of the approximation of A at the upper bound of the integral of Eq. 3.35 such that

$$\left| \int_0^{\chi} \phi A_i(\zeta) d\zeta - \frac{\Delta x \phi}{2} \sum_{i=1}^{I} (\Delta y_i + \Delta y_{i+1}) \right| \propto |A(\chi) - \Delta y(\chi)| \tag{3.36}$$

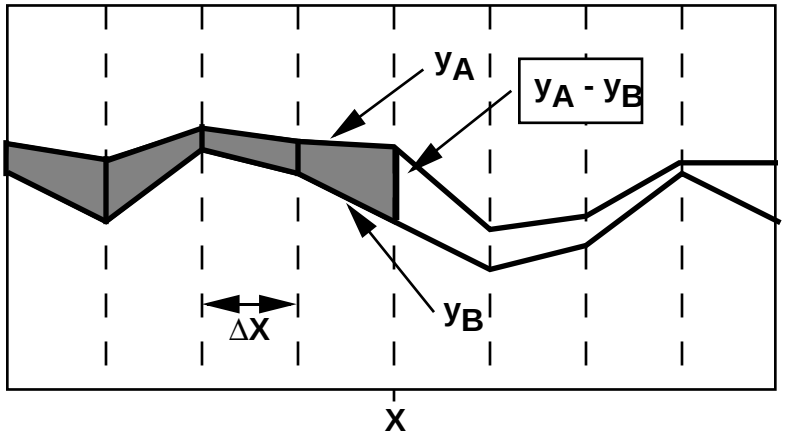

Figure 3.5: *Simple integration method along streamtube to determine the cumulative pore volume at point* χ.

---

where $\Delta y = y_A - y_B$.

3.7.2 Mapping of a 1D Solution - Method B

Although the error in finding the pore volume of a particular streamtube using Method A outlined in the previous section is small, particularly if sufficient streamtubes are used, it does have the disadvantage of implicitly stating that fronts can be mapped as vertical lines along a streamtube. This may result in rather 'jagged' looking fronts, especially if there strong vertical flow. A method that will avoid this is shown graphically in Fig. 3.6. Instead of using a single vertical line to approximate the cross sectional area A, two perpendicular lines are dropped from the center streamline to the bounding streamlines. When a perpendicular line can not be dropped onto one of the streamlines, a vertical segment as in Method A is assumed. Although this will not improve the error caused by Method A, it does result in smoother looking fronts. It is worth noting that neither method A nor method B will be able to capture streamlines that actually flow 'backwards'. Although this may happen, it is not considered here.

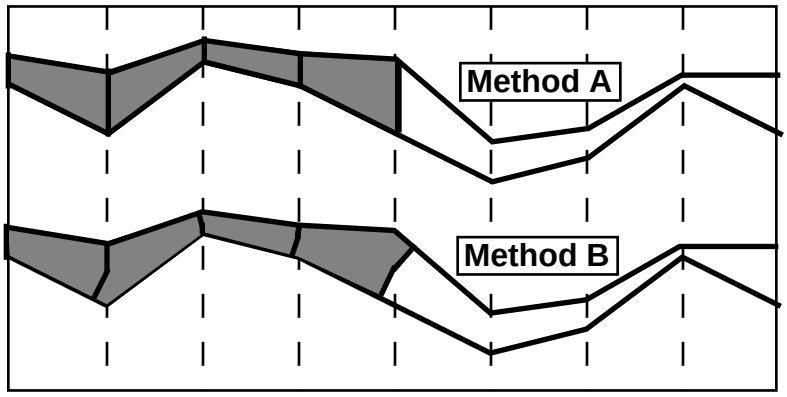

Figure 3.6: *Schematic of integration methods A & B. Although method B will not improve the error in the integration, it will generate smoother front profiles.*

3.7.3 Mapping 1D Solutions Onto a 2D Cartesian Grid

The final step in constructing the desired two-dimensional solution for the heterogeneous domain of interest is to map the one-dimensional solution onto each streamtube. In fact, the solution must also be mapped back onto the underlying regular cartesian grid in order to update mobilities for nonlinear problems as well as for simple plotting purposes.

The algorithm used here closely follows the approach used by *Renard* (1990), and is shown schematically in Fig. 3.7. The idea is that each cartesian grid block has $N \times N$ regularly distributed points in its interior. Each point will therefore fall within a particular streamtube and can be associated with a value of the streamtube's dimensionless pore volume x_D. For a particular time t_D it therefore 'sees' a concentration/saturation value as dictated by the one-dimensional solution. The average grid block value is then simply computed from all the values of the points within it. It is clear that given 'sufficient' streamtubes and 'sufficient' points within each grid block, the errors caused by the mapping algorithm will be minor. The sensitivity of the number of streamtubes and mapping nodes on the solution is examined in the next Chapter (Fig. 4.6).

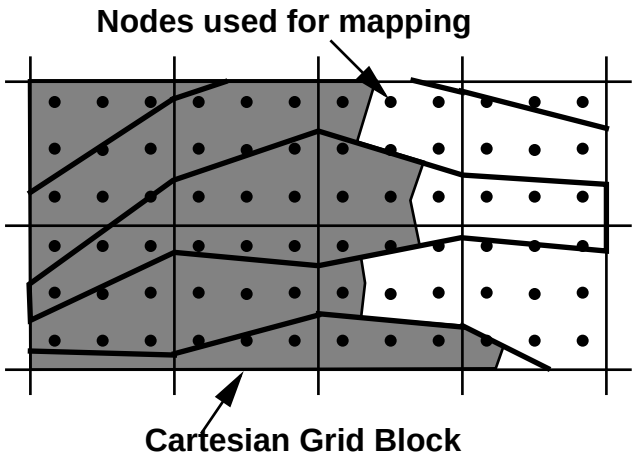

Figure 3.7: *Mapping of one-dimensional solution along streamtubes onto a regular underlying cartesian grid.*

Chapter 4

Unit Mobility Displacements

This chapter discusses modeling of unit mobility (tracer) displacements using streamtubes. Two-dimensional solutions devoid of numerical diffusion are found by mapping a one-dimensional, piston-like solution along streamtubes. Longitudinal physical diffusion is added to the two-dimensional solution by using a convection-diffusion solution along the streamtubes. Under unit mobility assumptions, the two-dimensional streamtube solution is shown to approach the exact solution in the limit of infinite streamtubes.

4.1 Introduction

Unit mobility displacements have been researched extensively in the past. They serve as a first stepping stone to understand the interaction of more complicated, nonlinear multiphase, multicomponent displacements with reservoir heterogeneity. The numerical advantage of tracer displacements is that the elliptic equation governing the potential flow field is decoupled from the mass conservation equations. The problem becomes linear in pressure/flow potential, and the numerically expensive pressure equation has to be solved only once to model the displacement over any desired time span, t_D. Tracer displacements have found widespread use in two major areas of petroleum research: to study numerical diffusion and to quantify the effects reservoir heterogeneities (*Abbaszadeh-Dehghani 1982, Wattenbarger 1993*).

The tracer assumption has also been used extensively in streamtube modeling

(see Chapter 2), because most authors consider the streamtubes as fixed in time, even for two-phase displacements where the total velocity is a function of saturation. This chapter introduces the streamtube approach for tracer displacements, outlining the underlying method to construct two-dimensional solutions for heterogeneous reservoirs that will be applied to nonlinear displacements in the following chapters.

4.2 Streamtubes

As presented in Chapter 3, the governing partial differential equation for the streamfunction in a heterogeneous domain is given by

$$\frac{\partial}{\partial x}\left(\frac{1}{\lambda_y}\frac{\partial \Psi}{\partial x}\right)+\frac{\partial}{\partial y}\left(\frac{1}{\lambda_x}\frac{\partial \Psi}{\partial y}\right)=0 \quad , \tag{4.1}$$

where λ_x and λ_y are the spatially varying fluid mobilities in the x and y directions given by

$$\lambda_x=\frac{k_x}{\mu} \quad , \quad \lambda_y=\frac{k_y}{\mu} \quad . \tag{4.2}$$

k_x and k_y are the absolute permeabilities in the x and y direction respectively, and μ is the constant, single-phase viscosity[1]. Considering the heterogeneous field[2] shown in Fig. 4.1 and applying a constant uniform flux boundary condition at the inlet and a constant pressure boundary condition at the outlet[3] produces the set of streamlines/streamtubes shown in Fig. 4.2. These streamtubes can now be combined with any one-dimensional tracer solution to find a two-dimensional displacement.

[1]Since μ is constant, Eq. 4.1 can be written as

$$\frac{\partial}{\partial x}\left(\frac{1}{k_y}\frac{\partial \Psi}{\partial x}\right)+\frac{\partial}{\partial y}\left(\frac{1}{k_x}\frac{\partial \Psi}{\partial y}\right)=0 \quad . \tag{4.3}$$

[2]See Appendix A for a description of the method used to generate permeability fields.
[3]See Chapter 3 for a discussion on boundary conditions.

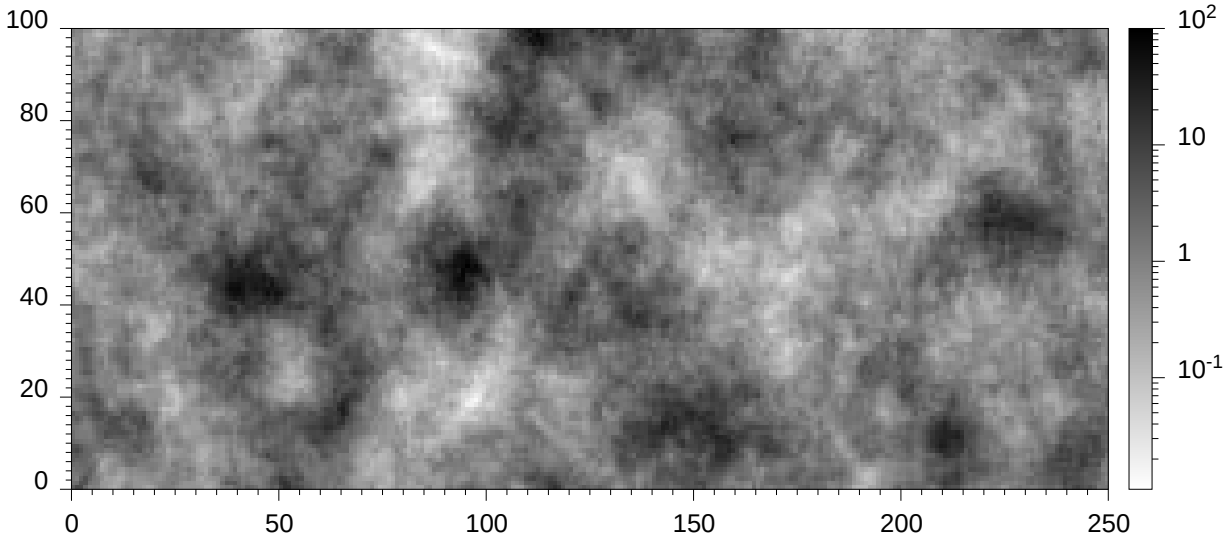

Figure 4.1: *Permeability map with logarithmic scaling on a 250x100 grid. The correlation length is* $\lambda \approx 0.3$ *and the standard deviation is* $\sigma_{\ln K} = 1.0$.

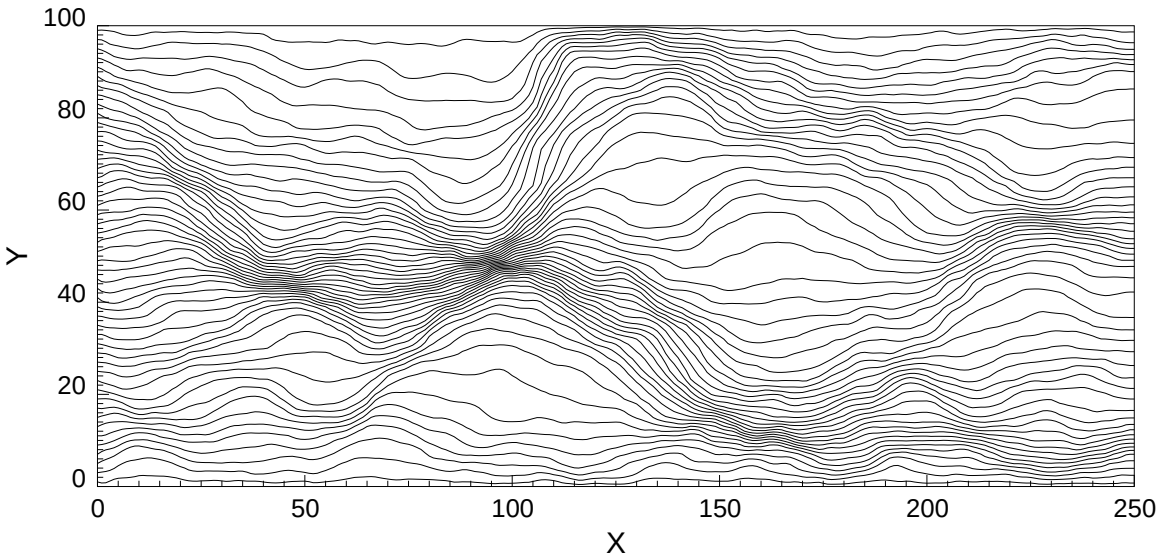

Figure 4.2: *Streamlines for permeability field shown in Fig. 4.1.*

4.3 2D Displacements - No Physical Diffusion

4.3.1 The 1D Solution

The general material balance for the isothermal flow of component i, assuming no chemical reactions and no adsorption/desorption, is given by (*Lake 1989, p.29*)

$$\frac{\partial}{\partial t}\left(\phi\sum_{j=1}^{N_P}\rho_j S_j\omega_{ij}\right) + \nabla\cdot\left(\sum_{j=1}^{N_P}\rho_j\omega_{ij}\vec{u}_j - \phi S_j\rho_j\vec{\vec{K}}_{ij}\cdot\nabla\omega_{ij}\right) = 0 \quad , \tag{4.4}$$

where

ρ_j = molar density of phase j ,
S_j = saturation of phase j ,
ω_{ij} = mole fraction of component i in phase j ,
u_j = Darcy velocity of phase j ,
K_{ij} = dispersion of component i in phase j,
N_p = number of phases present .

The Darcy velocity for phase j is given by

$$\vec{u}_j = -\frac{k_{rj}\vec{\vec{k}}}{\mu_j}\cdot\left(\vec{\nabla}P_j + \rho_j\vec{g}\right) \quad , \tag{4.5}$$

where

k_{rj} = relative permeability of phase j ,
μ_j = viscosity of phase j ,
$\vec{\vec{k}}$ = absolute permeability tensor ,
P = pressure,
$\vec{g}$ = gravity .

Assuming (1) single-phase flow[4], (2) horizontal, one-dimensional flow[5], (3) no diffusion[6], (4) incompressible fluid and rock properties[7], (6) ideal mixing[8], (7) constant phase

[4] $N_P = 1$; $S_1 = 1$; $P_1 = P$; $u_1 = u$
[5] $\vec{g} = 0$; $\vec{\vec{K}}_{i1} = K_{i1}$; $\vec{\vec{k}} = k$
[6] $K_{i1} = 0$
[7] $\rho_1 = \rho \neq \rho(P)$; $\phi \neq \phi(P)$
[8] $\rho = \sum_{i=1}^{N_c}\rho_i^{\circ}\omega_{i1}$

viscosity[9], and (8) homogeneous domain[10] the conservation equation for species i becomes

$$\phi\frac{\partial(\rho w_i)}{\partial t}+u\frac{\partial(\rho w_i)}{\partial x}=0 \qquad i=1,\cdots,N_c\ . \tag{4.6}$$

$\rho w_i = C_i$ is the volumetric concentration of component i. Introducing the dimensionless variables

$$t_D = \frac{1}{\phi L}\int_0^t u dt=\frac{ut}{\phi L} \tag{4.7}$$

$$x_D = \frac{x}{L} \tag{4.8}$$

$$C_{Di} = \frac{C_i}{C_i^*}\ , \tag{4.9}$$

gives

$$\frac{\partial C_{Di}}{\partial x_D}+\frac{\partial C_{Di}}{\partial t_D}=0 \qquad i=1,\cdots,N_c\ . \tag{4.10}$$

Restricting flow to two components only ($N_c = 2$) gives a single independent conservation equation, where the component subscript is dropped for convenience, as

$$\frac{\partial C_D}{\partial x_D}+\frac{\partial C_D}{\partial t_D}=0\ . \tag{4.11}$$

Eq. 4.11 is a linear hyperbolic conservation equation. For constant initial data of the type

$$C_D(x_D,0)\begin{cases} C_{Dl} & \text{for } x_D\le 0 \\ C_{Dr} & \text{for } x_D\ge 0 \end{cases}\ , \tag{4.12}$$

Eq. 4.11 is easily solved by the method of characteristics (*Zauderer 1989, LeVeque 1992*). The initial data of Eq. 4.12 has a discontinuity at $x_D = 0$. Problems with this type of initial data are called Riemann problems, where the subscript r refers to the state to the right of the discontinuity and l refers to the state to the left of the discontinuity.

[9] $\mu_1 = \mu$
[10] k = constant

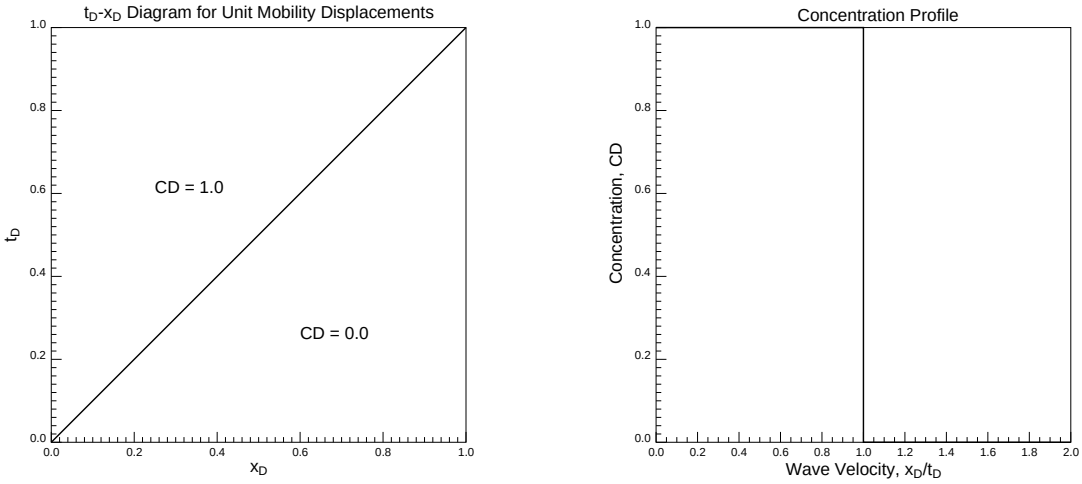

Figure 4.3: *Analytical solution for unit mobility displacement with no physical diffusion.*

The solution to Eq. 4.11 with the initial data given by Eq. 4.12 is an indifferent wave traveling at unit velocity, expressed mathematically as

$$C_D(x_D, t_D) = \begin{cases} 1 & \text{for } x_D \leq t_D \\ 0 & \text{for } x_D \geq t_D \end{cases} , \tag{4.13}$$

and shown graphically in Fig. 4.3. Clearly, Eq. 4.13 is a limiting solution, since it represents a sharp front traveling at unit velocity without ever diffusing. In fluid flow through porous media, both molecular diffusion and velocity variations at the pore scale cause the front to diffuse with time (*Bear 1972*). But as with all limiting solutions, Eq. 4.13 is important because it is a reference solution against which to measure numerical solutions that invariably include numerical diffusion. In a similar way then, mapping Eq. 4.13 onto streamtubes will lead to a limiting, diffusion-free, two-dimensional solution that can be used as a benchmark for testing numerical schemes.

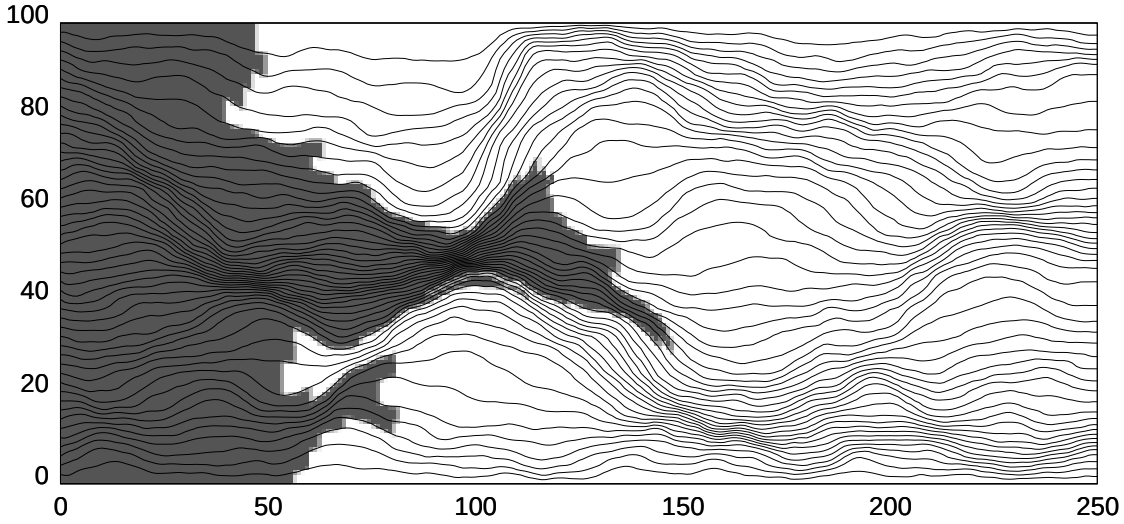

Figure 4.4: *Example solution for the two dimensional domain by mapping the diffusion-free tracer solution at $t_D = 0.3$ along each streamtube of Fig. 4.1.*

4.3.2 The 2D Solution

Using the one-dimensional tracer solution given by Eq. 4.13 and the streamtubes for the heterogeneous domain of Fig. 4.1, a two-dimensional solution is constructed by mapping Eq. 4.13 onto each streamtube as outlined in Chapter 3. An example solution at $t_D = 0.3$ is shown in Fig. 4.4.

Generating the streamtube solution in Fig. 4.4 does not involve any 'time-stepping', as is the case for finite difference approaches. Instead, because the dimensionless distance (Eq. 3.27) is known along each streamtube, the location of the tracer front can be positioned immediately in each streamtube by simply finding the $x_D = t_D$ point. All points along a streamtube associated with $x_D < t_D$ will see a tracer concentration of $C_D = 1$, whereas all points associated with $x_D > t_D$ will see a concentration of $C_D = 0$. To generate a solution at some later time then, the streamtube approach does not move the old front position by a Δt_D, but instead generates a solution for the new cumulative time $t_D + \Delta t_D$. A profile history is constructed by mapping the analytical solution for different dimensionless times, as illustrated in Fig. 4.5.

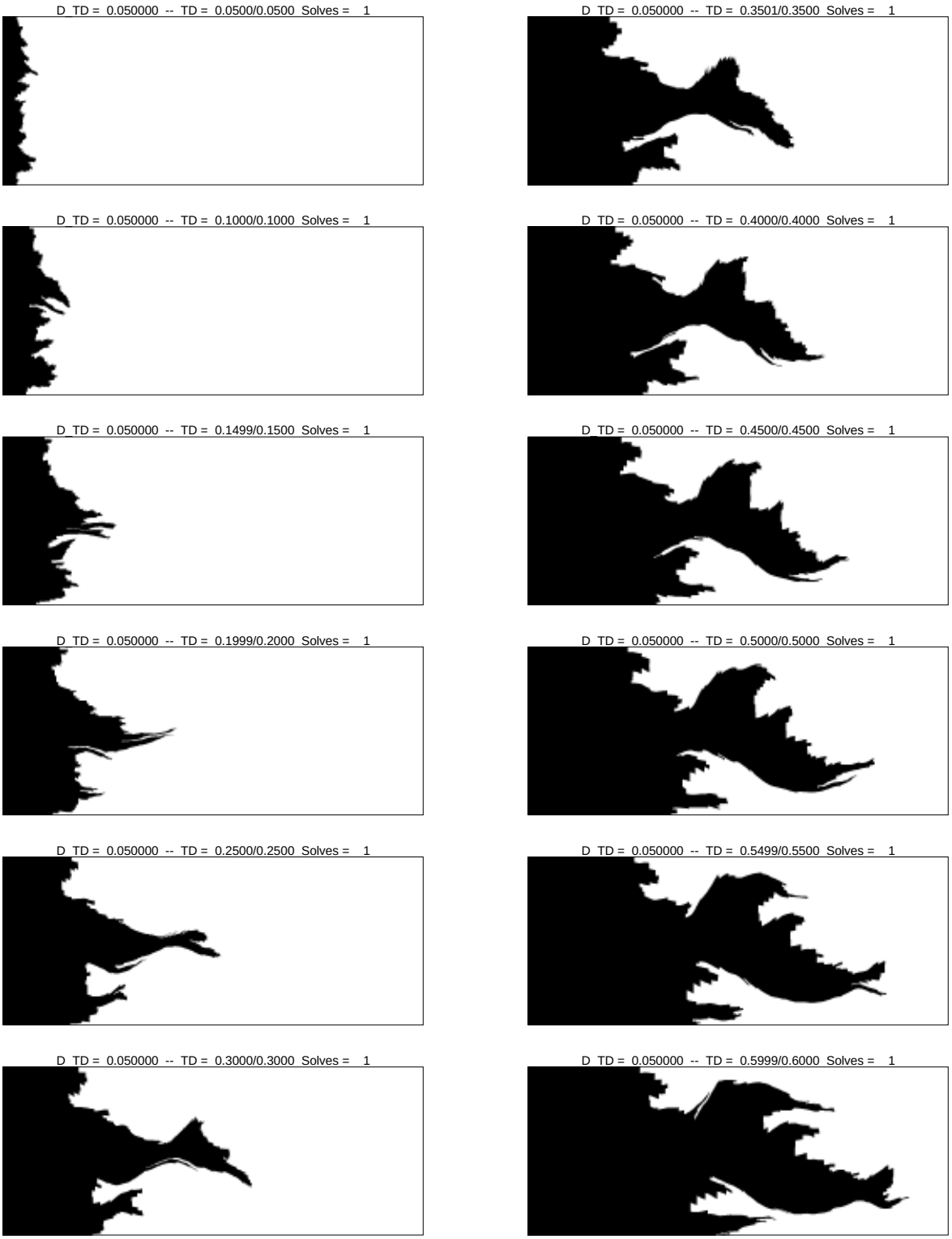

Figure 4.5: *Displacement history at $\Delta t_D = 0.05$ intervals for the permeability map (250x100 grid blocks) shown in Fig. 4.1.*

Except for the averaging occurring at the grid block level due to the mapping algorithm used for transferring the one-dimensional solution onto the underlying regular cartesian grid as outlined in Chapter 3 (see Fig. 3.7), there is no numerical diffusion in the resulting two-dimensional solution. Instead, an area having a maximum width of a single grid block along the front, in which the concentration can be between 0 and 1, represent the minimum level of resolution imposed by the number of grid blocks used in the underlying cartesian grid. The displacement history in Fig. 4.5 is significant, because it represents the limiting numerical-diffusion-free tracer solution for the heterogeneous reservoir shown in Fig. 4.1.

4.3.3 Sensitivity of 2D Solution

As pointed out in Chapter 3, the accuracy of the two-dimensional solution will depend on the number of streamtubes used to map the one-dimensional solution as well as on the number of 'mapping nodes' used to transfer the solution from the streamtubes back onto the regular cartesian grid. Clearly, the more streamtubes and mapping nodes are used, the better the solution. On the other hand, there must exist a limit on the number of streamtubes necessary to represent the two-dimensional solution: if each streamtube has a maximum width that is smaller than the underlying cartesian grid block, then the resolution of the front due to the large number of streamtubes will be lost to the averaging at the grid block level.

The sensitivity of the two-dimensional solution to the number of streamtubes and mapping nodes is demonstrated in Fig. 4.6. The same 50×50 heterogeneous permeability field is solved using 10, 50, and 100 streamtubes with respectively 4, 9, and 25 mapping nodes per grid block. Although a different permeability field may give a slightly different result, especially if there is strong vertical flow, Fig. 4.6 indicates that using approximately the same number of streamtubes as blocks in the y-direction and 4 mapping nodes per grid block is sufficient to capture the details of the two-dimensional solution. In fact, because fast flow regions produce a bunching of streamtubes, these areas will automatically produce a better resolution compared to slow flow regions, which give rise to 'fatter' streamtubes. Since the high flow regions are the regions of primary interest, relatively few streamtubes (compared to

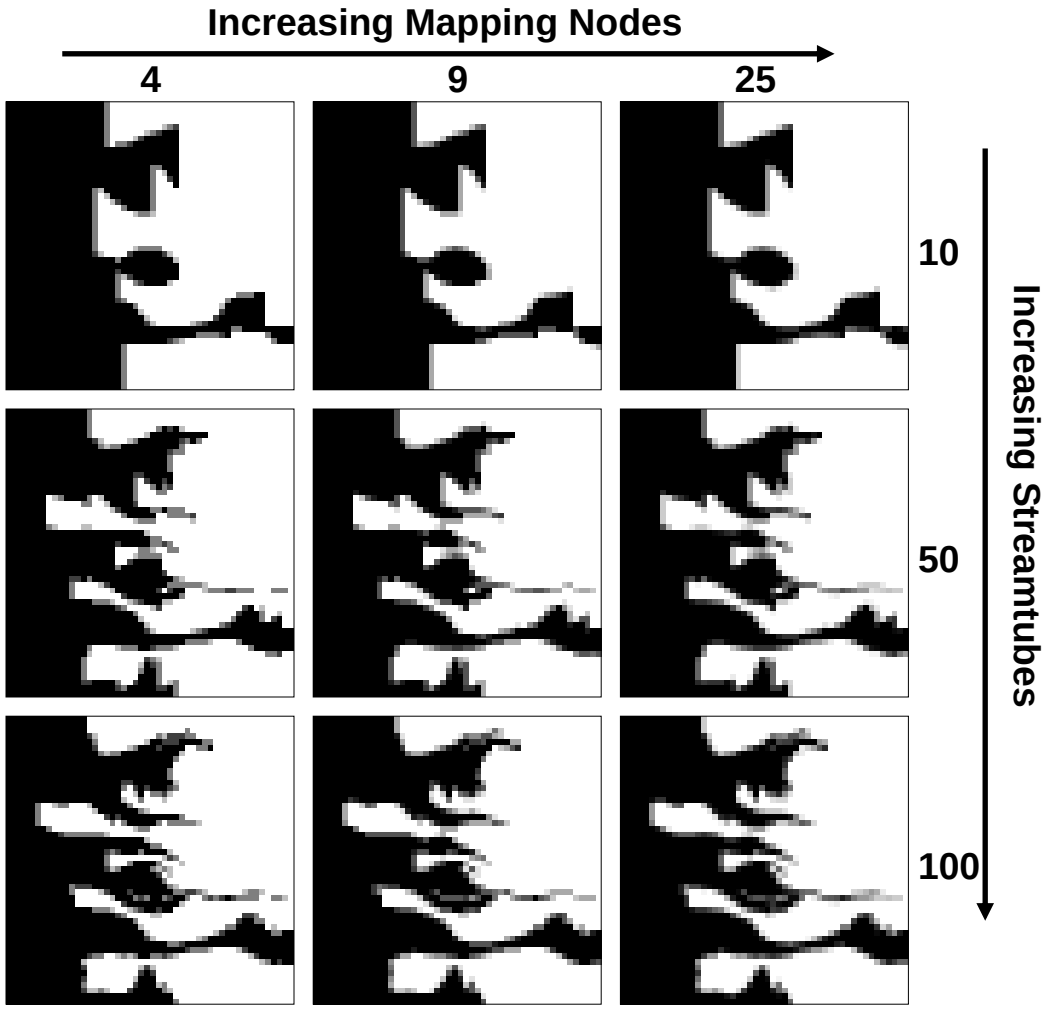

Figure 4.6: *Sensitivity of two-dimensional solution on the number of streamtubes and mapping nodes per grid block. The number of streamtubes increases from top to bottom (10,50,100) and the number of mapping nodes increases from left to right (4, 9, 25). The underlying heterogeneous permeability field is on a* 50×50 *cartesian grid with five orders of magnitude variation in permeability and* $\lambda_x = 0.2$, $\lambda_y = 0.1$.

the number of NY grid blocks) can still produce acceptable results.

Because the number of streamtubes produces negligible overhead in the code used in this dissertation (STREAM), the majority of the results presented here used $2\times NY$ streamtubes and 9 mapping nodes per grid block.

4.4 2D Displacements - Physical Diffusion

4.4.1 The 1D Solution

In real porous media, the indifferent wave solution derived in the previous section is subject to 'smearing' due to a combination of molecular diffusion and velocity variations at the pore scale that induce mixing. Effects of molecular diffusion are generally assumed to be small compared to the effects of local velocity variations (*Perkins and Johnston 1963, Bear 1972, Gelhar and Axness 1983, Lake 1989*). A more realistic tracer displacement is one that accounts for such diffusive effects. The derivation is analogous to the derivation of Eq. 4.11, except that now the diffusion coefficient K is nonzero (but spatially constant) which leads to

$$\phi\frac{\partial(\rho w_i)}{\partial t} + u\frac{\partial(\rho w_i)}{\partial x} = \phi K\frac{\partial^2(\rho w_i)}{\partial x^2} \qquad i = 1,\cdots,N_c \ , \tag{4.14}$$

the well-known convection-diffusion equation. Using the same dimensionless variables as before gives the dimensionless form of the CD-equation as

$$\frac{\partial C_D}{\partial t_D} + \frac{\partial C_D}{\partial x_D} = \frac{1}{N_{Pe}}\frac{\partial^2 C_D}{\partial x_D^2} \ , \tag{4.15}$$

where N_{Pe} is a dimensionless number called the Peclet number and given by

$$N_{Pe} = \frac{uL}{K} \ . \tag{4.16}$$

A 'velocity dependent' model is sometimes used to express the coefficient K as (*Lake 1989*)

$$K = K_m + \alpha u \ , \tag{4.17}$$

where K_m is the molecular diffusion coefficient and α is the dispersivity of the permeable medium[11]. If the molecular diffusion coefficient is assumed to be small compared to the product αu then the Peclet number may be written as

$$N_{Pe} = \frac{L}{\alpha} \quad . \tag{4.18}$$

Although Eq. 4.18 is very appealing because it gives a 'velocity independent' expression for the Peclet number, it must be used with caution. In general, α is not a fundamental property of the medium and has been shown to increase with travel distance in observed field data[12] (*Neuman 1990, Arya et al.1988*). On the other hand, for a completely uncorrelated log-permeability field, α is indeed constant and can be approximated from the covariance of the permeability field (*Gelhar and Axness 1983, Dagan 1988*). Although Eq. 4.16 and Eq. 4.18 are different, both equations must give rise to the same constant value of N_{Pe} in order to honor the assumption (a spatially constant coefficient K) used in deriving the CD-equation.

Eq. 4.15 is now of parabolic form and thus requires an additional boundary condition compared to its hyperbolic, diffusion-free counterpart. An approximate solution to Eq. 4.15 using the following initial and boundary conditions (*Lake 1989*),

$$C_D(x_D, t_D = 0) = 0 \tag{4.19}$$

$$C_D(x_D = 0, t_D) = 1 \tag{4.20}$$

$$C_D(x_D \to \infty, t_D) = 0 \tag{4.21}$$

[11]The use of the dispersivity α is the reason why the convection-diffusion equation is often referred to as the convection-dispersion equation. In the published literature, diffusion is used to indicate mixing due to molecular diffusion whereas dispersion is used to indicate mixing due to local velocity variations.

[12]The fact that α is found to increase with distance traveled in field data results from the attempt to use a one-dimensional diffusive/dispersive model to capture three-dimensional, convective dominated flow. Effects due to heterogeneities across various scales are lumped into a single parameter, leading to a dependence of α on distance traveled. In the streamtube method, however, at least two heterogeneity scales are being separated explicitly: field scale heterogeneities are defined by the streamtube geometries, while sub-streamtube heterogeneities may be captured using α. See Section 4.4.2 for a discussion on the subject.

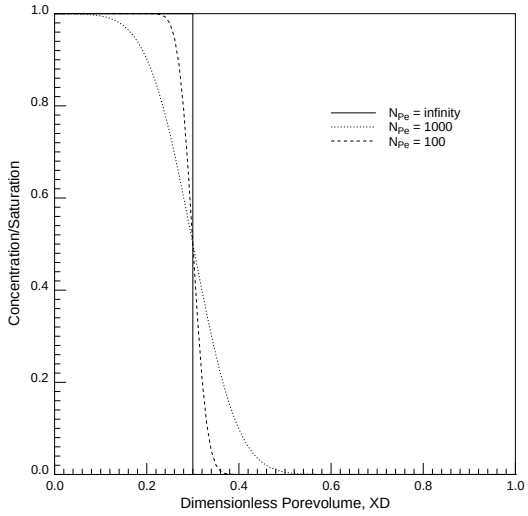

Figure 4.7: *One-dimensional analytical solutions for the convection-diffusion equation at* $t_D = 0.3$ *and three values of* N_{Pe}.

---

is given by[13]

$$C_D(x_D, t_D) = \frac{1}{2}\text{erfc}\left(\frac{x_D - t_D}{2\sqrt{\frac{t_D}{N_{Pe}}}}\right) \quad . \tag{4.22}$$

Adding physical diffusion to a two-dimensional displacements therefore amounts to mapping Eq. (4.22) onto each streamtube for a given value of N_{Pe}. Example solutions at $t_D = 0.3$ and three values of N_{Pe} are shown in Fig. 4.7.

4.4.2 The 2D Solution

Mapping Eq. 4.22 onto streamtubes is slightly different from mapping the no-diffusion solution, since Eq. 4.22 is clearly not scalable by x_D/t_D. To find the solution for a particular time t_D, Eq. 4.22 must be evaluated explicitly for that time. Nevertheless, it is important to realize that as in the no-diffusion case, there is no time-stepping

[13]The exact solution is

$$C_D(x_D, t_D) = \frac{1}{2}\text{erfc}\left(\frac{x_D - t_D}{2\sqrt{\frac{t_D}{N_{Pe}}}}\right) + \frac{1}{2}e^{x_D N_{Pe}}\text{erfc}\left(\frac{x_D + t_D}{2\sqrt{\frac{t_D}{N_{Pe}}}}\right) \quad ,$$

but the second term goes to zero exponentially as t_D, x_D, and N_{Pe} grow.

involved in finding the two-dimensional solution, since Eq. 4.22 is an analytic expression, which can be evaluated directly for any dimensionless time t_D and mapped onto the streamtubes.

Example two-dimensional solutions for the heterogeneous domain of Fig. 4.1 (250×100 grid blocks) at $t_D = 0.3$ and three Peclet numbers ($N_{Pe} \rightarrow \infty$, $N_{Pe} = 1000$, and $N_{Pe} = 100$) are shown in Fig. 4.8. The following issues are addressed by Fig. 4.8:

Convection vs. Diffusion

Field-scale Peclet numbers can range from 10-10000 (*Arya et al. 1988*) and are typically of order 1000. Figure 4.8 shows that for this range of Peclet number physical diffusion is likely to be a second-order effect. The large-scale, correlated permeability field dictates the overall profile of the tracer and where it preferentially wants to go. This first order effect remains dominant in the presence of small amounts of physical diffusion.

Longitudinal vs. Transverse Diffusion

Since a streamtube is a one-dimensional system, only longitudinal diffusion is accounted for in Fig. 4.8, and transverse diffusion is assumed to be negligible. The question must be asked whether the solutions in Fig. 4.8 would have been substantially different if transverse diffusion had been included. *Blackwell* (1962) studied the relative importance of longitudinal to transverse diffusion in sand-packed columns and found that at slow flow rates, transverse diffusion may be on the same order of longitudinal diffusion. However, as the flow rate increases, longitudinal diffusion begins to dominate the displacement and several orders of magnitude difference may exist between the two diffusion coefficients. This conclusion carries over to field scale displacements as well. Using stochastic continuum theory *Gelhar and Axness* (1983) show that for isotropic permeability fields the transverse macrodispersivity is several orders of magnitude smaller than the longitudinal dispersivity. In the case of an arbitrarily oriented permeability field, the ratio of longitudinal to transverse dispersivity is still on the order of 10^{-1}. This is generally confirmed by field data (*Gelhar 1993*).

Figure 4.8: *Including physical diffusion in M=1 displacement by mapping the convection-diffusion equation along each streamtube at* $t_D = 0.3$. *Examples at* $N_{Pe} \to \infty$, $N_{Pe} = 1000$, *and* $N_{Pe} = 100$.

Thus, it is fair to say that if the solutions in Fig. 4.8 are assumed on a field scale, transverse diffusion would not change them significantly.

Scale of the 2D Solution

Mapping a convection-diffusion solution onto the streamtubes automatically attaches a length scale to the system. The asymptotic behavior of the longitudinal dispersivity through a low variance, second-order stationary, permeability field may be expressed as (*Gelhar and Axness 1983, Dagan 1988, Neumann 1990*)

$$\alpha = \int_0^\infty C(h)dh \approx \int_0^{L_{rep}} C(h)dh \approx B\sigma^2 L_{rep} \tag{4.23}$$

where L_{rep} is a representative length scale beyond which the system looks 'diffusive' (or Fickian), $C(h)$ is the covariance as a function of separation length h, and B is a constant. For example, if the $C(h)$ is linear between 0 and L_{rep} then $B = 0.5$ and using Eq. 4.23, the Peclet number can be expressed as

$$N_{Pe} = \frac{2}{\sigma^2}\frac{L}{L_{rep}} \quad . \tag{4.24}$$

By choosing a Peclet number then, a representative length scale (L_{rep}) is automatically introduced beyond which the systems is said to be diffusive. What order of magnitude L_{rep} can have though, is a matter of heated debate. If the porous medium is modeled as a series of well–stirred 'tanks' (*Aris and Amundson 1957*), then in the limit of a large number of pores a Fickian diffusion model is indeed valid. In this case, L_{rep} is on the order of the representative element volume (REV) used in the continuum approach to porous media. Laboratory displacements through 'homogeneous' cores have generally confirmed this (*Brigham et al. 1961, Blackwell 1962*). If L_{rep} is on the order of the REV, then the two–dimensional streamtube scale could be several orders of magnitude larger, maybe on a $\mathcal{O}(1m)$ or possibly even $\mathcal{O}(10m)$ scale.

For field scales, however, there exists considerable uncertainty what L_{rep} should be, or even if a such number has a meaning at all. Ample experimental data from field tracer tests demonstrate convincingly the inadequacy of the convection–diffusion model in matching the integrated concentration response at the production wells (*Arya et al. 1988*). Nevertheless, considerable effort has gone into showing under

what conditions the convection–diffusion equation may be applicable to field scale displacements and when not (*Matheron and de Marsily 1980, Gelhar and Axeness 1983, Dagan 1983;1984;1988, Arya et al. 1988, Neumann 1990*). Numerical experiments (*Smith and Schwartz 1980, Desbartes 1990, Wattenbarger 1993*) have also shown that a diffusive limit is reached only for $L_{rep} << \lambda_c << L$ and $\sigma^2_{\ln k}$ small, where L_{rep} is the diffusive length scale at the pore level, λ_c is the correlation length scale of the permeability field, and L is the domain dimension in the main direction of flow. Others (*Waggoner et al. 1992*), on the other hand, have reported relatively large 'dispersive' regions in λ–$\sigma^2_{\ln k}$ parameter space.

The real question in applying in the CD–model to field–scale streamtubes though, is whether a sub–field scale L_{rep} exists that allows the CD–solution to hold along field–scale streamtubes. A numerical example of this idea is given by *Wattenbarger* (1993) In essence, the idea is that each streamtube can be treated as a system having the necessary characteristics ($L_{rep} << \lambda_c << L$ and $\sigma^2_{\ln k}$ small) so as to allow a Fickian limit to be reached within each streamtube. Considering that the streamtubes, by definition, will conform to the flow units (heterogeneity) of the system, the assumption of treating each streamtube as a pseudo homogeneous unit that reaches a diffusive limit is not unreasonable. In other words, a small L_{rep} does not necessarily preclude the streamtubes to be on a field scale. For example, successful matching of field tracer data using this approach has been demonstrated by *Abbaszadeh–Dehghani* (1982). In summary, mapping the CD-model along field-scale streamtubes is an attempt to capture sub-tube heterogeneities, which are represented numerically by specifying an appropriate Peclet number. It represents a 'nested' approach to modeling heterogeneities that dominate at different scales: the streamtubes capture the large-scale heterogeneities of the reservoir while the CD-solution models sub-grid block/sub-streamtube features.

Limiting Two-Dimensional Solution

The $N_{Pe} \to \infty$ solution is the limiting no-diffusion solution and serves as the reference point to quantify any diffusive behavior. The no-diffusion solution is an important ingredient in quantifying numerical diffusion, as will be discussed in the next section.

4.5 Quantifying Numerical Diffusion

Mapping analytical solutions, such as Eq. 4.13 or Eq. 4.22, onto streamtubes results in two-dimensional solutions that are completely devoid of numerical diffusion. Streamtube solutions can therefore be used to quantify the extent of numerical diffusion in other numerical solutions obtained by using finite differences or finite elements.

An example of such a comparison is given in Fig. 4.9, which shows the tracer solution without physical diffusion at $t_D = 0.3$ compared to no-diffusion solutions obtained using Mistress (CFL=0.2), a research code with flux corrected transport developed at British Petroleum (*Christie and Bond 1985*) and Eclipse, a commercially available reservoir simulator with single point upstream weighting.

In the limit of a large number of streamtubes, the streamtube solution is the exact limiting solution for the no diffusion case, and can be used to calculate the spatial error

$$\Delta C_{\rm err} = \mid C(x,y)_{\rm Stubes} - C(x,y)_{\rm FD} \mid \ , \tag{4.25}$$

where the subscript FD stands for finite difference. A spatial rendering of $\Delta C_{\rm err}$ is shown in Fig. 4.10.

4.6 Concluding Remarks

This chapter introduced the basic concept involved in mapping a one-dimensional solution onto streamtubes to generate a two-dimensional solution for a heterogeneous reservoir. The key aspect in constructing a two-dimensional solution is to map the one-dimensional solution at the new time level by going back to time $t_D = 0$ and integrating forward to $t_D = t_D + \Delta t_D$, rather than time-stepping from t_D to $t_D + \Delta t_D$. For the special case of tracer flow, mapping the one-dimensional solution as a Riemann solution does not involve any assumptions, since the streamtubes are fixed in time. In the limit of 'sufficient' streamtubes, the no-diffusion, two-dimensional tracer solution is the exact limiting solution and can be used to quantify the numerical error of traditional numerical approaches. Longitudinal physical diffusion is added by mapping a convection-diffusion solution along streamtubes. By choosing a value for

Figure 4.9: *Comparison of concentration profiles showing the extent of numerical diffusion in finite difference simulators. Streamtube method versus Mistress, a research code with flux corrected transport (FCT) and Eclipse, a commercially available reservoir simulator with single point upstream weighting and automatic time step selection.*

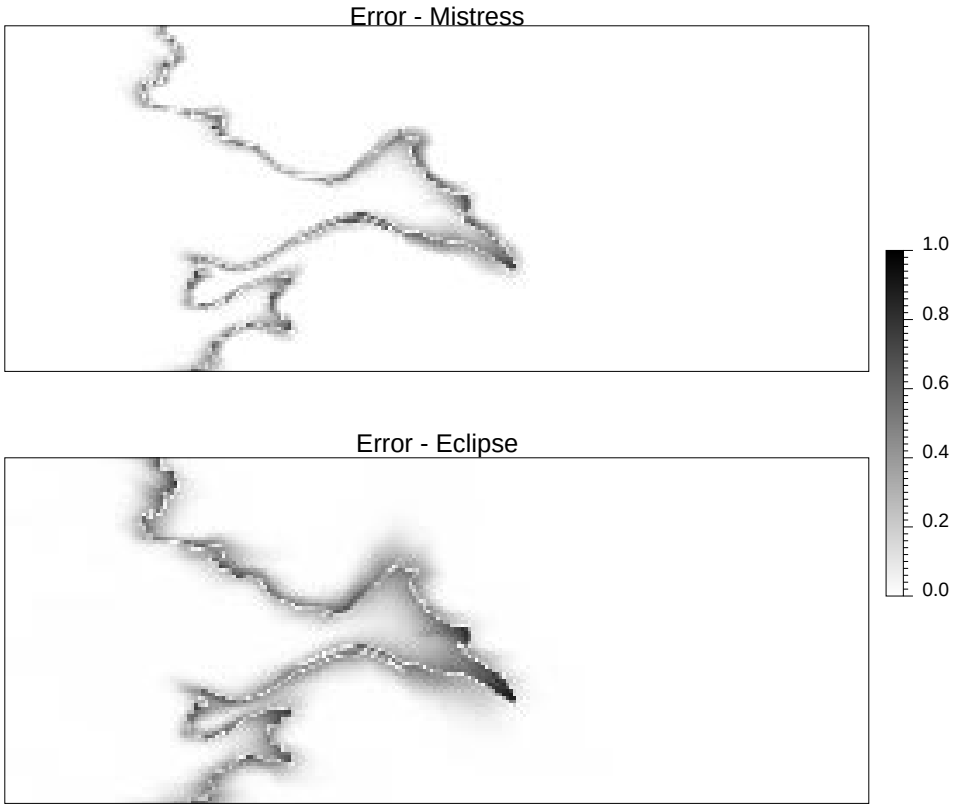

Figure 4.10: *Spatial distribution of the error caused by numerical diffusion in the Mistress and Eclipse simulations shown in Fig. 4.9.*

---

the Peclet number in the convection-diffusion model, an implicit assumption about the scale of the two-dimensional solutions is made. In particular, sub-streamtube heterogeneities are assumed to lead to a Fickian limit. Thus, the streamtube approach is an example of how physical phenomena that take place at different scales can be nested into a single model: the geometries of the streamtube explicitly model large scale heterogeneities that give rise to fast and slow flow regions, while the convection-diffusion solution implicitly models sub-streamtube heterogeneities that cause local mixing.

Chapter 5

Immiscible Displacements

This chapter discusses modeling of two-phase, immiscible displacements using streamtubes. The concept of mapping one–dimensional Riemann solutions along streamtubes is developed further, and the resulting two–dimensional solutions are shown to match solutions obtained using a conventional finite difference approach.The immiscible problem is found to be only weakly nonlinear resulting in converged solutions using two orders of magnitude fewer matrix inversions than in traditional finite difference simulation. The speed of the streamtube approach is used to study the interaction of nonlinearity and reservoir heterogeneity in immiscible displacements, demonstrating an increasing uncertainty in recovery with increasing reservoir heterogeneity.

5.1 Introduction

When *Higgins and Leighton* (1962) introduced the streamtube approach as a fast method to predict two–phase flow in a five–spot pattern, they reported excellent agreement with experimental data for mobility ratios ranging from 0.083 to 754. Other authors (*Higgins et al. 1964, Doyle and Wurl 1971, LeBlanc and Caudle 1971, Martin and Wegner 1979*) also reported good matches with either field or laboratory data for similar values of mobility ratios. All authors were able to account for the nonlinearity inherent in the total velocity field by keeping the streamtubes fixed and adjusting the flowrates instead. The only published note on the failure of the streamtube approach is by *Martin et al.* (1973) and, surprisingly, it is for a favorable

mobility ratio case. Intuitively, high unfavorable mobility ratio displacements are expected to have a 'stronger' nonlinearity and thus be more difficult to model numerically, whereas the favorable mobility ratio displacements are by definition stable. The answer is that while the end–point mobility ratios reported by many authors are very high, the resulting 1D solutions exhibit a very long rarefaction wave leading to smooth changes in the velocity fields. Favorable mobility ratios, on the other hand, have self-sharpening shocks, across which properties vary abruptly leading to much sharper changes in the velocity fields. Two–phase immiscible displacements with unfavorable mobility ratios and reasonable rock curves will therefore either have shock–front mobility ratios close to 1 or just long rarefaction waves.

It is this weak nonlinearity in the velocity field that allows for the assumption of constant streamtube geometries, which are almost universally applied in the petroleum literature[1]. The assumption of fixed streamtubes is also reinforced by the areal geometry used by all authors since, by continuity, a streamline must start and end at a source point, leaving little room for the streamtubes to change their shape during the displacement. Adjusting the flow rates for each streamtube according to the total resistance of the system is sufficient to capture the nonlinear allocation of fluids that would result from changing streamtubes. Although the approaches differ slightly from author to author, all show convincingly that constant streamtubes can successfully and inexpensively predict recovery for most two-dimensional, areal waterflood problems.

5.1.1 The Riemann Approach

In this chapter, the waterflood problem is approached differently and used principally to demonstrate the applicability of the Riemann approach proposed in this work and to be used for multiphase, multicomponent displacements in later chapters. As in the tracer case, the domain is considered to be heterogeneous and the geometry to be cross-sectional. Compared to the areal domain, the streamlines are now no longer pinned down by two (or more) singularities, making them 'freer' to move and to reflect

[1] A notable exception is *Renard* (1990)

the nonlinearity in the flow field.

The principal difference to work done by previous authors lies is in the mapping of the one-dimensional solution along streamtubes which are periodically updated to model the nonlinearity of the displacement. In the Riemann approach used here, the one-dimensional solution is treated as a solution to a Riemann problem, although the streamtubes are updated periodically. Thus, the solution along a new streamtube for the time level $t_D + \Delta t_D$ is not given by an integration from t_D to $t_D + \Delta t_D$, as in conventional time-stepping algorithms, but rather as an integration from 0 to $t_D + \Delta t_D$, where the initial conditions are assumed to be constant right and left states. The Riemann approach centers on treating each periodically updated streamtube as a true one-dimensional system on which the Buckley-Leverett solution is mapped repeatedly for different times. The underlying assumption in the Riemann approach is that the fluid entering a streamtube remains in the streamtube and exits only at the outlet end, even if the streamtube changes location and geometry as a function of time. The validity of this approach is considered in the sections that follow.

5.1.2 Reasons for the Riemann Approach

A legitimate question is to ask what motivates the Riemann approach. The answer centers on the attempt to capture the nonlinearities that exist in multiphase flow. Only three authors (*Martin et al. 1973, Martin and Wegner 1979, Renard 1990*) address the idea of updating the streamtubes, rather than using total flow resistance to capture the nonlinear behavior of the displacement. Mathematically, updating the streamtubes is an appealing approach because the local flow velocities are updated, and the original definition of a streamtube as carrying a volumetric rate equal to the difference in the value of its bounding streamlines is maintained. However, updating the streamtubes poses one problem related to the initial conditions associated with each streamtube: each time a streamtube is updated it must be initialized so that the conservation equation(s) can be solved. The only reasonable possibility to assign new initial conditions along an updated streamtube is to use the old, two–dimensional saturation distribution on the underlying cartesian grid. Because updating a streamtube literally means changing its position in x–y space, it is easy to see that the new initial

conditions will not correspond to the old saturation distribution along the streamtube. The resulting hyperbolic problem that must be solved will be one with general, nonconstant initial conditions. No analytical solutions exist for such problems and the saturation distribution along the new streamtube can be moved forward in time either (1) numerically by using a standard one–dimensional finite–difference solution along each streamtube (*Bommer and Schechter 1979*), or (2) by using a moving interface, front–tracking algorithm (*Sheldon and Dougherty 1964, Glimm et al. 1983, Bratvedt et al. 1989*). The Riemann approach, on the other hand, completely circumvents the problem of initial conditions that arises with streamtube updating: the two–dimensional solution is approximated by N one–dimensional Riemann solutions along changing streamtubes.

5.2 The 1D Buckley–Leverett Solution

The one-dimensional Buckley–Leverett solution is well known and well documented in the petroleum literature (*Buckley and Leverett 1941, Dake 1978, Lake 1989*). Starting from the general material balance for component i (*Lake 1989, p.29*)

$$\frac{\partial}{\partial t}\left(\phi \sum_{j=1}^{N_P} \rho_j S_j \omega_{ij}\right) + \nabla \cdot \left(\sum_{j=1}^{N_P} \rho_j \omega_{ij} \vec{u}_j - \phi S_j \rho_j \vec{\vec{K}}_{ij} \cdot \nabla \omega_{ij}\right) = 0 \quad , \tag{5.1}$$

and assuming (1) two component, two–phase, immiscible flow[2], (2) no diffusion[3], (3) constant and equal phase densities[4], and (4) one–dimensional flow gives the well known equation

$$\phi \frac{\partial S_w}{\partial t} + \frac{\partial u_w}{\partial x} = 0 \quad , \tag{5.2}$$

where the subscript for component $i = 1$ has been replaced with w, to keep with the traditional application to oil–water systems. Eq. 5.2 is generally used in its dimensionless form

$$\frac{\partial S_w}{\partial t_D} + \frac{\partial f_w}{\partial x_D} = 0 \quad , \tag{5.3}$$

[2] $\omega_{11} = \omega_{22} = 1$; $\omega_{12} = \omega_{21} = 0$

[3] $\vec{\vec{K}}_{ij} = 0$

[4] $\rho_1 = \rho_2$

where $t_D = tu_t/L$ and $x_D = \phi x/L$ are usual definitions of dimensionless time and distance respectively, u_t is the total (constant) Darcy velocity given by $u_t = u_w + u_o$, and f_w is the fractional flow of water given by

$$f_w = \frac{u_w}{u_w + u_o} = \frac{1}{1 + \frac{k_{ro}\mu_w}{k_{rw}\mu_o}} \quad . \tag{5.4}$$

k_{ro}, k_{rw}, μ_o, and μ_w are the relative permeabilities and viscosities of oil and water as indicated by the subscript[5]. The solution to Eq. 5.3 subject to Riemann conditions of the form

$$S_w(x_D, 0) \begin{cases} S_{wl} & \text{for } x_D \leq 0 \\ S_{wr} & \text{for } x_D \geq 0 \end{cases} \quad , \tag{5.5}$$

where, as in the tracer case (Eq. 4.12), the subscripts l and r refer to the left and right constant states of the discontinuity at $x_D = 0$, can be found easily using the method of characteristics (*Zauderer 1989, LeVeque 1992*). Depending on the shape of the fractional flow curve, f_w, the solution can contain rarefaction waves and shocks, which are found using the velocity constraint and the entropy condition (*Johns 1992*). A rarefaction wave is composed of saturations having characteristic velocities given by

$$\frac{dx_D}{dt_D} = \frac{df_w}{dS_w} \quad , \tag{5.6}$$

whereas a shock travels with a characteristic velocity given by

$$\frac{dx_D}{dt_D} = \frac{f_w^U - f_w^D}{S_w^U - S_w^D} \quad . \tag{5.7}$$

The superscripts U and D stand for upstream and downstream respectively. An example solution for a two–phase problem with an end–point mobility ratio of 10 is shown in Fig. 5.1.

5.3 Validation of the Riemann Approach

The Riemann approach was tested by the following numerical experiment. Using a standard finite difference simulator (Eclipse), the velocity fields were stored for

[5]Eq. 5.4 assumes that the one–dimensional reservoir is homogeneous.

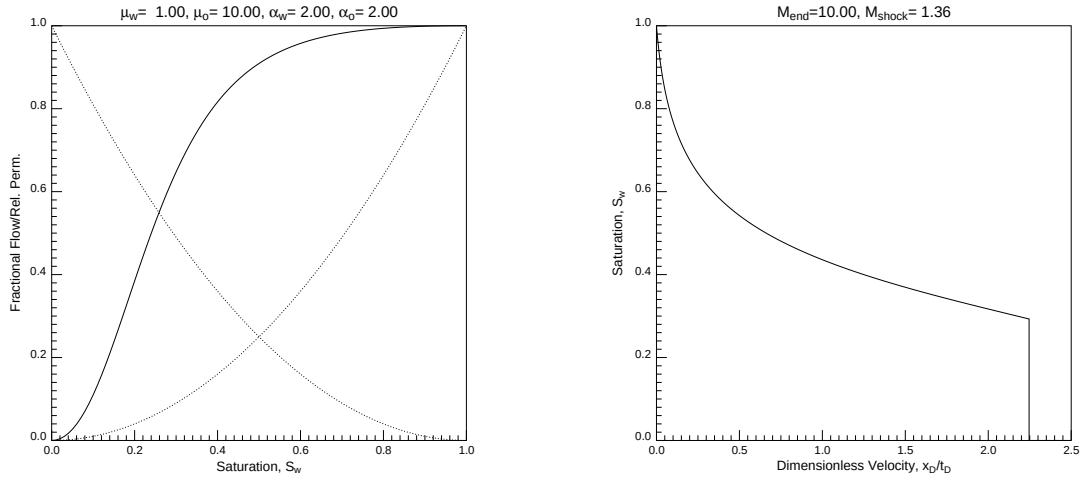

Figure 5.1: *Relative permeability curves ($k_{rw} = S_w^2$, $k_{ro} = S_o^2$), corresponding fractional flow function for a viscosity ratio of 10 ($\mu_o = 10$, $\mu_w = 1$), and Buckley–Leverett analytical solution used for testing the Riemann approach. The mobility ratio at the shock front is $M_{\text{shock}} = 1.36$.*

---

regular increments of dimensionless time. From each velocity field, the corresponding streamtubes were then constructed and used to find the saturation profiles by mapping a Riemann solution along the streamtubes for that particular time. The saturation profiles obtained by this method were then compared to the saturation profiles obtained by the direct Riemann approach.

The one–dimensional solution used to test the Riemann approach is shown in Fig. 5.1. Although the end-point mobility ratio is 10, the shock–front mobility ratio is, in fact, only 1.36, resulting in a more stable displacement than suggested by the end-point value alone. As was mentioned previously, this is generally true for many waterfloods with 'reasonable' relative permeability curves: the frontal mobility ratio is of order 1 even though the end-point can be of order 10 or 100 leading to a weak nonlinearity in the total velocity. The absolute permeability field used in the numerical experiment is shown in Fig. 5.2, and was derived from the finer 250x100 field used in Chapter 4 by a simple geometric averaging of 2x2 blocks.

As demonstrated in Fig. 5.3, the Riemann approach agrees well with the mixed

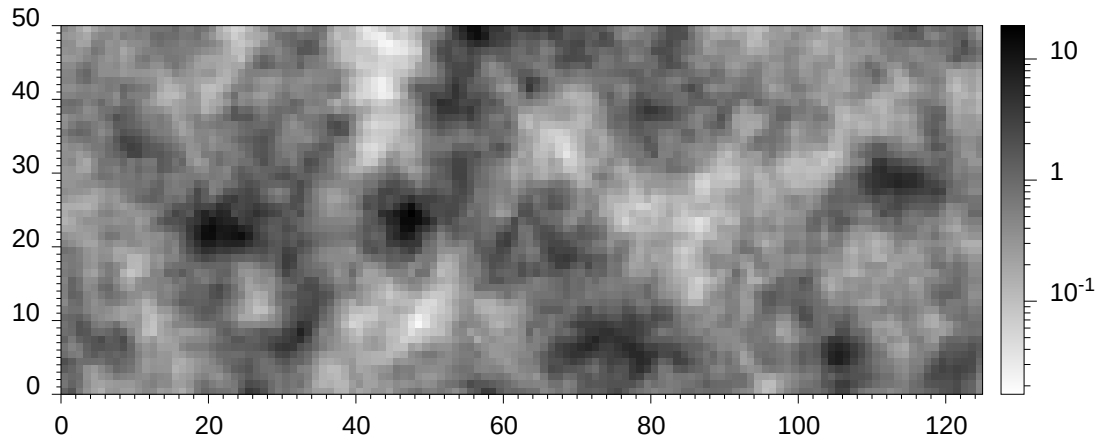

Figure 5.2: *Permeability map with logarithmic scaling – (125x50 Grid).*

method (Eclipse velocity field + Riemann approach). Both solutions are seen to be devoid of numerical diffusion compared to the saturation profiles obtained directly from Eclipse. Figure 5.3 displays example solutions at $t_D = 0.2$ and $t_D = 0.4$. The upper row shows saturation maps obtained directly from Eclipse; the middle row shows maps obtained using the velocity from Eclipse, but mapping the solution using the Riemann approach; and the last row shows profiles obtained by using the Riemann approach only.

A direct comparison of saturation maps (Fig. 5.3) as well as the integrated response (Fig. 5.4) demonstrate that the difference between the two methods (Eclipse velocity field + Riemann approach and direct Riemann approach) is indeed small and the nonlinearity of the velocity field is captured accurately by the direct Riemann approach. In fact, it is interesting to note that numerical diffusion causes a larger difference in recovery between the two methods than the approximation introduced by the Riemann approach. This conclusion can be drawn from the fact that the velocity fields for the two recovery curves are identical and therefore the difference must be attributed to numerical diffusion. That numerical diffusion has the upper hand in the Eclipse solution is also suggested by the comparison of the saturation histories shown in Fig. 5.5. This numerical experiment indicates that the error in the velocity

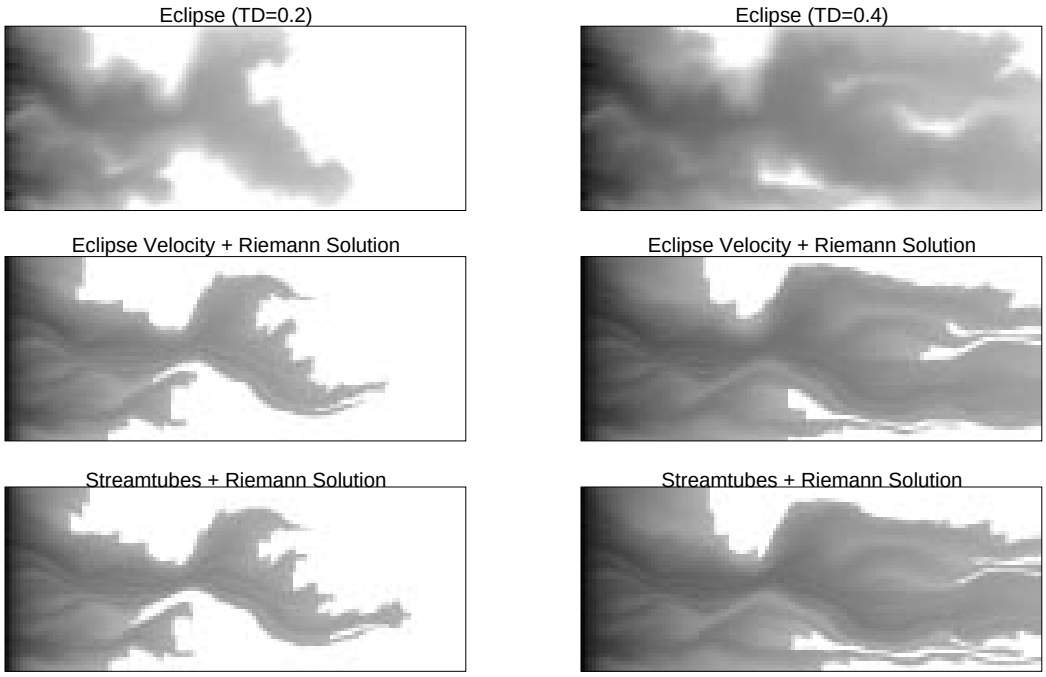

Figure 5.3: *Saturation maps at times $t_D = 0.2$ and $t_D = 0.4$. From top to bottom: profiles obtained directly from Eclipse; profiles obtained by using the velocity field from Eclipse but mapping a Riemann solution along streamtubes; profiles obtained by the method proposed in this thesis.*

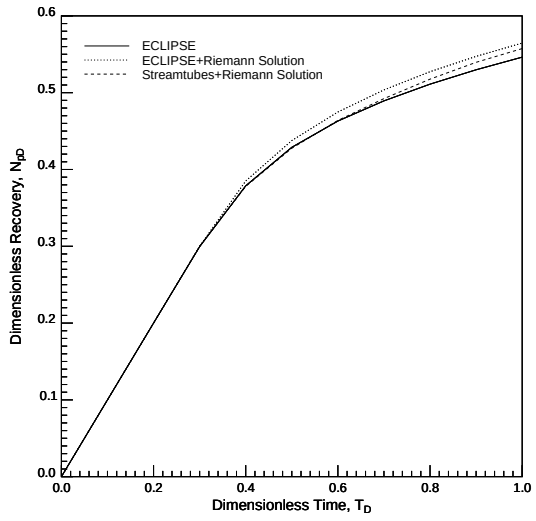

Figure 5.4: *Recovery curves for the three different solution methods used to generate the profiles in Fig. 5.3.*

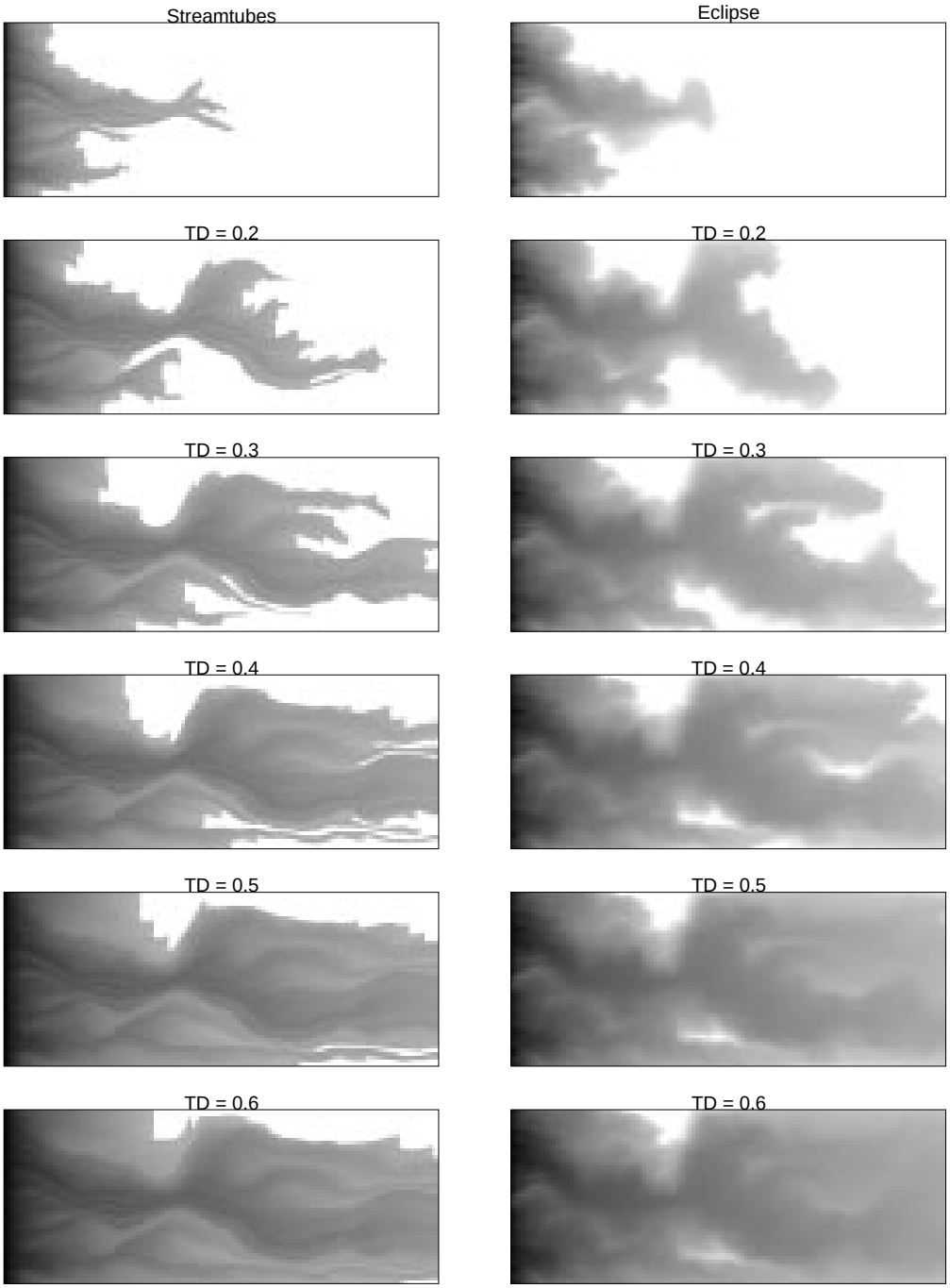

Figure 5.5: *Displacement history at $\Delta t_D = 0.1$ intervals for a Buckley–Leverett problem with a fractional flow function given by Fig. 5.1*

field caused by the Riemann approach is indeed small compared to traditional finite difference solutions. In particular, numerical diffusion is shown to cause larger errors than the assumption used in the Riemann approach.

5.4 Convergence of the Riemann Approach

Before using the Riemann approach to investigate other immiscible cases, the issue of convergence is addressed in this section. In other words, at what rate must the streamtubes be recalculated in order to consider the solution converged? If the two-phase immiscible problem is indeed weakly nonlinear, then it may require fewer updatings of the pressure (or Ψ–field) than currently used in finite difference simulators which would lead to a substantial speed-up. Finite difference simulators use a CFL-type (*Courant et al. 1928, LeVeque 1992*) stability criterion for the discretized hyperbolic conservation equation to determine when to resolve for the pressure field. Strictly speaking, this is not necessary. The CFL-condition simply states that the domain of dependence of the finite difference method must include the domain of dependence of the hyperbolic conservation equation (*LeVeque 1992*), but says nothing about the elliptic pressure equation. Solving for the pressure field at every time step required by the CFL condition may be 'overkilling' the problem in order to be on the safe side, but obviously carries an enormous cost in terms of computer time.

In the streamtube approach the conservation equation is not discretized and therefore there is no CFL condition to worry about. The question of how many times the streamtubes must be updated to consider the solution converged arises naturally and is addressed by solving the previous problem repeatedly with an increasing number of streamtube updates. Recovery curves for 1, 10, 20, 40, and 100 streamtube updates are shown in Fig. 5.6. It is rather surprising to find that 20 solves are sufficient to consider the problem converged over a range of two pore volumes. With only 20 solves, the new approach represents a reduction in computation time by two orders of magnitude compared to the thousands of solves needed by a traditional finite difference simulator like Eclipse. For this particular problem ($M_{\text{end}} = 10$), Eclipse required 1600 solves which translates into a speed-up of 8000% .

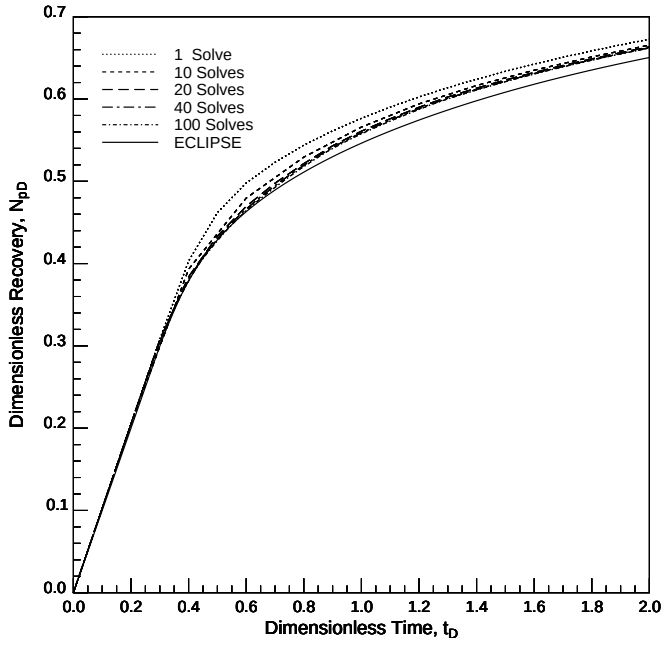

Figure 5.6: *Recovery curves for 1, 10, 20, 40, and 100 streamtube updates over two pore volumes injected ($t_D = 2$) showing that the problem can be considered converged if more than 20 updates are used.*

5.5 Other Immiscible Solutions

This section considers other immiscible cases intended to verify the streamtube approach further as well as to use it to gain some physical insight into two–phase displacements. Although several parameters affect the displacement efficiency of an immiscible displacement, only two parameters are investigated here: (a) the end-point mobility ratio and (b) reservoir heterogeneity. Except where noted, the relative permeabilities are assumed fixed and given by $k_{rw} = S_w^2$, $k_{ro} = S_o^2$.

5.5.1 End-Point Mobility Ratio

The end-point mobility is defined as

$$M_{\text{end}} = \frac{\lambda_J}{\lambda_I} = \left(\frac{k_r}{\mu}\right)_J \left(\frac{\mu}{k_r}\right)_I \quad , \tag{5.8}$$

where the subscripts I and J refer to initial and injected conditions respectively. For the relative permeabilities used here, $k_{r_I} = k_{r_J} = 1$, and the end-point mobility ratio is simply given by the viscosity ratio,

$$M_{\text{end}} = \frac{\mu_o}{\mu_w} \quad . \tag{5.9}$$

Figures 5.7 and 5.8 show that the end-point mobility ratio only affects the rate of convergence, with the $M_{end} = 1$ case requiring one solve, $M_{end} = 3$ less than ten, $M_{end} = 5$ approximately ten, and the $M_{end} = 10$ case twenty solves as. The converged recovery curves all compare in the same manner with the recovery curves obtained from Eclipse (Fig. 5.8) due to numerical diffusion in the Eclipse solution. A more surprising result though is that Eclipse consistently underestimates recovery compared to the streamtube solutions — surprising because it is usually assumed that numerical diffusion increases recovery by mitigating viscous instability, thereby reducing viscous fingering and early breakthrough.

A possible reason for this is that numerical diffusion in the Eclipse solution smears the shock front and reduces its effectiveness in recovering the oil ahead of it. The streamtube solution, on the other hand, maintains the piston-like recovery mechanism by mapping an analytical solution and therefore predicts a higher oil recovery from the reservoir. The true physical answer may lie somewhere between the two, but these results are significant because the effects of numerical diffusion on recovery become quantifiable through the streamtube approach.

Another example is shown in Fig. 5.9. For this case, the end-point relative permeability of the oil phase is $k_{ro}|_{\text{S}_o=1} = 0.25$. Keeping the same exponents as before and assuming an oil-to-water viscosity ratio of ten ($\mu_o = 10, \mu_w = 1$) leads to an end-point mobility ratio of $M_{\text{end}} = 40$. Even in this case, as the recovery curves in Fig. 5.10 demonstrate, the streamtube method is able to capture the nonlinearity with only 20 updates.

5.5.2 Reservoir Heterogeneity

To study the impact of reservoir heterogeneity on recovery, the $M_{end} = 10$ one-dimensional solution of Fig. 5.1 was used to find recoveries up to two pore volumes

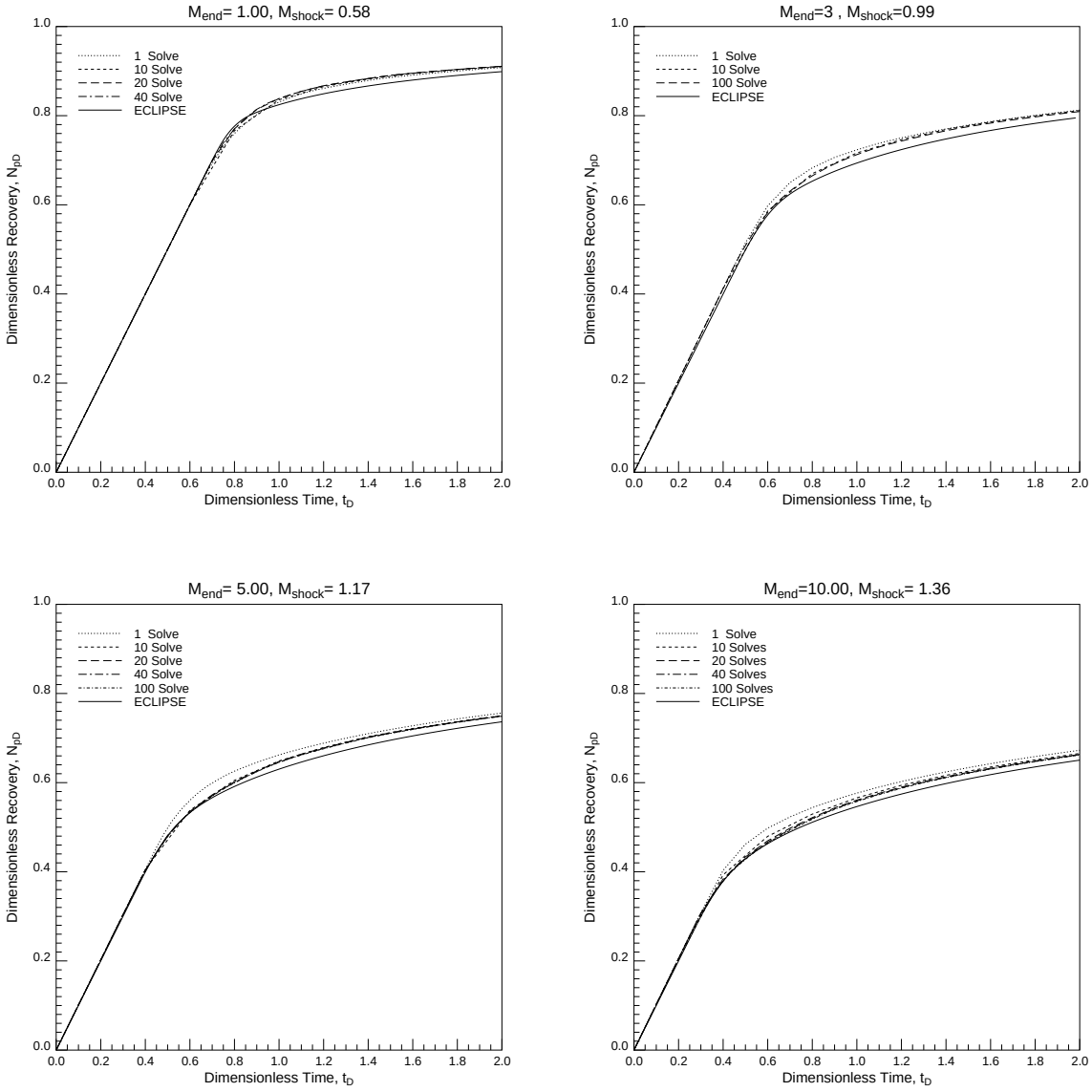

Figure 5.7: *Recovery curves for for M=1, 3, 5, and 10 showing convergence of the streamtube approach and comparison with recovery curves obtained from Eclipse. The permeability field is shown in Fig. 5.2.*

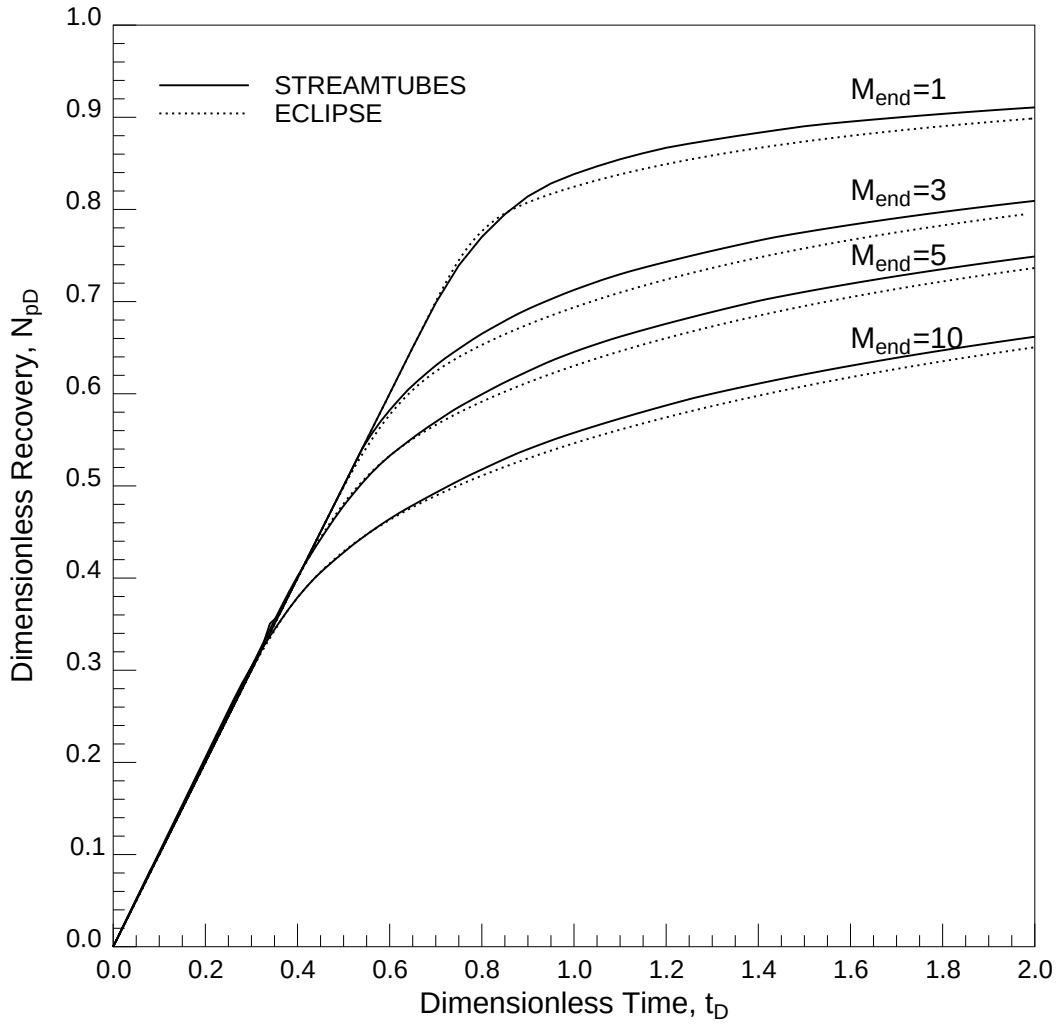

Figure 5.8: *Summary of converged recovery curves.*

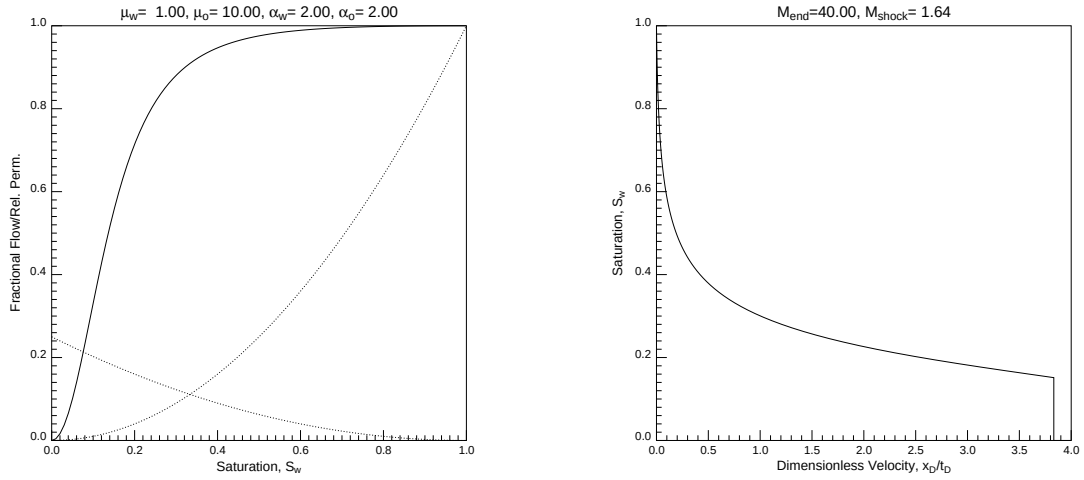

Figure 5.9: *Relative permeabilities, fractional flow, and one-dimensional saturation profile for* $M_{\text{end}} = 40$. *The shock-front mobility ratio is* $M_{\text{shock}} = 1.64$. ($k_{rw} = S_w^2,\ k_{ro} = 0.25,\ S_o^2,\ \mu_o = 10,\ \mu_w = 1$).

injected for the three permeability fields shown in Fig. 5.11. All three permeability fields are log-normally distributed, have four orders of magnitude variation in absolute permeability and differ only in their correlation lengths. Although there are several parameters to 'quantify' reservoir heterogeneity, the heterogeneity index (HI), which originated from the work of *Gelhar and Axness* (1983) and has been used by other authors since (*Mishra 1987, Araktingi and Orr 1993, Sorbie et al. 1992*), is used here. The heterogeneity index is given by

$$HI = \sigma^2_{\ln k} \lambda_c \quad , \tag{5.10}$$

where $\sigma^2_{\ln k}$ is the variance of the $\ln k$–field and λ_c is the correlation length in the x–direction. The higher HI, the 'more' heterogeneous the system is said to be.

The heterogeneity index is an attractive parameter because it combines information about the variability of the permeability field ($\sigma^2_{\ln k}$) with information about the correlation structure of the heterogeneity (λ_c). The traditional Dykstra–Parson coefficient can be recovered from HI by recalling that

$$\sigma_{\ln k} = -\ln(1 - V_{DP}) \quad . \tag{5.11}$$

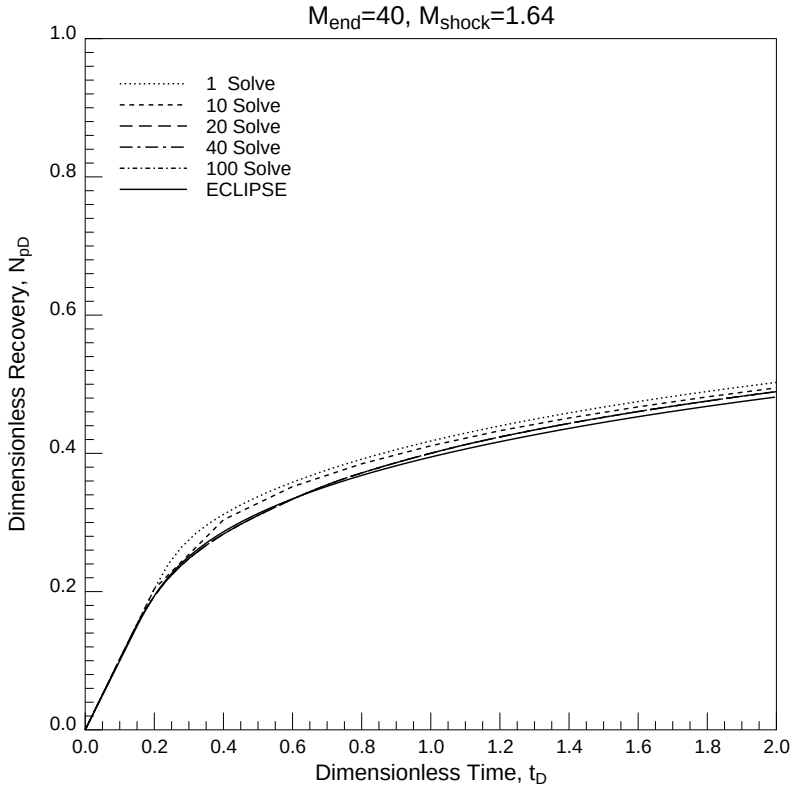

Figure 5.10: *Recovery curves for the data shown in Fig. 5.9.*

The streamtube method is able to give some valuable insight that may have not been as easily observable using a standard finite difference simulator. The recovery curves of Fig. 5.12, for example, suggest that the influence of the nonlinearity in the velocity field on recovery will depend on reservoir heterogeneity. Permeability fields with very short correlation lengths tend to mitigate the nonlinearity (see the case with $\lambda_c = 0.02$) requiring only a few solves to converge, while longer correlation lengths allow for stronger nonlinear behavior (see case with $\lambda_c = 0.6$) requiring more solves.

In reservoirs with short correlation lengths, the nonlinearity is not noticeable in the geometry of the streamtubes. The streamtubes expand and contract many times over the duration of the displacement but end–up, on average, to behave like streamtubes from the tracer case. Thus, the recovery curves can be found by simply solving for the streamtubes once and mapping the appropriate Buckley-Leverett solution, as Fig. 5.12 clearly shows.

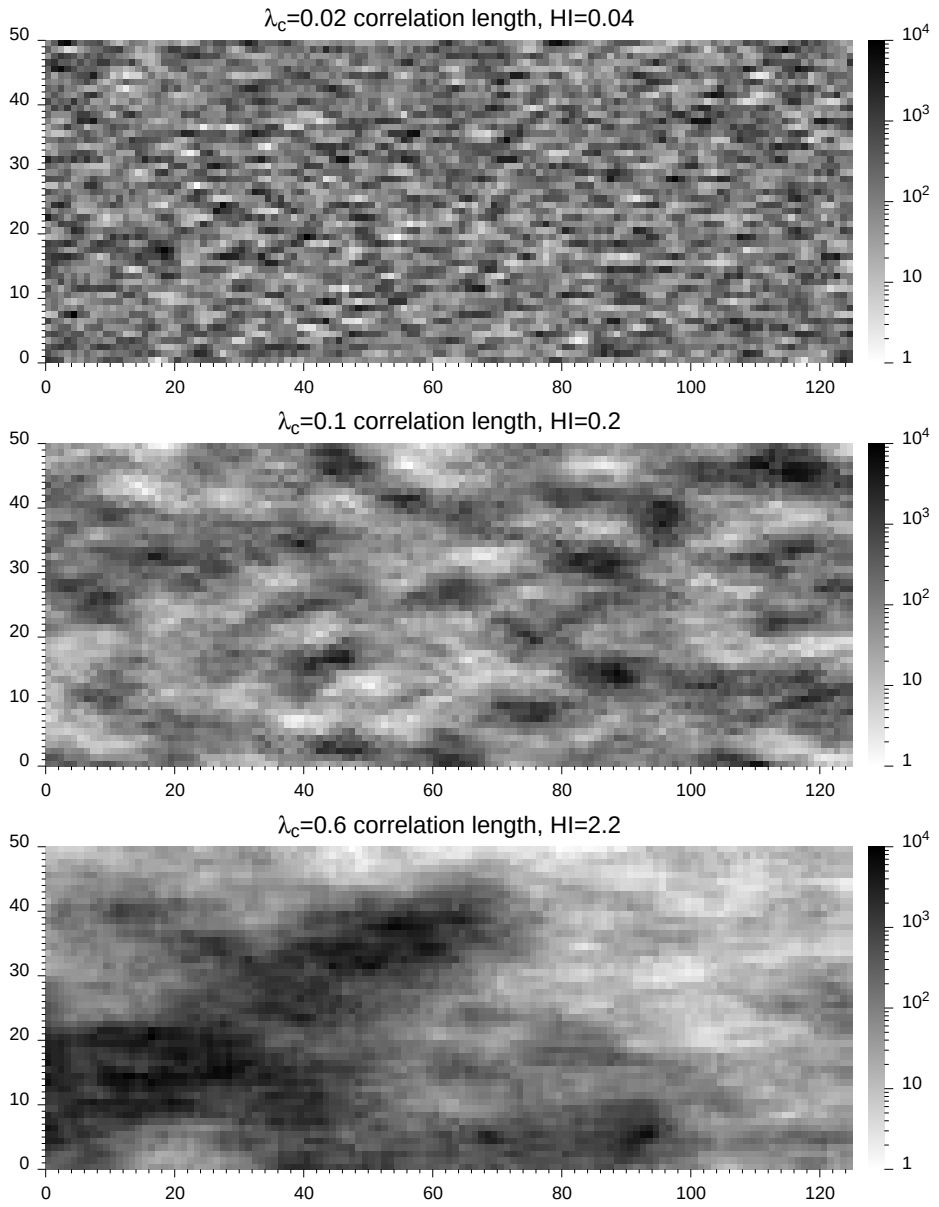

Figure 5.11: *Permeability fields differing only in correlation length. Correlation lengths from top to bottom: 0.02 (HI=0.04), 0.1 (HI=0.2), and 0.6 (HI=2.2). The grid size is 125x50.*

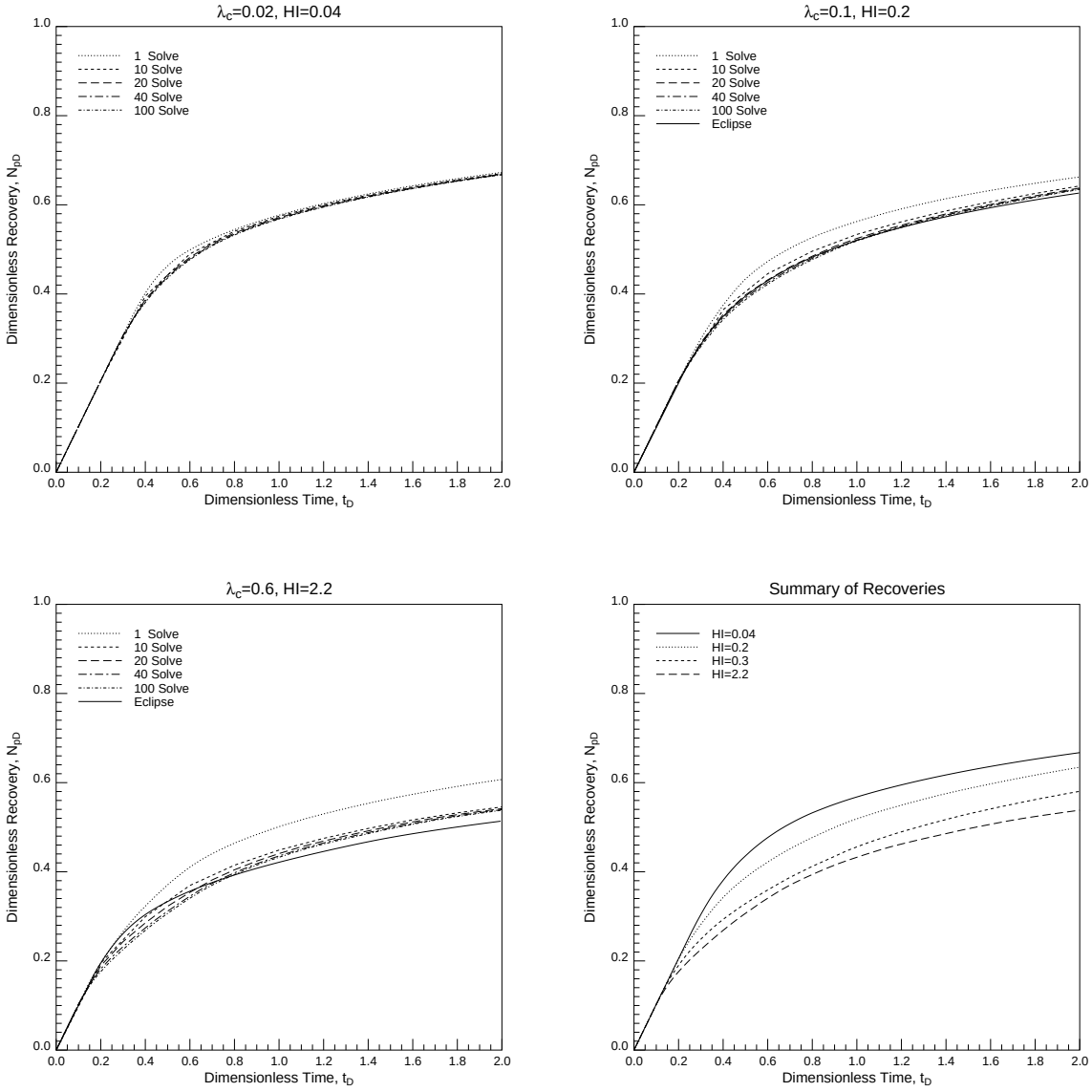

Figure 5.12: *Recovery curves for permeability fields of Fig. 5.11 showing convergence of the streamtube approach and comparison with recovery curves obtained from Eclipse.*

As the correlation length increases the nonlinearity becomes more noticeable, and for the extreme case of $\lambda_c = 0.6$, 40 updates are necessary to converge onto the solution. Well defined flow paths of least resistance between the inlet and outlet now exist, and a dominant flow channel is created, leading to early breakthrough. The nonlinearity of the problem is accentuated because the injected phase increases its total velocity along the easy flow path until it reaches the outlet end. To capture this continuous increase in total velocity requires more updates of the streamtubes compared to the shorter correlation length cases. 'More', in this case, is to be understood within the context of streamtubes, but still compares very favorably to the many solves required by a traditional finite difference simulator. That the $\lambda_c = 0.6$ case leads to a much stronger nonlinearity in the flow field is also suggested by a noticeable difference between the streamtube and the Eclipse solution.

To study further how the nonlinearity in the velocity field interacts with reservoir heterogeneity, 30 geostatistical realizations, twelve of which are shown in Fig. 5.13, having identical statistics ($\lambda_c = 0.2, HI = 0.2$, and 3 order of magnitude in k) were generated. Example saturation maps at $t_D = 0.3$ for the twelve permeability field are shown in Fig. 5.14. Similarly, 30 other permeability fields with identical statistics ($\lambda_c = 0.4, HI = 0.88$, and 4 orders of magnitude in k) were produced with example permeability fields and saturation maps given by Fig. 5.15 and Fig. 5.16. Although the saturation maps give an indication of the nonlinearity present in both cases, the story is best told using the recovery curves shown in Fig. 5.17 and Fig. 5.18. The 60 recovery curves (there are 30 for each case) suggest that nonlinearity and reservoir heterogeneity interact to give an increasing spread in recovery with increasing reservoir heterogeneity. In other words, it is generally not correct to state that increasing reservoir heterogeneity will always lower recovery. A more accurate statement is that the probability that recovery will fall in a desired interval (that may be specified by economic considerations, for example) decreases with increasing heterogeneity and nonlinearity. It is interesting to note that the spread in recoveries for $HI = 0.2$ is almost contained within the larger spread of recoveries for $HI = 0.88$. It is therefore entirely possible that a given realization with $HI = 0.2$ ('low heterogeneity') can return a lower recovery than a realization with $HI = 0.88$ ('high heterogeneity').

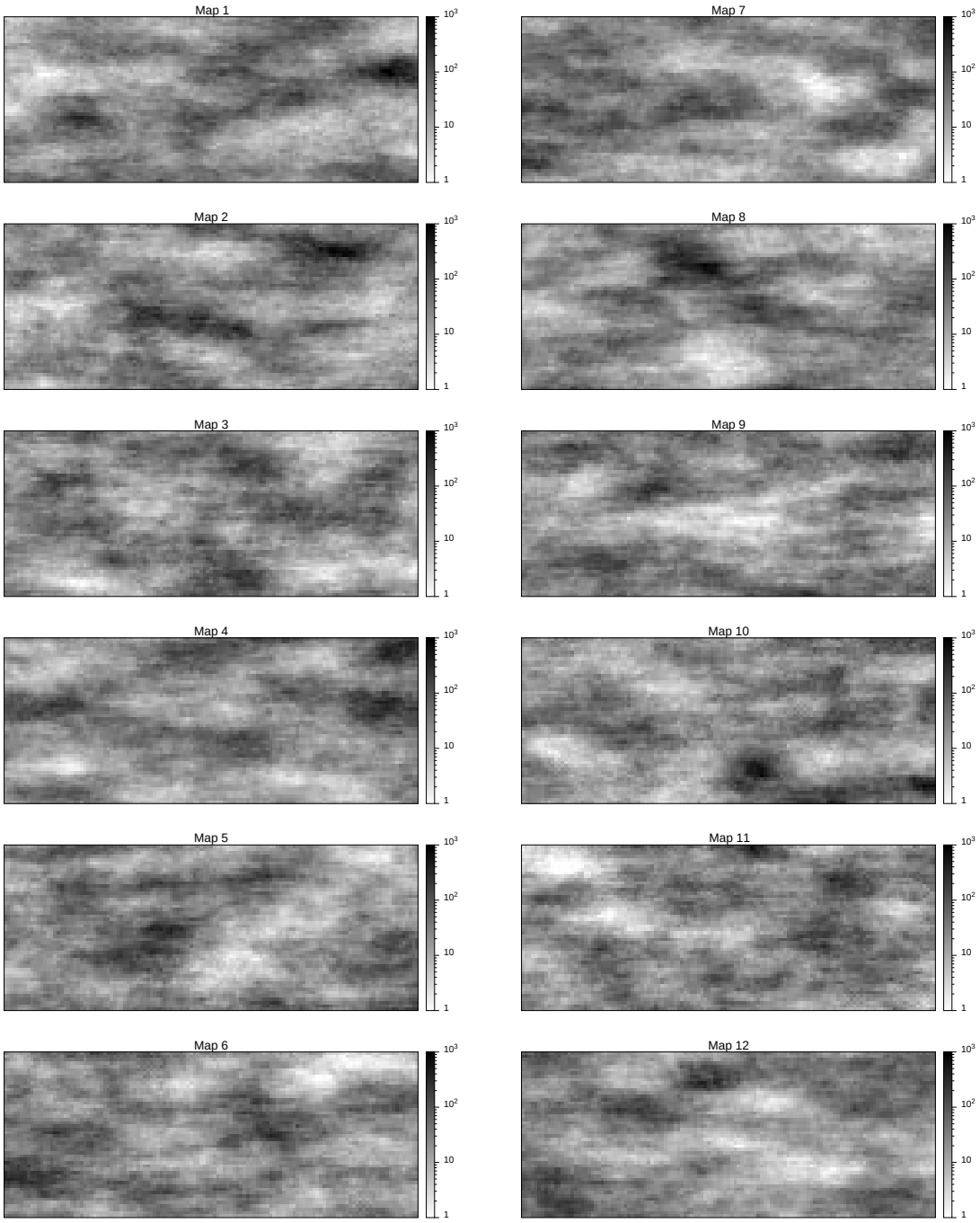

Figure 5.13: *Twelve permeability fields having identical statistics:* $\lambda_c = 0.2, HI = 0.2$, *and three orders of magnitude variation in absolute permeability.*

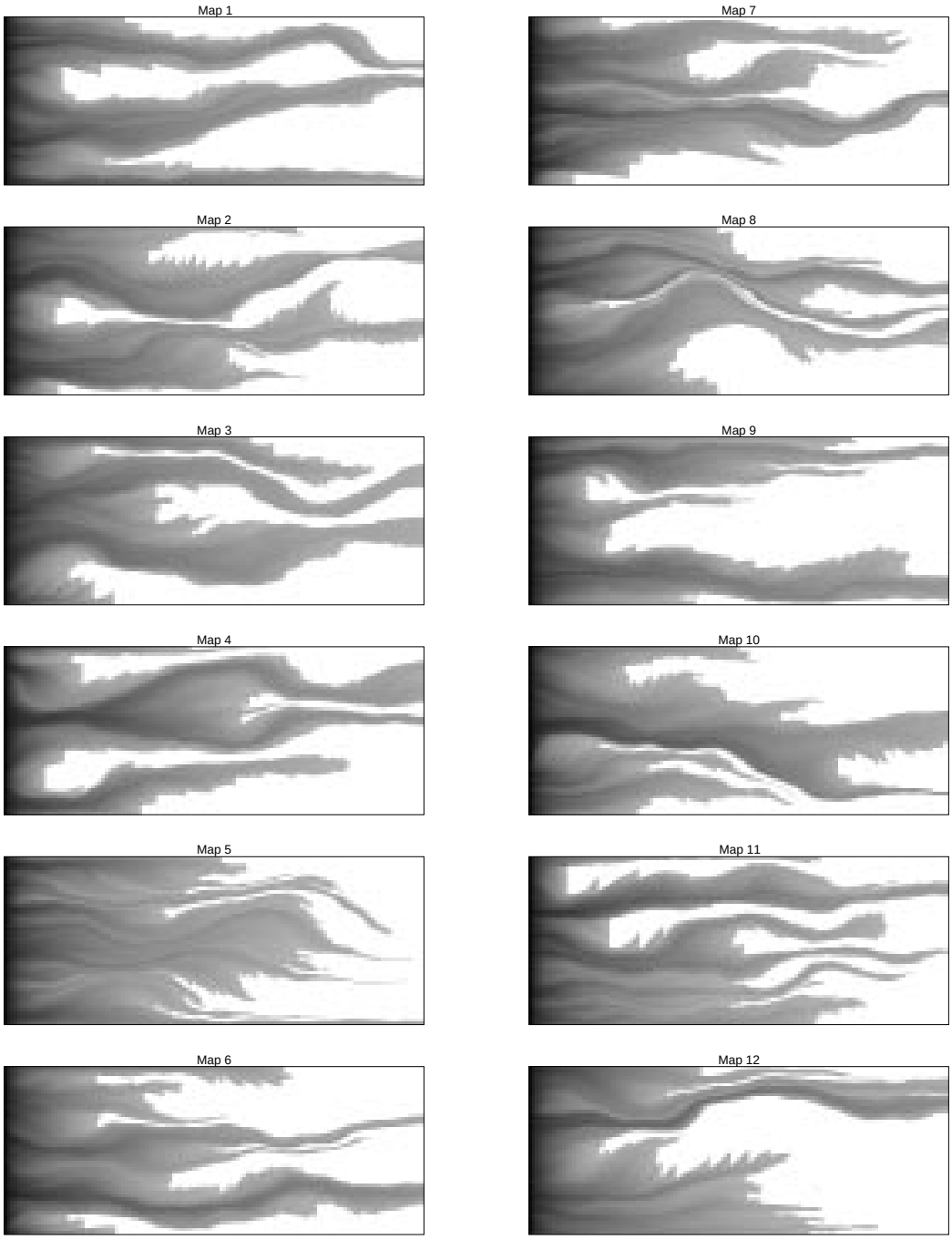

Figure 5.14: *Saturation profiles at $t_D = 0.3$ for each permeability map shown in Fig. 5.13.*

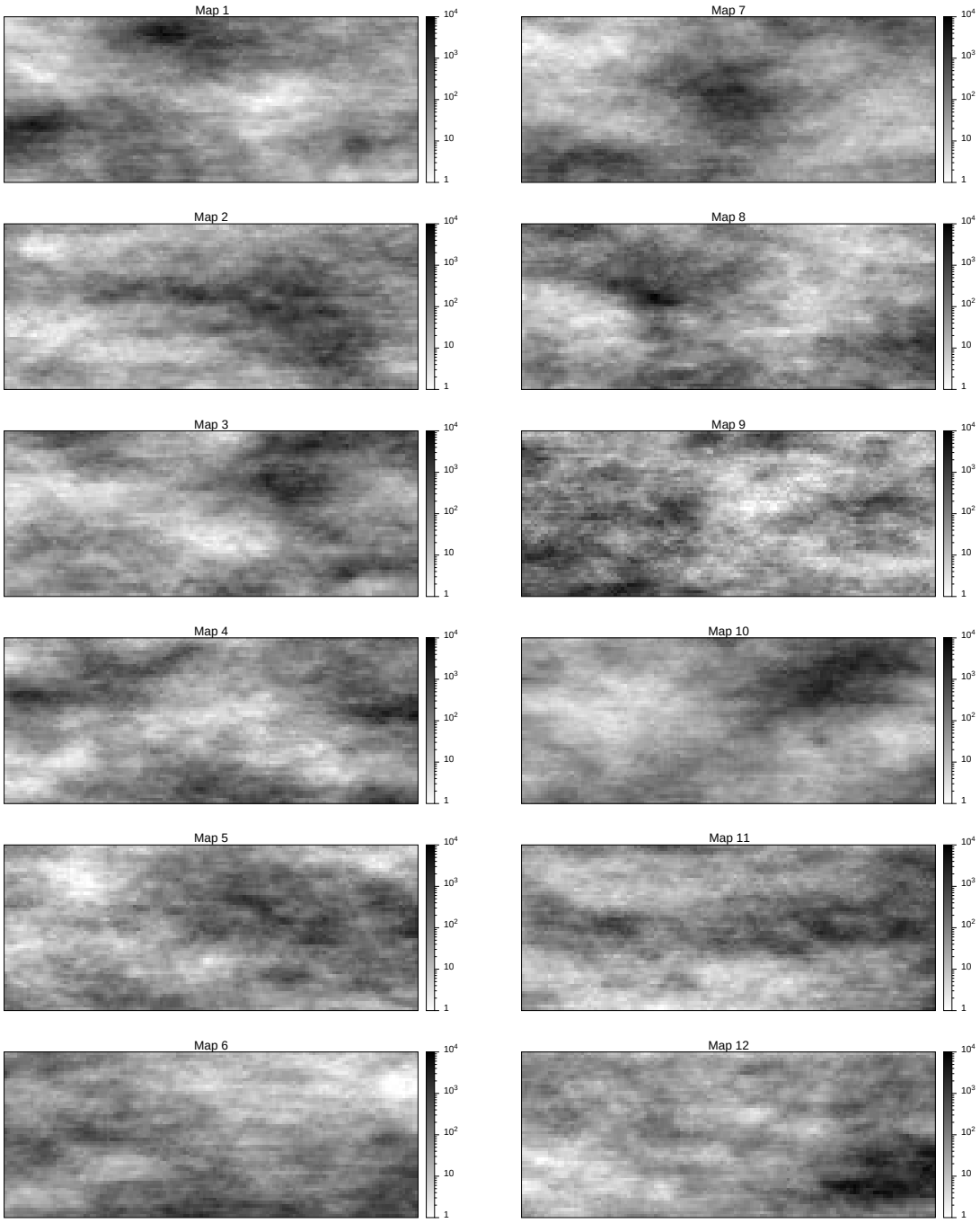

Figure 5.15: *Twelve permeability fields having identical statistics:* $\lambda_c = 0.4, HI = 0.88$*, and four orders of magnitude variation in absolute permeability.*

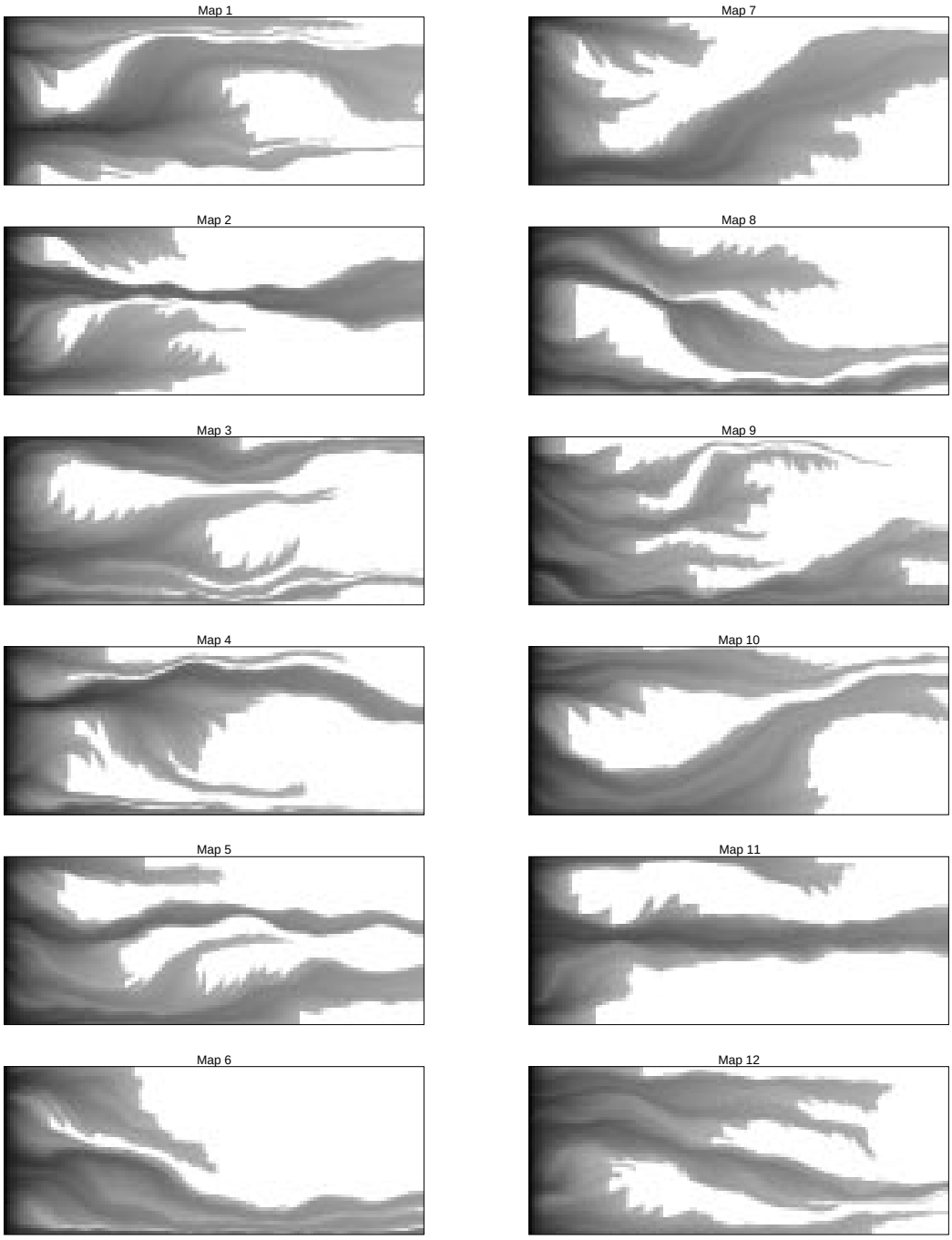

Figure 5.16: *Saturation profiles at $t_D = 0.3$ for each permeability map shown in Fig. 5.15.*

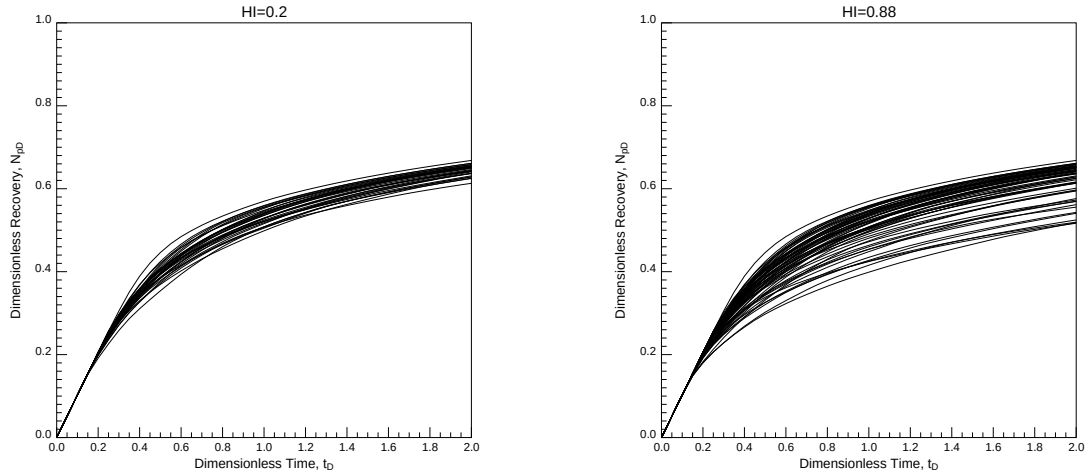

Figure 5.17: *Range of recovery curves for 30 permeability fields with* $\lambda_c = 0.2, HI = 0.2$*, and three orders of magnitude variation in absolute permeability (left) and 30 permeability fields with* $\lambda_c = 0.4, HI = 0.88$*, and four orders of magnitude variation in absolute permeability (right).*

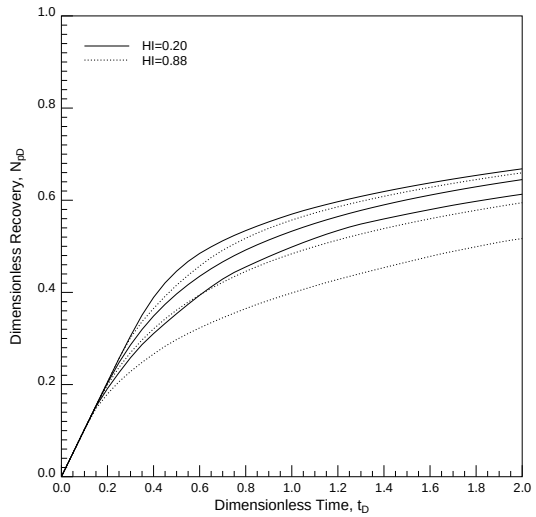

Figure 5.18: *Summary of recovery range for the above cases: minimum, maximum, and average recoveries for* $HI = 0.2$ *and* $HI = 0.88$.

These results suggest that the interaction of nonlinearity and reservoir heterogeneity can be quantified as a probability on recovery or spread in recoveries. In order to determine such probabilities, nonlinear displacements using multiple realizations of the same field must be possible in a reasonable amount of computation time. The streamtube method combined with a one-dimensional Riemann approach is a very quick and accurate alternative to traditional reservoir simulation approaches and therefore offers a way to evaluate the recovery probabilities statistically for a given end-point mobility ratio and heterogeneity structure.

5.6 The Higgins and Leighton Method

The streamtube approach originally proposed by Higgins and Leighton (*1962a, 1962b, 1964*), and subsequently used by many investigators[6], centers on capturing the nonlinear behavior of the displacement by keeping the streamtube fixed but allocating the total flow into each streamtube in proportion to the total flow resistance along each streamtube. For areal problems, the Higgins and Leighton method has been shown to give good approximation of recovery for both, homogeneous domains (*Doyle and Wurl 1971, Martin and Wegner 1971*) and heterogeneous domains (*Emanuel et al. 1989, Mathews et al. 1989*). The total resistance along a streamtube i is given by

$$R_i = \int_0^S \frac{d\zeta}{A(\zeta)\lambda_t(\zeta)} \quad , \tag{5.12}$$

where ζ is a length coordinate along a streamtube (i.e. the center streamline in a streamtube), S is the total length of each streamtube[7], $A(\zeta)$ is the cross-sectional area along the streamtube, and λ_t is the total mobility. The flow is then allocated in proportion to (*Hewett and Behrens, 1991*)

$$\frac{R_T}{R_i} \quad , \tag{5.13}$$

[6]See Chapter 2: Literature Review

[7]Not to be confused with x_D, the dimensionless pore volume coordinate along a streamtube defined by the Eq. 3.27

where R_T is given by

$$\frac{1}{R_T} = \sum_{i=1}^{N_S} \frac{1}{R_i} \quad . \tag{5.14}$$

Unlike finding the pore volume along a streamtube using Eq. 3.34, which is all that is required to map one-dimensional Riemann solutions along periodically changing streamtubes (see Section 3.7) and is easily found, evaluating the integral in Eq. 5.12 is more difficult. The reason is that to calculate R_i the product $A(\zeta)K(\zeta)$, where $K(\zeta)$ is the absolute permeability, must be determined along ζ. For a general heterogeneous domain, in which the permeability field is specified by K_x and K_y components on a regular cartesian grid, finding the directional permeability $K(\zeta)$ becomes a nontrivial exercise. Furthermore, if the streamtube encompasses more than one grid block then $K(\zeta)$ should really be an average of the directional permeabilities along $A(\zeta)$. Finding the area, $A(\zeta)$, is easier than finding $K(\zeta)$, but must be approximated in the absence of isobars to trace across streamtubes, much in the same way as it has to be approximated when finding the pore volume. The difference though is that in finding the pore volume the error in A is only felt through the upper bound of the integral (Eq. 3.7.1), whereas in finding the total resistance the error is integrated over the entire length of the streamtube.

Fig. 5.19 compares recoveries for the Higgins and Leighton method to recoveries found using the streamtube approach proposed here as well as recoveries from Eclipse. Although the Higgins and Leighton method returns acceptable recoveries, the difficulty it has in capturing breakthrough time correctly with increasing mobility ratio suggests a weakness of the method in trying to model the nonlinear part of the displacement. The Higgins and Leighton method requires a single solve for the streamfunction and thus is clearly faster than the streamtube approach proposed here. But given that the streamtubes have to be updated at most twenty times over two pore volumes injected to capture the nonlinearity of the displacement, the small savings in computation time of the Higgins and Leighton method are probably not worth the loss of accuracy in recovery as well as the difficulties associated with finding R_i. The fact that the Higgins and Leighton method fails to predict breakthrough correctly as the mobility ratio of the displacement increases shows that the changing

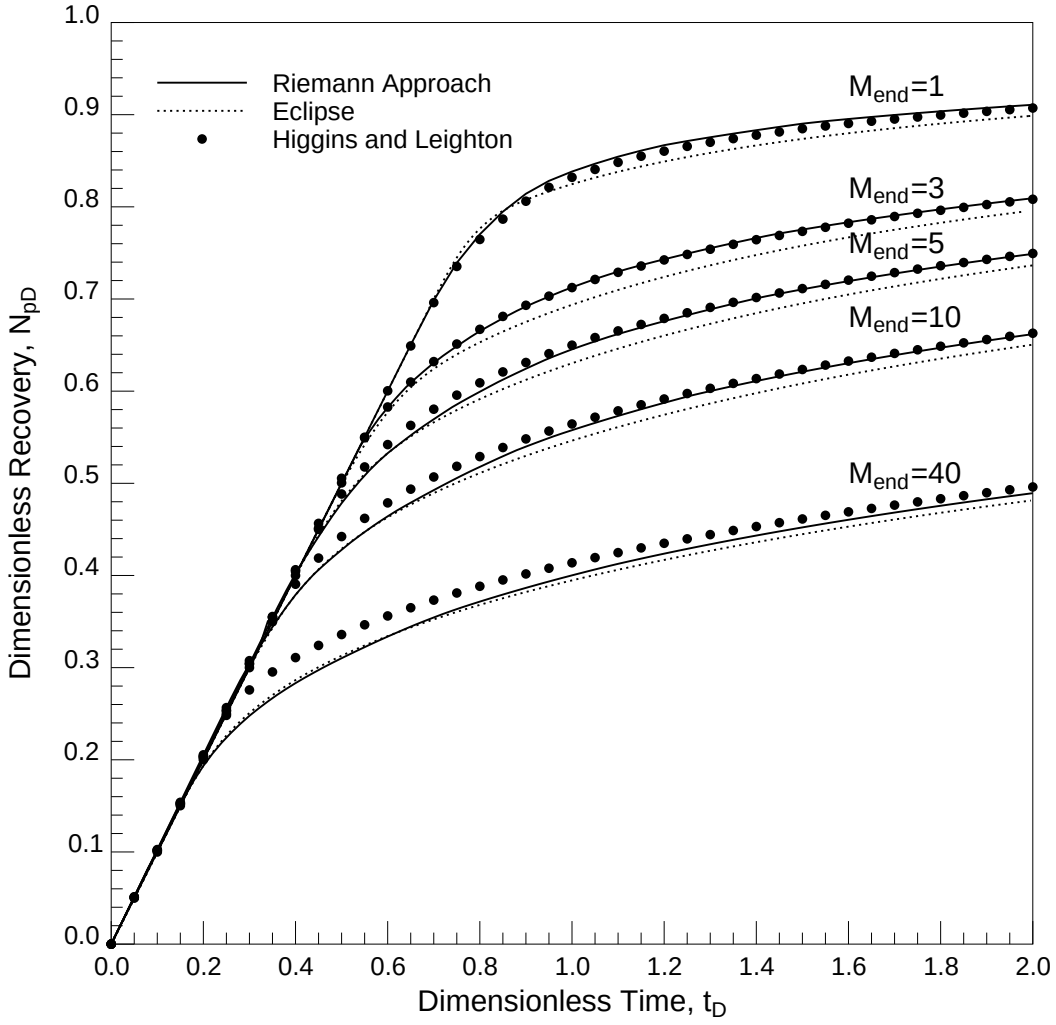

Figure 5.19: *Comparison of recovery curves found using the streamtube approach proposed here, Eclipse, and the Higgins and Leighton method. The Higgins and Leighton method keeps the streamtube fixed but allocates the flow in proportion to the total flow resistance along each streamtube.*

velocity can only roughly be approximated using a fixed streamtube/total resistance approach.

5.7 Concluding Remarks

In this chapter, the streamtube approach was extended to model two–phase, immiscible displacements. To account for the changing total velocity field, the streamtubes were updated periodically. The one–dimensional Buckley–Leverett solution was then mapped along the new streamtubes as a true Riemann solution. The key result of this chapter is to demonstrate that the error caused by the Riemann approach used for mapping a one–dimensional solution along periodically updated streamtubes is small and, in fact, is less significant than the error introduced by numerical diffusion in finite difference solutions. Another key result is that the weak nonlinearity of the total velocity field allows for converged solutions using at most 20 streamtube updates over two pore volumes. As a result, speed–ups by two orders of magnitude with respect to traditional finite difference solutions are achieved. The speed of the streamtube method is put to use in a statistical approach to reservoir forecasting, demonstrating that the spread in recovery due to equiprobable permeability fields can be substantial. The spread in recovery is particularly important, because it suggests that the error caused by the numerical scheme itself may be small compared to the uncertainty introduced by the statistics of the reservoir description. Finally, the streamtube approach proposed here was also compared to the Higgins and Leighton method, demonstrating that the nonlinear part of the flow problem cannot be accounted for by using a fixed streamtube/total resistance approach. In the next chapter, the streamtube approach is extended to ideal miscible displacements.

Chapter 6

First-Contact Miscible Displacements

This chapter applies the streamtube approach to modeling first contact miscible (FCM) displacements through heterogeneous reservoirs. Three one-dimensional solutions are presented that may be combined with streamtubes to construct two-dimensional solutions for heterogeneous systems: (1) a piston-like, unit wave velocity solution, (2) a convection-diffusion solution, and (3) a viscous fingering solution. The displacement scale implied by each of these three one-dimensional solutions is discussed. The resulting two-dimensional streamtube solutions are shown to capture overall recovery and first-order displacement features seen in traditional finite difference solutions. The superior speed of the streamtube solution is put to use in a statistical approach to reservoir forecasting: recovery curves for 180 permeability fields are used to demonstrate how nonlinearity in the total velocity field and heterogeneity interact to determine overall recovery.

6.1 Introduction

First-contact miscible (FCM) displacements[1] in heterogeneous systems have been studied by several authors (*Araktingi and Orr, 1993, Gorell 1992, Sorbie et al. 1992,*

[1]Sometimes also referred to as ideal miscible displacements.

Waggoner et al. 1992, Christie 1989). An extensive treatment of the subject was recently given by *Tchelepi* (1994). The strong interest in first-contact miscible displacements is motivated principally by the possibility of learning more about displacements which are near-miscible, such as gas and carbon-dioxide flooding. The assumptions used in first-contact miscible flow isolate the convective part of the displacement problem from any phase behavior considerations and allow a study of the interaction of reservoir heterogeneity and the nonlinearity of the total velocity field in determining sweep efficiency. But the absence of any phase behavior and multiphase flow aspects enhances the nonlinearity of the problem. Diffusive mechanisms, such as molecular diffusion and pore scale mixing, are the only physical mechanisms available to mitigate the original mobility contrast. As a result, first-contact miscible displacements are very challenging to simulate numerically and are far more difficult than the two-phase immiscible problem discussed in Chapter 5. High mobility contrasts lead to extreme velocity variations and sufficient grid blocks must be used to ensure that numerical diffusion is as close as possible to representing true physical diffusion at the grid block scale. To find physically meaningful simulations of first-contact miscible displacements require substantial computer resources (*Tchelepi 1994, Christie and Bond 1987*).

6.2 The Assumptions in FCM Flow

The assumptions for first-contact miscible flow are analogous to the assumptions used to derive the tracer solution presented in Chapter 4. The general material balance formulation for a component i with no chemical reactions and adsorption/desorption given by (*Lake 1989, p. 29*) is

$$\frac{\partial}{\partial t}\left(\phi \sum_{j=1}^{N_P} \rho_j S_j \omega_{ij}\right) + \nabla \cdot \left(\sum_{j=1}^{N_P} \rho_j \omega_{ij} \vec{u}_j - \phi S_j \rho_j \vec{\vec{K}}_{ij} \cdot \nabla \omega_{ij}\right) = 0, \qquad (6.1)$$

and assuming (a) single-phase flow, (b) incompressible fluid and rock properties, (c) constant phase density, and (d) ideal mixing gives

$$\phi \frac{\partial C_i}{\partial t} + \nabla \cdot \left(C_i \vec{u} - \phi \vec{\vec{K}}_i \cdot \nabla C_i\right) = 0 \ . \qquad (6.2)$$

Expanding the divergence term in Eq. 6.2 and applying continuity ($\nabla \cdot \vec{u} = 0$) gives the governing equation for miscible displacements as

$$\phi \frac{\partial C_i}{\partial t} + \vec{u} \cdot \nabla C_i - \phi \nabla \cdot \left(\vec{\vec{K}}_i \cdot \nabla C_i \right) \quad = 0 \quad . \tag{6.3}$$

Eq. 6.3 is identical to the tracer formulation. The difference is hidden in the Darcy velocity $\vec{u}$ which is now given by

$$\vec{u} = \frac{\vec{\vec{k}}}{\mu(C)} \cdot \nabla P \quad , \tag{6.4}$$

where the viscosity μ is assumed a function of concentration C. A quarter power mixing rule, given by

$$\mu(C) = \left(\frac{C}{\mu_s^{1/4}} + \frac{1 - C}{\mu_o^{1/4}} \right)^{-4} \quad , \tag{6.5}$$

is usually used as a functional relationship between μ and C. μ_s is the 'solvent' viscosity and μ_o is the 'oil' viscosity, which are simply the viscosities at $C = 1$ and $C = 0$ respectively, and also define the end-point mobility ratio as

$$M = \frac{\mu_o}{\mu_s} \quad . \tag{6.6}$$

Eq. 6.3 is the starting PDE for all first-contact miscible unstable displacements. The 'strength' of the nonlinearity in the flow field will depend on the coupling between Eq. 6.3 and Eq. 6.4 through the mixture viscosity, $\mu(C)$, and the relative magnitude of the convective term ($\vec{u} \cdot \nabla C_i$) to the diffusive term ($\nabla \cdot \vec{\vec{K}}_i \cdot \nabla C_i$). If the diffusive term is large compared the convective term (small Peclet numbers), then instabilities will tend to be mitigated. Conversely, if the convective term dominates, then the displacement will see the growth of viscous fingers and/or strong channeling. It is therefore important to use a numerical scheme that will ensure a numerical diffusion term (which behaves much in the same way as physical diffusion) that is small — preferably on the order of the physical diffusion that is expected at the local grid block level— so as not to mask the true physics of the displacement.

6.3 The One-Dimensional Solution(s)

The use of streamtubes to model first-contact miscible displacements in heterogeneous systems requires a one-dimensional solution. For first-contact miscible flow, the governing one-dimensional PDE is easily derived from Eq. 6.3 as

$$\phi\frac{\partial C_i}{\partial t} + u\frac{\partial C_i}{\partial x} - \phi\frac{\partial}{\partial x}K_i\frac{\partial C_i}{\partial x} \quad = 0 \quad . \tag{6.7}$$

Using the usual definitions of dimensionless time, distance, and concentration assuming two components only, and a spatially constant K_i gives the familiar convection-diffusion equation

$$\frac{\partial C_D}{\partial t_D} + \frac{\partial C_D}{\partial x_D} = \frac{1}{N_{Pe}}\frac{\partial^2 C_D}{\partial x_D^2} \quad . \tag{6.8}$$

Eq. 6.8 is linear. The nonlinearity of the problem is accounted for by the coefficients in the governing PDE for the streamfunction that include the concentration-dependent viscosity

$$\frac{\partial}{\partial x}\left(\frac{\mu(C_D)}{k_y}\frac{\partial \Psi}{\partial x}\right) + \frac{\partial}{\partial y}\left(\frac{\mu(C_D)}{k_x}\frac{\partial \Psi}{\partial y}\right) = 0 \quad . \tag{6.9}$$

Thus, as the spatial concentration distribution changes, the coefficients of Eq. 6.9 change resulting in new streamtubes.

Unlike the two-phase immiscible problem, the first-contact miscible case has a subtle one-dimensional solution. For example, the no-diffusion form of Eq. 6.8 is given by

$$\frac{\partial C_D}{\partial t_D} + \frac{\partial C_D}{\partial x_D} = 0 \quad . \tag{6.10}$$

Eq. 6.10 is of hyperbolic type (*Zauderer 1989*) and can be solved using initial data of the type (Riemann conditions)

$$C_D(x_D, 0) \begin{cases} C_{Dl} & \text{for } x_D \leq 0 \\ C_{Dr} & \text{for } x_D \geq 0 \end{cases} \quad , \tag{6.11}$$

giving the well-known indifferent wave solution traveling at unit velocity (see Fig. 4.3). For favorable mobility ratios, the 'physical' solution is indeed a wave traveling at unit velocity, although the wave is no longer indifferent but self-sharpening. For unfavorable mobility ratios, on the other hand, the solution to Eq. 6.10 is misleading

because it still gives a piston-like displacement, when the system is in fact unstable. The problem, of course, is that the displacement model given by Eq. 6.10 is unable to distinguish between stable and unstable displacements since it is linear; by not having concentration dependent coefficients, the solution cannot account for any viscosity induced mobility contrast as a function of x_D and t_D. Furthermore, Eq. 6.10 has no characteristic length scale, resulting in a sharp, but unstable front at all length scales and for all times. A physically meaningful solution, on the other hand, would require some cut-off length scale across which the frontal instability is mitigated.

Adding a cut-off length scale can be done mathematically by retaining the second order diffusion term in Eq. 6.8. That implies that the cut-off length scale is now given by the diffusive length scale associated with N_{Pe}. It is important to note that Eq. 6.7, by its very derivation, has no way of modeling any other instability mitigation phenomena. In particular, there is no convective induced mixing beyond the pore scale that can be accounted for.

It is unlikely that at the field scale molecular diffusion and pore level mixing are first-order type physical processes that affect recovery. Convective mixing at the macroscale, such as viscous fingering and channeling are probably more important. To account for such phenomena in an averaged, one-dimensional sense, an analogy to two-phase flow was first proposed by *Koval* (1963). In the Koval model, straight line relative permeabilities and a quarter-power mixing rule are combined to define a flux function $f(C_D)$ that models convective mixing of the fluids. The governing PDE for Koval's model is[2]

$$\frac{\partial C_D}{\partial t_D} + \frac{\partial f(C_D)}{\partial x_D} = 0 \quad , \tag{6.12}$$

where $f(C_D)$ is given by

$$f(C_D) = \frac{1}{1 + \frac{1-C_D}{C_D}\frac{1}{M_{\text{eff}}}} \quad . \tag{6.13}$$

M_{eff} is the effective mobility ratio defined as

$$M_{\text{eff}} = \left(0.78 + 0.22 M^{1/4}\right)^4 \quad , \tag{6.14}$$

[2]Koval's original model also includes a heterogeneity factor H. This factor is set to $H = 1$ (homogeneous) for all Koval solutions presented in this dissertation, since the model is used only to capture viscous fingering in an averaged one-dimensional sense along streamtubes.

and $M = \mu_o/\mu_s$ is the usual definition of the mobility ratio.

A criticism of Koval's model is that he validated his model against experimental data by *Blackwell et al.* (1959), thereby lumping diffusive effects into the convective flux function. On the other hand, overall recovery from viscous fingering experiments has been shown to be remarkably insensitive to N_{pe}. In fact, Koval's method for homogeneous domains is surprisingly robust and has lead other investigators to propose similar models (*Dougherty 1963, Todd and Longstaff 1972, Fayers 1988*) .

For combining with streamtubes though, a better one-dimensional model to use is the Todd–Longstaff formulation. The Todd–Longstaff model includes Koval's model as a special case and is a single parameter function (not including M) given by

$$f(C_D) = \frac{1}{1 + \frac{1-C_D}{C_D}\left(\frac{1}{M}\right)^{1-\omega}} \quad . \tag{6.15}$$

By choosing ω as

$$\omega = 1 - 4\frac{\ln\left(0.78 + 0.22M^{1/4}\right)}{\ln M} \tag{6.16}$$

the Todd–Longstaff model is equivalent to Koval's model. Setting $\omega = 1$ gives the piston-like, no-diffusion solution, while $\omega = 0$ returns the 'equivalent' two-phase problem using straight line relative permeabilities. Varying ω therefore allows investigation of an entire range of possible solutions for the unstable case. Example fractional flow functions and concentration profiles for an end-point mobility ratio of ten are shown in Fig. 6.1. What value of ω to choose for generating a one-dimensional solution to use along streamtubes is discussed in Section 6.6.

6.3.1 Scale of 1D Solutions

Three one-dimensional solutions exist for the first-contact miscible case that may be mapped onto streamtubes: (1) a no-diffusion, piston-like solution, (2) a convection-diffusion solution, and (3) a viscous fingering solution. Of these three solutions, only two are really physically meaningful (2 and 3), each one emphasizing a different fluid flow mechanism to mitigate the inherent instabilities for unfavorable mobility ratio displacements. The CD-solution models 'mixing' at a scale at which the flow is

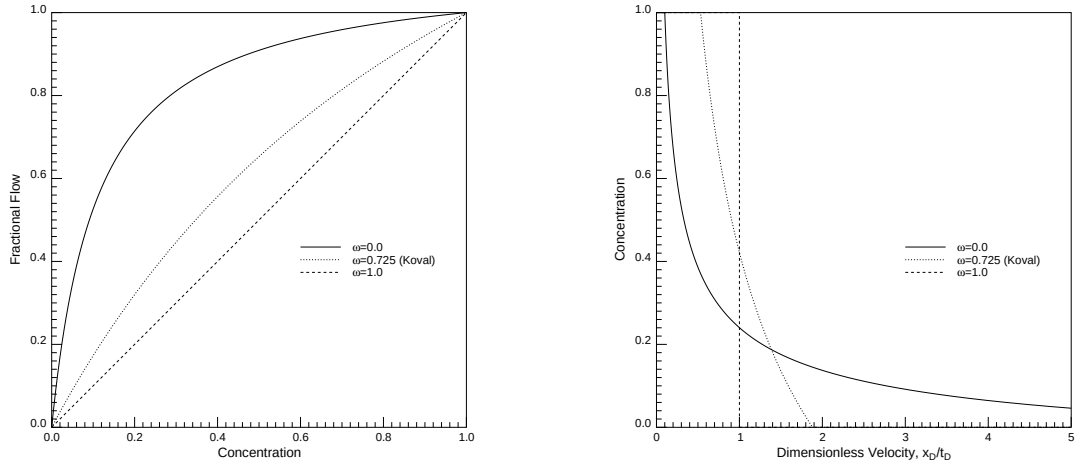

Figure 6.1: *Fractional flow curves and corresponding velocity profiles for* $M = 10$ *and different values of* ω *in the Todd–Longstaff model.*

assumed Fickian, while the viscous fingering model attempts to capture the average linear growth of viscous fingers in two dimensions. Which one-dimensional solution is used along streamtubes will make an implicit statement about the physical scale of the resulting two-dimensional solution.

The discussion on tracer displacements in Section 4.4.2 already discussed the diffusive length scale introduced by the convection-diffusion model. Choosing a Peclet number introduces a representative length scale, L_{rep}, beyond which the systems is said to be diffusive at the sub-streamtube level. On the other hand, if a viscous fingering model is used along streamtubes, such as the Todd–Longstaff model, then the scaling argument no longer rests on a diffusive length scale[3], and a representative length scale must be extracted from the viscous fingering model itself and the physics it is attempting to capture. The most convincing physical argument for attaching a length scale to the two-dimensional streamtube solution is to consider each streamtube as a 'homogeneous' medium that will attain a Fickian limit in the unit mobility ratio case, but will generate viscous fingers for $M > 1$.

[3]Although it is possible to argue that the size of viscous fingers may be scaled by L_{rep}.

6.4 2D Solutions With No Diffusion

Considerable effort has gone into trying to reduce the diffusive length scale associated with numerical solutions of unstable miscible displacements by using higher order numerical methods, a large number of grid-blocks (*Christie 1989, Christie and Bond 1987*), and alternative numerical techniques such as particle tracking (*Araktingi and Orr 1993, Tchelepi 1994,*). Mapping the no-diffusion analytical solution along streamtubes is therefore particularly appealing, since it would represent a completely diffusion-free, two-dimensional, unstable solution. Although such diffusion-free solutions can be found, they are unstable at all length scales, amplifying the assumptions inherent in the Riemann approach. It is easy to see that mapping a one-dimensional solution along streamtubes that is unstable at all length scales must necessarily lead to a similarly unstable two-dimensional solution. By not allowing any diffusive mechanism, the initial instability given by the end-point mobility ratio is preserved throughout the life of the displacement. As a result, moving the solution forward in time may result in large changes in the streamtube geometries, even for small time steps ($t + \Delta t$). For example, a permeability field that would normally give rise to a viscous fingering flow regime (see Fig. 6.2) will generate streamtubes that alternate between a 'very narrow' and 'very fat' state. This may be an extreme example, particularly given the fact that the streamtube approach by its very nature of conforming to the reservoir heterogeneity is not suited for modeling 'pure' viscous fingering since it can never capture the mechanisms of shielding, spreading, and tip splitting (*Homsy 1987*). Nevertheless, it explains why the 'fingers' in the streamtube solution of Fig. 6.2 are so narrow (basically one or two grid blocks in width) followed by a swept-out region. The Mistress finite difference solution, on the other hand, clearly indicates extensive fingering.

As the permeability field becomes more correlated (Fig. 6.3-Fig. 6.4), the instability in the streamtube solution is accentuated. Channels rapidly change direction and size and appear and disappear until some dominant flow path to the outlet boundary is found. At this point, all the flow is diverted into this (usually one) preferential

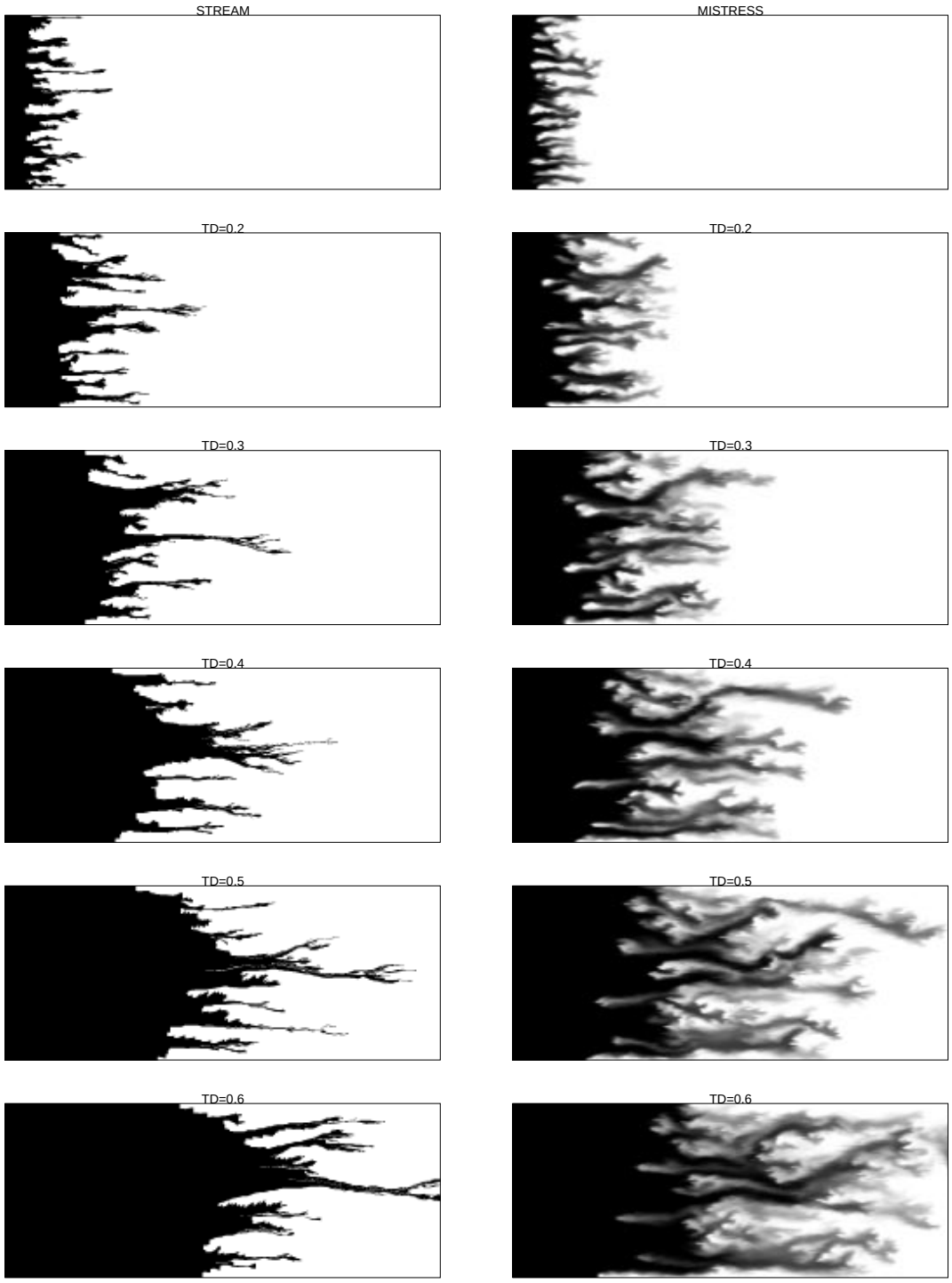

Figure 6.2: *Evolution of a 2D, M=10, no-diffusion solution in a 250x100 block permeability field with short correlation length. (PERM 5 — $\lambda = 0.01$, $\sigma_{\ln k} = 0.5$, $HI = 0.0025$)*

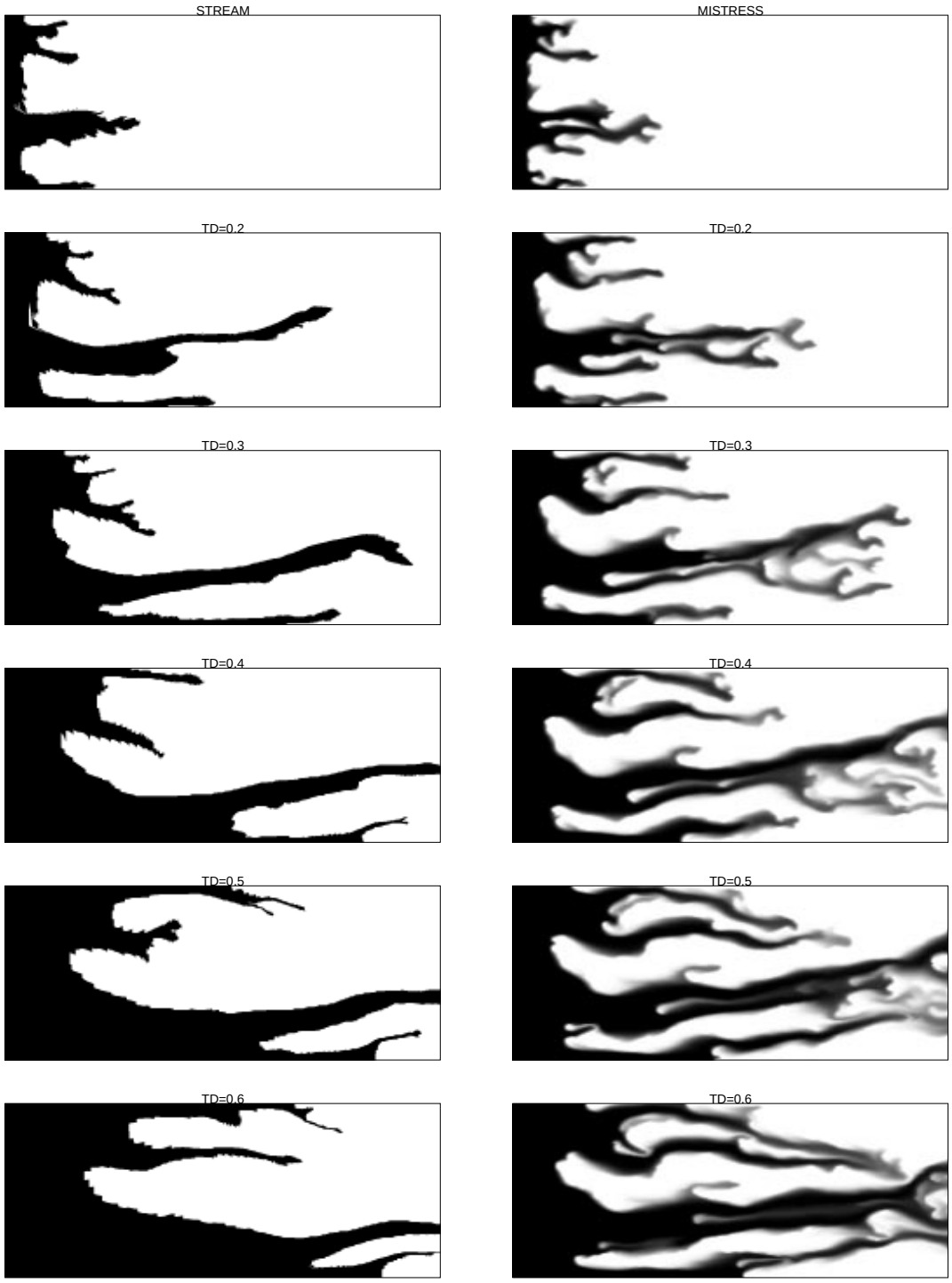

Figure 6.3: *Evolution of a 2D, M=10, no-diffusion solution in a 250x100 block permeability field with intermediate correlation length. (PERM 2 — $\lambda = 0.25$, $\sigma_{\ln k} = 0.5$,$HI = 0.0625$)*

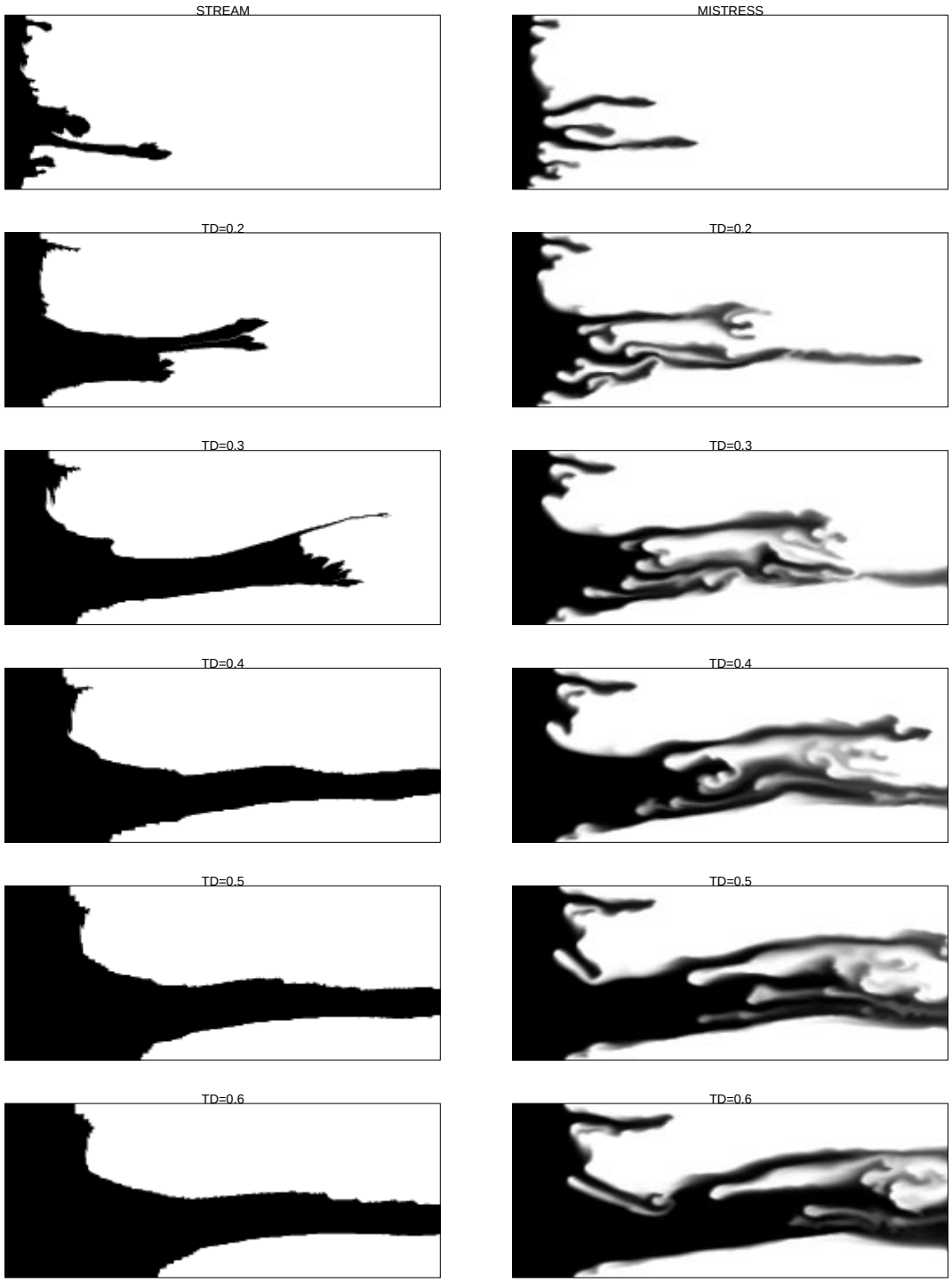

Figure 6.4: *Evolution of a 2D, M=10, no-diffusion solution in a 250x100 block permeability field with long correlation length. (PERM 8 —* $\lambda = 1.00$, $\sigma_{\ln k} = 0.5$,$HI = 0.25$*)*

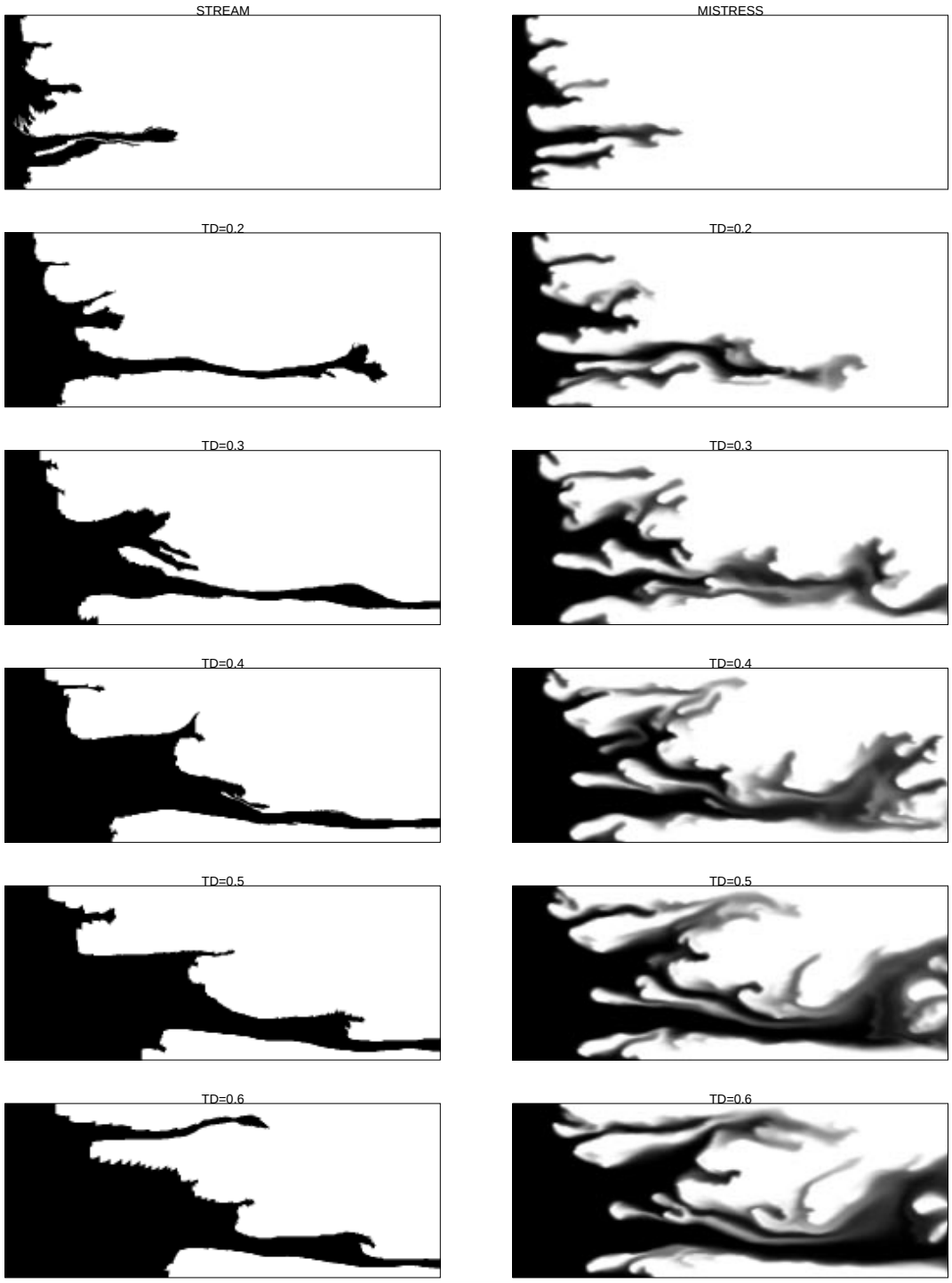

Figure 6.5: *Evolution of a 2D, M=10, no-diffusion solution in a 250x100 block permeability field with intermediate correlation length. (PERM 4 — $\lambda = 0.5$, $\sigma_{\ln k} = 1.0$,$HI = 0.50$)*

flow path, causing the fronts to retract in many of the other channels, giving the impression of 'backwards' flow. Although visible to a certain extent in Fig. 6.2-Fig. 6.4, the instability of the solution is best demonstrated in an animated version of the displacement. The recovery curves for the different displacements, shown in Fig. 6.6, are particularly interesting. Given the completely unstable nature of the displacements, overall recoveries are remarkably good and breakthrough is predicted correctly in all cases. The reason for this must be that the first-order effect due to the underlying heterogeneity structure is still captured by the streamtubes.

Possibly the 'best' solution in the no-diffusion case can be obtained for systems in which the correlation length is on the same order, or greater, of the system length ($\lambda_c > L$); the least resistant flow path is found immediately and the competition between several streamtubes never materializes. The problem with systems of this type is that the large channel(s) could now be considered homogeneous systems in their own right, giving rise to a viscous fingering dominated flow regime within them. Fig. 6.4 shows just that. The streamtube solution correctly identifies the preferential flow path, but the finite difference solution does display viscous fingering within the channel.

The examples in this section demonstrate that mapping a piston-like, $M > 1$ solution along the streamtubes results in unstable two-dimensional solutions. All the solutions were for an end-point mobility ratio of ten ($M = 10$). Choosing $M < 10$ would certainly give better behaved solution (in the limit of $M = 1$ the no-diffusion tracer solution is obtained), whereas choosing $M > 10$ would make things worse. As with the one-dimensional solution, the problem is that there is no characteristic length scale on which to mitigate the instability, causing streamtubes to abruptly change in size and direction. Streamtubes are able to find dominant flow channels, if they exist, and are even able to return a particularly good match of breakthrough. Nevertheless, it is evident that, in general, the solutions will be unstable and nonphysical.

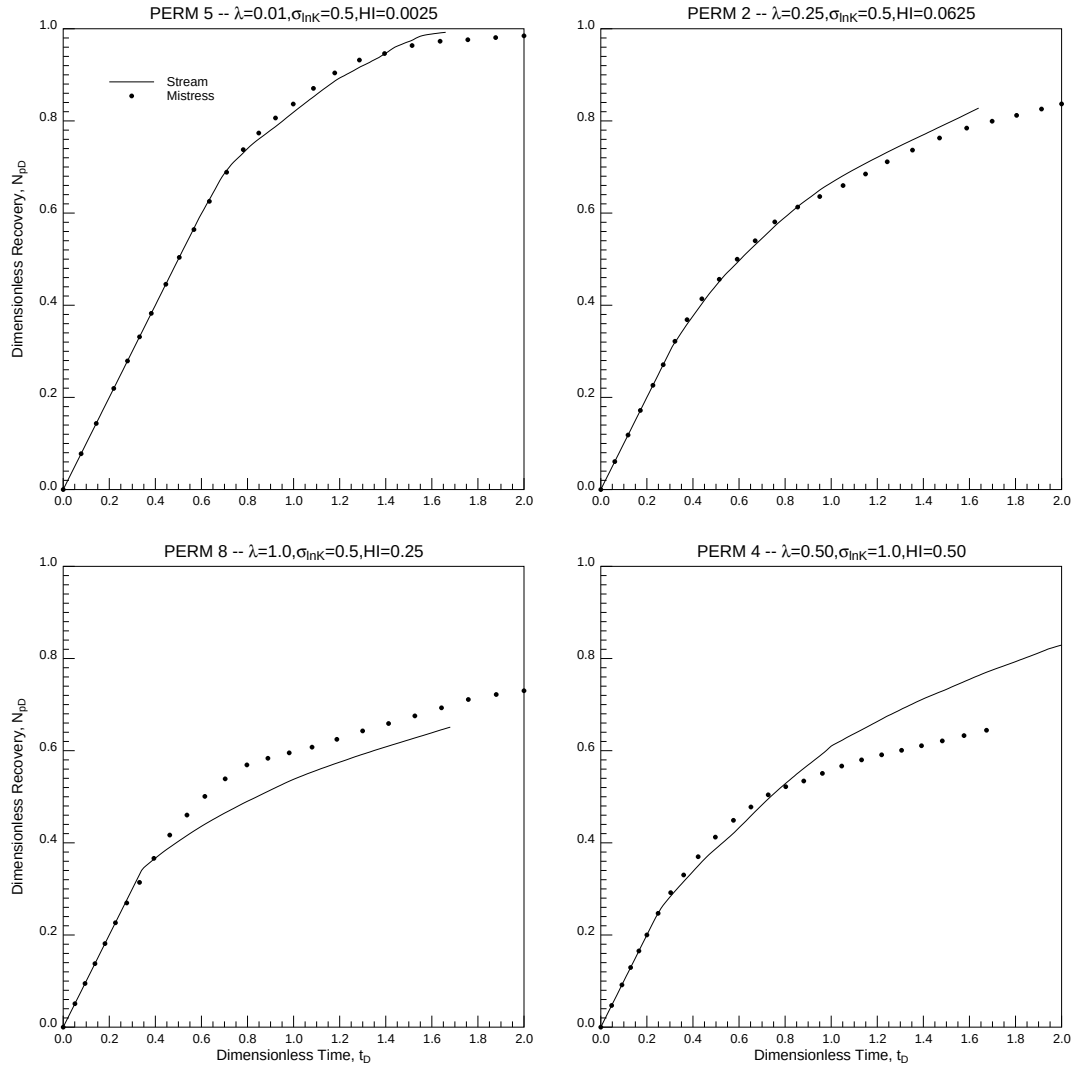

Figure 6.6: *Recovery curves for the displacements shown in Fig. 6.2 - Fig. 6.4.*

6.5 2D Solutions Using the CD-Equation

Mapping the approximate solution to the convection-diffusion equation using semi-infinite boundary conditions, given by

$$C(x_D, t_D) = \frac{1}{2}\text{erfc}\left(\frac{x_D - t_D}{2\sqrt{\frac{N_{Pe}}{t_D}}}\right) \quad , \tag{6.17}$$

introduces a mixing zone that grows proportionally to the square root of time. In other words, the frontal instability is mitigated as the concentration varies smoothly from $C_D = 1$ to $C_D = 0$ across a zone of length Δx_D which grows proportionally to $\sqrt{t_D}$. In case of unit mobility ratio displacements, Eq. 6.17 makes an implicit assumption about the probable scale of system: each streamtube is assumed to have a Fickian limit given by the particular choice of the Peclet number, Pe. For unfavorable mobility ratios, on the other hand, that same streamtube should give rise to viscous fingering dominated flow regime. Thus, mapping a CD-solution along streamtubes for $M > 1$ would be a contradiction or force a different scale on the solution.

The principal idea to be investigated here though, is whether longitudinal diffusion can be a sufficiently strong mechanism to mitigate the initial mobility contrast. In particular, this implies that physical diffusion can prevent the growth of viscous fingers. For diffusion to have such an effect the scale of the system can no longer be the same one as it was for unit mobility ratio case, but must necessarily be smaller so as to emphasize the mechanical mixing action at the REV-scale. Just how much physical diffusion is necessary to mitigate the initial instability is difficult to quantify, since it will depend strongly on the extent of heterogeneity. Furthermore, simply comparing snapshots at particular times may be misleading. A series of still images that look 'right' may display instabilities if viewed as an animated sequence. As an example, Fig. 6.7 shows concentration maps at $t_D = 0.3$ for $Pe = 10, 50$, and 200 as compared to the reference Mistress solution with no physical diffusion (but with numerical diffusion) for a 250x100 block permeability field with a correlation length of $\lambda_c = 0.3$ and $\sigma_{\ln k} = 1.0$. Fig. 6.8 shows the corresponding recovery curves. Mapping a convection-diffusion solution along the streamtubes introduces a mixing zone across which the instability is mitigated, but it does not alter the main features of

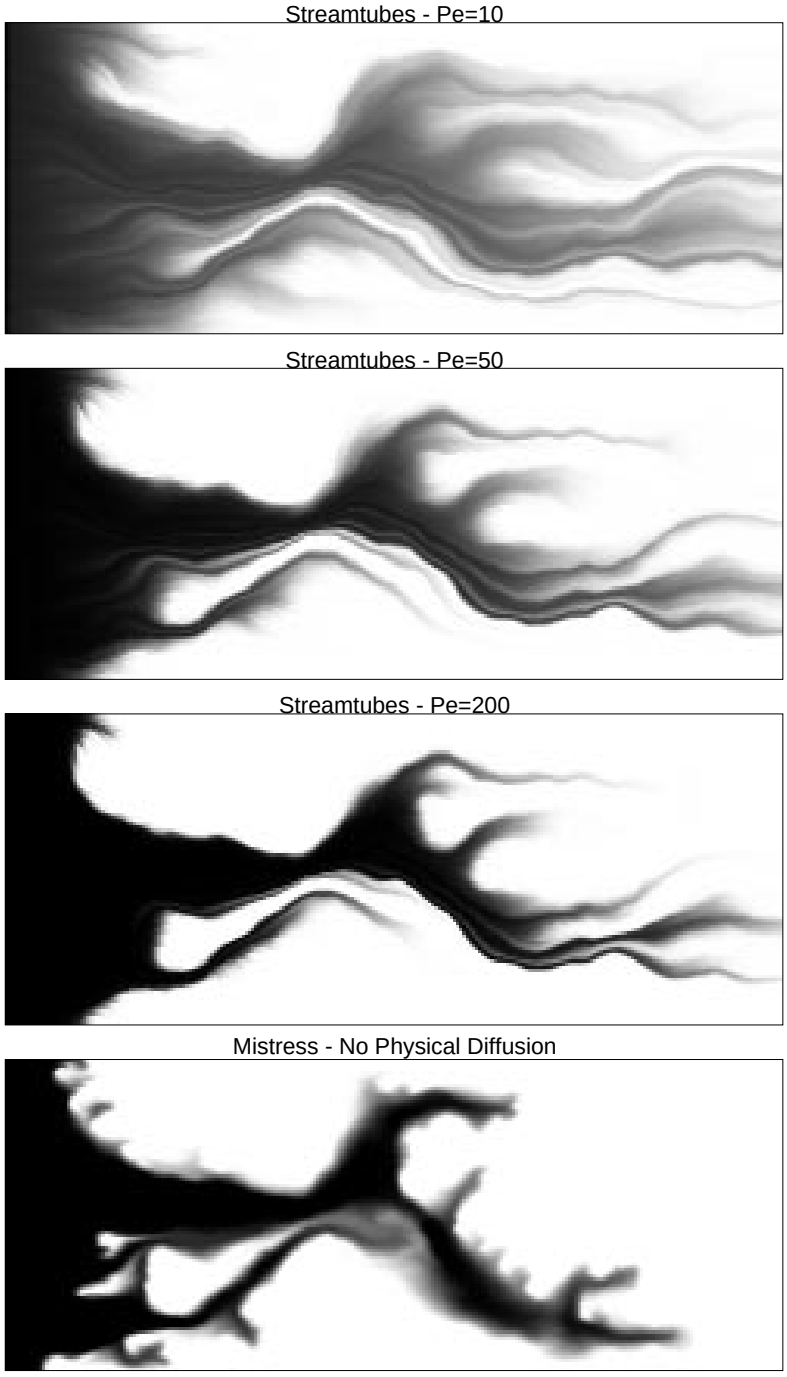

Figure 6.7: *Comparison of concentration maps at $t_D = 0.3$ for different values of Pe in a 250x100 block permeability field. The reference Mistress solution for the same time is given as well. The Mistress solution has no physical diffusion added to it.*

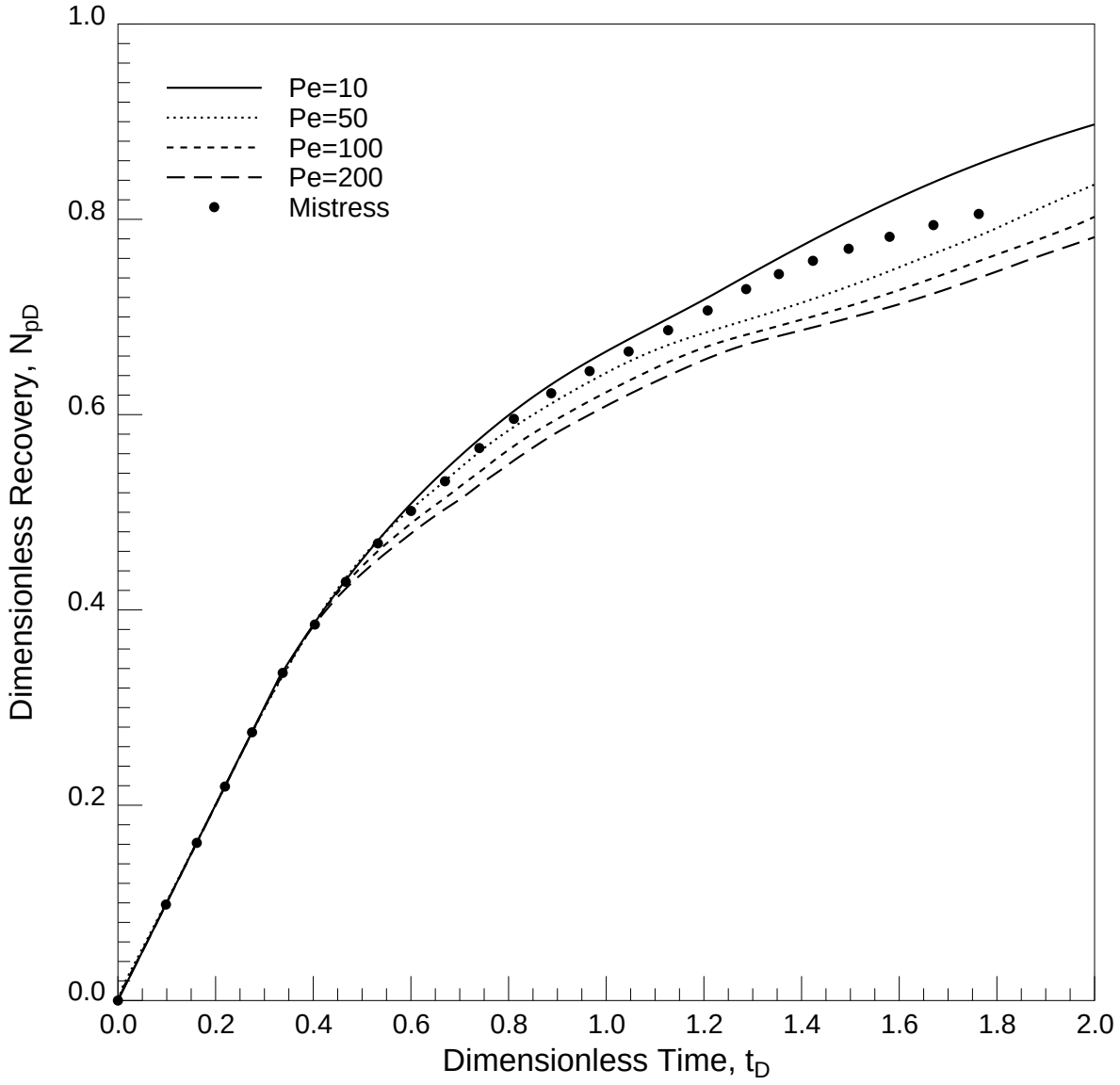

Figure 6.8: *Recovery curves for the permeability field used in Fig. 6.7 and for different values of* Pe.

the displacement, which remain dictated by the underlying permeability field. This is summarized by the recovery curves of Fig. 6.8, which show a weak dependence of overall recovery on Pe. In fact, breakthrough time is practically independent of Pe, suggesting that it is a convective, permeability-dominated phenomenon. This result relaxes to a certain extent the constraint on the scale of the system imposed by mapping a CD-solution for an $M > 1$ displacement, and thus it is possible that the concentration maps in Fig. 6.7 apply on a field scale as well.

A slight discrepancy exists on what the 'correct' value of Pe should be for the streamtube solution: a visual comparison of the concentration maps in Fig. 6.7 point to a value closer to 200, whereas the recovery curves of Fig. 6.8 suggest a value between 10-50. The reason for this discrepancy must be that the streamtube solution does not capture the viscous fingering details of the Mistress solution. The only way to account for the additional recovery given by viscous fingering and the derived mobility reduction, is to increase the physical diffusion in the overall streamtube solution. Example displacements for $Pe = 50$ and $Pe = 200$ are given in Fig. 6.9-Fig. 6.10. The difference in the streamtube solution is in fact negligible.

Many more runs would be necessary to cover thoroughly the relevant parameter space given by M, Pe, λ and σ. Three additional example solutions for $M = 10$ and $HI = 0.0625, 0.25$ are shown in Fig. 6.11 – Fig. 6.13, which also give the Mistress reference solutions[4]. The recovery curves for the four cases are reported in Fig. 6.14. The solutions presented in this section demonstrate that by adding sufficient physical diffusion it is possible to mitigate the initial instability and obtain meaningful physical solutions. The first-order features of the displacements though, which were also seen in the no-diffusion solutions, remain unchanged and are dictated by reservoir heterogeneity. The argument for not using the CD-solution in the case of unstable displacements is probably still valid although less restrictive due to the second-order effect of diffusion on displacement performance.

[4]As a comparison, the equivalent no-diffusion solutions are given in Figs. 6.3 and 6.4.

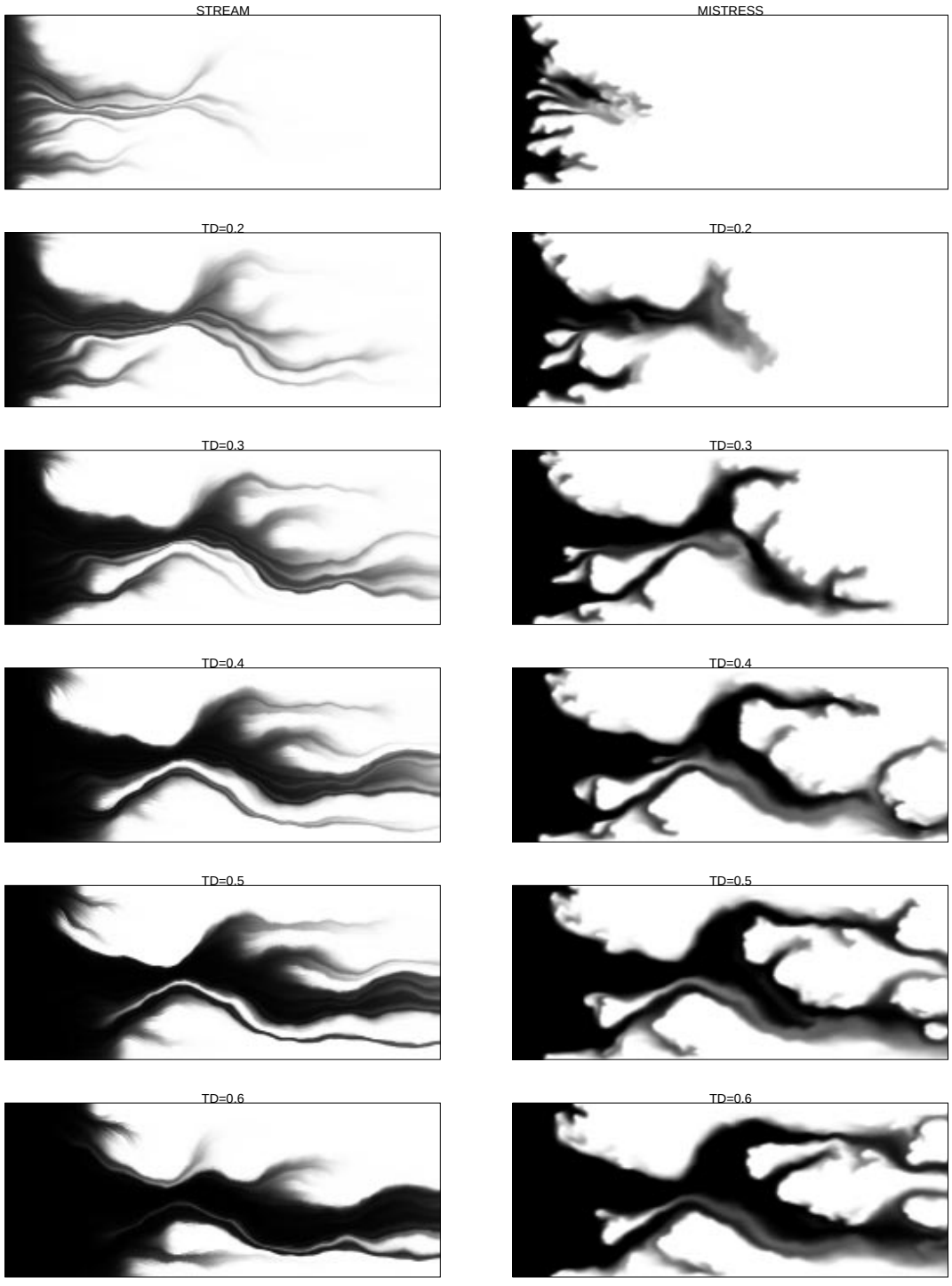

Figure 6.9: *Evolution of a 2D, $M = 10$, $Pe = 50$ CD-solution in a 250x100 block permeability field with intermediate correlation length (PERM BP — $\lambda_c = 0.3$, $\sigma_{\ln k} = 1.0$, $HI = 0.3$).*

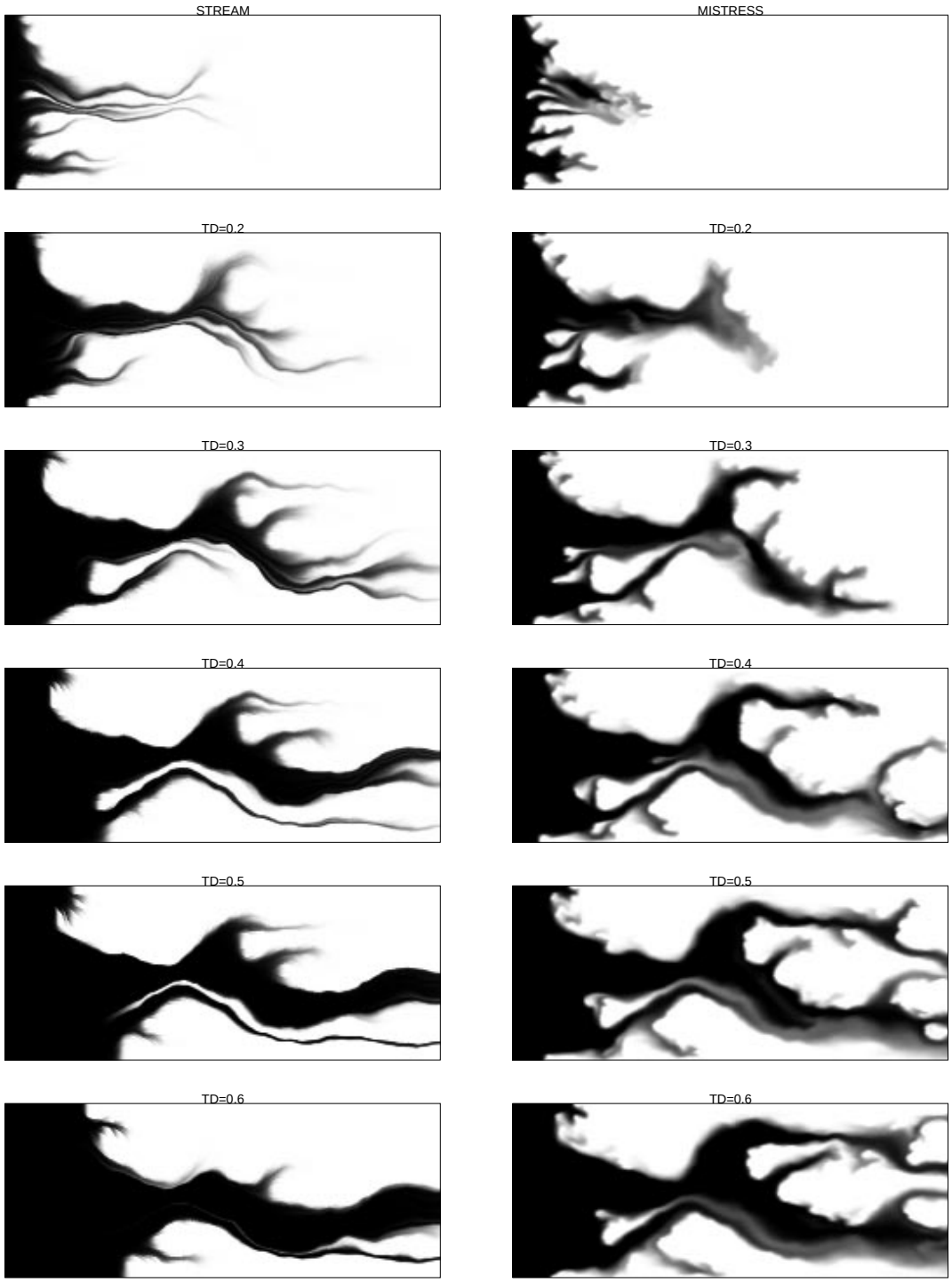

Figure 6.10: *Evolution of a 2D, $M = 10$, $Pe = 200$ CD-solution in a 250x100 block permeability field with intermediate correlation length (PERM BP — $\lambda_c = 0.3$, $\sigma_{\ln k} = 1.0$, $HI = 0.3$).*

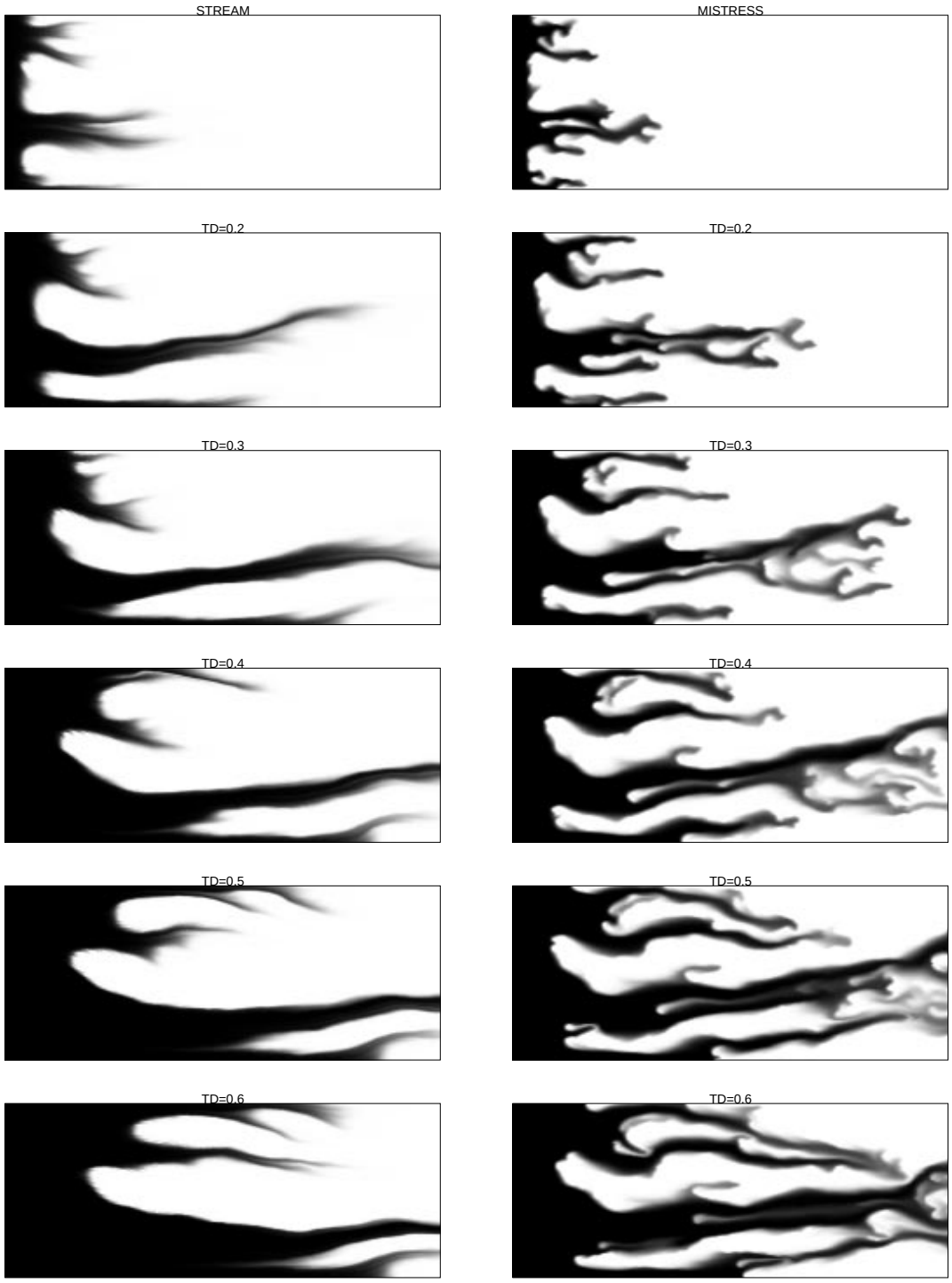

Figure 6.11: *Evolution of a 2D,* $M = 10$, $Pe = 200$ *CD-solution in a 250x100 block permeability field with intermediate correlation length (PERM 2 —* $\lambda = 0.25$, $\sigma_{\ln k} = 0.5$,$HI = 0.0625$*).*

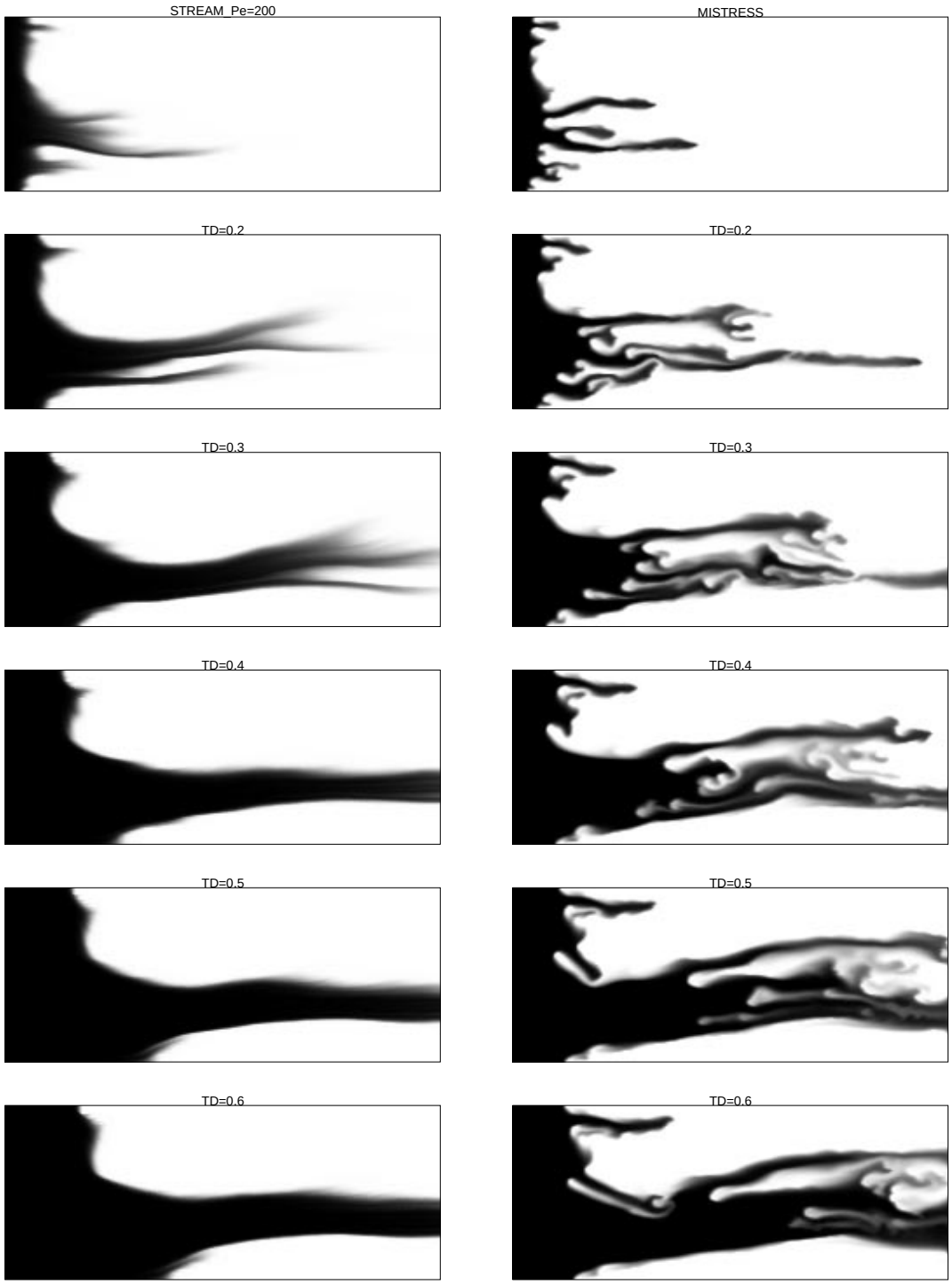

Figure 6.12: *Evolution of a 2D, $M = 10$, $Pe = 200$ CD-solution in a 250x100 block permeability field with long correlation length (PERM 8 — $\lambda = 1.00$, $\sigma_{\ln k} = 0.5$,$HI = 0.25$).*

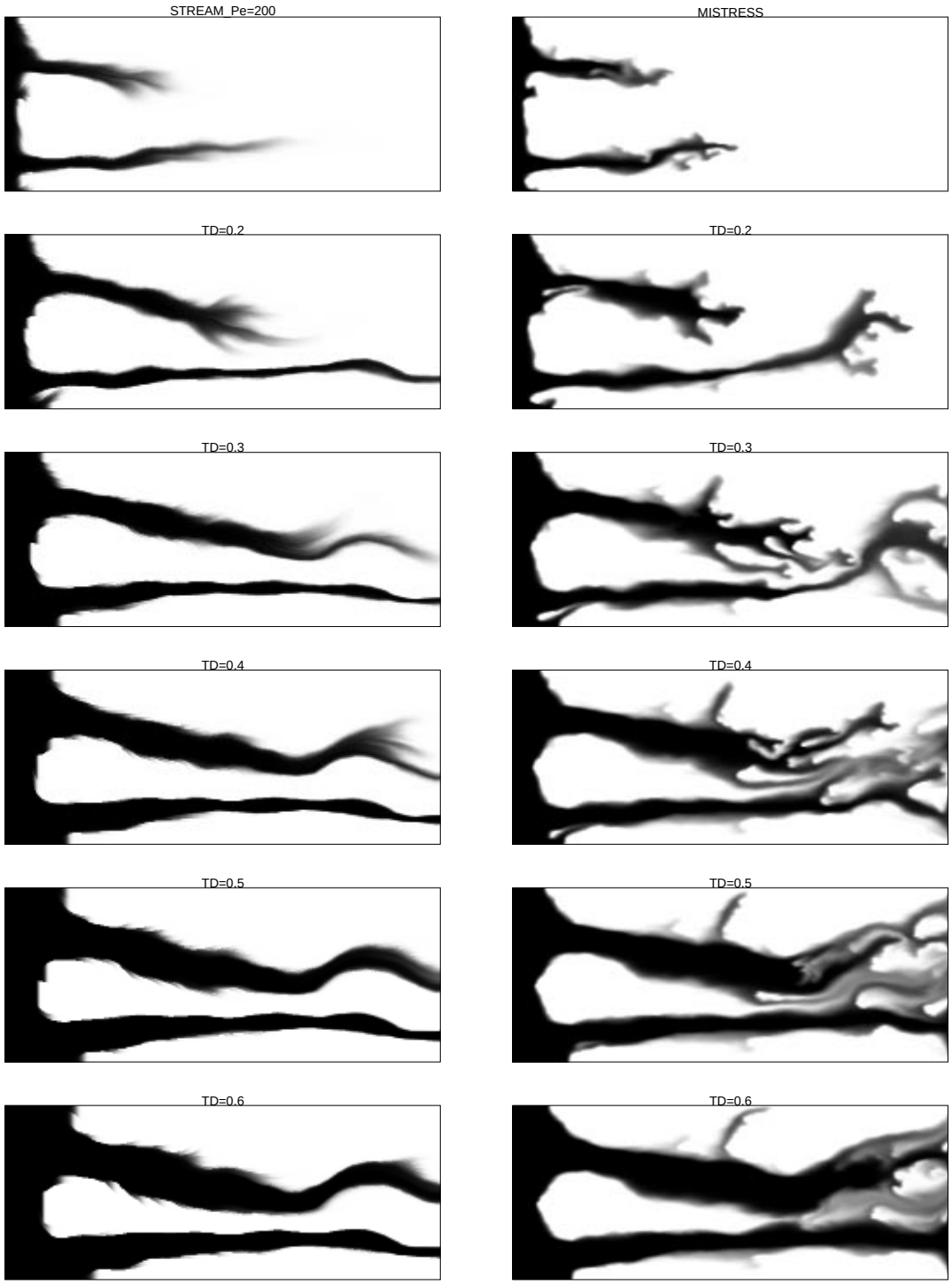

Figure 6.13: *Evolution of a 2D, $M = 10$, $Pe = 200$ CD-solution in a 250x100 block permeability field with intermediate correlation length but with larger variance. (PERM 9 — $\lambda = 0.25$, $\sigma_{\ln k} = 1.0$,$HI = 0.25$).*

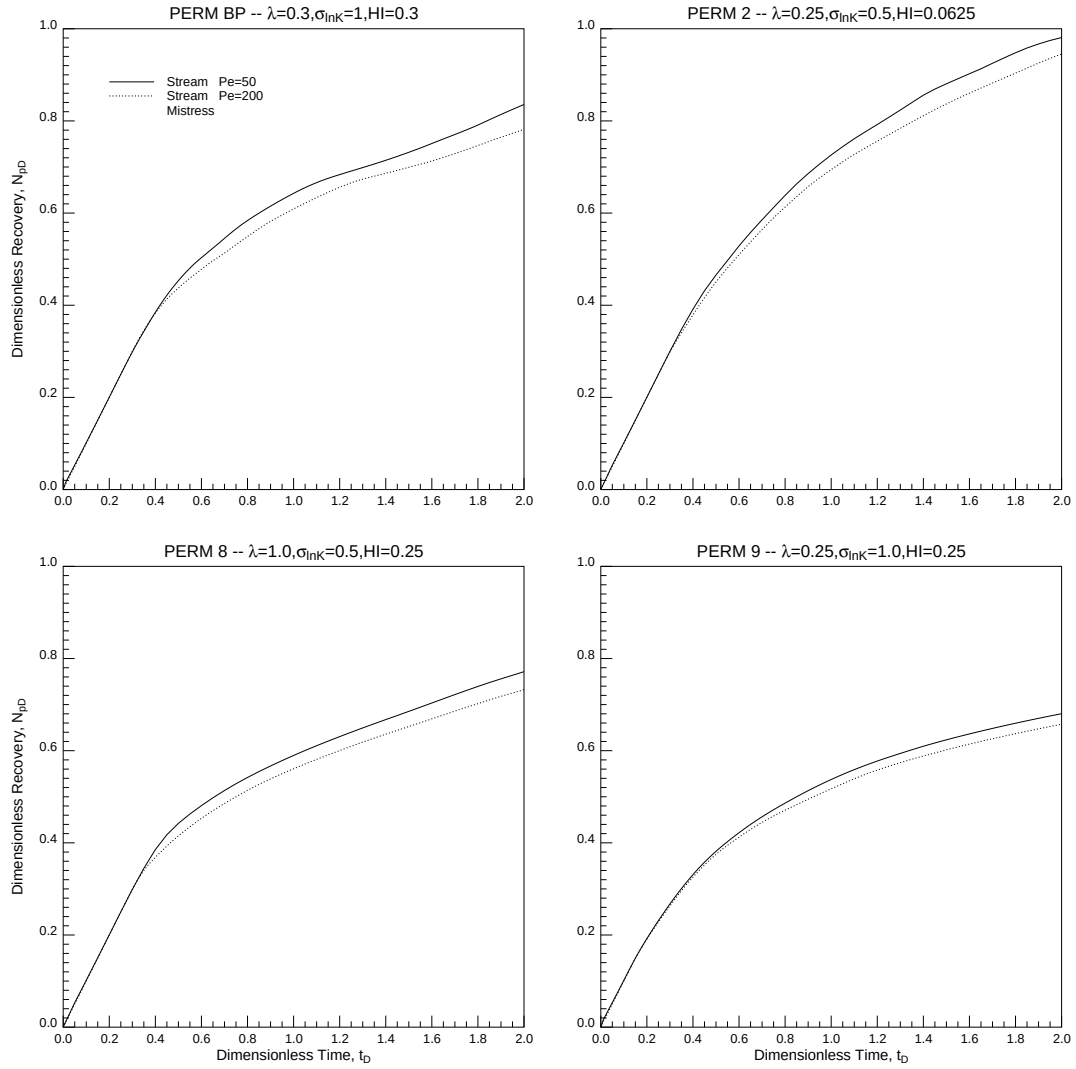

Figure 6.14: *Recovery curves for the displacements shown in Fig. 6.9 - Fig. 6.13.*

6.6 2D Solutions Using Viscous Fingering Model

If the streamtubes are considered to be on a field scale, then a one-dimensional viscous fingering solution is probably more appropriate than the convection-diffusion solution to capture the first contact miscible displacement of the resident oil. In other words, each streamtube is considered large enough and homogeneous enough to reach a Fickian limit for $M = 1$ and to generate a viscous fingering flow regime for $M > 1$. The effective 'mixing' zone now grows linearly with time, allowing the instability to be mitigated even more than in the convection-diffusion approach.

In generating a two-dimensional solutions using the Todd–Longstaff model, a value for ω must be chosen. An $\omega \approx 2/3$ is widely used and has been found to match both, experimental and numerical displacements through homogeneous media (*Todd and Longstaff 1972, Fayers et al. 1992*). If the Todd–Longstaff model is made to match Koval's model then ω becomes a (weak) function of end-point mobility ratio as given by Eq. 6.16, since Koval's model assumes a fixed solvent concentration of 0.22 to find the mixture viscosity using the quarter power mixing rule. It is unreasonable to believe that a constant value for ω is able to match all secondary miscible displacements in homogeneous media, and therefore some functional dependence on M is probably desired. On the other hand, given the physical limits of $\omega = 1$ (no mixing) and $\omega = 0$ (complete mixing), the large uncertainties in the input data, and the general nonlinearity of the problem, it is unlikely that a dependence of ω on M can actually be detected with the desired degree of accuracy by numerical or laboratory experiments.

To quantify the sensitivity of the streamtube solution on ω, the same $M = 10$ displacement through a 125x50 block heterogeneous system was simulated using incremental values of ω, starting from $\omega = 0$ up to $\omega = 1$, with $\Delta\omega = 0.1$. Example concentration maps at $t_D = 0.3$ are shown in Fig. 6.15 and the recovery curves are shown in Fig. 6.16. The particularly interesting feature of the recovery curves is that they are not monotonic as a function of ω. Recovery increases starting from $\omega = 0$, reaches a maximum at around $\omega = 0.6$ - 0.7, and then decreases again as it tends to $\omega = 1.0$. It is difficult to make any general statements about why recovery reaches a maximum in the range of $\omega = 0.6$ - 0.7, and particularly if it is simply a coincidence

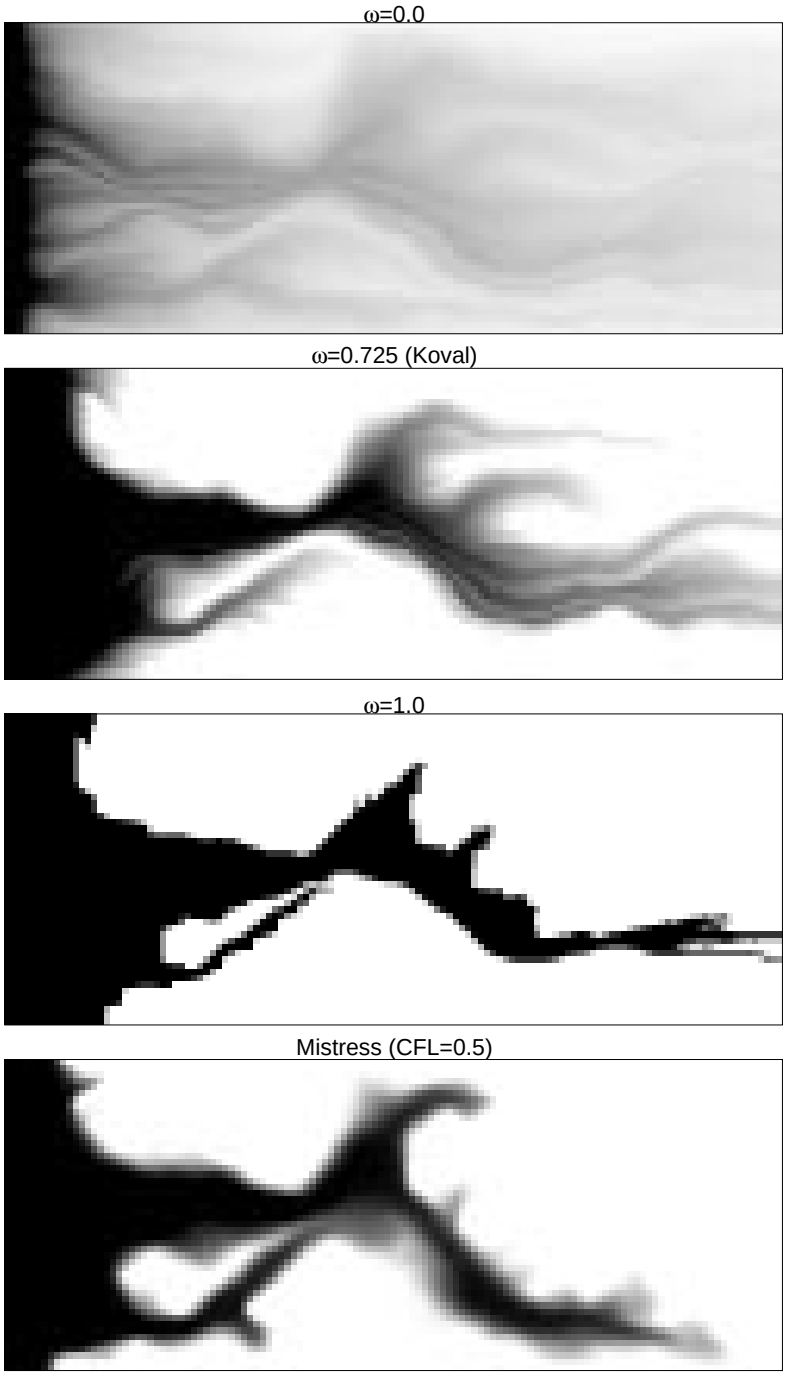

Figure 6.15: *Example concentration maps for $\omega = 0$ (complete mixing), $\omega = 0.725$, and $\omega = 1$ (no mixing) at $t_D = 0.3$ and $M = 10$. The Mistress solution is shown at the bottom.*

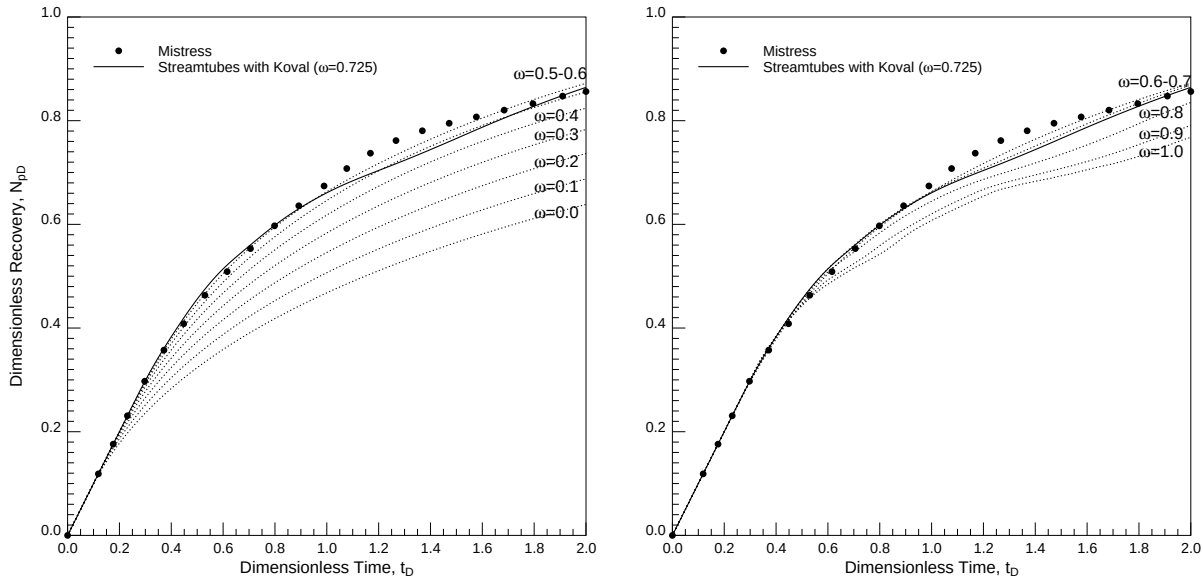

Figure 6.16: *Recovery curves for increasing values of ω showing the non-monotonic change in recovery.*

---

that the widely accepted value of $\omega = 2/3$ falls within this range. Many more runs for a wide range of permeability fields and mobility ratios would be necessary. On the other hand, from the solutions presented so far and particularly from the discussion on the no-diffusion case, it is possible to argue that both, $\omega = 0$ and $\omega = 1$, cannot possibly give the maximum recovery. $\omega = 0$ represents complete mixing, with the one-dimensional solution given by the 'equivalent' two-phase formulation using straight line relative permeabilities. As a result, a long rarefaction wave with the maximum concentration velocity given by M and the minimum velocity given by $1/M$ causes a poor sweep of each streamtube. $\omega = 1$, on the other hand is equivalent to the no-diffusion solution, emphasizing the least resistant flow paths and returning an nonphysical solution due to the absence of any diffusive length scale. Between these two extreme cases then, an ω_{max} must exists that mitigates the instability by allowing some mixing while at the same time retaining sufficient frontal character to ensure a 'good' sweep. That ω_{max} is closer to 1 than to 0 could be explained by the fact that mixing is less important in defining the overall character of the solution

than the heterogeneity of the system. In other words, mixing must be introduced mainly as an instability mitigator. In fact, the stronger the heterogeneity, the more the displacement would look like the no-diffusion solution; displacements dominated strongly by heterogeneity would become rather insensitive to the higher values of ω with possibly all values between 0.6 and 1.0 giving more or less the same recovery.

Fig. 6.17 - Fig. 6.22 show example $M = 10$ solutions through 250x100 block reservoirs with varying degree of heterogeneity. A value of $\omega = 0.725$ is used in each case (equivalent to Koval's model) to capture the 'viscous fingering induced mixing' along each streamtube. The comparison with the Mistress solution in each case raises the interesting question whether the streamtube solutions and the Mistress solutions are indeed on the same scale. All Mistress solutions have some viscous fingering features, whereas all the fingering in the streamtube solutions is assumed to take place within the streamtubes and captured in an averaged one-dimensional sense. As a result, it could be argued that the streamtube solution is probably representing a larger scale than the Mistress solution.

The recoveries for the displacements shown in Fig. 6.17 - Fig. 6.20 are summarized in Fig. 6.23. The recovery for the very short correlation length system is expected to be good, since it amounts to the recovery predicted by the one-dimensional Koval solution. For the other cases, the recovery curves tell an interesting story, particularly for the $HI = 0.0625$ (PERM 2) and $HI = 0.64$ (PERM 3) heterogeneity distributions. The $HI = 0.0625$ permeability field has a correlation length of $\lambda_c = 0.25$, but only a standard deviation of $\sigma_{\ln k} = 0.5$. In other words, the system is only mildly heterogeneous, and although there are preferential flow channels, the streamtube solution see a rather homogeneous reservoir, whereas the Mistress solution allows fingers to grow along these channels (Fig. 6.19). The predicted recoveries are accordingly higher for the more homogeneous streamtube solution and lower for the viscous fingering dominated Mistress solution. The interesting point about this displacement is that it identifies a flow regime in which the streamtube model fails to capture the dominant displacement mechanism: field scale fingering induced by a mildly heterogeneous systems.

The much more heterogeneous $HI = 0.64$ case (Fig. 6.22), on the other hand,

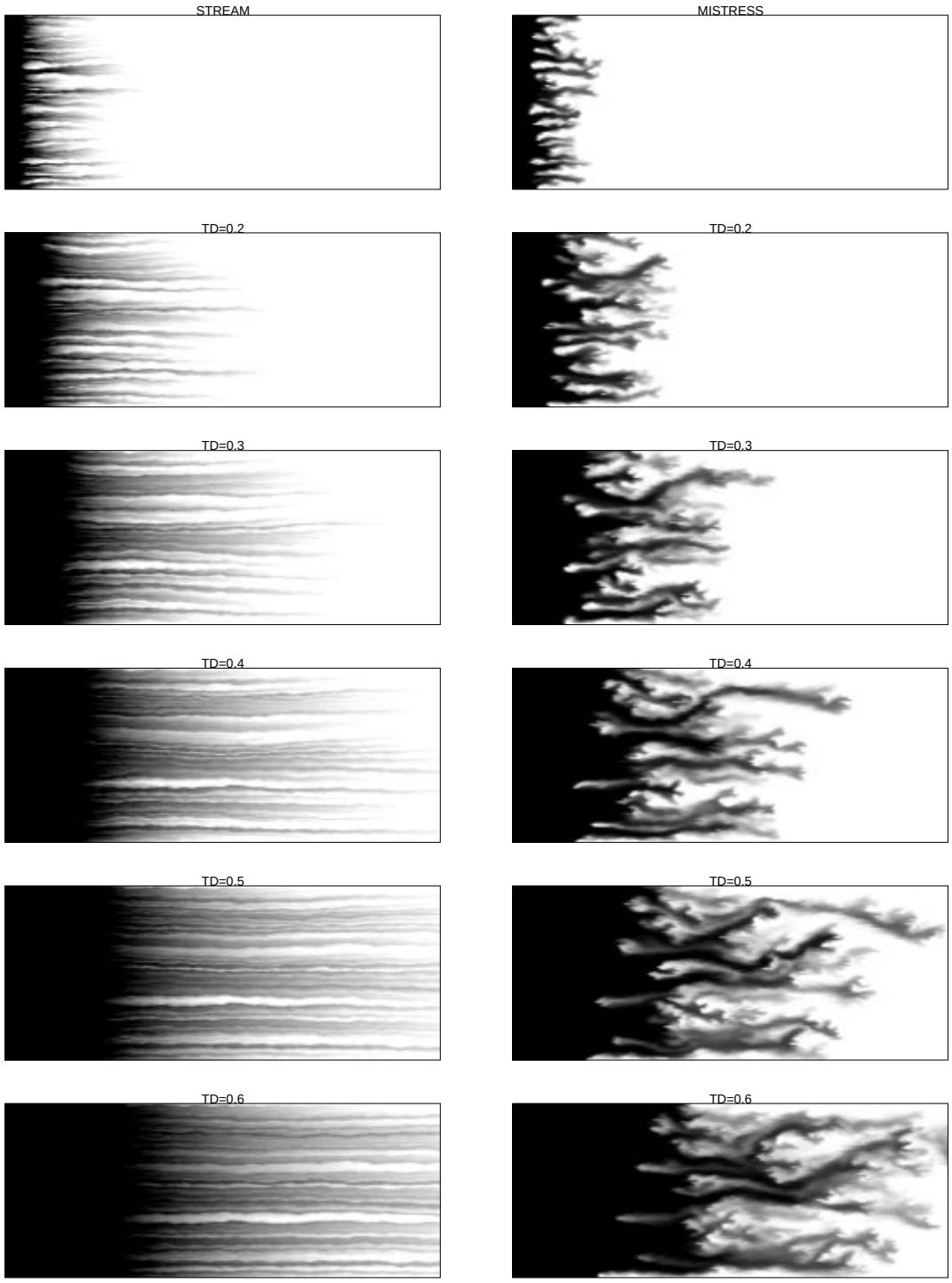

Figure 6.17: *Displacement history for a $M = 10$ displacement using Koval's model along streamtubes in a 250x100 block heterogeneous reservoir with very short correlation length (PERM 5 — $\lambda = 0.01$, $\sigma_{\ln k} = 0.5$, $HI = 0.0025$).*

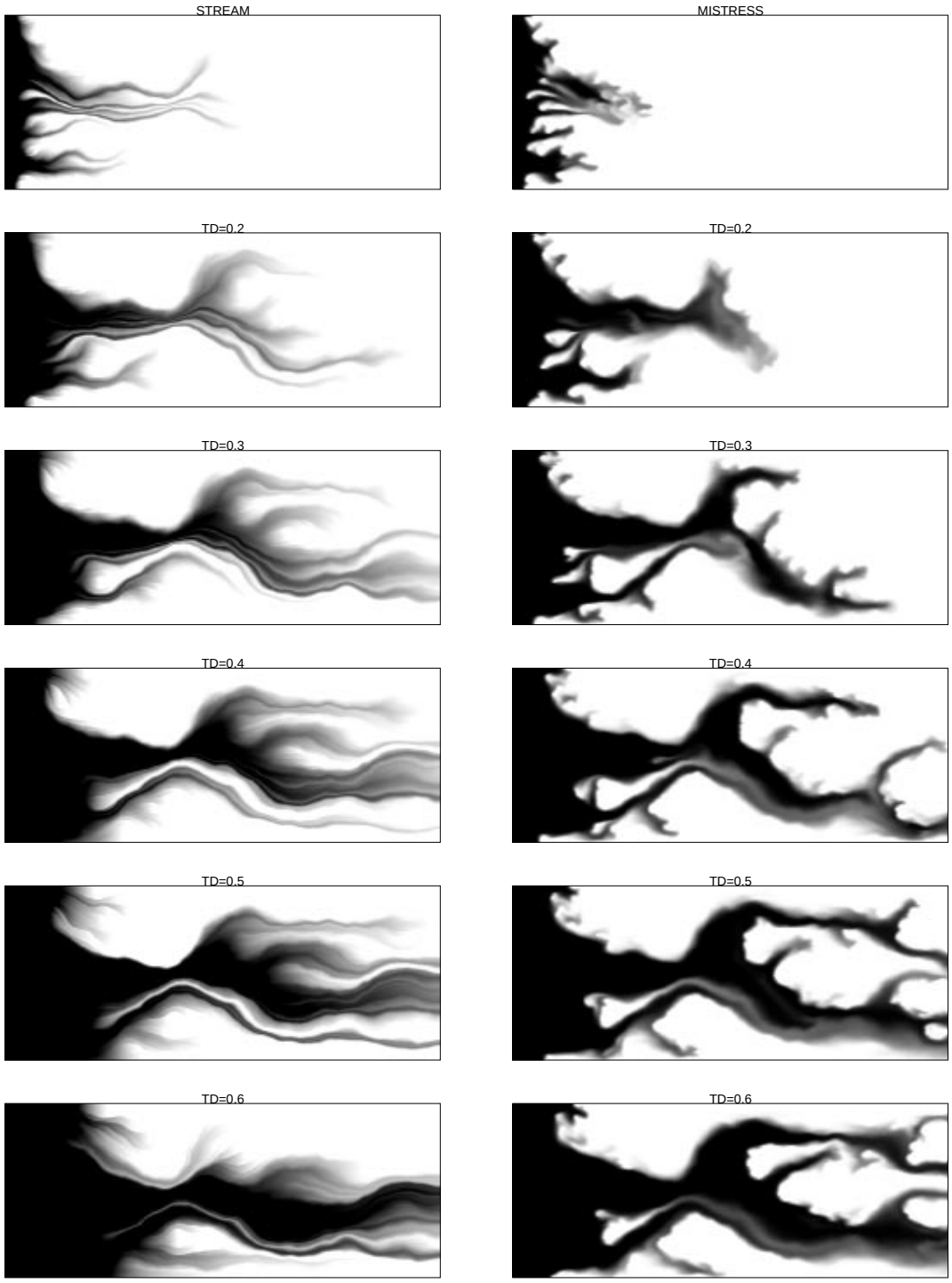

Figure 6.18: *Displacement history for a $M = 10$ displacement using Koval's model along streamtubes in a 250x100 block heterogeneous reservoir with intermediate correlation length (PERM BP — $\lambda = 0.3$, $\sigma_{\ln k} = 1$,$HI = 0.3$).*

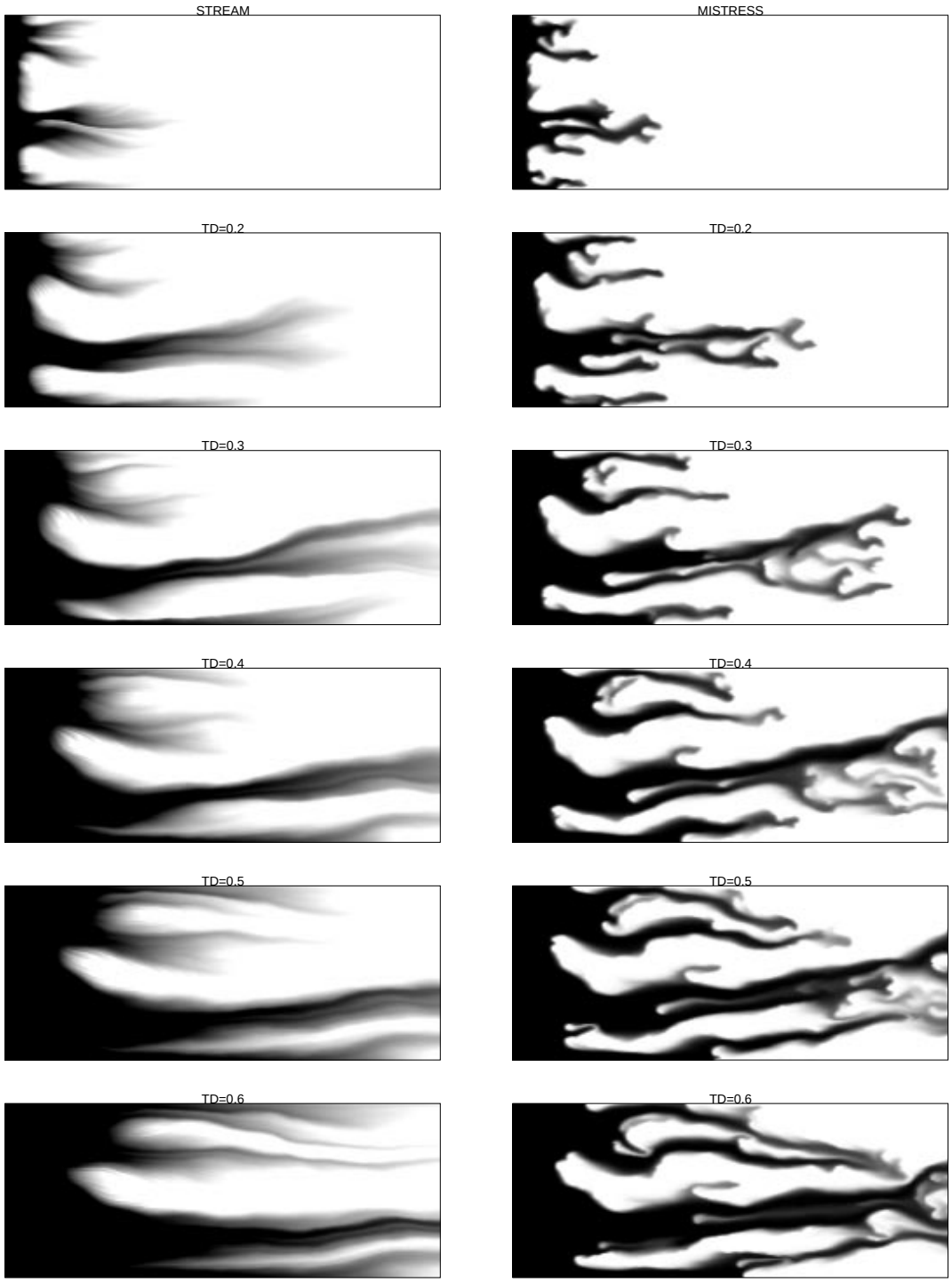

Figure 6.19: *Displacement history for a $M = 10$ displacement using Koval's model along streamtubes in a 250x100 block heterogeneous reservoir with intermediate correlation length (PERM 2 — $\lambda = 0.25$, $\sigma_{\ln k} = 0.5$,$HI = 0.0625$).*

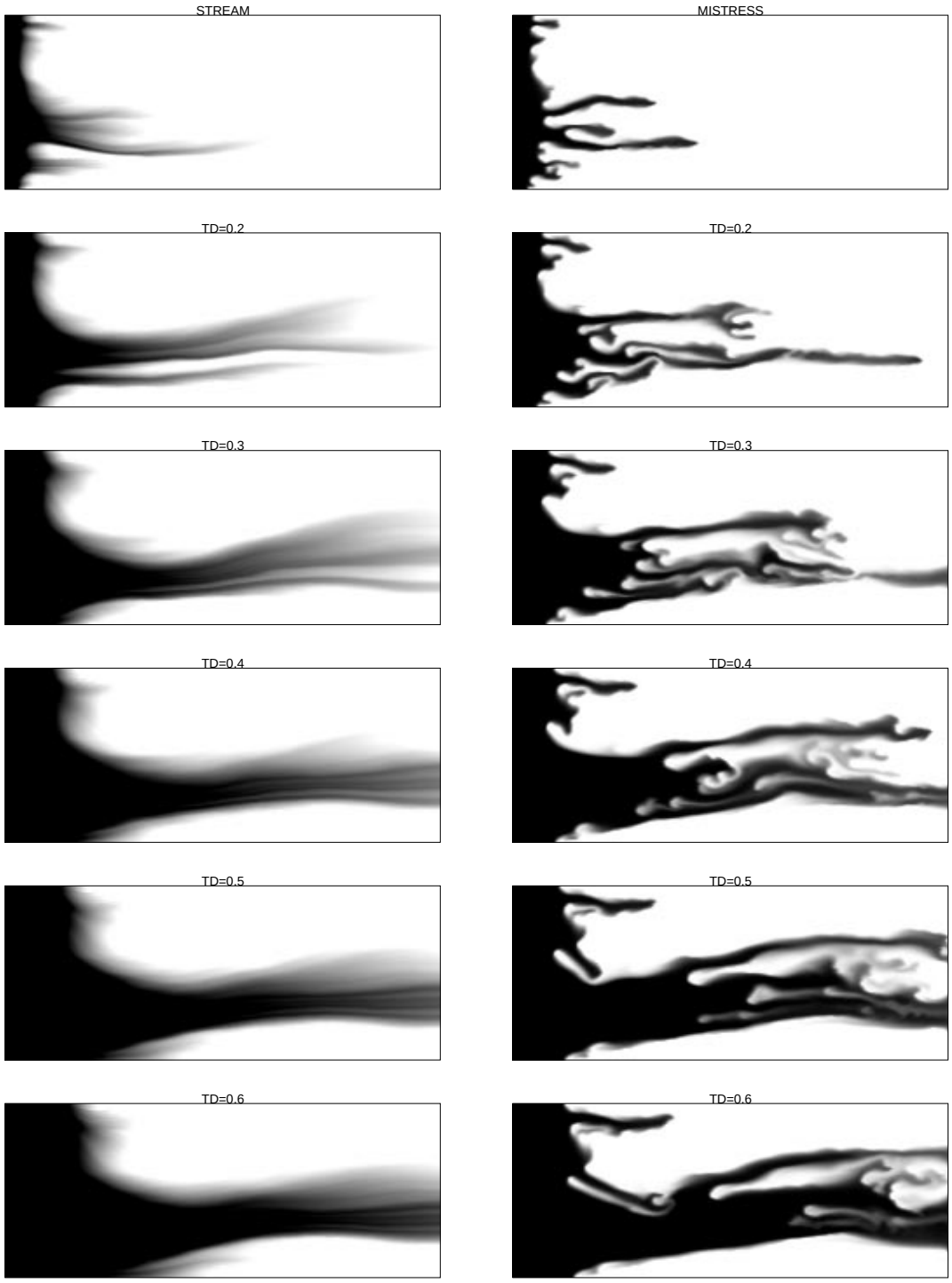

Figure 6.20: *Displacement history for a $M = 10$ displacement using Koval's model along streamtubes in a 250x100 block heterogeneous reservoir with long correlation length (PERM 8 — $\lambda = 1.00$, $\sigma_{\ln k} = 0.5$,$HI = 0.25$).*

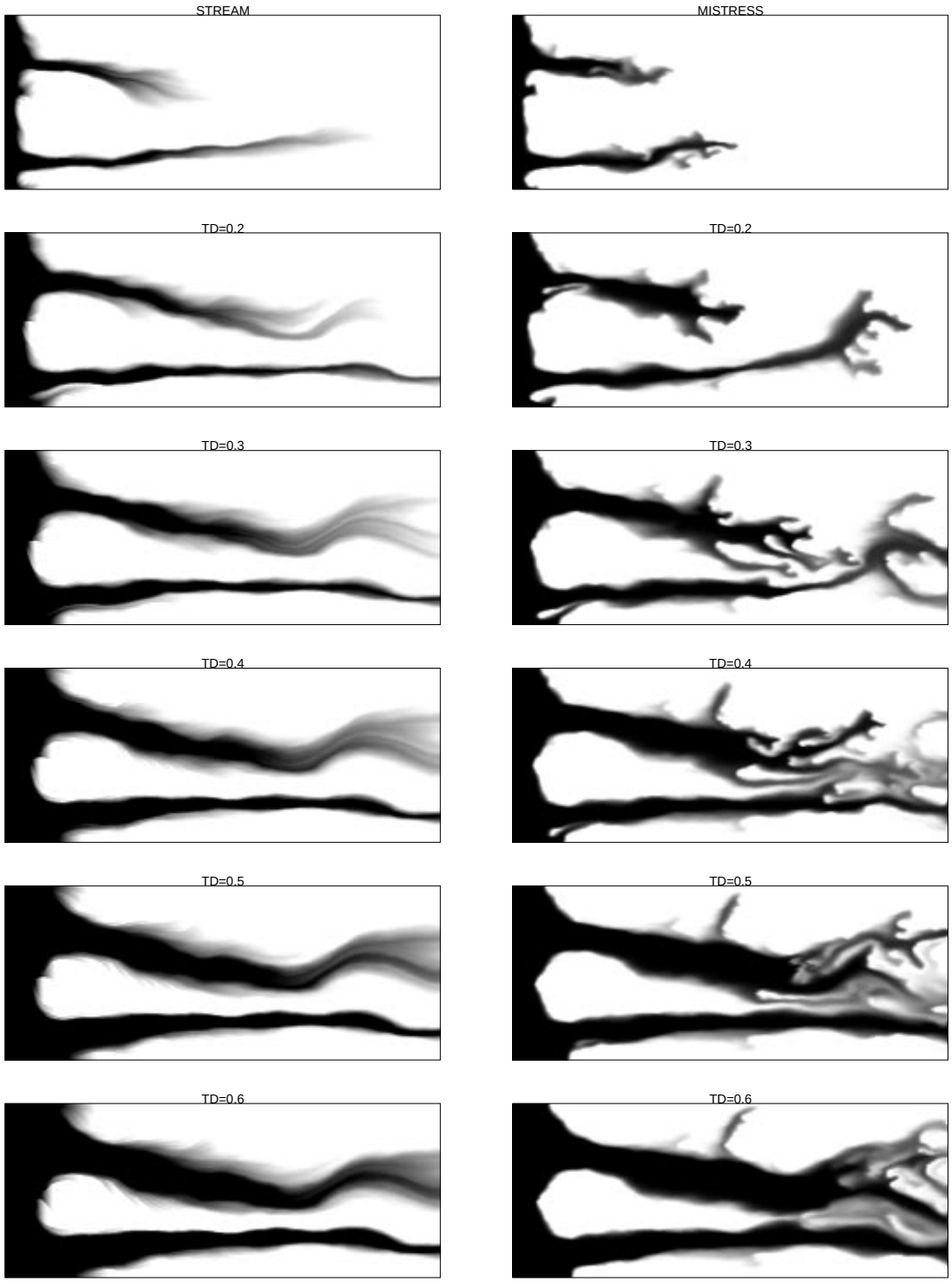

Figure 6.21: *Displacement history for a $M = 10$ displacement using Koval's model along streamtubes in a 250x100 block heterogeneous reservoir with long correlation length (PERM 9 — $\lambda = 0.25$, $\sigma_{\ln k} = 1.0$,$HI = 0.25$).*

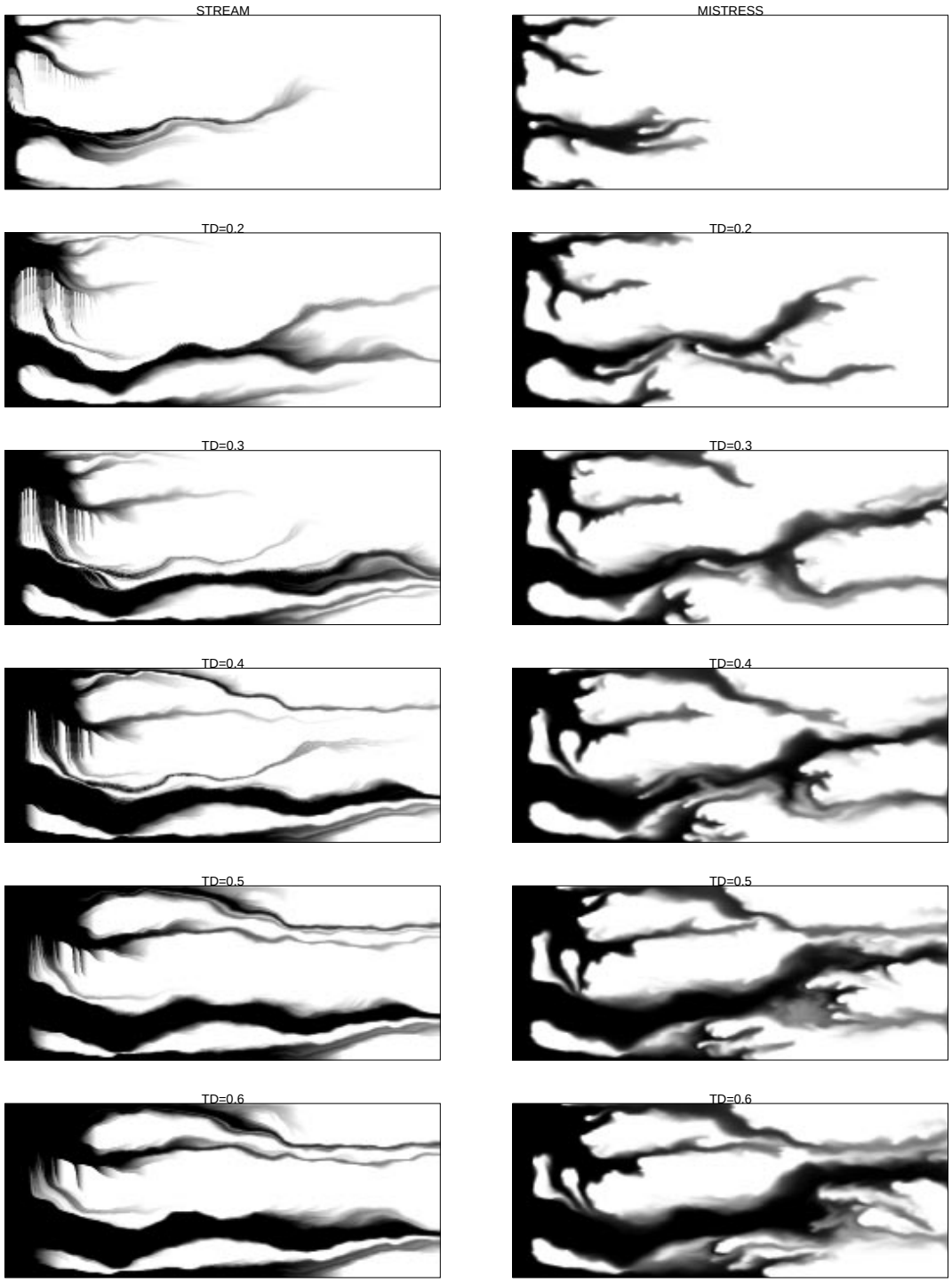

Figure 6.22: *Displacement history for a $M = 10$ displacement using Koval's model along streamtubes in a 250x100 block heterogeneous reservoir with long correlation length (PERM 3 — $\lambda = 0.25$, $\sigma_{\ln k} = 1.6$,$HI = 0.64$).*

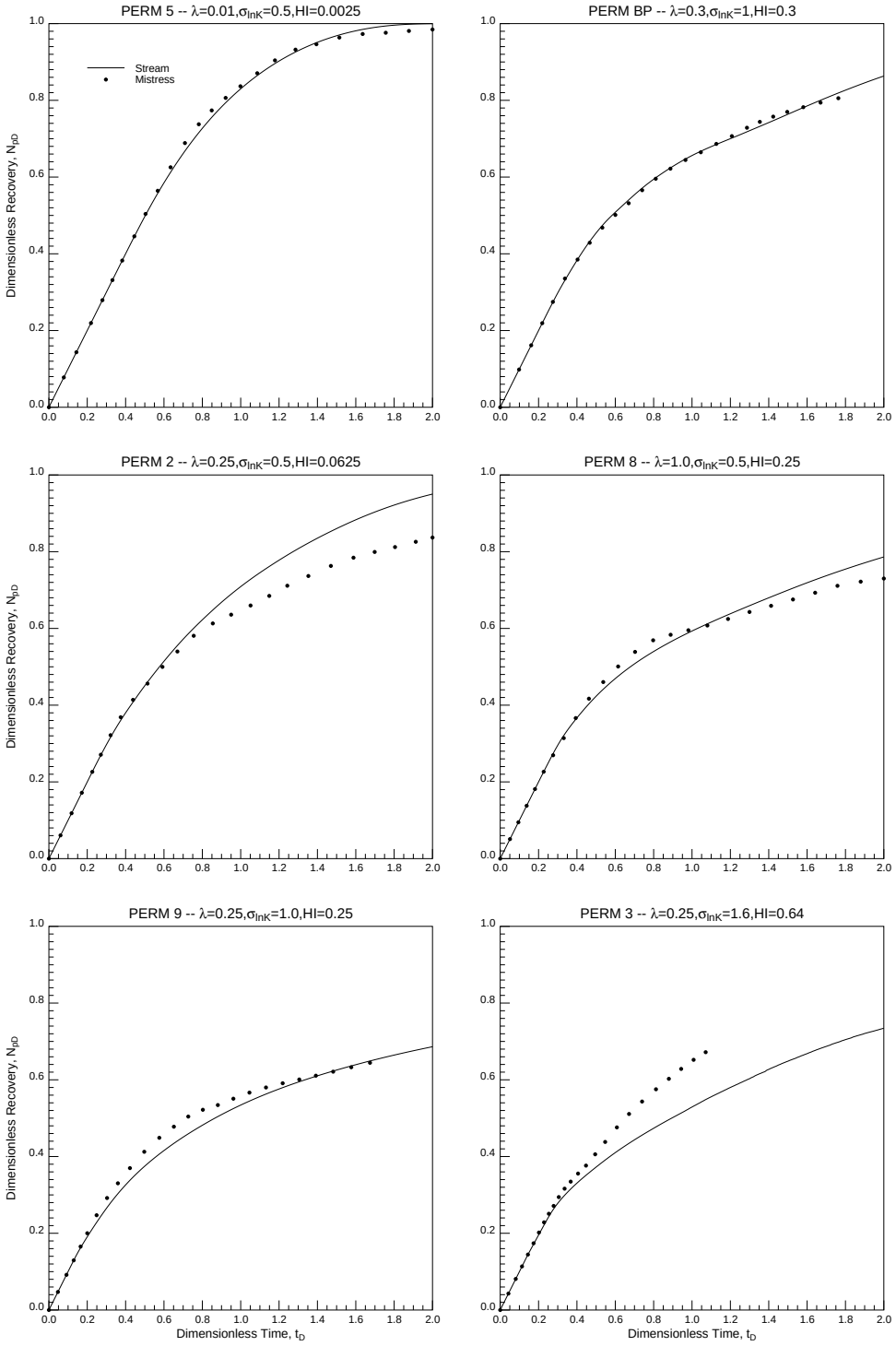

Figure 6.23: *Recovery curves for the displacements shown in Fig. 6.17 - Fig. 6.22.*

behaves quite differently. Heterogeneity is clearly the dominating factor in this displacement, which the streamtube model is able to capture. Mistress also resolves the heterogeneity, but the many fingers, channels, and numerical diffusion cause sufficient 'mixing' to lower the mobility contrast and lead to a substantially higher overall recovery. It is likely that transverse numerical diffusion is significant in this displacement as well. Compared to the streamtube solution, the flow channels in the Mistress solution are thicker, and they coalesce leading to higher recoveries. Mistress also had some numerical difficulties with this particular field due to the extreme permeability contrasts. As a result, run time exceeded 14000 Cray seconds, which was set as a limit for all the other cases, and resulted in the truncated recovery curve[5]. In the remaining cases, the streamtube and Mistress recoveries match, demonstrating the ability of the streamtube approach to capture overall recovery and the main displacement features.

6.7 Convergence

As was mentioned in Chapter 5, the streamtube approach does not have the equivalent of a CFL condition: there is no numerical limitation to the size of the time step, and the solution is always numerically stable. Instead, the question of whether the solution has converged must be addressed explicitly through the number of times the streamtubes are updated to capture the nonlinearity in the total velocity field. A solution is considered converged when the overall recovery does not change with increasing number of updates over a fixed total time t_D.

All the solutions presented in this chapter implicitly used 'sufficient' updates for a converged solution. Fig. 6.24 shows overall recoveries as a function of mobility ratio and number of streamtube updates for the same 250x100 permeability field used in Fig. 6.18. In both cases, $M = 5$ and $M = 10$, the solution can be considered converged by using between 40 and 100 streamtube updates over two pore volumes injected. In fact, the big difference in recovery occurs by going from a single solve (tracer case) to 10 updates. Even by using only 20 updates an acceptable solution

[5]This case actually exhibits some backward flow (vertical finger growing from the second finger at the top to the main flow channel). This is also the reason for the vertical streaks in the streamtube solution.

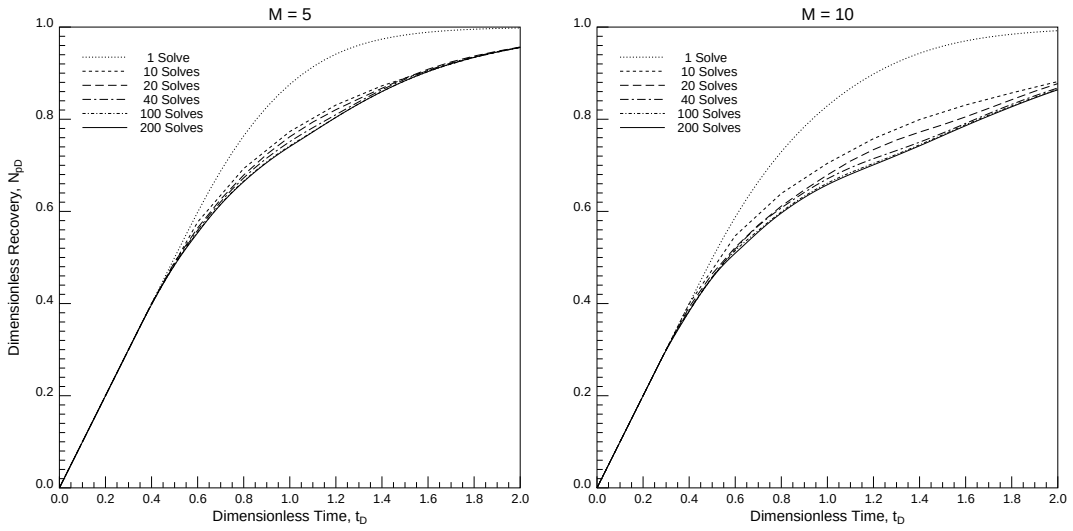

Figure 6.24: *Example of the convergence of the 2D solution for the first-contact miscible case for end-point mobility ratios of 5 and 10 over two pore volumes injected. The permeability field is 125x100 blocks.*

---

can be obtained, with breakthrough predicted correctly. The speed-up,compared to the many thousands of pressure solves required by Mistres, is by two to three orders of magnitude. Herein lies the great advantage of the streamtube approach. Although it makes strong assumptions in generating the two-dimensional solutions and does not capture the subtleties of viscous fingering, it is nevertheless able to find solutions that contain all the main features imposed by the heterogeneity and return accurate overall recoveries, particularly breakthrough times, using orders of magnitude fewer matrix inversions than a traditional finite difference or finite element approach. A particularly good example is given by the strongly heterogeneous case discussed previously and shown in Fig. 6.22. Mistress required 14,400 Cray seconds to reach approximately $t_D = 1$. The streamtube solution, on the other hand, used 100 streamtube updates, which translates to approximately 100 Cray seconds and a speed-up by a factor of 144. A good answer could have been found using fewer solves, as Fig. 6.24 indicates. Using just 20 solves the speed-up would be by a factor of 720.

The recovery curves in Fig. 6.24 are for a permeability field with an intermediate correlation length ($\lambda_c = 0.3$). Fig. 6.25 shows how the number of updates varies

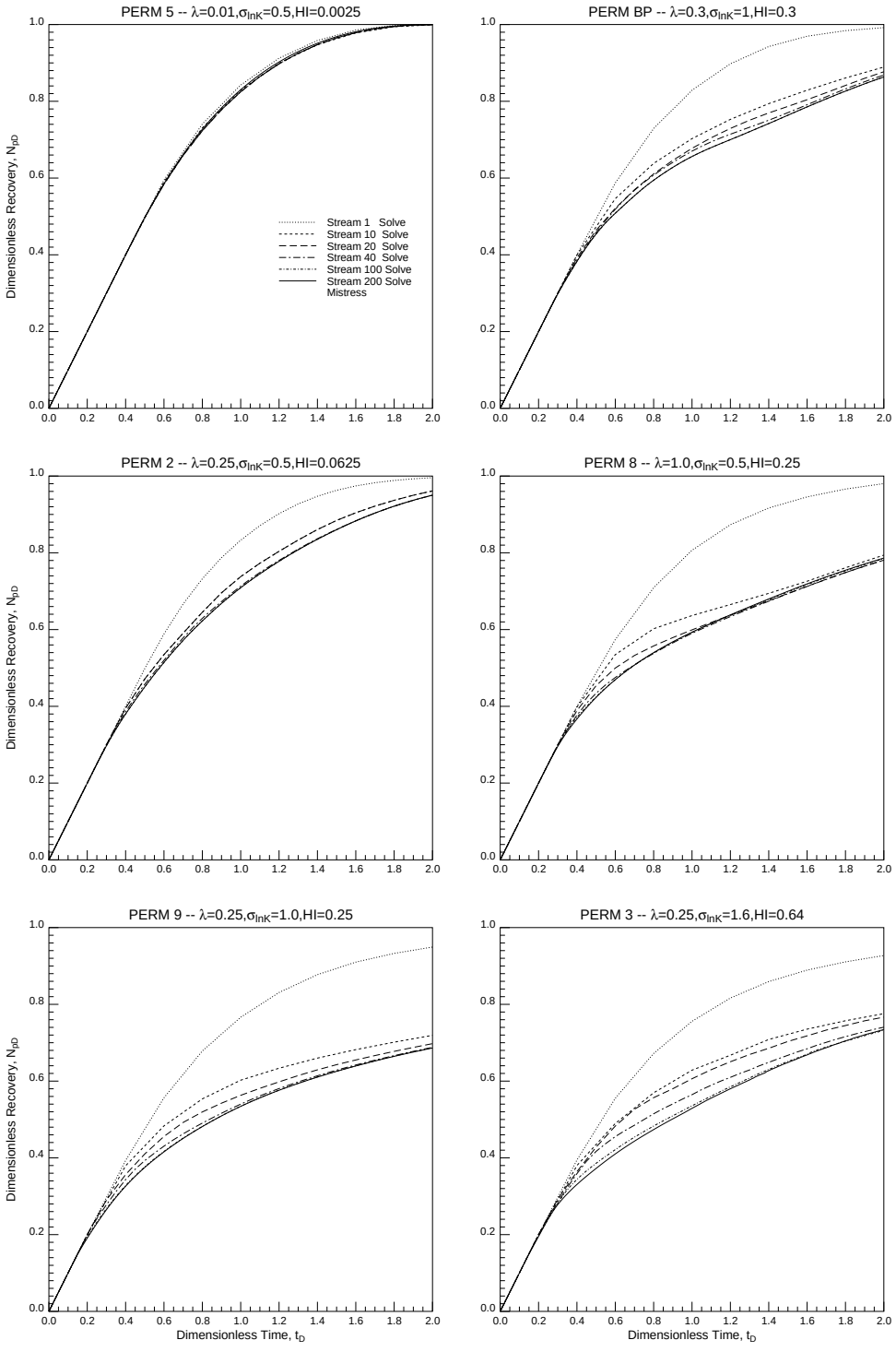

Figure 6.25: *Number of streamtube updates required for convergence of $M = 10$ displacements as a function of heterogeneity of the permeability fields. Koval's one-dimensional solution along the streamtubes was used in all cases.*

with correlation length and the variability of the permeability field. The correlation length is the more important parameter in setting the number of updates to reach a converged solution. For short correlation lengths, there are no particular flow paths for the streamtubes to identify. On average, the streamtubes will not see a major change in their geometry or direction and the recovery is matched because of the one-dimensional viscous fingering model along each streamtube. As the correlation length increases, flow paths are created leading to more dramatic changes in the streamtube geometries. Streamtubes in the high permeability zones will progressively become thinner whereas streamtubes in the low permeability zones progressively become thicker. In order to capture this progressive change in streamtube geometries, the streamtubes must be updated more frequently. Nevertheless, in all cases, the streamtube approach is able to capture overall recoveries requiring approximately 100 solves (or fewer) which represent a speed-up of at least two orders of magnitude compared to the reference finite-difference solutions presented in this chapter.

6.7.1 The Higgins and Leighton Approach

As in the two-phase immiscible case, an alternative to updating the streamtubes to capture the nonlinearity of the displacement is to keep the streamtubes fixed and allocate the flow according to the total flow resistance of each streamtube. Although the Higgins and Leighton approach gave reasonably good recovery curves in the immiscible case, the error in breakthrough time is expected to be more pronounced for first-contact miscible flow due to the stronger nonlinearity of the formulation.

King et al. (1993) modified the Higgins and Leighton's approach and found 'boost' factors for each streamline by calculating the total flow resistance as an integration from the inlet to the isobar located at the tip of the leading finger, rather than using the total length of the streamline from inlet to outlet as required in Eq. 5.12. King et al. realized that at early times the resistance, R_i, would be dominated by the unswept part of the streamtube, thus underestimating the nonlinearity of the displacement. The placement of an isobar at the leading finger is a clever way to reduce the influence of the unswept region on flow resistance, but is also an indication that the approach of Higgins and Leighton will likely fail for displacements that are

strongly nonlinear. Using the isobar modification may be an alternative though it clearly has some problems as well. For example, it may be difficult to pick the 'leading' finger at early times —in fact, choosing the wrong finger will cause convergence onto a wrong solution, because it will force the smallest flow resistance on that particular finger and allow it to grow the fastest. The problem might be corrected by using an isobar that is removed from the leading finger by some appropriate length (although that in turn raises the question of how much to remove the isobar from the leading finger). It is worth noting that the difficulties found by King et al. were anticipated by *Martin et al.* (1973), who found that immiscible displacement with favorable mobility ratios (i.e. piston-like displacements with a mobility difference across the front) could not be predicted as well unfavorable mobility ratio displacement using fixed streamtubes.

Fig. 6.26 compares recoveries for six different permeability fields. Except for the uncorrelated permeability case, the Higgins and Leighton approach falls between the single-solve and the converged streamtube solution, underestimating the nonlinearity of the displacement, particularly breakthrough. By how much the Higgins and Leighton approach will, in general, underestimate the nonlinearity of the displacement though is hard to quantify, because it will depend strongly on the type of correlated permeability structure. Furthermore, the Higgins and Leighton method must be used with caution in light of the inevitable error that is introduced when evaluating the flow resistances using Eq. 5.12, which is likely to become more significant the stronger the system heterogeneity. A case in point is the recovery curves for strongly heterogeneous permeability field (PERM 3) in Fig. 6.26. It is likely that that Higgins and Leighton solution is seeing a substantial error due to the strong heterogeneity of the system (see Fig. 6.22). Thus, the conclusion drawn for the immiscible case applies here as well: given that 40 streamtube updates will generally result in a converged streamtube solution, the small gain in speed offered by the Higgins and Leighton method does not offset the error in recovery that may result.

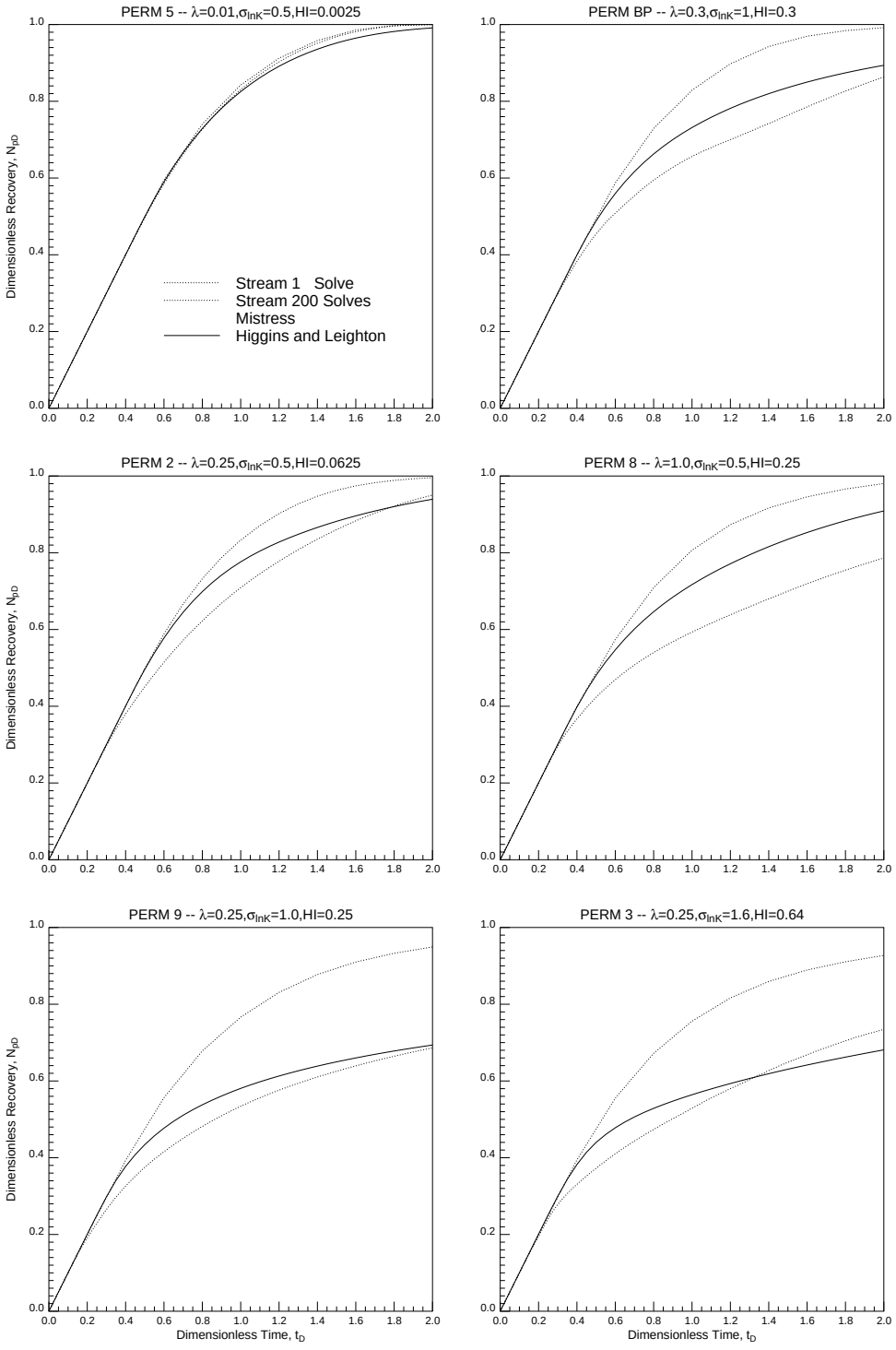

Figure 6.26: *Comparison of the streamtube approach proposed here and the Higgins and Leighton method.*

6.8 Applications

The real power of the streamtube approach lies in its ability to produce solutions that capture the main features imposed by the underlying permeability field while using orders of magnitude less CPU time than traditional simulation techniques. Its strength is not in resolving the details of the displacements, although the control on numerical diffusion may suggest it, but in being able to produce reasonably accurate recoveries very quickly. As such, it is ideally suited for a statistical approach to reservoir forecasting. A large number of statistically identical permeability realizations can be processed to generate a spread in recovery for a particular combination of reservoir geology and displacement mechanism. The streamtube approach may also be used as a filter: the permeability fields that returned the maximum and minimum recoveries can be singled out and used in a much more expensive finite-difference simulation to confirm the uncertainty.

The speed of the streamtube approach can be used in many ways, but becomes particularly appealing when a parameter space of interest includes reservoir heterogeneity, in which case many simulations are required to obtain a statistically meaningful answer. An example of a parameter space that has received considerable attention recently (*Tchelepi 1994, Araktingi and Orr 1993, Waggoner et. al 1992, Sorbie et. al 1992*) has been in the area of unstable displacements through heterogeneous systems. In its most simple representation, the parameter space is given by the end-point mobility ratio (instability) and heterogeneity index HI (heterogeneity), although HI is clearly an incomplete parameter for quantifying the complex geologic structure of a real reservoir. Nevertheless, HI can give some indication of the degree of heterogeneity of the reservoir, particularly if it is used in a statistical sense. A partial sweep of the parameter space is shown in Fig. 6.27. There are 30 recovery curves for each of the six M-HI pairs. Mobility ratio increases from left to right and heterogeneity increases from top to bottom. All underlying permeability fields have 125x50 grid blocks.

Fig. 6.27 quantifies how nonlinearity in the velocity field and heterogeneity interact, but does so statistically, rather than using a single recovery for each case. As

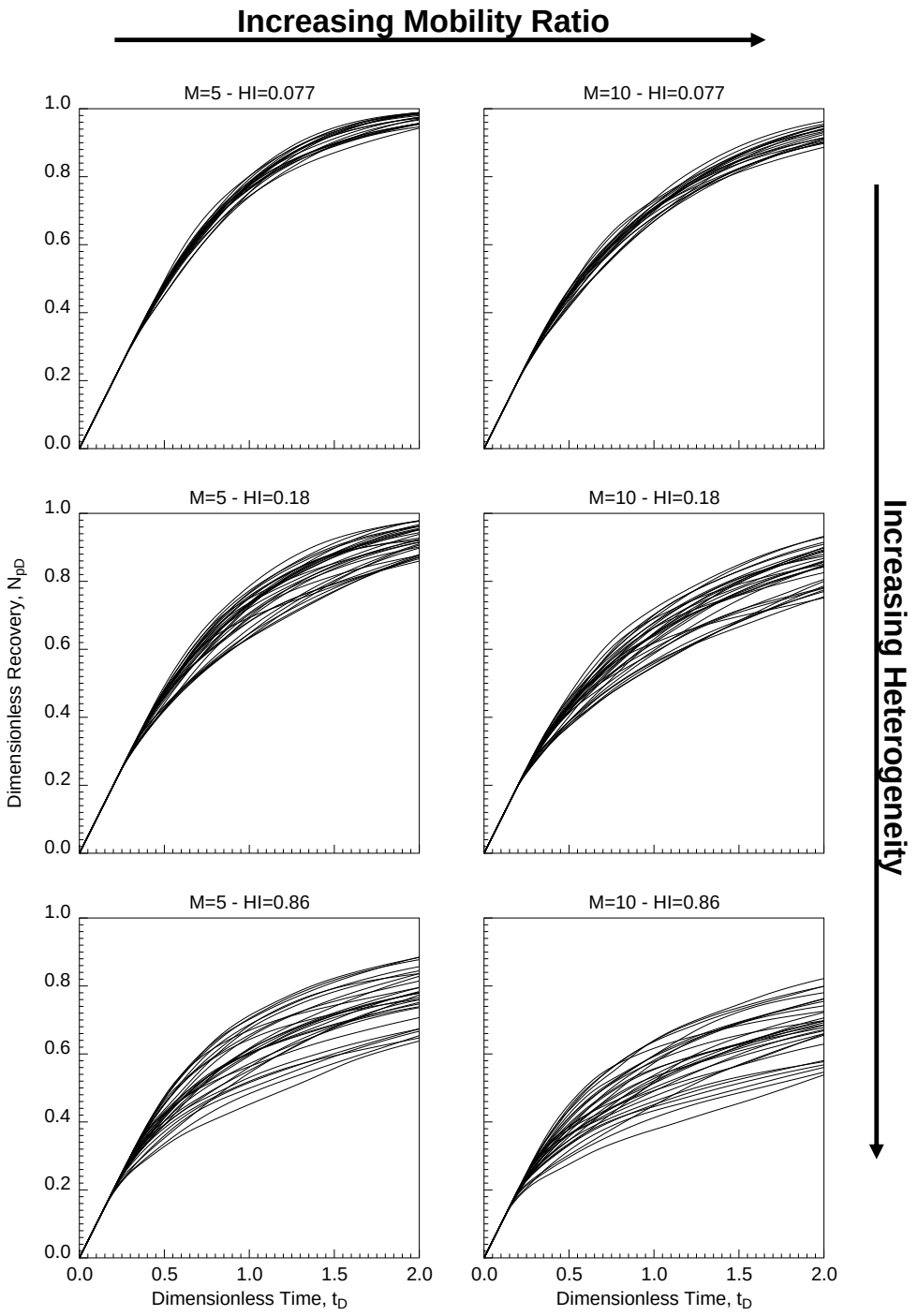

Figure 6.27: *180 recovery curves used in partially sweeping the M-HI parameter space to determine how nonlinearity and heterogeneity interact.*

a result, the weakness of HI as a parameter is traded for a more convincing spread in recovery given by the 30 curves for each case. Some interesting observations may be made from Fig. 6.27: (1) nonlinearity and reservoir heterogeneity interact to create a spread in recovery that increases with increasing mobility ratio and increasing heterogeneity; (2) of the two parameters, heterogeneity is clearly the dominant factor in establishing recovery, although an increasing mobility ratio causes the spread between minimum and maximum recovery to increase slightly; (3) the most important conclusion to be drawn comes from realizing that the recovery areas partially overlap from one case to the next. A higher heterogeneity index or mobility ratio does not automatically lead to lower recoveries compared to a system with lower heterogeneity or mobility ratio, although on average this conclusion does hold. For example, an $M = 5$-$HI = 0.86$ pair exists that will return a higher recovery then an $M = 10$-$HI = 0.86$ pair.

The 180 recoveries of Fig. 6.28 would have taken a prohibitively long time using a traditional finite difference approach. Instead, if the streamtube approach is used as a filter for the 180 images, the number of solutions required to establish firmly the spread in recoveries is just six — two per case — as shown in Fig. 6.28.

6.9 Concluding Remarks

This section demonstrated that the streamtube approach is able to model first-contact miscible displacements in heterogeneous systems using several orders of magnitude fewer matrix inversions than traditional finite difference solutions. Reservoir heterogeneity emerged as the dominant factor in establishing sweep and recovery efficiency. Although diffusion or a viscous fingering model improve on the instabilities inherent in the Riemann approach, they do not change the first-order displacement features imposed by the underlying permeability field. This also holds for all the Mistress solutions presented as comparisons. Thus, the main conclusion to be drawn from this chapter is that it may be sufficient to capture the field scale reservoir heterogeneity structure to obtain a good first order estimate of recovery, even in strongly nonlinear displacements. The variation in recovery due to a specific choice of permeability

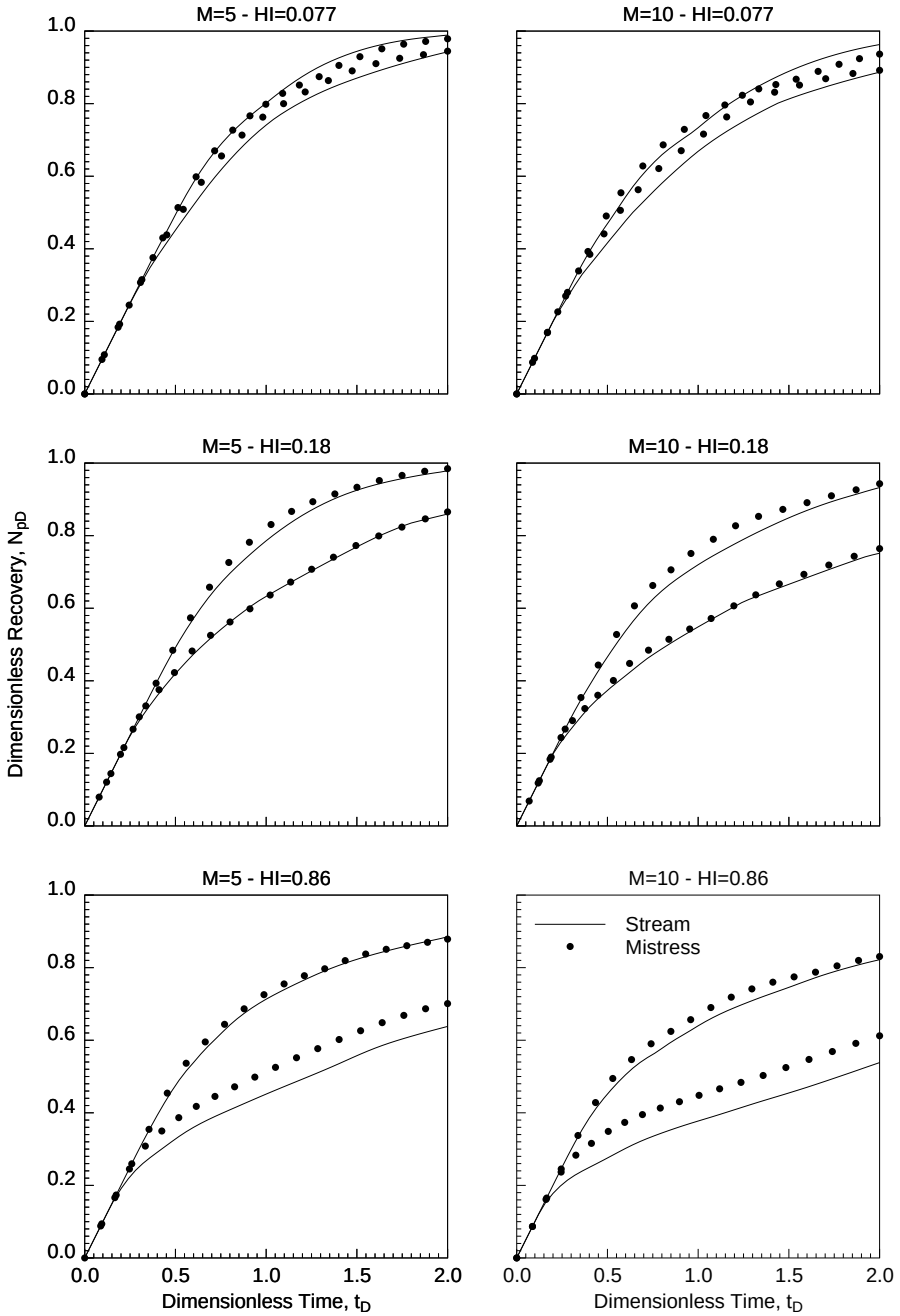

Figure 6.28: *Confirming the spread in recoveries predicted by the streamtube approach by running Mistress on permeability fields associated with the maximum and minimum recoveries for each case predicted by the streamtube approach.*

realization is shown to be substantially larger than the error due to approximations in the streamtube approach. For field scale displacements then, it is preferable to have the capability of processing many geostatistical images to capture the impact of reservoir heterogeneity by a method like the streamtube approach, rather than the capability of accounting for all possible physical phenomena at various scales for a single reservoir image.

Chapter 7

Compositional Displacements

This chapter applies the streamtube approach to compositional displacements through heterogeneous reservoirs. One-dimensional compositional solutions are mapped along streamtubes to model condensing/vaporizing gas displacements. By comparing the diffusion-free streamtube solutions to finite difference solutions, numerical diffusion is shown to mitigate substantially and to eliminate completely any mobility contrast. The streamtube approach is shown to be many orders of magnitude faster than traditional numerical simulation approaches, while still capturing the first order effects on displacement due to reservoir heterogeneity and phase behavior.

7.1 Introduction

Phase equilibrium considerations add a substantial degree of complexity to compositional displacements compared to two-phase immiscible and first-contact miscible displacements. The local equilibrium assumption requires a flash calculation for each grid block at every time step, while the traditional difficulties associated with numerical diffusion and frontal instabilities remain. Simulations become enormously expensive and yet may yield less than satisfactory solutions. Compared to the 'simple' physics described by two-phase relative permeabilities in immiscible displacements or the quarter power mixing rule in first-contact miscible displacements, phase equilibrium and its coupling to multiphase flow poses daunting numerical difficulties. Because of the large computation times involved, compositional simulations are often

run on coarse grids and therefore have substantial amounts of numerical diffusion. It can be difficult to distinguish whether a particular feature is genuinely part of the solution and the physics of the problem or whether it is simply an artifact of the numerical scheme. The problem of numerical diffusion is particularly subtle in compositional simulation because it interacts with the phase behavior to alter displacement performance, sometimes substantially (*Johns et al. 1994, Walsh and Orr 1990, Pande and Orr 1989*).

The streamtube approach is a powerful tool for investigating compositional displacements. With a one-dimensional solution known, the two-dimensional solution for a heterogeneous system can be constructed with the same ease as the tracer, immiscible, or first-contact miscible case. Furthermore, because the one-dimensional solution may be calculated numerically using a large number of grid blocks, or analytically for some special cases (*Johns et al. 1993, Dindoruk et al. 1992, Orr et al. 1993*), numerical diffusion is minimized or even completely absent. Computation times are reduced dramatically, since beyond the savings resulting from the comparably small number of streamtube updates required to capture the nonlinear convective part of the displacement, all the phase behavior is contained within the one-dimensional solution that is mapped along the streamtubes. In other words, the phase behavior is completely decoupled from the underlying cartesian grid used to solve for the local flow velocity, and flash calculations are no longer necessary for each grid block. The streamtube approach also has the substantial advantage of being always numerically stable. Its simple formulation, particularly the decoupling of the phase behavior from the flow field, makes for very robust simulations. The only issue, as in in the displacements described in the previous chapters, is the number of times the streamtubes must be updated to capture the change in the total mobility field. The simplicity of the streamtube approach is in stark contrast to traditional compositional simulation, which faces significant numerical difficulties, particularly in strongly heterogeneous systems, where extreme differences in local flow velocities impose very small time steps and convergence problems.

The interest in multiphase, compositional displacements is spurred principally by enhanced oil recovery methods, such as miscible or near miscible gas injection

processes that can achieve high displacement efficiencies. For modeling purposes, the phase behavior of real hydrocarbon systems is simplified by introducing pseudo components. Pseudo components are created by lumping together components with 'similar' properties in a way that the original phase behavior of the system can be reproduced. For example, *Newley and Merrill* (1991) suggest lumping components with similar K-values at some 'appropriate' feed composition. Using this technique, *Johns et al.* (1993) are able to match successfully a 12-component model using only four pseudo-components. Reducing the number of components to a manageable size is important in numerical simulation, since it impacts directly on the time spent per grid block and time step by the flash routine in calculating equilibrium compositions of the phases. On the other hand, as with all pseudo properties, undesired numerical artifacts may arise, particularly at conditions further away from the ones used to calibrate the model.

The key mechanism to achieve better oil recoveries exploited in high pressure gas injection methods is mass transfer between the highly mobile gas phase and the resident oil phase[1]. If the main recovery mechanism is the partitioning of the oil components into the gas phase, the displacement is said to be vaporizing. Conversely, if the gas components partition into the oil phase, the displacement is said to be condensing (*Stalkup 1983*). Both, vaporizing and condensing mechanisms, lead to better sweep efficiencies by moving towards miscibility, although the gain in recovery is partly offset by increased viscous instability that can lead to fingering and channeling. A vaporizing mechanism can also increase oil recovery by transporting oil components through the more mobile gas phase to the production well. Displacements that are vaporizing and/or condensing can lead to multicontact miscibility (MCM) by repeated mass transfer between the phases. Although the injected gas phase and the resident oil phase may not be miscible at first, as the displacement takes place, repeated vaporization of the volatile oil components into the gas phase or condensation of injected components into the oil phase can lead to a miscible

[1]In real reservoirs, particularly reservoirs that have been previously waterflooded, a third, aqueous phase is generally present as well, thereby considerably complicating the flow aspect since three-phase relative permeabilities are required. All the work presented here assumes only two, non-aqueous flowing phases to be present.

displacement. Multicontact miscibility is usually illustrated using a pseudoternary system (*Stalkup 1983*). The key condition for achieving multicontact miscibility is that the initial oil composition and the injected gas composition lie on opposite sides of the critical tie-line extension. In a ternary system, a MCM displacement can be classified as vaporizing or condensing depending on the position of the initial and injected compositions: if the injected gas composition is in the area of tie-line extensions, the displacement will be vaporizing. However, if the oil composition is in the area of tie line extensions then the displacement will be condensing.

Ternary representations allow explanation of vaporizing or condensing gas drives only. Yet experimental observations of enriched gas floods (*Stalkup 1965*) show that displacements may be both condensing and vaporizing at the same time (*Zick 1986, Stalkup 1987, Lee et al. 1988*). The leading edge of the displacement may show condensation of components into the oil phase, while the trailing edge may show vaporization of components into the gas phase. Depending on initial and injected compositions of the oil and gas phase as well as pressure and temperature of the reservoir, a displacement may therefore be purely vaporizing, purely condensing, or both. If the displacement has vaporizing as well as condensing characteristics, a pseudoternary system is no longer able to capture this type of behavior. In order to model a combined vaporizing/ condensing displacement a minimum of four pseudo components is necessary (*Zick 1986, Johns et. al. 1992*).

7.2 One-Dimensional Solutions

As for all displacement mechanisms discussed in the preceding chapters, applying the streamtube technique to model compositional displacements in heterogeneous systems centers on the availability of a one-dimensional solution. Substantial progress on analytical solutions has been reported recently (*Johns et al. 1993, Dindoruk et al. 1992, Orr et al. 1993, Johns 1992, Dindoruk 1992, Monroe et al. 1990, Monroe 1986*), and analytical solutions have been presented for multicomponent problems that have constant initial and injected conditions (Riemann conditions) with either no volume change on mixing (*Johns et al. 1993, Johns 1992*) or volume change on mixing

(*Dindoruk et al. 1992, Dindoruk 1992*). For an extensive treatment on the subject the reader is referred to the dissertations of *Johns* (1992) and *Dindoruk* (1992). The key results presented by Johns, Dindoruk, and Orr include a method to construct two-phase, multicomponent solutions without having to resort to a systematic elimination technique, the existence of $n_c - 1$ key tie lines ($n_c - 3$ of which are called crossover tie lines), and the classification of the displacement according to the volatility of its individual components (K-values).

The starting point for the analytical solutions is the $i = 1, \cdots, n_c$ one-dimensional, mass balance equations given by (*Lake 1989, p.29*)

$$\frac{\partial}{\partial t}\left(\phi \sum_{j=1}^{N_P} \rho_j S_j \omega_{ij}\right) + \frac{\partial}{\partial x}\left(\sum_{j=1}^{N_P} \rho_j \omega_{ij} u_j - \phi S_j \rho_j K_{ij} \frac{\partial \omega_{ij}}{\partial x}\right) = 0 \quad . \tag{7.1}$$

Assuming (1) no diffusion/dispersion and (2) defining the fractional flow of phase j as

$$f_j = \frac{u_j}{u_t} \quad , \tag{7.2}$$

where u_t is simply the total Darcy velocity, gives the governing material balance equations as

$$\frac{\partial}{\partial t}\left(\sum_{j=1}^{N_P} \rho_j S_j \omega_{ij}\right) + \frac{\partial}{\partial x}\left(\frac{u_t}{\phi} \sum_{j=1}^{N_P} \rho_j \omega_{ij} f_j\right) = 0 \quad , \quad i = 1, n_c \quad . \tag{7.3}$$

Eq. 7.3 are n_c coupled, first order hyperbolic equations. In fact, only $n_c - 1$ need to be solved since the normalized overall compositions z_i

$$z_i = \frac{\sum_{j=1}^{N_P} \rho_j S_j \omega_{ij}}{\sum_{j=1}^{N_P} \rho_j S_j} \tag{7.4}$$

add-up to one, i.e.

$$\sum_{i}^{n_c} z_i = 1 \quad . \tag{7.5}$$

If there is no volume change on mixing, then the phase density ρ_j is a function of the phase composition and the pure component (constant) densities ρ_{ci} and given by

$$\rho_j = \frac{1}{\sum_i^{n_c} \frac{x_{ij}}{\rho_{ci}}} \quad . \tag{7.6}$$

In this case, the total velocity u_t is constant and the equations can be simplified by

expressing them in terms of volumetric concentrations. If there is volume change on mixing, then the volume of the mixture is no longer a linear function of the phase compositions; the phase density ρ_j must be found through an equation of state model and u_t will no longer be constant (*Dindoruk 1992*).

The solution to Eq. 7.3 subject to Riemann boundary conditions will be composed of shocks, constant states, and rarefaction waves. Shocks are introduced when the continuous solution to Eq. 7.3 is nonphysical, as in the case of multivaluedness, for example. Constant states are necessary to connect shocks and rarefaction waves into a continuous solution and occur when a path switching point in composition space has two velocities associated with it. Finally, rarefaction waves are simply genuine smooth continuous solutions to Eq. 7.3. The key in constructing the unique solution for a particular set of Riemann conditions centers on imposing (1) the velocity constraint and (2) the entropy condition on the multiple, mathematically possible solutions (*Johns 1992, Dindoruk 1992*).

Analytical solutions are invaluable. They are the reference solutions against which to compare numerical solutions, and allow a rigorous analysis of the physics at play, as the extensive discussions on vaporizing and condensing gas drives by *Johns et al.* (1993), *Dindoruk et al.* (1992), and *Orr el al.* (1992) demonstrate. Nevertheless, all one-dimensional solutions used here were obtained numerically. The reason for this was to guarantee consistency in the phase behavior representation between the one-dimensional solutions used along the streamtubes and the two-dimensional 'reference' solutions found using the same compositional simulator in 2D. In other words, the two-dimensional compositional solutions used for comparing the streamtube solutions were obtained by simply increasing the number of blocks in the second dimension and specifying the heterogeneous permeability field, while leaving the PVT data section untouched.

7.3 Reservoir Heterogeneity and Phase Behavior

A key issue in multiphase, multicomponent flow through heterogeneous porous media revolves around the question of how phase behavior and reservoir heterogeneity

interact to define the displacement of resident hydrocarbons. Although several investigators have studied the problem, many questions remain, particularly with regard to conclusions drawn from numerical simulations due to the insufficient number of grid blocks generally used in the published studies.

The most convincing results on how phase behavior and heterogeneity interact, albeit on a microscopic scale, come from flow-visualization experiments (*Campbell and Orr 1985, Bahralolom et al. 1988*). *Bahralolom et al.* (1988) show the existence of a relatively high residual oil saturation in preferential flow paths of a CO_2/crude-oil displacements. They point out that although three different mechanisms –transverse dispersion, viscous crossflow, and capillary crossflow– may have contributed to creating this type of residual saturation, capillary crossflow is the most likely mechanism responsible for their observations. They are also quick to point out that their experiments are not to scale: pores are an order of magnitude larger than those in actual rocks and the flow velocity is also larger than what would be observed on a field scale. Nevertheless, the results are substantial in that they directly link higher residual oil saturations to the heterogeneity of the system. Thus, preferential flow paths not only cause early breakthrough, but may also cause an increased residual saturation.

Similar behavior was predicted by *Gardner and Ypma* (1984) by numerical simulations of CO_2 corefloods. They noticed that residual oil saturations increased in zones where pure CO_2 fingers had first displaced the resident oil and attributed this phenomenon to the combined action of transverse dispersion and viscous crossflow. The numerical simulations of Gardner and Ypma were for mildly heterogeneous systems on 100x10 and 40x10 grids, and all permeability fields were uncorrelated. The phase behavior of a CO_2/Wasson crude system was represented using two pseudo components, and the phase viscosities were computed using a quarter-power mixing rule. The results by Gardner and Ypma are important, but are also symptomatic of the difficulties associated with extracting information from numerical simulations of compositional displacements. The small number of blocks in the vertical direction, the uncorrelated permeability field, the two pseudo-component phase behavior, and the quarter-power mixing rule for the phase viscosities introduce errors and assumptions that may substantially 'contaminate' the final answer. As a result, it becomes

extremely difficult to give any conclusive answer as to how phase behavior and heterogeneity may interact, and to what extent their results were due to numerical artifacts.

A more recent attempt to numerically study CO_2 displacements, this time on a field scale, has been by *Chang et al.* (1994). Chang et al. simulated the displacement of a three-component characterization of a Maljamar separator oil by pure CO_2 at 1200 psi and $90°F$ through a variety of different heterogeneous systems. With their simulator's third-order finite difference scheme as justification, Chang et al. used a relatively coarse 80x20 mesh for their simulations. In light of this, their main conclusion —that viscous fingering is not a dominant flow pattern in field-scale CO_2 displacements— is questionable. The study by Chang et al. again underlines the inherent difficulties in extracting meaningful physical insight from compositional simulations; although channeling and gravity override may in fact be dominant displacement mechanisms on a field scale (as Chang et al. suggest) the large number of degrees of freedom introduced by the phase behavior description (number of pseudo components, equation of state model, viscosity correlations, etc...) and reservoir heterogeneity, coupled with the well-known difficulties introduced by numerical diffusion and uncertainties in the relative two and three-phase flow properties combine to give a highly nonlinear, uncertain problem formulation from which it is almost impossible to conclude that viscous fingering is not important on a field scale.

Given the difficulties associated with compositional simulations, one of the central issues of this chapter is to try to understand how 'good' finite difference solutions really are, and what they may be expressing about the interaction of phase behavior and reservoir heterogeneity. The strategy is to combine the accurate one-dimensional, multiphase, multicomponent solutions with the simple streamtube formulation and compare the resulting two-dimensional solution to full, two-dimensional finite-difference solutions. In particular, because the streamtube solutions do not account for transverse mixing mechanisms, have no numerical diffusion, and emphasize the system heterogeneity, the hope is that by comparing them to finite difference solutions something can be inferred about the relative importance of these mechanisms.

7.4 UTCOMP - A Finite Difference Simulator

UTCOMP (*Version 3.2, 1993*) is an IMPES-type, isothermal, three-dimensional, compositional simulator developed at the University of Texas at Austin. The formulation of UTCOMP is described by *Chang* (1990) and *Chang et al.* (1990). A rigorous Gibbs stability test is done before all flash calculations to determine the number of phases. Nonaqueous fluid properties can be modeled using either the Peng-Robinson or Redlich-Kwong equation of state. Phase viscosities are found using the Lohrenz-Bray-Clark correlation (*Lohrenz et al. 1964*). A particularly nice feature of UTCOMP is the possibility of controlling numerical diffusion by specifying the numerical scheme for generating the system of linear equations. Single-point upstream weighting and a third order, total variation diminishing (TVD) scheme were used here to study the impact of numerical diffusion on the solutions.

7.5 Three-Component Solution

An example of a high volatility intermediate (HVI) ternary system is given by CH_4 /CO_2/C_{10} at 1600 *psia* and 160°*F* (*Johns 1992, p. 122*). The name 'high volatility intermediate' refers to the strict ordering of the K-values for all compositions and the fact that the intermediate component K-value is greater than one ($K_{CO_2} > 1$)[2]. This means that CO_2 will preferentially reside in the more mobile gas phase. A HVI-system can give rise to either a condensing or vaporizing drive depending on the initial and injected compositions. The displacement of a 30/70 CH_4/C_{10} oil by pure CO_2, for example, is a condensing gas drive.

The CH_4/CO_2/C_{10} system shown will not develop MCM since the injection and initial compositions are both in the region of tie line extensions.

The one-dimensional solution shown was found by *Johns* (1992) using the Peng-Robinson equation of state (*Peng and Robinson 1976*), the Lohrenz-Bray-Clark correlation for the phase viscosities (*Lohrenz et al. 1964*), and Corey-type relative

[2]In other words, $K_{CH_4} > K_{CO_2} > 1$ while $K_{C_{10}} < 1$. If all K-values were greater than one, $K_{CH_4} > K_{CO_2} > K_{C_{10}} > 1$, the system would be first-contact miscible.

Component	M_w	P_c (psia)	T_c (oF)	V_c (ft^3/lb-mol)	ω
CO_2	44.01	1071.0	87.90	1.5060	0.2250
CH_4	16.04	667.8	-116.63	1.5899	0.0104
C_{10}	142.29	305.7	652.10	9.6610	0.4900

Component	Interaction Parameters		
	CO_2	CH_4	C_{10}
CO_2	0.0000	0.1000	0.0942
CH_4	—	0.0000	0.0420
C_{10}	—	—	0.0000

Table 7.1: *Component properties for the three-component model.*

permeabilities with an exponent of 2 and a residual oil saturation of $S_{or} = 0.2$: $k_{rg} = S_g^2$; $k_{ro} = (1 - S_{or} - S_g)^2$. Pressure and temperature were 1600 *psia* and $160°F$ respectively. Component properties as shown in Table 7.1. The composition profiles in Finding the one-dimensional composition profiles is the first step in constructing a two-dimensional compositional solution for a heterogeneous system using streamtubes. In addition though, the one-dimensional profile for the total mobility is required as well. In the two-phase, immiscible problem and in the first-contact miscible case, finding the total mobility for each grid block was a simple function of the block saturation/concentration. In compositional flow finding the total mobility is complicated by the fact that the phase viscosities are functions of composition. For the purposes of this work, UTCOMP , which also uses the Lohrenz-Bray-Clark correlation, was simply modified to output total mobility as well. Example numerical solutions (including the total mobility profile) for the $CH_4/CO_2/C_{10}$ system, found using 100 and 500 grid blocks and the third order TVD-option, are shown in Fig. 7.1.

The numerical solutions in Fig. 7.1 are able to capture all the essential shocks in this condensing gas drive, and particularly the 500-block solution has an acceptable level of numerical diffusion. The numerical solutions do not have exactly the same shock speeds as the analytical solution found by *Johns* (1992), because the residual oil saturation was set to zero for simplicity, and the solutions account for volume

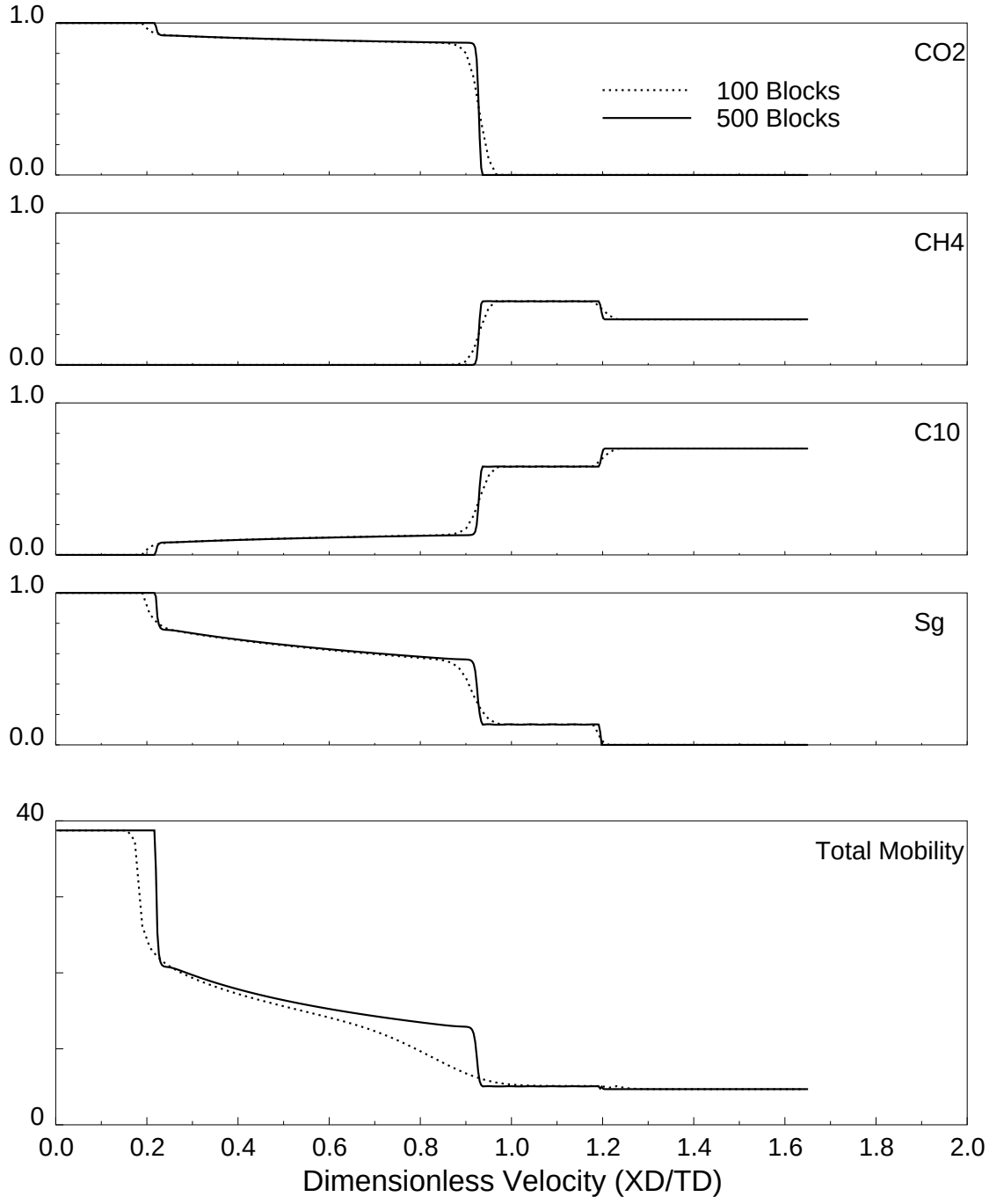

Figure 7.1: UTCOMP *one-dimensional numerical solution, using 100 and 500 grid blocks and a third order TVD-scheme to control numerical diffusion, for the* $CH_4/CO_2/C_{10}$ *condensing gas drive.*

change on mixing, whereas Johns used a value of 0.2 for the residual oil saturation and did not account for volume change. For streamtube modeling purposes, the total mobility profile is possibly the most important piece of information, because it indicates the strength of the nonlinearity of the total flow velocity and directly ties into the solution of the streamtubes. For this particular case, although the end-point mobility ratio is approximately 8, the mobility ratios across the two fronts, which are separated by a long rarefaction wave, are approximately 3 and 2. In other words, the mobility contrast is reduced considerably by the phase behavior alone. To what extent numerical diffusion may affect total mobility is already anticipated by the disappearance of the leading mobility front due to numerical diffusion in the 100 grid block solution.

An almost diffusion-free compositional solution through a heterogeneous domain can now be found by mapping the 500 grid block, TVD solution along streamtubes. Composition and saturation maps for a 125x50 block heterogeneous reservoir[3] at $t_D = 0.3$ and $t_D = 0.5$ are shown in Fig. 7.2. As expected, the fronts are clearly visible and, although the end-point mobility ratio is $M \approx 8$, the displacement does not suffer from the 'instabilities' seen in the no-diffusion solutions of Chapter 6. The reason for the stability, of course, is that the phase behavior mitigates the initial mobility ratio contrast by creating two 'weaker' fronts which are separated by a long rarefaction wave. As in Chapter 6, it is important to remember that all the scaling arguments brought forward there apply here as well. In other words, the 500 grid block numerical solution used along the streamtubes has a very small diffusive length scale, and although the two resulting fronts have smaller mobility ratios than the original end-point mobility ratio, they remain unstable and can be thought of in the same way as the no-diffusion, unit velocity wave solution in the ideal miscible case for $M > 1$. Technically then, the instability across the two fronts, even if small, would require some form of mitigation, possibly using a viscous fingering model as suggested by *Blunt et al.* (1994).

Figs. 7.3 and 7.4 compare the two-dimensional UTCOMP solution found using a

[3]The permeability field used in this example is an upscaled version of the 250x100 permeability field used in Fig. 4.1, Fig. 6.7, and Fig. 6.15. The upscaling was done by simply taking a geometric average of 2x2 grid blocks.

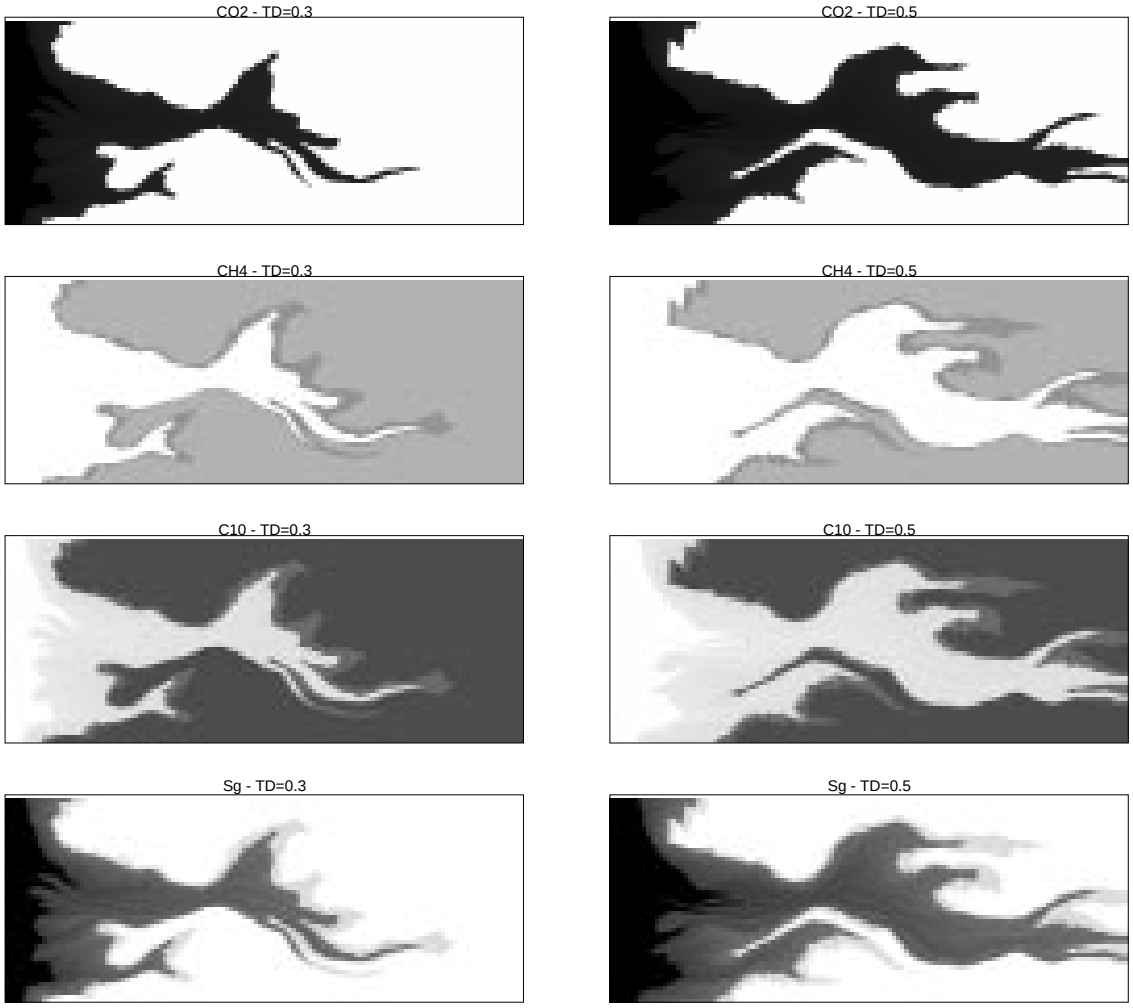

Figure 7.2: *Two-dimensional, 3 component condensing gas drive in a 125x50 heterogeneous block reservoir at* $t_D = 0.3$ *and* $t_D = 0.5$. *The one-dimensional solution is shown in Fig. 7.1.*

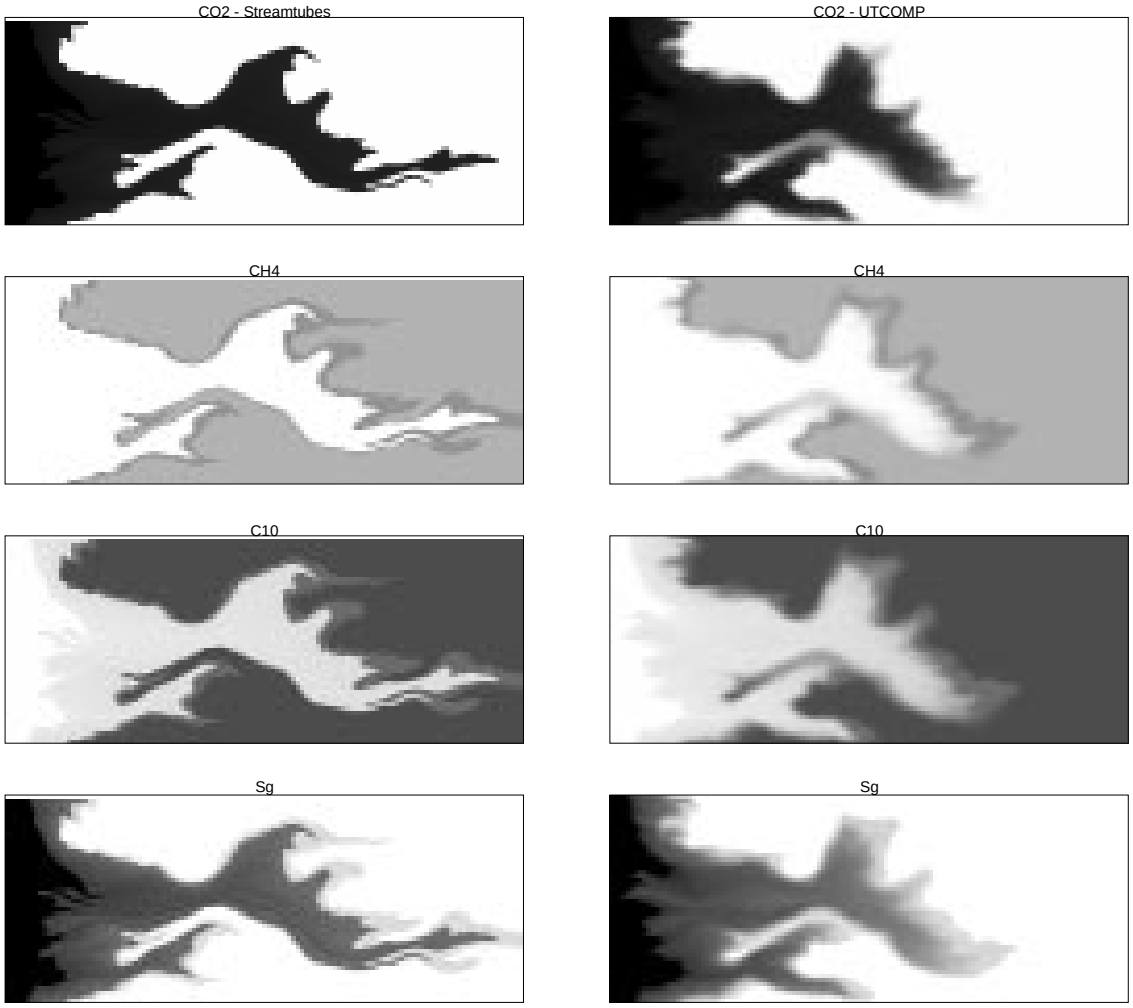

Figure 7.3: *Comparison of the streamtube solution with the UTCOMP solution at* $t_D = 0.4$. *The UTCOMP solution was found using a third-order TVD scheme.*

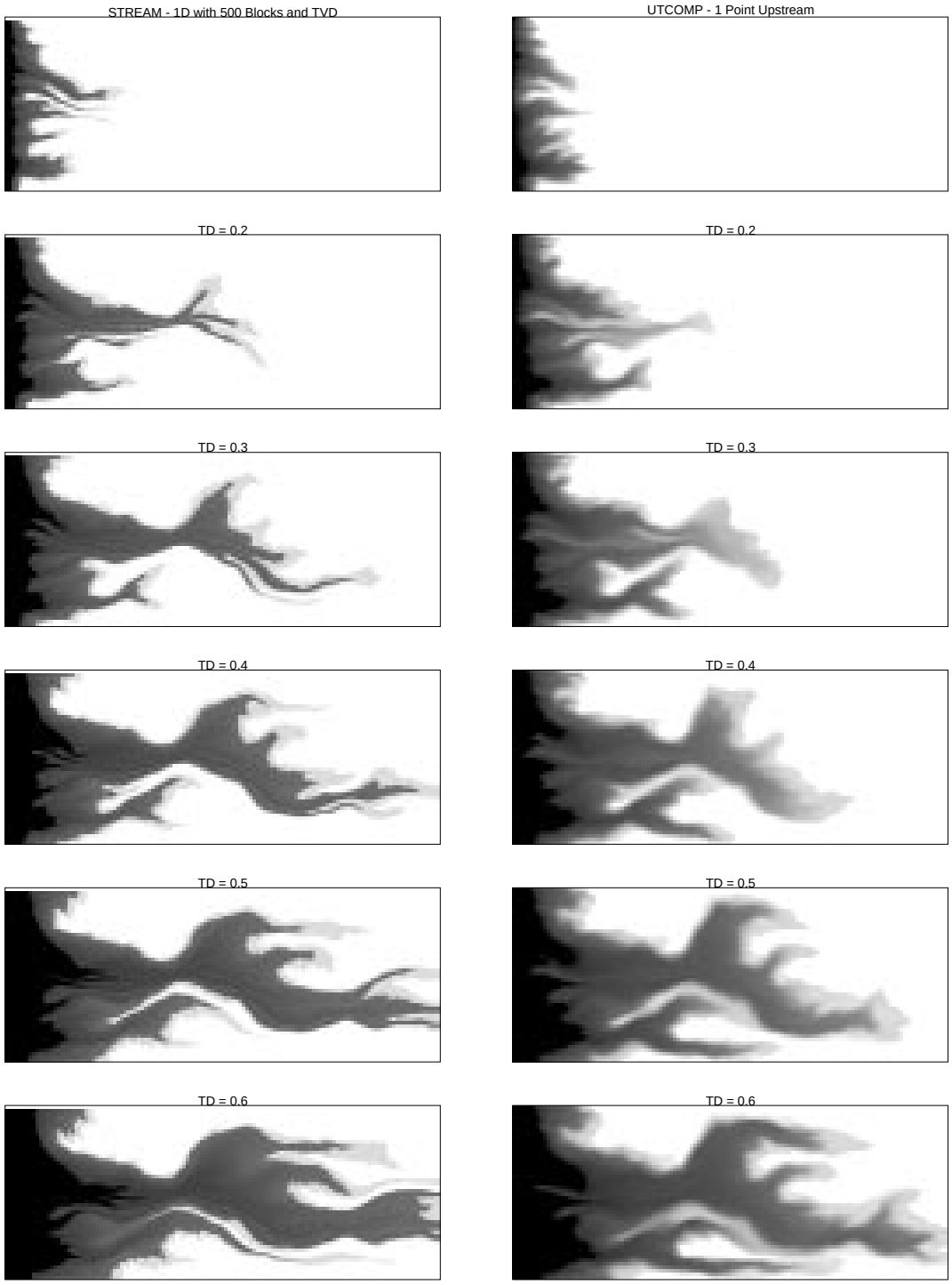

Figure 7.4: *Comparison of the evolution in time of the gas saturation. The streamtube solution was found using a 500 grid block one-dimensional solution, while the UTCOMP solution was found using a third-order TVD scheme.*

third-order TVD scheme to the streamtube solution; Fig. 7.3 compares composition and saturation profiles at $t_D = 0.4$, whereas Fig. 7.4 compares only the gas saturation profiles from $t_D = 0.1$ to $t_D = 0.6$. The agreement is very good, particularly considering that UTCOMP required approximately 5000 Cray seconds per 0.1PV injected, whereas the streamtube solution required approximately 2-3 Cray seconds, a speed-up factor of more than three orders of magnitude. Both solutions clearly capture the same overall flow characteristics imposed by the underlying heterogeneity field. Figs. 7.3 and 7.4 are encouraging, because they suggest that the streamtubes can be combined successfully with a one-dimensional compositional solution to model a two-dimensional displacement at a significantly reduced cost, with the error introduced by the Riemann approach remaining 'small' thereby not significantly altering the displacement mechanism.

Nevertheless, although the comparison is good and the streamtube solution looks like a 'sharper' UTCOMP solution, a noticeable difference is the more stable behavior of the UTCOMP solution in which the leading front has not penetrated as far as in the streamtube solution. This difference raises an important question: is the stability in the finite difference solution an artifact due to numerical diffusion or a genuine physical phenomenon, possibly resulting from mixing due to viscous cross-flow? Considering that the number of blocks in the main direction of flow is only 125, and that a TVD-scheme in 2D does not result in the same numerical diffusion control as in 1D, it is possible that numerical diffusion is the main reason for the more stable looking UTCOMP solution. Two additional simulations were performed in an attempt to answer this question: (1) a UTCOMP solution was found for the same 125x50 grid but using a one-point upstream scheme to show the effects of numerical diffusion more clearly, and (2) a diffused one-dimensional compositional solution was mapped along the streamtubes in an attempt to include numerical diffusion in the streamtube solution[4].

[4]A simulation with a refined 250x100 grid and a third-order TVD scheme, while maintaining the same heterogeneity structure, was attempted using UTCOMP as well. Unfortunately, computation costs approached 70,000 Cray seconds ($\approx 20hr$) per 0.1 PV injected, forcing the simulation to be aborted.

(1) - 125x50 1Pt Upstream Solution

Fig. 7.5 compares the UTCOMP one-point upstream weighting solution to the streamtube solution. The degradation in the UTCOMP solution is noticeable compared to the TVD solution: the fronts are more diffused, the solution now looks more stable, and breakthrough occurs later still than in the TVD solution. Fig. 7.5 suggests that the mitigation of the original mobility contrast in UTCOMP solutions is likely due to numerical diffusion rather than to crossflow.

(2) - Diffused Streamtube Solution

The comparison of UTCOMP solutions with TVD and single-point upstream weighting suggest that the frontal instability is mitigated substantially by numerical diffusion. To corroborate this, it should be possible to find a 'diffused' one-dimensional solution along the streamtubes that would lead to a solution similar to the one obtained using finite differences. The one-dimensional solution used in the streamtube solution was obtained using 500 grid blocks and a third-order TVD scheme, which produced a solution with relatively sharp fronts. But given the fact that only 125 blocks are present in the main direction of flow and that a TVD scheme in two-dimensions does not necessarily have the same numerical diffusion control as it does in one dimension[5], a one-dimensional solution using 100 grid blocks and single point upstream weighting was mapped along the streamtubes. A difficulty associated with mapping a 'diffused' one-dimensional solution is that the solution is no longer scalable by x_D/t_D, as is shown in Fig. 7.6. There are 10 curves in Fig. 7.6, each representing a solution at time increments of $\Delta t_D = 0.1$ starting from $t_D = 0.1$. The solution clearly tends to 'sharpen-up' with time, although even at $t_D = 1.0$, the solution is still suffering from numerical diffusion. To capture the time dependence of the diffused, one-dimensional solution in Fig. 7.6, the solution was mapped along the streamtube for the corresponding time interval: the first curve was used in the streamtube simulator to find solutions in the range of $t_D = 0.0$ and $t_D = 0.1$, the second curve for solutions between $t_D = 0.1$ and $t_D = 0.2$, and so on. Although this approach is only a rough attempt to

[5]In general, any method that is TVD in two dimensions will be at most first order accurate, although the accuracy can be increased to second order if Strang splitting is used (*LeVeque 1992*).

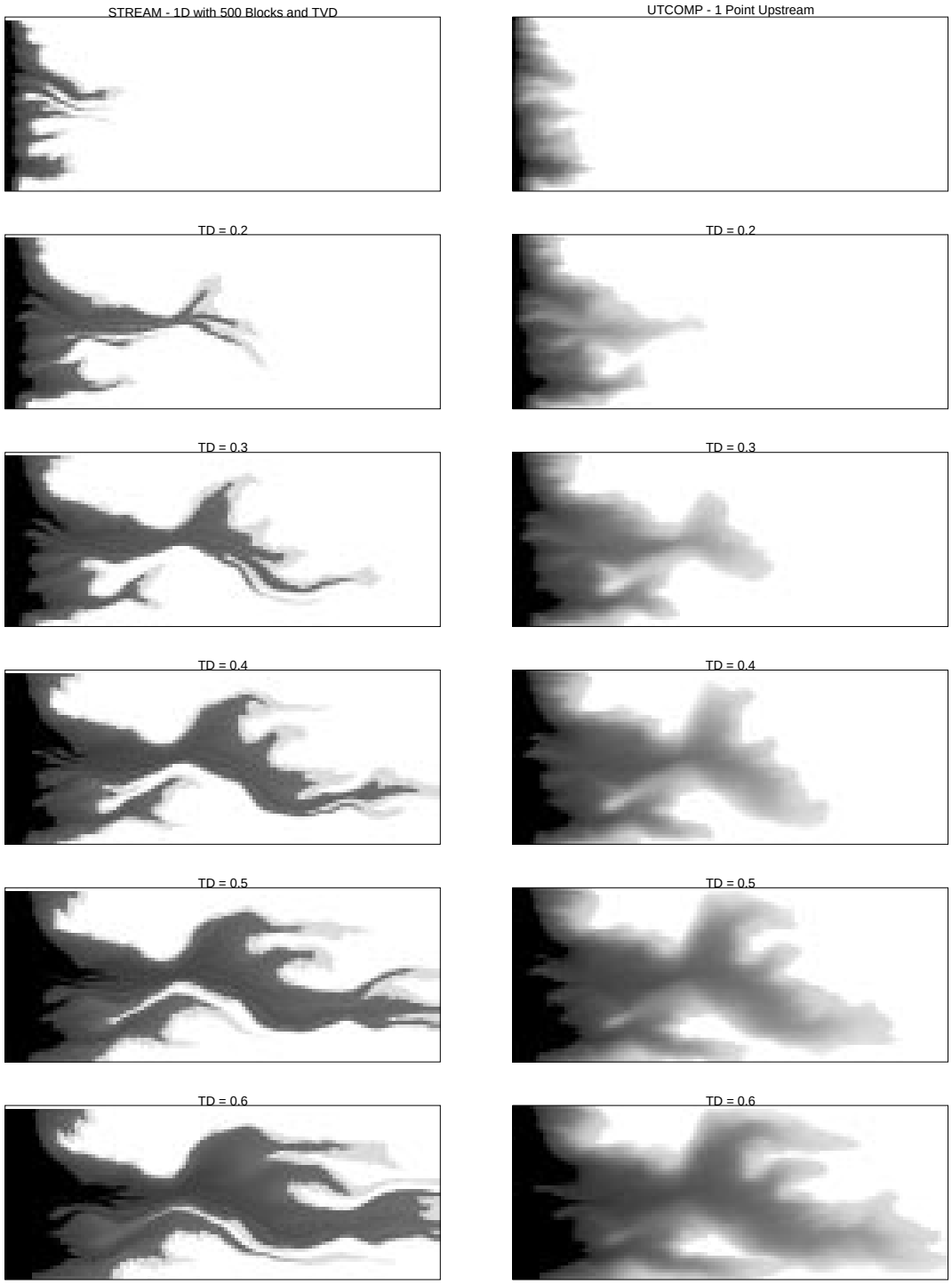

Figure 7.5: *Comparison of the evolution in time of the gas saturation. The streamtube solution was found using a 500 grid block one-dimensional solution while the* UTCOMP *solution was found using a single-point upstream weighting scheme.*

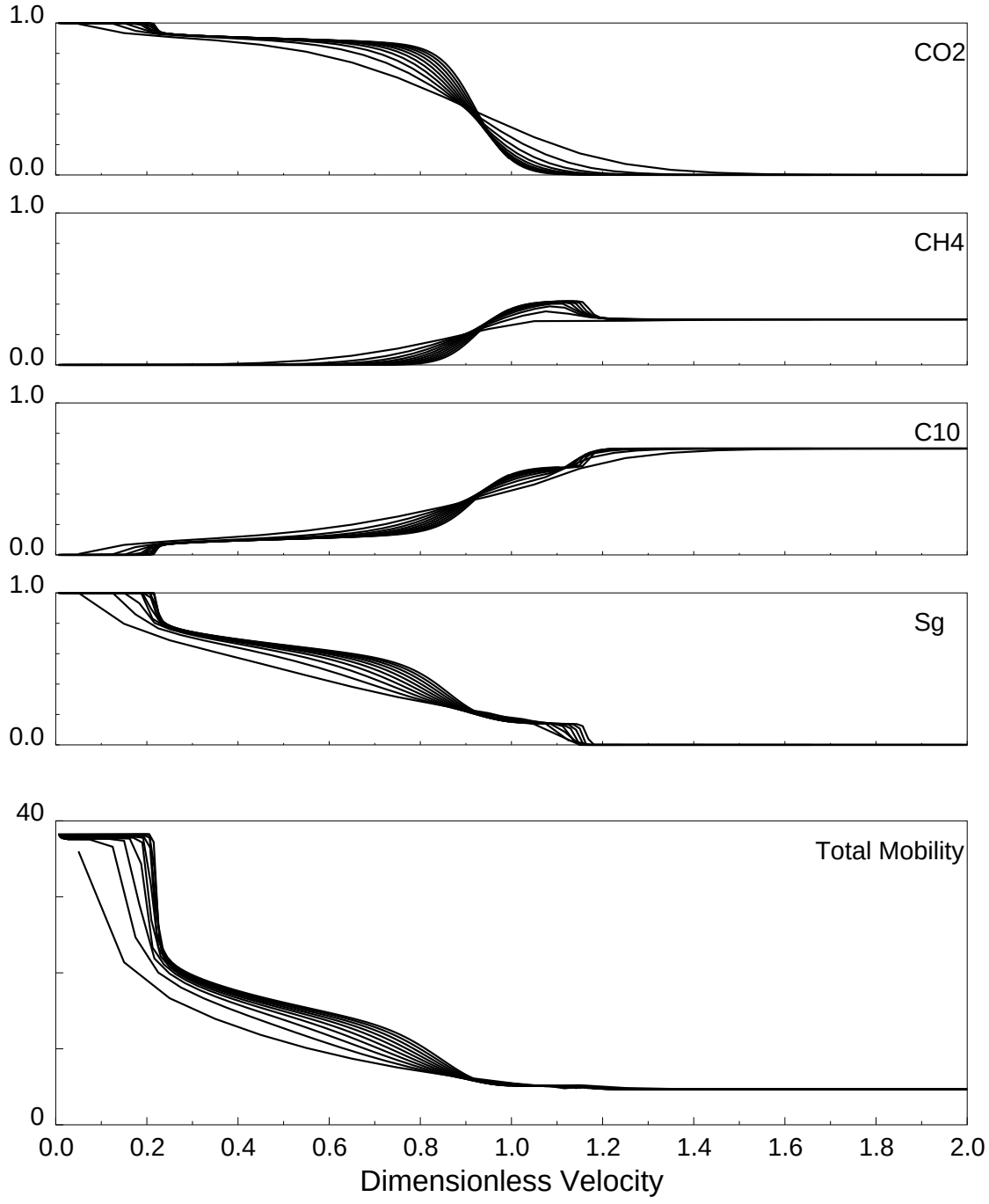

Figure 7.6: *Ten one-dimensional UTCOMP solutions using 100 grid blocks and one point upstream weighting. Each solution represent an increment of* $\Delta t_D = 0.1$.

include longitudinal 'numerical'-type diffusion into the streamtube solution, it does mitigate the mobility contrast.

Fig. 7.7 shows a comparison of the UTCOMP and the streamtube saturation maps. The streamtube displacement is indeed more stable than the one found using a 500 grid block, 1D solution (compare with Fig. 7.4), and it is apparent from this comparison that by adding 'numerical diffusion' to the streamtube solution, the finite difference solution can be approximated. It is important to realize that the diffused one-dimensional solution mapped along the streamtubes can, at best, approximate longitudinal numerical diffusion only. Clearly, the UTCOMP solution will also have some transverse diffusion, which cannot be accounted for in the streamtube solution. Transverse numerical diffusion would slow down the leading shock velocities and lead to a more stable displacement.

Fig. 7.8 shows a summary of the gas saturation maps for the various cases discussed previously. Two key issues are summarized in Fig. 7.8: (1) longitudinal and transverse numerical diffusion combine with phase behavior to mitigate substantially the original instability of the displacement and (2) the streamtube solution with the sharp, 500 grid block solution may in fact be considered as the limiting no-diffusion solution to the three-component problem. The large difference in computation times, 3000-10000 Cray seconds per 0.1 PV injected depending on numerical scheme and grid size for UTCOMP as opposed to 2-3 Cray seconds for the streamtube solution makes the streamtube solution very attractive, despite the underlying Riemann assumption used in mapping the one-dimensional solutions along the streamtubes. Fig. 7.8 is interesting because it shows how numerical diffusion is able to mitigate the instability of the displacement. It is likely that both UTCOMP solutions in Fig. 7.8 are not converged solutions; grid refinement and time-step reduction would likely reveal a stronger instability.

Cumulative recoveries for the three-component problem are shown in Fig. 7.9, which quantifies the more stable displacement seen by UTCOMP . It is interesting to note that the difference in recovery due to the different one-dimensional solutions used along the streamtubes — 500 grid blocks and TVD versus 100 grid blocks and one-point upstream — is negligible. The one-dimensional recovery is shown as well

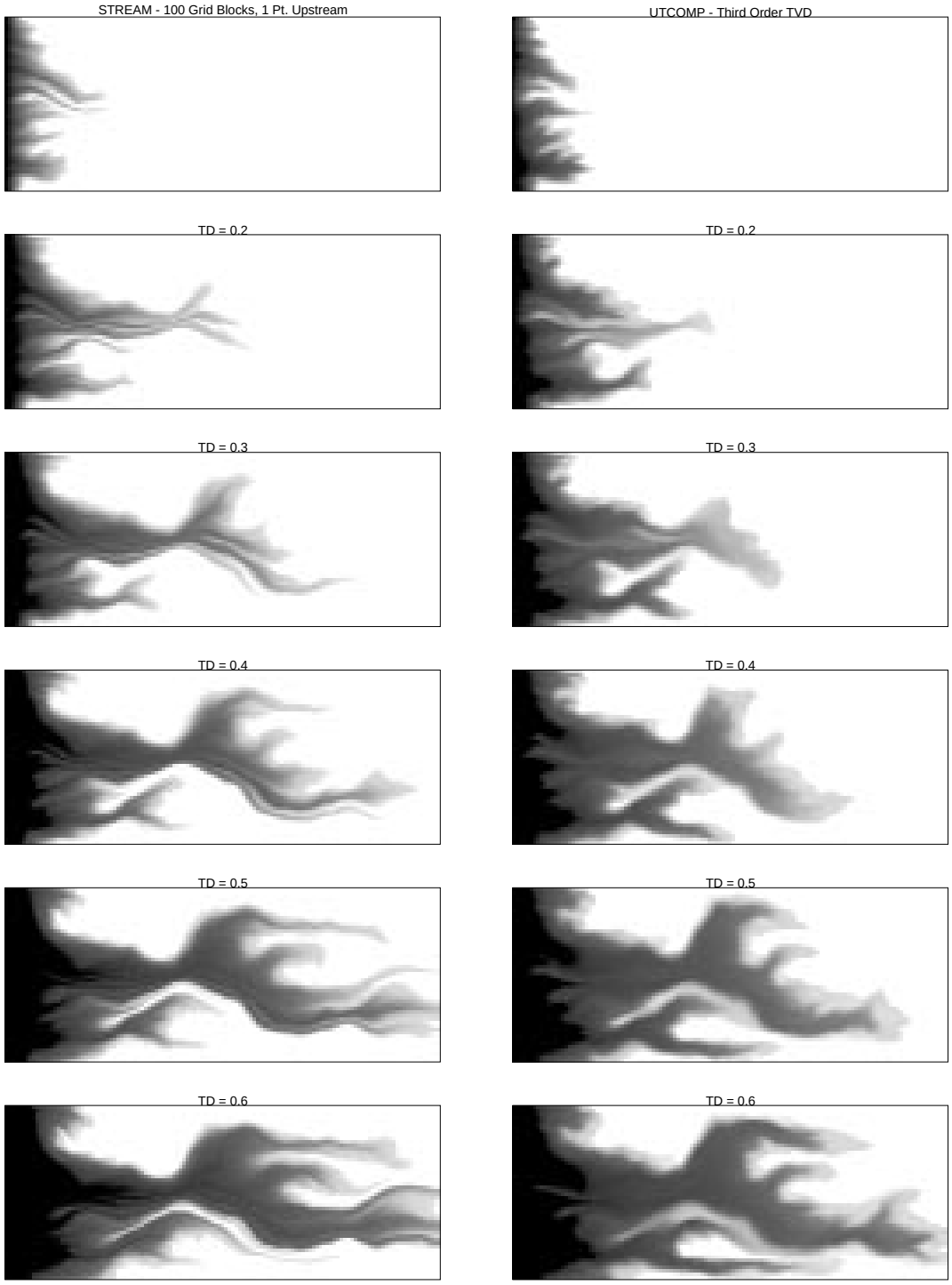

Figure 7.7: *Comparison of the evolution in time of the gas saturation. The streamtube solution was found using single point upstream, 100 grid block, 1D solutions while the UTCOMP solution was found using a third-order TVD scheme on a 125x50 grid.*

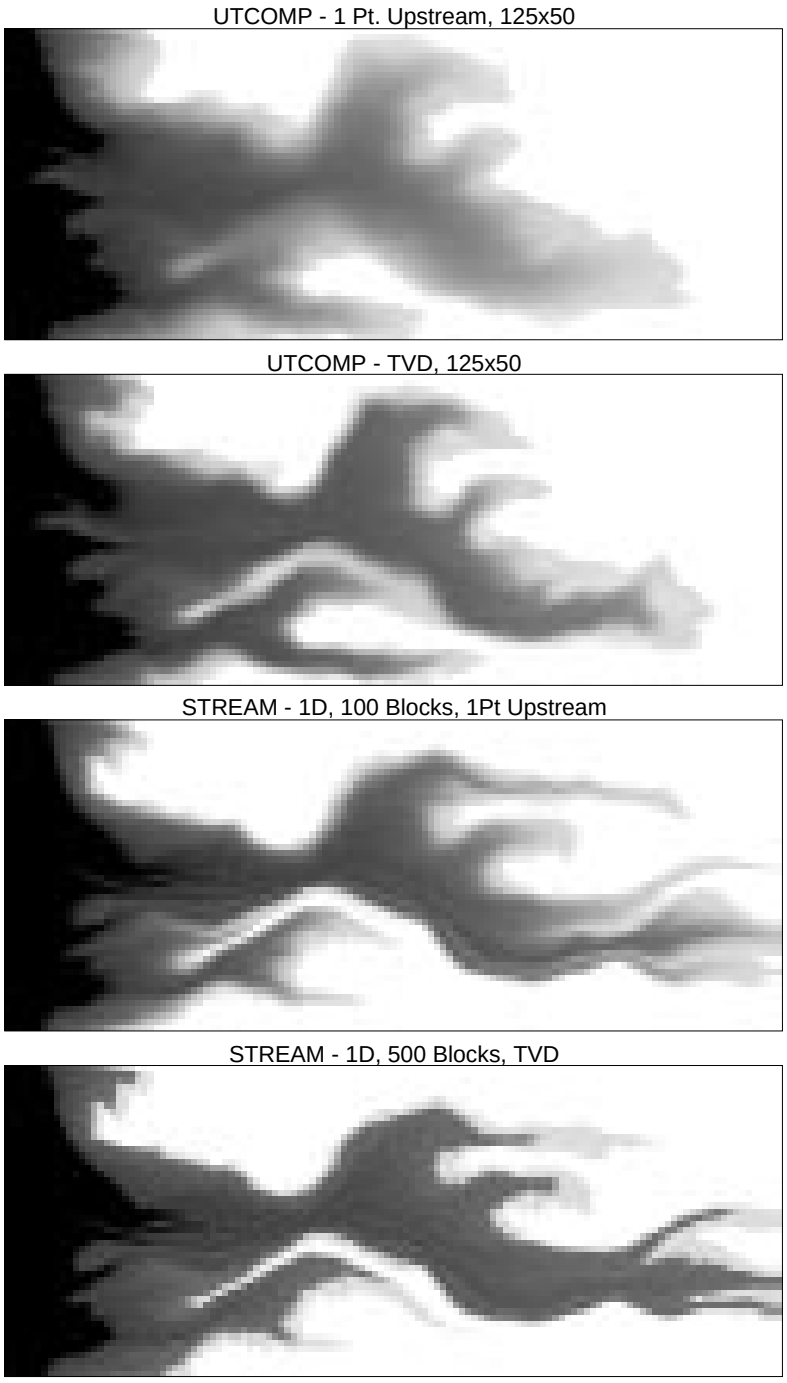

Figure 7.8: *Summary of gas saturation maps at $t_D = 0.5$: From top to bottom: UTCOMP solution with single-point upstream weighting, UTCOMP solution third order TVD scheme, streamtube solution using a 1D, 100 blocks, single-point upstream solution, and streamtube solution using a 1D, 500 grid block-TVD solution.*

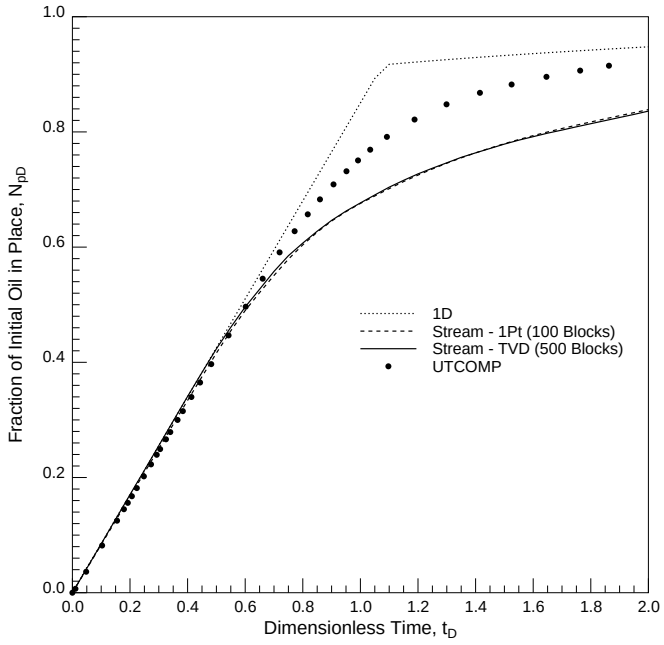

Figure 7.9: *Recovery curves for the* $CO_2/CH_4/C_{10}$ *system.*

as a way to quantify the impact on recovery due to heterogeneity and a nonlinear velocity field. Fig. 7.10 shows the convergence of the streamtube solution. Forty streamtubes updates are sufficient to capture the first order effect imposed by reservoir heterogeneity on recovery, and, as expected, the UTCOMP recovery falls between the streamtube solutions using a single solve and ten solves.

Fig. 7.11 shows the same three-component, two-phase displacement through a less heterogeneous system. The permeability field is an upscaled version (125x50) of the same permeability field used for the displacements shown in Fig. 6.20 ($\lambda = 1.00$, $\sigma_{\ln k} = 0.5$,$HI = 0.25$). The interesting feature of Fig. 7.11 is that while the UTCOMP single-point upstream solution shows no viscous fingering whatsoever, the same solution using a third-order TVD scheme is able to retain sufficient mobility contrast to result in some fingering in the channel demonstrating again that numerical diffusion can have a substantial impact on flow behavior and supress fingering. The streamtube solution, of course, is not able to reproduce any viscous fingering, but captures the main flow path and the first order effect of heterogeneity on the displacement at a

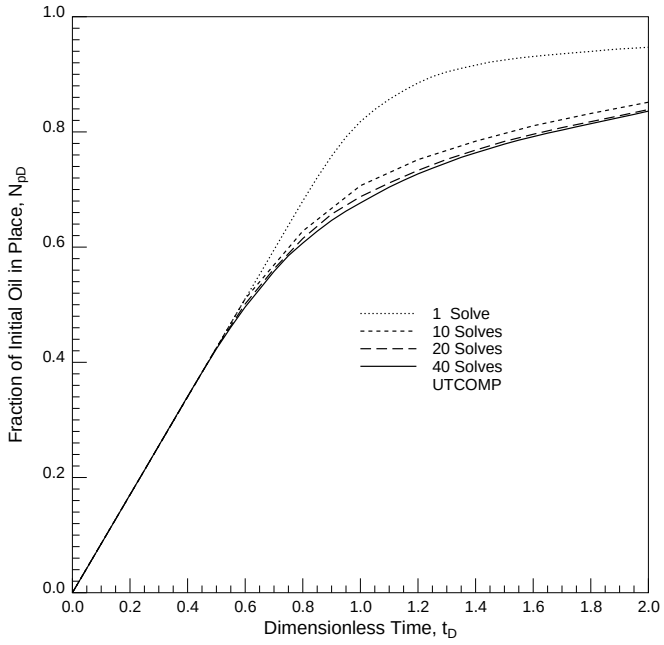

Figure 7.10: *Convergence for the* $CO_2/CH_4/C_{10}$ *system, showing that overall recovery can be predicted using fewer than 40 streamtube updates over 2* PV_{inj}.

much lower computational cost.

7.6 Four-Component Solution

The three-component system presented in the previous section was characterized by a condensing displacement mechanism. In this section, the displacement of a three-component oil —CH_4, C_6, C_{16}— by an enriched gas, composed of a mixture of CH_4 and C_3, at 2000 psia and 200°F is used as an example of a displacement exhibiting condensing behavior at the leading edge and vaporizing behavior at the trailing edge. The example is taken from *Johns* (1992, p. 194) and is discussed in detail there. Component properties are shown in Table 7.2. The initial composition of the oil in mole fractions is $CH_4 = 0.2$, $C_6 = 0.4$, $C_{16} = 0.4$ and the injected composition of the enriched gas is $CH_4 = 0.65$ and $C_3 = 0.35$. The injected conditions are close to the minimum enrichment composition for miscibility ($CH_4 = 0.615$ and $C_3 = 0.385$),

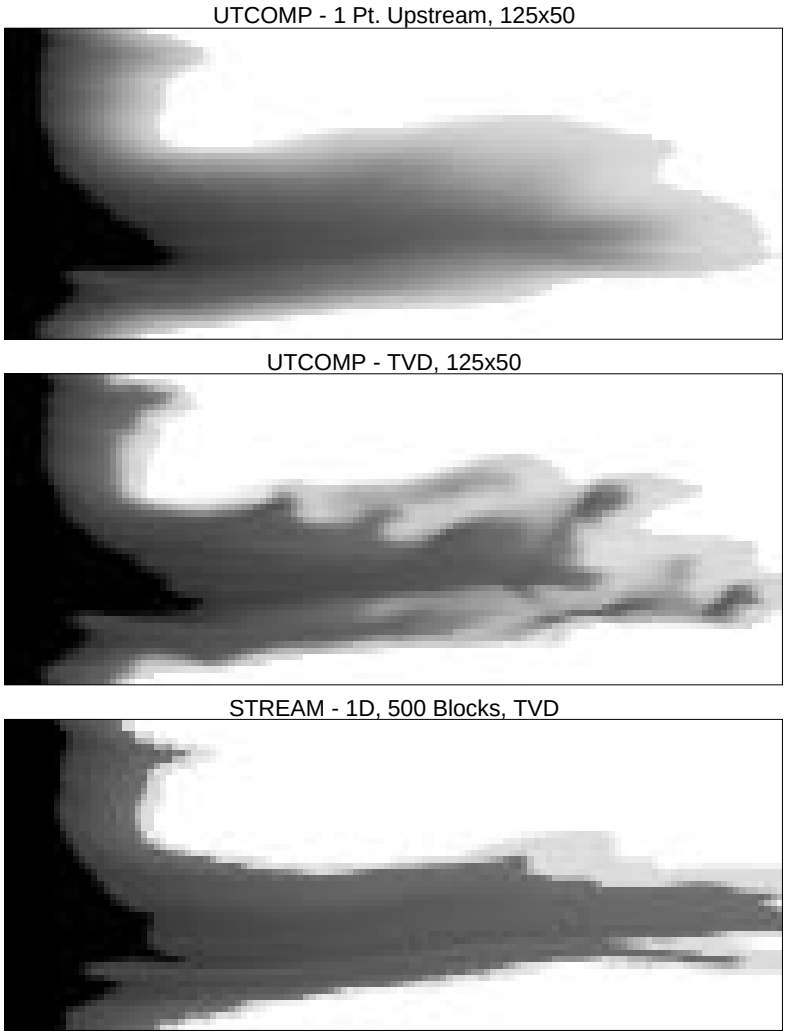

Figure 7.11: $CH_4/CO_2/C_{10}$ *displacement in a mildly heterogeneous system (compare with Fig. 6.20) showing the suppression of viscous fingers due to numerical diffusion.*

Component	M_w	P_c (psia)	T_c °F	V_c (ft^3/lb-mol)	ω
CH_4	16.04	667.8	-116.63	1.5899	0.0104
C_3	44.087	615.8	205.85	3.2534	0.1530
C_6	86.18	430.6	453.63	5.9299	0.2990
C_{16}	226.448	205.7	830.91	15.000	0.7420

Component	Interaction Parameters			
	CH_4	C_3	C_6	C_{16}
CH_4	0.0000	0.0000	0.0250	0.0350
C_3	—	0.0000	0.0100	0.0100
C_6	—	—	0.0000	0.0000
C_{16}	—	—	—	0.0000

Table 7.2: *Component properties for the four-component model.*

characterizing the system as near-miscible (*Johns 1992*).

Fig. 7.12 shows the numerical one-dimensional solutions obtained from UTCOMP using 100 and 500 grid blocks and a third-order TVD scheme to control numerical diffusion. Unlike the three-component solution, UTCOMP has some problems in resolving the one-dimensional solution for this case. Numerical difficulties are evident in the diffused fronts as well as in the 'dip' in the total mobility profile. Nevertheless, the 500 grid block solution does seem to capture the main feature of the displacement and sees the condition of near miscibility: the main part of the two-phase region is small and the the total mobility profile shows a substantial mobility contrast across the two-phase region. Again, the mobility profile is the main indicator of the instability that will control the streamtube solution. For this case, the initial mobility contrast is $M \approx 8.4$, but unlike the three-component solution which had a similar end-point mobility ratio, the main two fronts are much closer to each other and lead to a mobility contrast of $M \approx 6$. Thus, the four-component streamtube solution is expected to be more unstable than the three-component solution discussed previously.

Fig. 7.13 shows the component and saturation maps for $t_D = 0.2$ and $t_D = 0.45$ obtained by mapping the 500 grid block TVD-solution along streamtubes. The stronger instability compared to the previous three-component solution is evident,

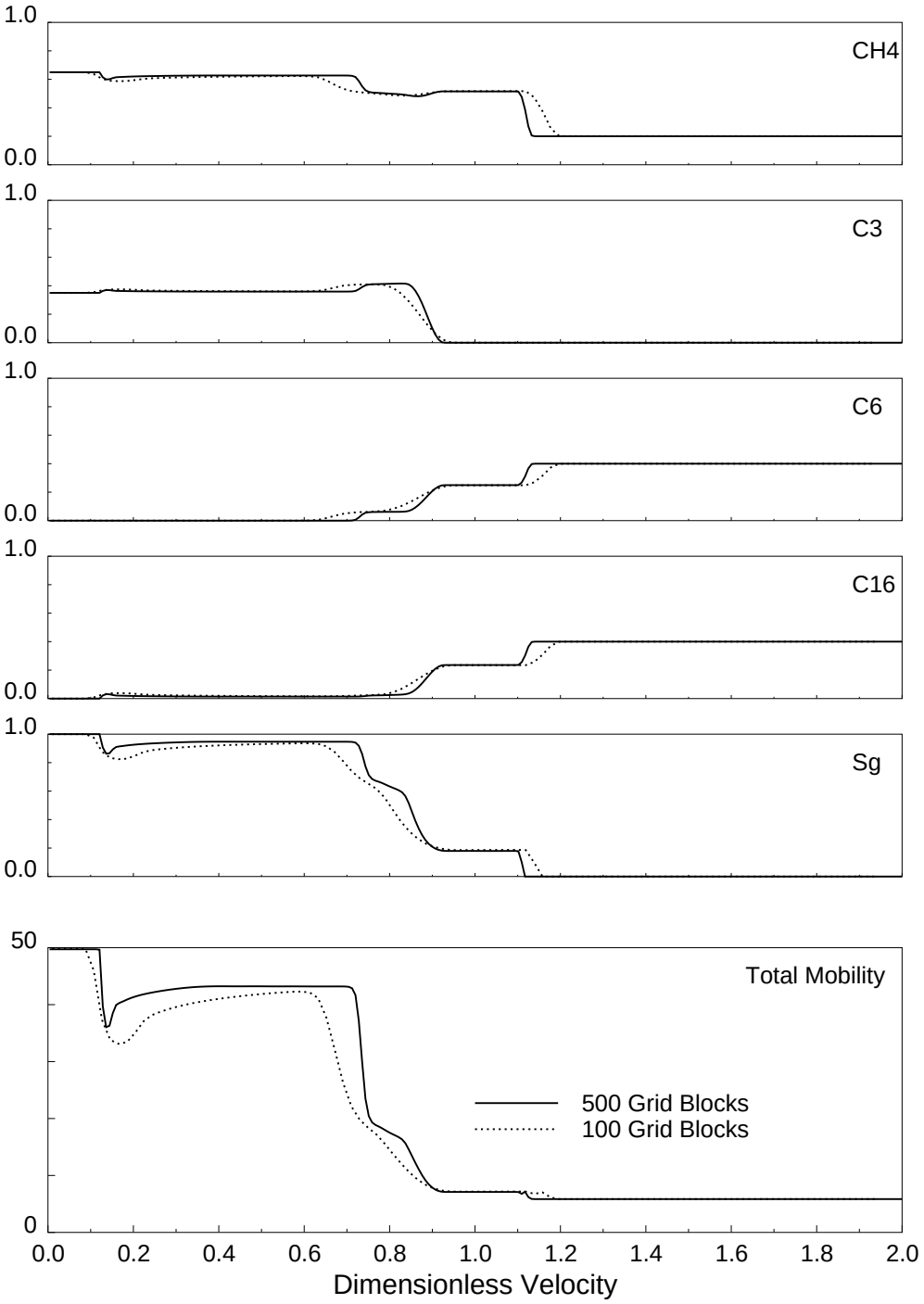

Figure 7.12: *One-dimensional numerical solution, using 100 and 500 grid blocks and a third-order TVD scheme to control numerical diffusion, for the* $CH_4/C_3/C_6/C_{16}$*-condensing/vaporizing gas drive.*

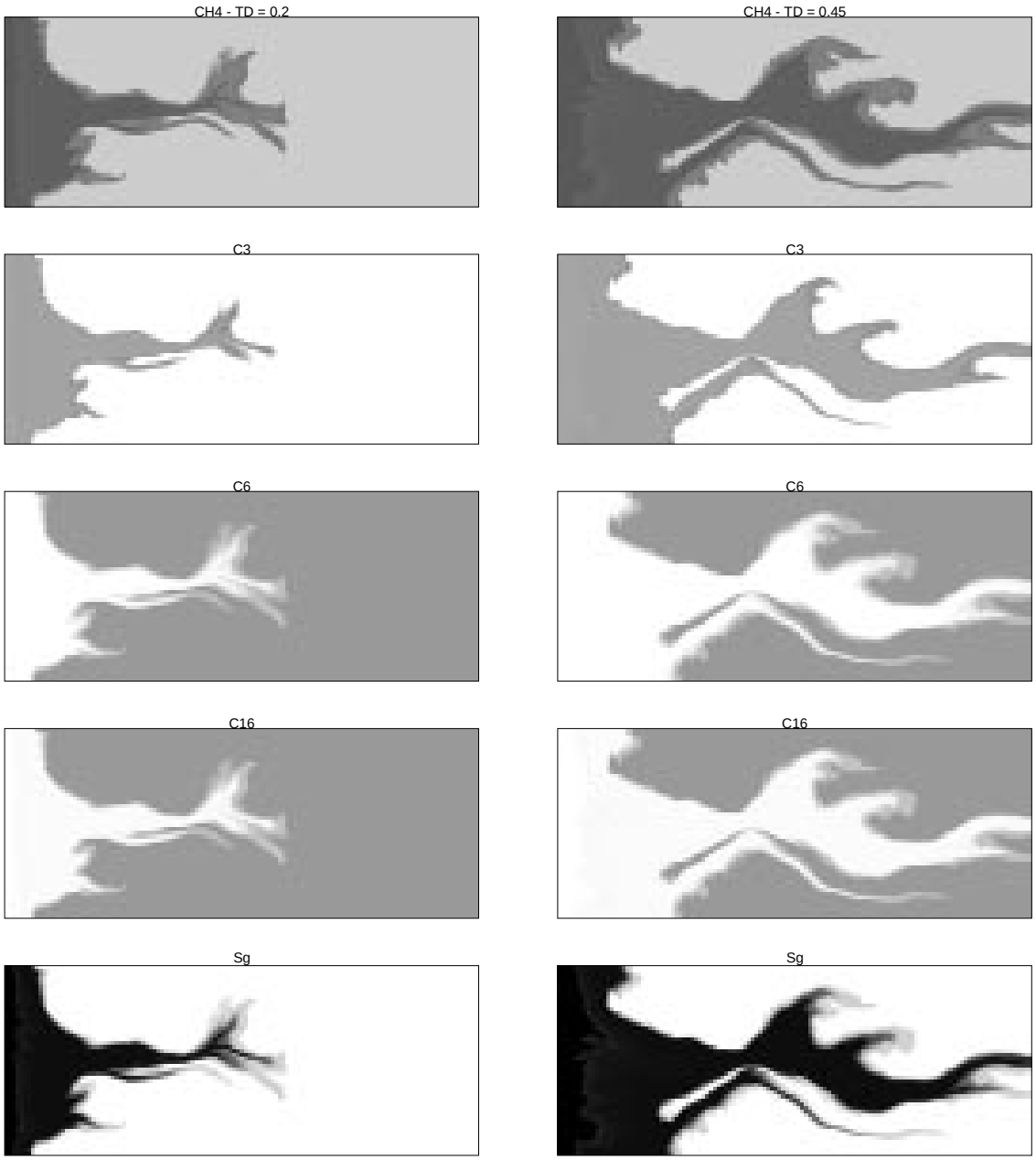

Figure 7.13: *Two-dimensional streamtube solutions at $t_D = 0.2$ and $t_D = 0.45$ for the $CH_4/C_3/C_6/C_{16}$ displacement using the 500 grid block 1D solution shown in Fig. 7.12.*

with break-through occurring well before $t_D = 0.45$. That the streamtube solution sees a much stronger instability is also demonstrated by Fig. 7.14 and Fig. 7.15, which show comparisons to TVD solutions from UTCOMP . As in the three-component case, the central question that arises from comparing the streamtube solutions to the UTCOMP solutions is whether the much more stable displacement simulated by UTCOMP is a result of numerical diffusion or is, indeed, a genuine physical feature of the displacement mechanism. The impact of numerical diffusion is again illustrated by using single-point upstream weighting in UTCOMP and a diffused one-dimensional solution along the streamtubes[6].

A comparison of UTCOMP saturation maps (single-point upstream weighting vs. third-order TVD) is shown in Fig. 7.16. The TVD-solution shows a noticeable improvement in the resolution of the leading shock compared to the single-point upstream solution, indicating again that numerical diffusion is substantially affecting the displacement. But the surprising feature of the comparison is that although the TVD-solution shows a marked improvement, the displacement remains rather stable, and the positions of the leading fronts are very similar. Clearly, the mitigating effect longitudinal and transverse diffusion have on the displacement by 'feeding' back into the phase behavior of the system is not offset by the improved numerical resolution of the third-order TVD-scheme. This raises an important issue regarding numerical diffusion control in compositional models: because numerical diffusion interacts with the phase behavior of the system, doubling the number of cells and/or using an improved numerical scheme may not show the same improvement as it would for ideal miscible or immiscible displacement. It also follows that increasing the 'complexity' of the phase behavior description will decrease the efficiency in controlling numerical diffusion. For example, the improvement of the TVD-solution compared to the single-point upstream solution in the four component case is not nearly as good as the improvement seen in the three-component case (see Fig. 7.4 and Fig. 7.5). The more serious implication of this discussion is that the UTCOMP solutions are not converged, but rather represent intermediate solutions in a possible refinement sequence

[6] As in the three component case, a simulation using a refined 250x100 grid with UTCOMP was attempted, but led to prohibitively high computation costs and had to be terminated.

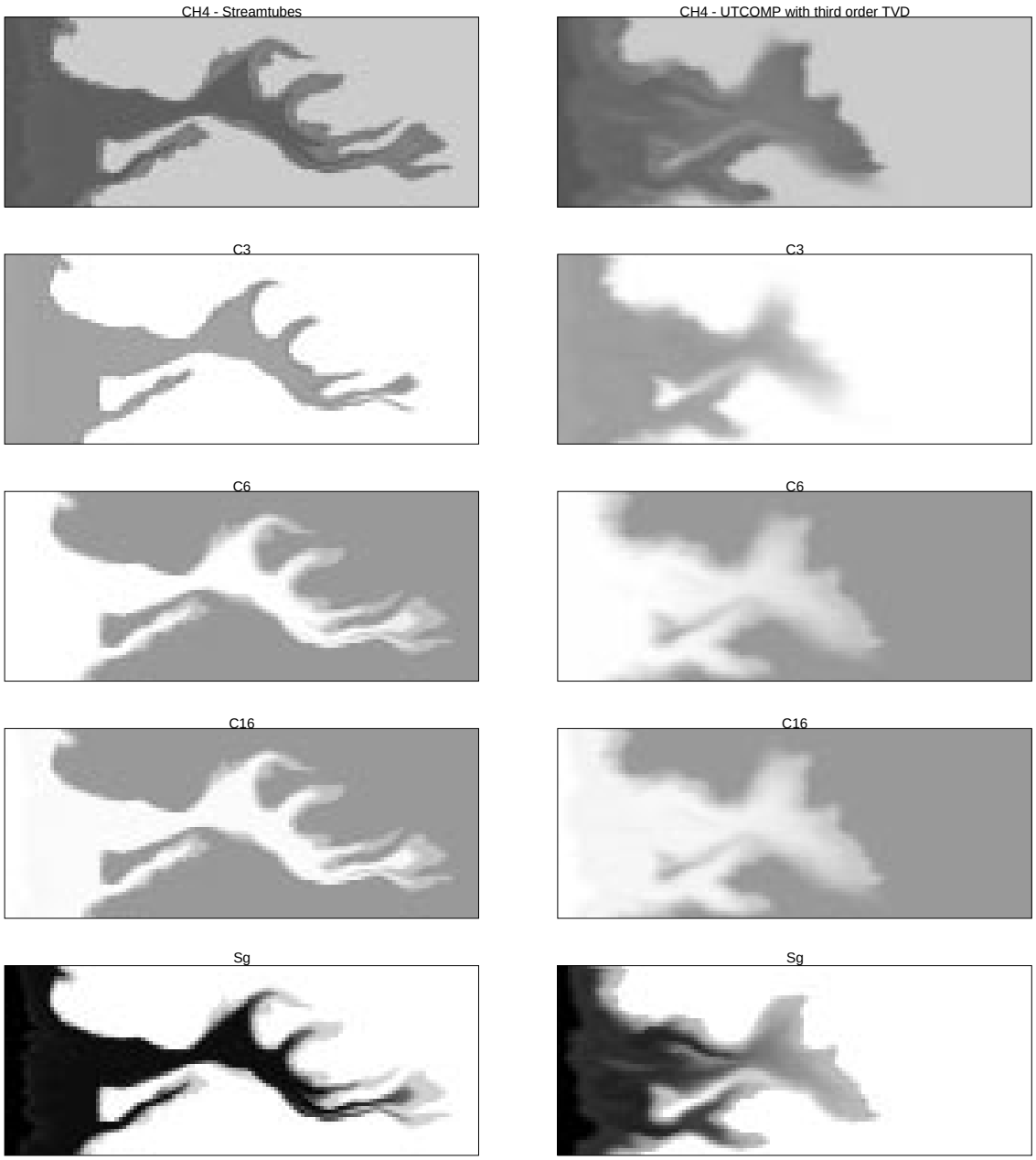

Figure 7.14: *Composition and saturation maps for the* $CH_4/C_3/C_6/C_{16}$ *displacement at* $t_D = 0.35$. *The UTCOMP solution was found using a third order TVD scheme, while the streamtube solution used the 1D, 500 grid block TVD solution.*

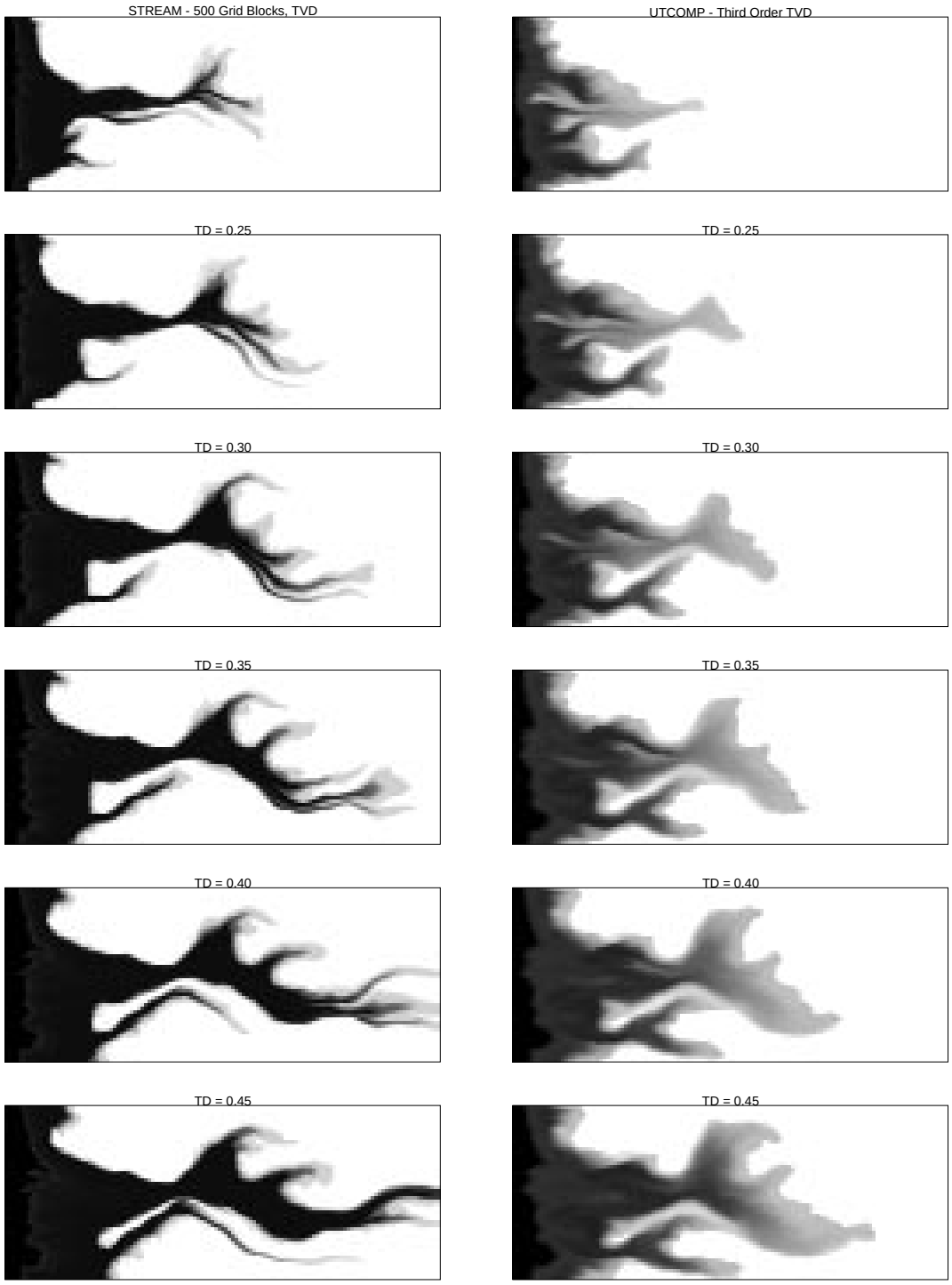

Figure 7.15: *Saturation maps for the* $CH_4/C_3/C_6/C_{16}$ *displacement at various times. The UTCOMP solution was found using a third order TVD scheme, while the streamtube solution used the 1D, 500 grid block TVD solution.*

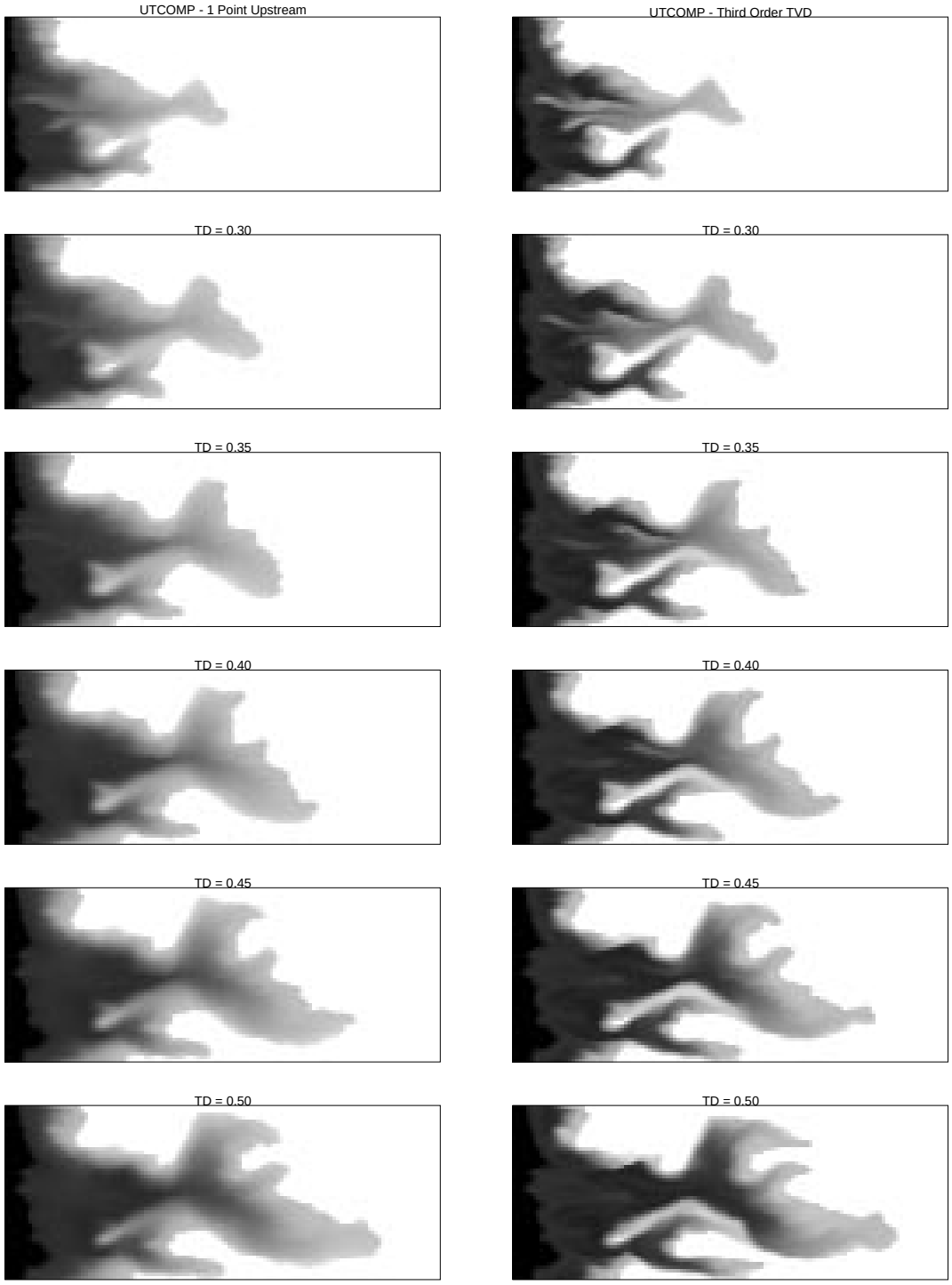

Figure 7.16: UTCOMP *saturation maps for the* $CH_4/C_3/C_6/C_{16}$ *displacement at various times. The* UTCOMP *solutions were found using single-point upstream weighting and a third order TVD scheme.*

that would ultimately show a displacement with substantial frontal instability, and possibly viscous fingering, and indeed much closer to the solution returned by the streamtube approach.

How significant numerical diffusion can be in reducing the inherent instability of the displacement is revealed by Fig. 7.17, which compares a 'diffused' streamtube solution to the UTCOMP (TVD) solution. The key issue in Fig. 7.17 is that the streamtube solution was generated using a 1D, 100 grid block, single-point upstream solution, but assuming a unit mobility ratio displacement ($M = 1$). In other words, the streamtubes were calculated only once, as in in the tracer case, and used to describe the velocity field for the entire duration of the displacement. What led to this was the discovery that even the most diffused mobility profile in the longitudinal direction would still return a displacement that looked more unstable than the equivalent UTCOMP solution. Thus, the entire mobility contrast was removed.

Using a one-dimensional solution devoid of any mobility contrast to match the UTCOMP solution has substantial implications. In particular, it suggest that numerical diffusion and phase behavior can combine to completely eliminate the original instability of a displacement in a heterogeneous system. Needless to say, the speed-up is now by four to five orders of magnitude, since the streamtube solution uses a single matrix inversion versus the many thousand pressure solves and flash calculations required by UTCOMP . The most dramatic conclusion to be drawn from the three- and four-component solutions is that two-dimensional compositional solutions, particularly those generated on coarse grids and with a simple single-point upstream weighting scheme are not likely to be converged solutions, and will predict optimistic recoveries.

Recoveries for various number of streamtube updates are shown in Fig. 7.18. All recoveries were obtained using the 500 grid block TVD solution (Fig. 7.12) along the streamtubes. As in the three-component solution, 40 updates over 2 pore volumes injected are sufficient to give a converged solution. Unfortunately, UTCOMP could not be run long enough to yield recovery after breakthrough due to the enormous computation time involved. Nevertheless, it is possible to argue, given the previous

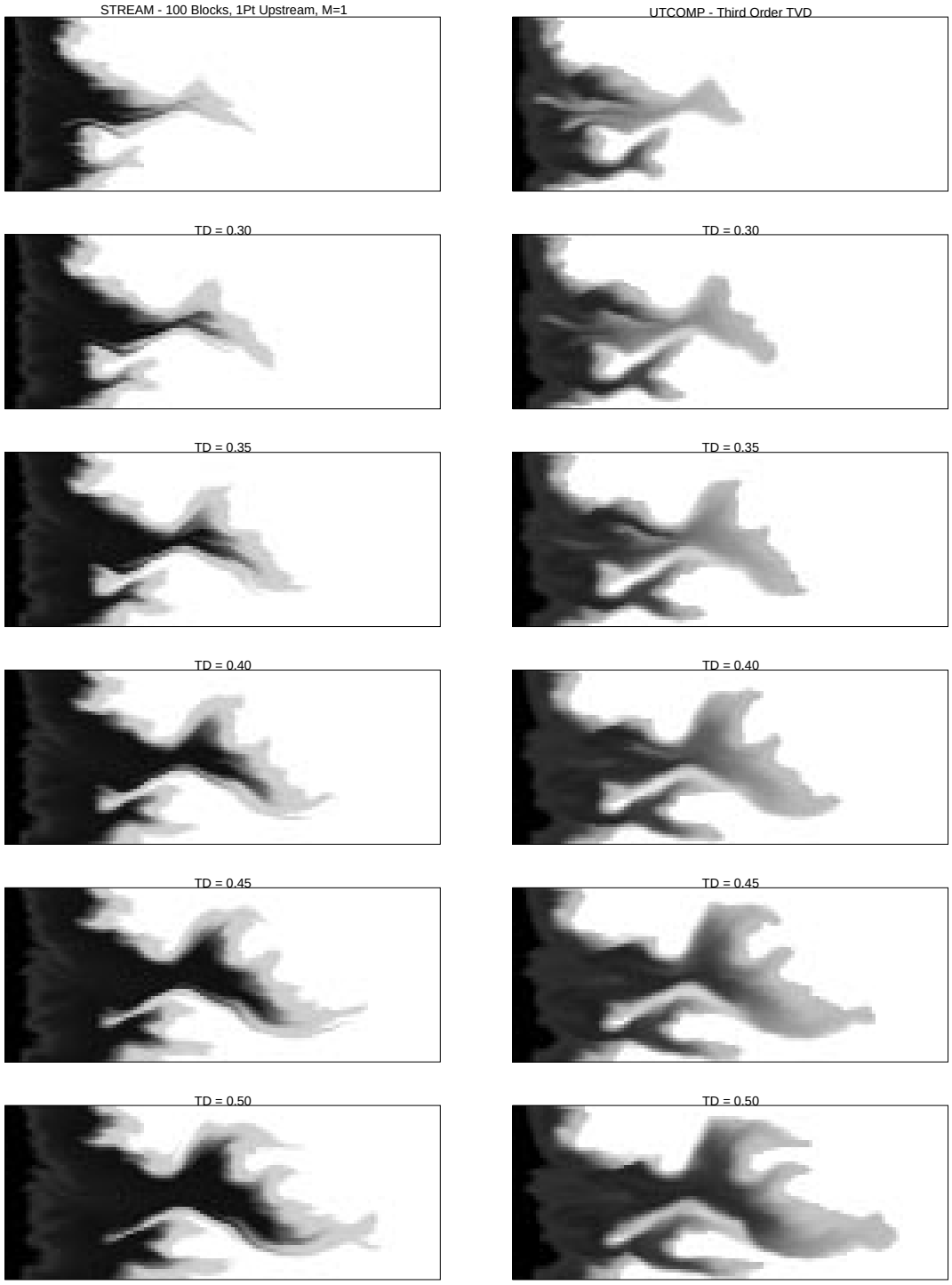

Figure 7.17: *Saturation maps for the two-dimensional* UTCOMP *and streamtube solutions for the* $CH_4/C_3/C_6/C_{16}$ *displacement. In this example, the streamtube solution was found by using a 100 grid block, 1D solution and* $M = 1$*. The UTCOMP solution is the same as shown in Fig. 7.16.*

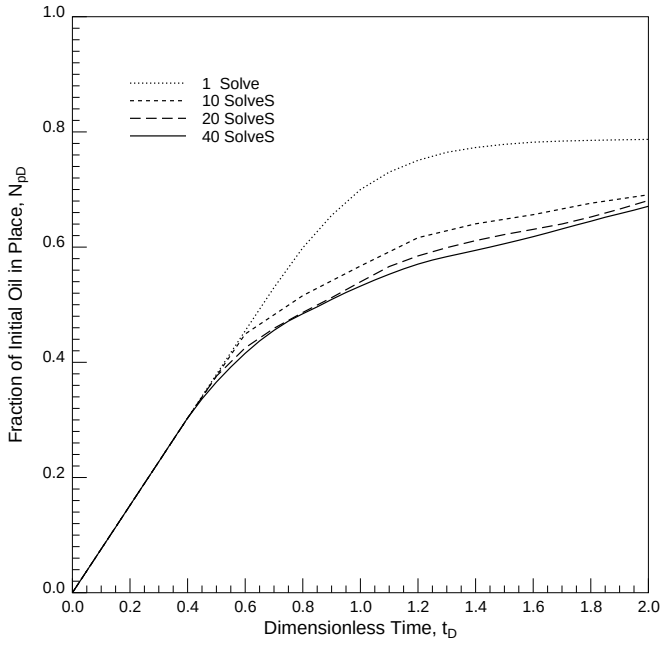

Figure 7.18: *Streamtube recovery curves for the* $CH_4/C_3/C_6/C_{16}$ *system. A 500 grid block TVD solution (Fig. 7.12) was used along the streamtubes.*

discussion and the comparisons of the concentration maps, that the UTCOMP recovery is likely to be bound by the streamtube recoveries found using 1 solve and 10 solves.

7.7 Numerical Diffusion vs. Crossflow

The previous section identified numerical diffusion as having a substantial impact on compositional displacements. To what extent crossflow may affect the displacement performance in a similar manner is an ongoing debate (*Fayers 1994, Fayers 1994b, Pande 1992, Pande and Orr 1989*), although all authors agree that crossflow aids overall recovery. Viscous crossflow is attributed to transverse pressure gradients that result from mobility differences.

Many questions remain though, particularly given the fact that numerical diffusion is usually not addressed explicitly in simulation studies that investigate viscous

crossflow. The difficulty is that crossflow, if it is present, will be subject to numerical diffusion as well. Separating the contribution of each mechanism therefore may be extremely difficult, if not impossible, because both manifest themselves in the same way: reduction of the mobility contrast by mixing. The examples of the previous sections are strong evidence that numerical diffusion — even when using an efficient third-order TVD scheme — can substantially reduce the mobility contrast. That raises the question whether the improved recovery reported by many authors and attributed to crossflow is in fact a combined effect of crossflow and numerical diffusion or even just numerical diffusion. For example, *Pande* (1992) found substantial improvement in recovery due to crossflow in a $C_2/C_4/C_{10}$ system for several different types of reservoir heterogeneity. Pande used a fairly coarse 50x30 (x-z) grid, with grid blocks of size 1 ft x 75 ft, and a single-point upstream weighting scheme. No-crossflow solutions were found by setting all vertical permeabilities to $K_z = 0.01K_x$.[7]

Fayers et al. (1994), on the other hand, did not report any crossflow effects while studying four component displacements through a mildly heterogeneous 128x64 system. Furthermore, comparison of the fine-grid 128x64 solution to a coarser 64x32 solution showed little evidence that numerical diffusion was a significant factor in reducing the instability of the displacement. It is likely, instead, that the numerical diffusion was so dominant as to mask any improvement in resolution between the two grid sizes, particularly considering that a single-point upstream scheme was used in all simulations. This interpretation would be in agreement with the three- and four-component UTCOMP solutions found here.

To consider the issue of numerical diffusion and crossflow further, this section uses the condensing/vaporizing four-pseudo-component system proposed by *Johns et al.* (1994) and detailed in Table 7.3. The four-component system was derived from a 12-component oil using the method proposed by *Newley and Merrill* (1991). The same four-pseudo-component system was used in the simulation study by *Fayers et al.* (1994). The strategy is to again rely on a comparison of the streamtube solution to the UTCOMP solution to gain a more detailed picture of the displacement mechanisms

[7] A convincing argument can be made here that by changing the ratio of K_z to K_x effectively generates a new permeability field. Thus, the change in recovery could just as well be attributed to a changing heterogeneity structure, rather than viscous crossflow.

Component	M_w	P_c (psia)	T_c (°F)	V_c (ft^3/lb-mol)	ω
CH_4N_2	16.0	671.17	-117.07	1.585	0.0130
C_{2+}	41.0	769.81	142.79	2.540	0.1592
C_{5+}	189.0	322.89	775.00	13.054	0.6736
C_{30+}	451.0	171.07	1136.59	30.644	1.0259

Component	Interaction Parameters			
	CH_4N_2	C_{2+}	C_{5+}	C_{30+}
CH_4N_2	0.0000	0.0286	0.0258	0.2000
C_{2+}	—	0.0000	0.0607	0.1268
C_{5+}	—	—	0.0000	0.0000
C_{30+}	—	—	—	0.0000

Table 7.3: *Component properties for the pseudo four-component model (*Johns et al. 1992*).*

at work. The four-pseudo-component system is particularly suitable for looking at viscous crossflow due to its very large end-point mobility ratio. The one-dimensional solution of an enriched CH_4N_2/C_{2+}-gas flood (0.3277/0.6733) displacing the four-component oil with initial compositions given by $CH_4N_2 = 0.3692$, $C_{2+} = 0.1155$, $C_{5+} = 0.4281$, and $C_{30+} = 0.0872$ at 3150 psia and 200°F is shown in Fig. 7.19. The total mobility profile was rescaled by the mobility of the oil at the initial conditions so that the y-axis could be used directly to get an indication of the mobility ratio of the displacement. The end-point mobility ratio is approximately $M \approx 70$. The leading shock has a mobility ratio of $M \approx 10$, the intermediate shock has a mobility ratio of $M \approx 6$, and the trailing shock has a mobility ratio of $M \approx 1.1$. A permeability field with 60x20 grid blocks and a heterogeneity index of $HI = 0.72$ ($\lambda_c = 0.5$, $\sigma_{\ln K} = 1.2$) was chosen, though it is clear that the grid is too coarse to possibly consider any resulting solution converged. But the opportunity for allowing at least one stage of refinement (120x40) that could be run using UTCOMP forced this choice.

A comparison of gas saturation at various times is shown in Fig. 7.20. The permeability field has a well defined main flow path that both solutions are able to see,

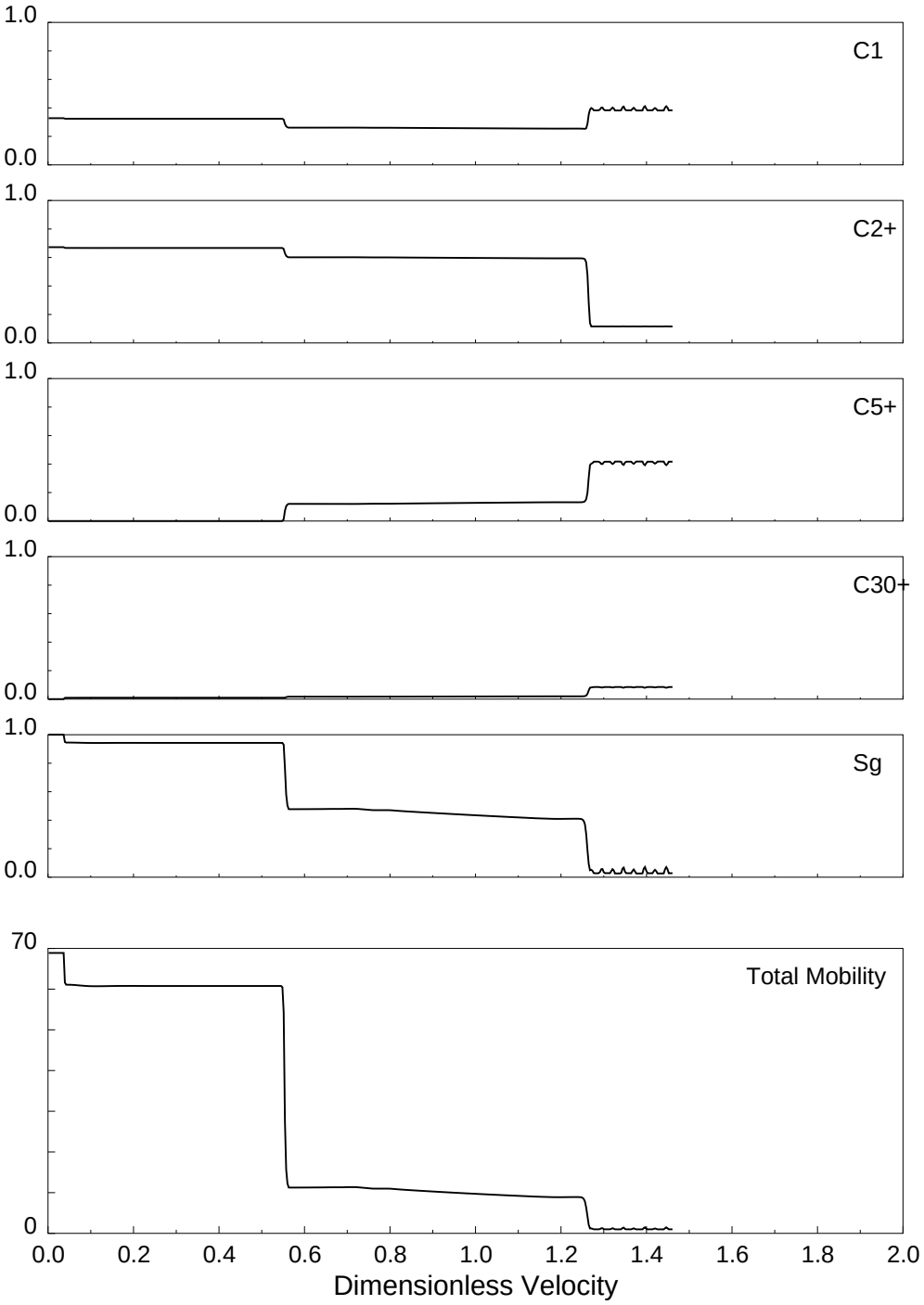

Figure 7.19: *One-dimensional numerical solution, using 500 grid blocks and a TVD-scheme for the* $CH_4N_2/C_{2+}/C_{5+}/C_{30+}$ *four-pseudo-component system proposed by* Johns et al. *(1994).*

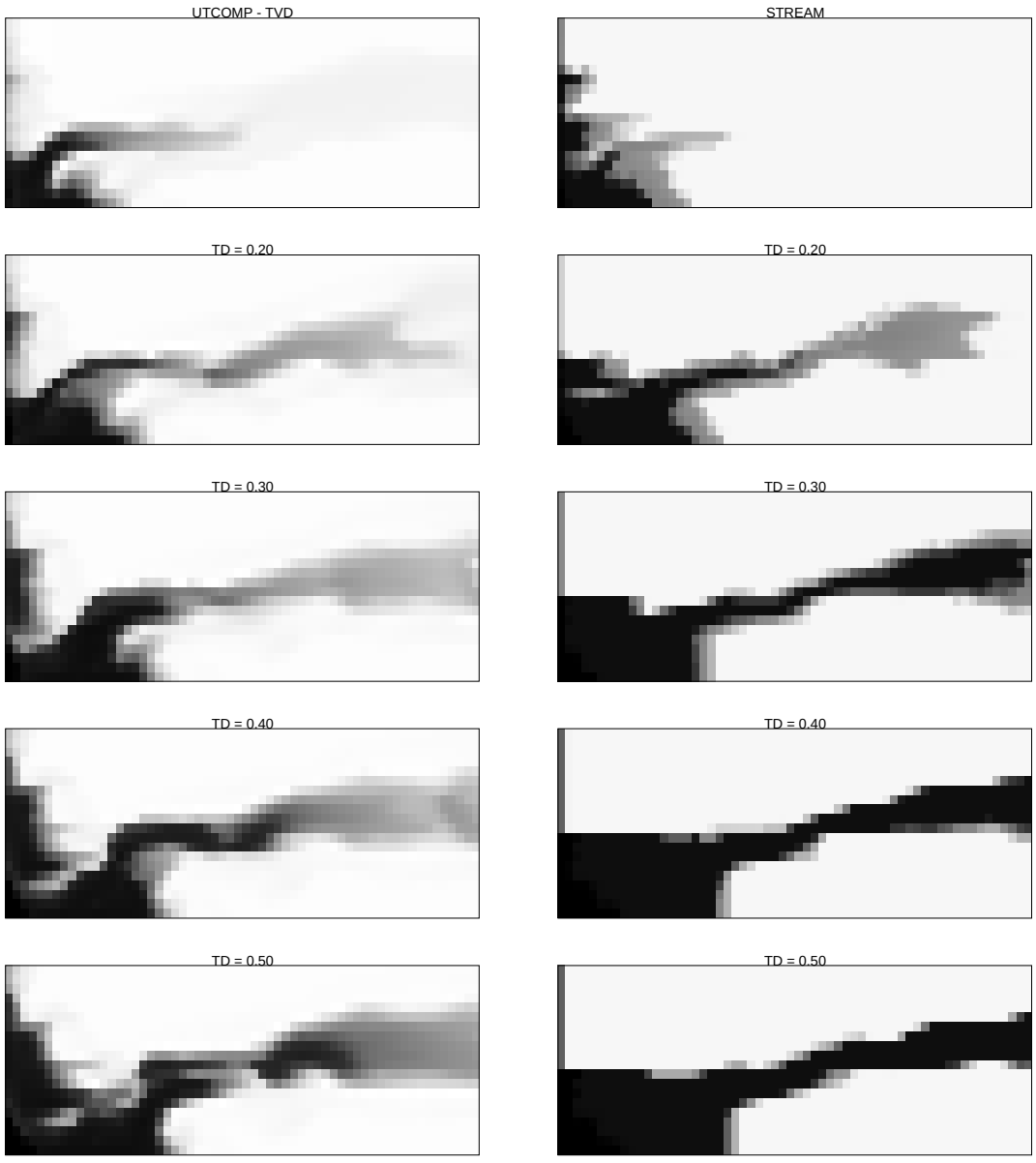

Figure 7.20: UTCOMP *and streamtube saturations for the* CH_4N_2/ C_{2+}/ C_{5+}/ C_{30+} *displacement. The one-dimensional solution used along the streamtubes is shown in Fig. 7.19. The* UTCOMP *solution was found using a third-order TVD scheme.*

but as in the previous cases, the UTCOMP solution clearly has a more diffused solution, particularly in the transverse direction. The issue then is whether viscous crossflow is the source for the mixing around the main flow channel or whether it is mainly numerical (transverse) diffusion. The example in Fig. 7.20 is particularly suited to help answer this question, because the single flow channel carries the high pressure into reservoir that allows for transverse pressure gradients that drive viscous crossflow. Both solutions suggest the presence of transverse pressure gradients by the thickening of the main flow channel as it progresses towards the outlet end. In fact, the shape of the main flow channel is reminiscent of a viscous finger: thin at the trailing end, where pressure gradients are pointing into the channel, and thick at the front where pressure gradients are pointing outwards. It is likely then that the 'mixed' zone around the main flow channel in the UTCOMP solution is due to viscous crossflow, since it too seems to thicken towards the outlet end.

To quantify how much numerical diffusion is affecting the solution, a comparison of the same displacement using several grid sizes is shown in Fig. 7.21. The 30x10 permeability field was found by simply taking a geometric average of 2x2 blocks in the original 60x20 field, whereas the 120x40 permeability field was generated by refining each cell into four smaller ones. All solutions clearly show the dominant flow channel, which thickens as it makes its way to the outlet end, suggesting that transverse pressure gradients are indeed at work. But the 120x40 UTCOMP solution also shows that numerical diffusion may be significant: the flow channel begins to have some higher gas saturation not visible in the coarser 60x20 grid, and it is possible that with further grid refinement numerical diffusion could be controlled further, leading to a solution closer to the streamtube solution.

Although both, the UTCOMP and streamtube solutions, indicate that transverse pressure gradients are present and possibly responsible for some mixing due to viscous crossflow in the UTCOMP solution, it is not apparent that crossflow is a dominant physical phenomenon. The real difficulty lies in the fact that the diffused or mixed region around the main flow channel is a sum of numerical transverse diffusion and mixing due to crossflow. Thus, it is difficult to quantify what the contribution of each mechanism really is. Given that numerical diffusion has such a mitigating effect in

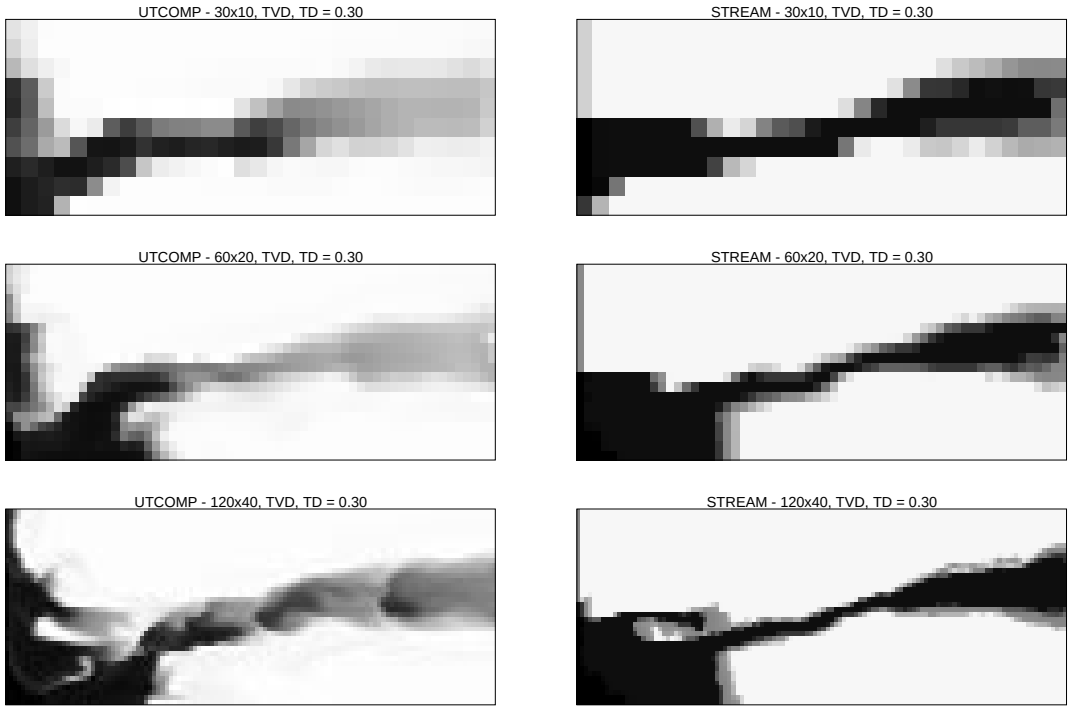

Figure 7.21: UTCOMP *and streamtube saturation for the* CH_4N_2/ C_{2+}/ C_{5+}/ C_{30+} *displacement for three different grids: 30x10, 60x20, 120x40. The one-dimensional solution used along the streamtubes is shown in Fig. 7.19. The* UTCOMP *solutions were found using a third order TVD scheme.*

---

the main flow direction it could be argued that it will cause a similiar effect in the transverse direction. But the key point to stress here is that the streamtube solution is a limiting no-crossflow solution. If crossflow is the primary cause for transverse mixing, then the solution is likely to look more like the UTCOMP solution. On the other hand, if crossflow is largely absent, then the UTCOMP solution is probably a result of transverse numerical diffusion, and the physical solution will be closer to the streamtube solution.

Unambiguous determination of the relative magnitudes of the effects of transverse diffusion and crossflow will require computations with finer grids than those that could be used here. A sufficiently high resolution must be obtainable on the underlying computational grid so as to minimize any numerical errors and resolve the

crossflow adequately. In that case, the impact of mixing due to crossflow could be assessed by direct comparison with the streamtube solutions presented here. Thus, the streamtube technique provides a basis for improved understanding of the effects of crossflow, given that the current computational cost limits of compositional simulations can be overcome.

7.8 Concluding Remarks

Unlike the previous chapters, the main issue raised here is not whether the streamtube approach can model compositional displacements, but rather how good traditional finite difference solutions to compositional problems really are. The simple and straightforward streamtube formulation is used to quantify numerical diffusion and demonstrates that its continuous feed-back into the phase behavior computation can substantially reduce the mobility contrast in a traditional finite difference formulation. In fact, the combination of numerical diffusion and phase behavior may be so strong that doubling the number of grid blocks or using third-order numerical schemes may simply not show substantial improvement in the solution, particularly in retaining the unstable characteristic of the displacement — in other words, the same numerical diffusion control that is achieved by doubling the grid blocks in a first-contact miscible displacement may require tripling or quadrupling the number of grid blocks for a compositional simulation. This type of numerical diffusion control, while retaining an acceptable level of reservoir description, is currently not possible with available computational resources. The streamtube approach is a simple and robust alternative that can solve very large problems without losing the underlying physics of the displacement to numerical diffusion and return a good approximation of overall recovery in four to five orders of magnitude less time than traditional simulation approaches. The streamtube solution cannot, by definition, model mixing due to viscous crossflow, and thus represents a no-crossflow limit. If mixing due to viscous crossflow is assumed to be a second-order effect, then the streamtube solution is a reasonable approximation to the true solution of a compositional displacement.

Chapter 8

Summary and Conclusions

The main ideas and conclusions discussed in this dissertation are summarized, and the limitations of the streamtube approach are reviewed.

8.1 Summary

The underlying assumption in applying the streamtube method to describe multiphase, multicomponent flow in heterogeneous porous media is that field scale displacements are dominated by reservoir heterogeneity and convective forces. Flow paths are captured by streamtubes, the geometry of which reflects the distribution of high and low flow regions in the reservoir. Each streamtube is treated as a one-dimensional system along which solutions to mass conservation equations for different displacement mechanisms can be mapped. The streamtube approach effectively decouples the 'channeling' imposed by the reservoir heterogeneity from the actual displacement mechanism taking place. In other words, regardless of the displacement type, the assumption is that there are predefined flow paths that will dominate the two-dimensional solution. The fluid velocity along these flow paths is reflected by the geometry of the streamtubes, and the inherent nonlinearity in the underlying velocity field is captured by periodically updating the streamtubes.

One-dimensional solutions are mapped along the streamtubes using a 'Riemann approach' — each streamtube is treated as a true one-dimensional system with constant initial and injected conditions, allowing to time-step by integrating from $t_D = 0$

to $t_D = t_D + \Delta t_D$. This approach allows analytical and numerical solutions to hyperbolic conservation equations (found using Riemann boundary conditions) to be mapped along periodically updated streamtubes. The reason for using the Riemann approach is to avoid difficulties associated with general-type initial conditions along streamtubes, in which case solutions could be found only numerically for each time step by either using a finite-difference approach or a front-tracking type approach. General-type initial conditions along streamtubes arise by updating the streamtubes while keeping the spatial saturation/concentration/composition distribution fixed. Initializing each new streamtube in this way produces initial conditions that are problem specific and of general-type.

Solutions for (1) tracer flow, (2) two-phase immiscible flow, (3) first-contact miscible flow, and (4) two-phase, multicomponent flow are found for a multitude of heterogeneous systems. For tracer flow the streamtubes are fixed in time and the Riemann approach is equivalent to time stepping from t_D to $t_D + \Delta t_D$. The only assumption in finding two-dimensional solutions involves neglecting transverse diffusion/dispersion mechanisms. In the limit of a piston-like front, a diffusion-free two-dimensional solution is found that can be used to quantify the error introduced by numerical diffusion in traditional simulation methods. Longitudinal physical diffusion can be added explicitly by mapping a CD-solution for a given Peclet number along streamtubes. Using the CD-solution is also an example of representing two different scales of reservoir heterogeneity: the large-scale heterogeneity captured by the geometry of the streamtubes and a smaller scale heterogeneity within each streamtube quantified indirectly by the Peclet number. The diffusive length scale associated with the choice of the Peclet number also allows scaling of the two-dimensional solution.

In the two-phase immiscible case the velocity field becomes a function of saturation and the streamtubes are updated periodically as the flood progresses. The Riemann approach is used to map the Buckley-Leverett solution along streamtubes. Evidence is presented to show that the error due to the Riemann approach is less than the error introduced by numerical diffusion in a traditional finite difference solution. The key result, though, is the convergence of the streamtube approach with orders of magnitude fewer matrix inversions (velocity field updates) than traditional solutions.

Only a few streamtube updates (less than 20 over 2 pore volumes injected) are necessary to predict overall recovery correctly. The speed of the streamtube approach is put to use by processing 60 geostatistical images to demonstrate the interaction of nonlinearity and reservoir heterogeneity.

Applying the streamtube approach to first-contact miscible flow raises the challenging question of the 'correct' one-dimensional solution to be used. Scaling arguments are used to suggest that streamtubes that gave rise to a Fickian limit for $M = 1$ displacements (tracer flow) should now see a viscous fingering flow regime for unstable $M > 1$ first-contact displacements. Thus, a Todd–Longstaff model is used to capture the sub-streamtube viscous fingering regime. Solutions are found using a piston-like one-dimensional solution and a CD-solution along streamtubes as well, although these solutions cannot be reconciled with the scale of the $M = 1$ solution. The streamtube method is again able to predict recoveries using orders (2-3) of magnitude less computation time than traditional simulation approaches. To demonstrate the power of this approach, 180 recoveries are found to show how nonlinearity and reservoir heterogeneity interact to define the uncertainty in overall recovery, and the usefulness of the streamtube approach as a fast filter is pointed out. Only permeability fields returning maximum and minimum overall recoveries in the streamtube approach need to be used to confirm the spread in recovery using an expensive finite difference/finite element simulation.

For compositional displacements the streamtube approach is shown to be particularly powerful due to its simplicity, robustness, and speed. The streamtube method is used to assess how good traditional numerical solutions to compositional displacements really are, particularly in view of interactions of numerical diffusion interacting with phase behavior calculations. The key result is the demonstration that numerical diffusion can substantially if not completely eliminate any mobility contrast in finite difference solutions. Streamtube solutions can be made to match finite difference solutions by simply using a unit mobility ratio calculation: mapping one-dimensional composition profiles along constant streamtubes. The resulting speed-up can range from 3 to 5 order of magnitude. In traditional finite difference simulation, convergence of the solution by progressive grid refinement is very slow, possibly requiring several

times (2-4) the number of grid refinements used in FCM displacements to demonstrate convergence. Finally, because mixing due to viscous crossflow and transverse numerical diffusion result in the same effect, their individual contribution can not be quantified readily. The streamtube solution is, by definition, a solution that cannot account for mixing due to viscous crossflow or transverse diffusion, and thus it represents a limiting solution where these mechanisms are assumed to have a second-order effect.

8.2 Limitations of the Streamtube Approach

As with all numerical techniques, the streamtube approach discussed in this dissertation clearly has its limitations. In part, the limitations are connected to the one-dimensional solutions used along the streamtube. The Riemann approach to mapping one-dimensional solutions along periodically updated streamtubes centers on the assumption of constant boundary conditions. If the boundary conditions change with time, as may happen in an areal domain where wells are shut-in, new wells are introduced, and flow rates vary, the Riemann approach may not work. Another key assumption in the streamtube method is the dominance of the heterogeneity in determining the flow response. If the reservoir is only mildly heterogeneous, though, viscous fingers, which the streamtube solution would fail to recognize, may actually dominate the displacement mechanism. The streamtube approach is not able to represent any transverse flow mechanism that leads to mixing explicitly. Thus, transverse diffusion and mixing due to viscous forces cannot be accounted for. Finally, accounting for gravity may not be as straightforward as modeling viscous forces, particularly in multiphase flow, because now the velocity vectors for each phase do not point in the direction of the total velocity.

8.3 Conclusions

The following main conclusions, in order of importance, are drawn from applying the streamtube approach to modeling multiphase, multicomponent flow:

Fast, accurate, and robust solutions. The streamtube approach produces fast, accurate, and robust solutions for displacements that are dominated by reservoir heterogeneity. Streamtube geometries capture the impact of heterogeneity on the flow field, while the one-dimensional solutions mapped along them retain the essential physics of the displacement mechanism. Speed-up is by two to three orders of magnitude for two-phase immiscible and first-contact miscible displacements and four to five orders for two-phase compositional displacements. The absence of any convergence criteria and the ability to capture all the essential physics of the displacement (like phase behavior) in the one-dimensional solution leads to particularly robust solutions.

Statistical reservoir forecasting. The speed of the streamtube approach makes it an ideal tool for statistical reservoir forecasting: hundreds of geostatistical images can be processed in a fraction of the time required by traditional reservoir simulators. Applications to two-phase immiscible and first-contact miscible displacements show a substantial uncertainty in overall recovery due to the combined effects of reservoir heterogeneity and the inherent nonlinearity of the displacements. As reservoir heterogeneity and nonlinearity increase so does the uncertainty in overall recovery. The streamtube approach can be used to quantify this uncertainty, which in turn can then be confirmed by a more expensive traditional approach using only the two geostatistical images that produces the maximum and minimum recoveries. Although the streamtube method makes strong assumptions in generating the two-dimensional solutions, the uncertainty in recovery due to heterogeneity is shown to be substantially larger than the error introduced by the Riemann approach.

Weak nonlinearity of Ψ. For all displacements, the necessary updates of the streamtubes to converge onto a solution are shown to be many orders of magnitude less than the equivalent number of pressure solves in traditional numerical simulation approaches. As a result, updating the streamtubes only periodically (20-40 times per 2 pore volumes injected) and using a one-dimensional solutions that captures the essential physics of the displacement is sufficient to give accurate

overall recoveries.

Impact of numerical diffusion on compositional displacements. Numerical diffusion is found to have a significant role in reducing the mobility contrast in traditional finite difference solutions of compositional displacements. Comparison of streamtube solutions to finite difference solutions it is found that the original mobility contrast is substantially reduced and even completely eliminated by the presence of numerical diffusion. Streamtube solutions can be made to match finite difference solutions by simply using a unit mobility ratio profile. Reservoir heterogeneity, phase behavior, and numerical diffusion are found to be so dominant in compositional displacements that convergence due to progressive grid refinement is very slow. Two to four times the refinement used in first-contact miscible displacements may be necessary in compositional displacements, particularly if a single-point upstream weighting scheme is being used, to see the equivalent improvement in the solution. As a result, compositional displacements on coarse grids obtained using a single-point upstream weighting scheme are not likely to result in converged solutions.

Decoupling of phase behavior from 2D grid. The streamtube approach is particularly powerful for multiphase compositional displacement. All the phase behavior is now contained in the one-dimensional solution that is mapped along the streamtubes, completely decoupling the underlying cartesian grid used to specify reservoir heterogeneity from phase behavior considerations. This approach differs from traditional approaches to reservoir simulation, which perform a flash calculation for each grid block at each time step. As a result, the streamtube approach makes for very robust solutions, particularly in the case of compositional displacements.

Crossflow. Because mixing due to viscous crossflow and transverse numerical diffusion result in the same effect, their individual contributions cannot be quantified readily. The streamtube solution is, by definition, a solution that cannot account for mixing due to viscous crossflow or transverse diffusion, and thus it represents a limiting solution where these mechanisms are assumed to have a

second-order effect. The streamtube solutions provide a useful limiting case against which the impact of crossflow can be measured.

Diffusion-free solutions. One-dimensional analytical solutions can be mapped along streamtubes to obtain numerical-diffusion-free solutions. For tracer flow, the solution is shown to be exact in the limit of infinite streamtubes and benchmark solutions can be generated in two dimensions, which can be used to test numerical schemes.

Scale of 2D solutions. By mapping a convection-diffusion model or a viscous fingering model an implicit assumption about the scale of the two-dimensional solutions is made in first-contact miscible displacements. Sub-streamtube heterogeneities are assumed to lead to a Fickian limit for $M = 1$ displacements, while giving rise to viscous fingering flow regime for unstable $M > 1$ displacements. Thus, the streamtube approach is an example of how physical phenomena that take place at different scales can be nested into a single model.

NOMENCLATURE

A	area, or coefficient
A_i	cross section of ith streamtube
B	coefficient
C	concentration, or coefficient
C_D	dimensionless concentration
f_w	water fractional flow
HI	heterogeneity index
h	separation length of permeability values
i	index, x-direction or streamtube; or $\sqrt{-1}$
j	index, y-direction
$\vec{\vec{K}}_{ij}$	diffusion/dispersion of component i in phase j, tensor
K	diffusion/dispersion, constant
K_m	molecular diffusion
$\vec{\vec{k}}$	absolute permeability, tensor
k_x	absolute permeability in x-direction
k_y	absolute permeability in y-direction
k_{rj}	relative permeability of phase j
L	system length
L_{rep}	representative diffusive length scale
M	mobility ratio
M_{eff}	effective mobility ratio
M_{end}	end-point mobility ratio
M_{shock}	shock front mobility ratio

M_w	molecular weight
N	number of streamtubes
NX	number of grid blocks in x-direction
NY	number of grid blocks in y-direction
N_p	number of phases
N_{Pe}	Peclet number
P	pressure
P_c	critical pressure
q_i	flow rate of ith streamtube
Q	flow rate
Q_{total}	total flow rate
S_j	saturation of phase j
S_w	water saturation
s	coordinate along a streamline
T_c	critical temperature
TVD	total variation diminishing
t	time
t_D	dimensionless time
t_{Di}	dimensionless time of ith streamtube
$u_{w,o}$	water, oil Darcy velocity
u_j	Darcy velocity of phase j
u_x	Darcy velocity in the x-direction
u_y	Darcy velocity in the y-direction
V_c	critical volume
V_{DP}	Dykstra–Parson coefficient
V_{Pi}	porevolume of ith streamtube
$\bar{V}_P$	porevolume used for scaling
v_{Di}	dimensionless velocity along ith streamtube
x	Cartesian direction
x_D	dimensionless distance
x_{D_i}	dimensionless distance along ith streamtube

y	Cartesian direction
y_A	y-coordinate of streamline A
y_B	y-coordinate of streamline B

Greek and symbols

α_L,α_T	longitudinal and transverse dispersivity
Δt_D	dimensionless time intervall
Δx	size of grid block in x-direction
Δy	size of grid block in y-direction,
	or difference in y-coordinate of streamlines at a fixed x
ζ	coordinate along streamtube/streamline
λ	mobility
λ_c	correlation length of permeability field
λ_x	mobility in the x-direction
λ_y	mobility in the y-direction
μ_j	viscosity of phase j
$\mu_{w,o,s}$	water, oil, solvent viscosity
ρ_j	density of phase j
σ	standard deviation
$\sigma_{\ln K}$	standard deviation of log-permeability distribution
ϕ	porosity
Φ	potential function
Ψ	streamfunction
Ω	complex potential
ω	Todd $ Longstaff parameter,
	or acentric factor
ω_i	mole fraction of component i
ω_{ij}	mole fraction of component i in phase j

Bibliography

[1] Abbaszadeh-Dehghani, M.: *Analysis of Unit Mobility Ratio Well-to-Well Tracer Flow to Determine Reservoir Heterogeneity*, PhD dissertation, Stanford University (December 1982).

[2] Abramowitz, M. and Stegun, I.A.: *Handbook of Mathematical Functions*, Dover (1970).

[3] Araktingi, U.G. and Orr, F.M., Jr.: "Viscous Fingering in Heterogeneous Porous Media," *Advanced Technology Series* (October 1993) **Vol.1, No.1**, 71–80.

[4] Aris, R. and Amundson, N.: "Some Remarks on Longitudinal Mixing or Diffusion in Fixed Beds," *AIChe Journal* (1957) 280.

[5] Arya, A., Hewett, T.A., Larson, R.G., and Lake, L.W.: "Dispersion and Reservoir Heterogeneity," *SPE Reservoir Engineering* (February 1988) 139–148.

[6] Aziz, K. and Settari, A.: *Petroleum Reservoir Simulation*, Applied Science Publishers, Essex, England (1979).

[7] Bahralolom, I., Bretz, R.E. and Orr, F.M., Jr.: "Experimental Investigation of the Interaction of Phase Behavior With Microscopic Heterogeneity in a CO2 Flood," *Soc. Pet. Eng. J.* (May 1988) **3**, No. 2, 662–672.

[8] Bear, J.: *Dynamics of Fluids in Porous Media*, American Elsevier, New York (1972).

[9] Blackwell, R.: "Laboratory Studies of Microdispersion Phenomena," *Society of Petroleum Engineers Journal* (March 1962) No. 1–8.

[10] Blackwell, R.J., Rayne, J.R. and Terry, W.M.: "Factors Influencing the Efficiency of Miscible Displacement," *Trans., AIME* (1959) **216**, 1–8.

[11] Blunt, M.J. et al.: "Predictive Theory for Viscous Fingering in Compositional Displacement," *SPE Reservoir Engineering* (February 1994) **9**, No. 1, pp. 73–80.

[12] Bommer, M.P. and Schechter, R.S.: "Mathematical Modeling of In-Situ Uranium Leaching," *Society of Petroleum Engineers Journal* (December 1979) 393–400.

[13] Bratvedt, F., Bratvedt, K., Buchholz, C.F. et al.: "A New Front-Tracking Method for Reservoir Simulation," paper SPE 19805 presented at the 1989 64th SPE Annual Technical Conference and Exhibition, San Antonio, TX, October.

[14] Brigham, W.E., Reed, P.W., and Dew, J.N.: "Experiments on Mixing During Miscible Displacements in Porous Media," *Society of Petroleum Engineers Journal* (March 1961) 1–8.

[15] Buckley, S.E. and Leverett, M.C.: "Mechanism of Fluid Displacement in Sands," *Trans., AIME* (1941) **249**, 107–116.

[16] Campbell, B. and Orr, F. J.: "Flow Visualization for CO_2/Crude–Oil Displacements," *Society of Petroleum Engineers Journal* (October 1985) 665–78.

[17] Chang, Y.-B.: *Development of Three–Dimensional, Equation–of–State Compositional Reservoir Simulator for Miscible Gas Flooding*, PhD dissertation, The University of Texas at Austin (1990).

[18] Chang, Y.-B., Lim, M.T., Pope, G.A., and Sepehrnoori, K.: "CO_2 Flow Patterns Under Multiphase Flow: Heterogeneous Field Scale Conditions," *SPE Reservoir Engineering* (August 1994) 208–216.

[19] Chang, Y.-B., Pope, G.A., and Sepehrnoori, K.: "A Higher–Order Finite Difference Compositional Simulator," *J. Phys. Sci. and Eng.* (November 1990).

[20] Cheng, A.-D.: "Darcy's Flow With Variable Permeability: A Boundary Integral Solution," *Water Resources Research* (July 1984) **20**, No. 7, 980–984.

[21] Christie, M.: "High Resolution Simulation of Unstable Flows in Porous Media," *SPE Reservoir Engineering* (1989) **4**, No. 3, 297–303.

[22] Christie, M. and Bond, D.: "Multidimensional Flux–Corrected Transport for Reservoir Simulation," paper SPE SPE 13505 presented at the 1985 Reservoir Simulation Symposium, Dallas.

[23] Christie, M.A. and Bond, D.J.: "Detailed Simulation of Unstable Processes in Miscible Flooding," *Soc. Pet. Eng. Res. Eng.* (November 1987) **2**, No. 4, 514–522.

[24] Churchill, R. and Brown, J.: *Complex Variables and Applications*, fifth edition edition, McGraw-Hill Publishing Company (1990).

[25] Courant, R., Friedrichs, K.O., and H. Lewy: "Ueber die partiellen Differenzgleichungen der mathematischen Physik," *Math. Ann.* (1928) **100**, pp. 32–74.

[26] Dagan, G.: "Time–Dependent Macrodispersion for Solute Transport in Anisotropic Heterogeneous Aquifers," *Water Resources Research* (September 1988) **24**, No. 9, 1491–1500.

[27] Dake, L.P.: *Fundamentals of Reservoir Engineering*, Elsevier Scientific Publishing Company (1978).

[28] Deutsch, C.V. and Journel, A.G.: *GSLIB Geostatistical Software Library and User's Guide*, Oxford University Press (1992).

[29] Dindoruk, B.: *Analytical Theory of Multiphase, Multicomponent Displacement in Porous Media*, PhD dissertation, Stanford University, Stanford, CA (1992).

[30] Dindoruk, B., Johns, R.T. and Orr, F.M., Jr.: "Analytical Solution for Four Component Gas Displacements with Volume Change on Mixing," (June 1992) Third European Conference on the Mathematics of Oil Recovery, Delft, Holland.

[31] Dougherty, E. and Sheldon, J.: "The Use of Fluid-Fluid Interfaces to Predict the Behavior of Oil Recovery Processes," *Society of Petroleum Engineers Journal* (June 1964) 171–182.

[32] Dougherty, E.L.: "Mathematical Model of an Unstable Miscible Displacement," *Soc. Pet. Eng. J.* (June 1963) 155–163.

[33] Douglas, J., Peaceman, D.W., and Rachford, H.H.: "A Method for Calculating Multi-Dimensional Immiscible Displacement," *Trans. AIME* (1959) **216**.

[34] Doyle, R.E. and Wurl, T.M.: "Stream Channel Concept Applied to Waterflood Performance Calculations For Multiwell, Multizone, Three-Component Cases," *Journal of Petroleum Technology* (March 1971) 373–380.

[35] Emanuel, A.S., Alameda, G.K., Behrens, R.A., and Hewett, T.A.: "Reservoir Performance Prediction Methods on Fractal Geostatistics," *SPE Reservoir Engineering* (August 1989) 311–318.

[36] Evans, D. and Raffensperger, J.: "On the Stream Function for Variable-Density Groundwater Flow," *Water Resources Research* (August 1992) **28**, No. 8, 2141–2145.

[37] Ewing, R.E, Russell, T.F., and Wheeler, M.F.: "Simulation of Miscible Displacement Using Mixed Methods and a Modified Method of Characteristics," paper SPE 12241 presented at the 1983 Reservoir Simulation Symposium, San Francisco, CA, November.

[38] Fayers, F. and Lee, S.: "Crossflow Mechanisms In Oil Displacements By Gas Drive In Heterogeneous Reservoirs," *In Situ* (1994) **18**, No. 4.

[39] Fayers, F.J.: "An Approximate Model with Physically Interpretable Parameters for Representing Miscible Viscous Fingering," *SPE Reservoir Engineering* (May 1988) **3**, 551–558.

[40] Fayers, F.J., Aléonard, B., and Jouaux, F.: "Progress with Compositional Studies in Heterogeneous Systems for Slightly Submiscible Gas Displacements," paper SPE SPE 27832 presented at the 1994 DOE/SPE Improved Oil Recovery Symposium, Tulsa, Oklahoma, April 17–20.

[41] Fayers, F.J., Blunt, M.J. and Christie, M.A.: "Comparison of Empirical Viscous Fingering Models and Their Calibration for Heterogeneous Problems," *SPE Reservoir Engineering* (May 1992) 195–202.

[42] Frind, E. and Matanga, G.: "The Dual Formulation of Flow for Contaminant Transport Modeling 1. Review of Theory and Accuracy Aspects," *Water Resources Research* (February 1985) **21**, No. 2, 159–169.

[43] Frind, E.O., Matanga, G.B., and Cherry, J.A.: "The Dual Formulation of Flow for Contaminant Transport Modeling 2. The Borden Aquifer," *Water Resources Research* (February 1985) **21**, No. 2, 170–182.

[44] Gardner, J.W. and Ypma, J.G.J.: "An Investigation of Phase-Behavior/Macroscopic-Bypassing Interaction in CO2 Flooding," *Soc. Pet. Eng. Journal* (October 1984) 508–520.

[45] Gelhar, L.: *Stochastic Subsurface Hydrology*, Prentice Hall (1993).

[46] Gelhar, L.W. and Axness, C.L.: "Three-Dimensional Stochastic Analysis of Macrodispersion in Aquifers," *Water Resources Research* (1983) **19**, No. 1, 161–180.

[47] Glimm, J., Lindquist, B., McBryan, O.A., Plohr, B., and Yaniv, S.: "Front Tracking for Petroleum Simulation," paper SPE 12238 presented at the 1983 Reservoir Simulation Symposium, San Francisco, CA, November.

[48] Gorell, S.: "Outlook for Calibration of Large Grid–Block Models for Miscible Flooding Applications," paper SPE 24186 presented at the 1992 1992 SPE/DOE Eight Symposium on Enhanced Oil Recovery, Tulsa, OK, April.

[49] Hauber, W.C.: "Prediction of Waterflood Performance for Arbitrary Well Patterns and Mobility Ratios," *Journal of Petroleum Technology* (January 1964) 94–103.

[50] Hewett, T. and Behrens, R.: "Scaling Laws in Reservoir Simulation and Their Use in a Hybrid Finite Difference/Streamtube Approach to Simulation the Effects of Permeability Heterogeneity," *Reservoir Characterization, II*, L. Lake and J. Carroll, H.B. (eds.), Academic Press, Inc., London (1991).

[51] Higgins R.V. and Leighton, A.J.: "A Computer Method to Calculate Two–Phase Flow in Any Irregularly Bounded Porous Medium," *Journal of Petroleum Technology* (June 1962) 679–683.

[52] Higgins R.V. and Leighton, A.J.: "Computer Prediction of Water Drive of Oil and Gas Mixtures Through Irregularly Bounded Pororus Media — Three-Phase Flow," *Journal of Petroleum Technology* (September 1962) 1048–1054.

[53] Higgins, R.V., Boley, D.W., and A.J. Leighton: "Aids to Forecasting The Performance of Water Floods," *Journal of Petroleum Technology* (September 1964) 1076–1082.

[54] Johns, R.T.: *Analytical Theory of Multicomponent Gas Drives With Two-Phase Mass Transfer*, PhD dissertation, Stanford University, Stanford, CA (1992).

[55] Johns, R.T., B. Dindoruk, and Orr, F.M. Jr.: "Analytical Theory of Combined Condensing/Vaporizing Gas Drives," paper SPE 24112 presented at the 1992 SPE/DOE Eighth Symposium on Enhanced Oil Recovery, Tulsa, OK, April.

[56] Johns, R.T., B. Dindoruk, and Orr, F.M. Jr.: "Analytical Theory of Combined Condensing/Vaporizing Gas Drives," *SPE Advanced Technology Series* (May 1993) **1**, No. 2, 7–16.

[57] Johns, R.T., Fayers, F.J. and Orr, F.M., Jr.: "Effect of Gas Enrichment and Dispersion on Nearly Miscible Displacements in Condensing/Vaporizing Drives," *SPE Advanced Technology Series* (1994) **2**, No. 2, 173–180.

[58] King, M.J., Blunt, M.J., Mansfield, M., and Christie, M.A.: "Rapid Evaluation of the Impact of Heterogeneity on Miscible Gas Injection," paper SPE 26079 presented at the 1993 Western Regional Meeting, Anchorage.

[59] Koval, E.J.: "A Method for Predicting the Performance of Unstable Miscible Displacements in Heterogeneous Media," *Soc. Pet. Eng. J.* (June 1963) 145–154.

[60] Lafe, O. and Cheng, A.-D.: "A Perturbation Boundary Element Code for Steady State Groundwater Flow in Heterogeneous Aquifers," *Water Resources Research* (June 1987) **23**, No. 6, 1079–1084.

[61] Lafe, O.E., Ligget, J.A., and Liu, P.L-F.: "BIEM Solutions to Combinations of Leaky, Layered, Confined, Unconfined, Nonisotropic Aquifers," *Water Resources Research* (October 1981) **17**, No. 5, 1431–1444.

[62] Lake, L.W., Johnston, J.R., and Stegemeier, G.L.: "Simulation and Performance Prediction of a Large-Scale Surfactant/Polymer Project," *Society of Petroleum Engineers Journal* (December 1981) 731–739.

[63] Lake, W.L.: *Enhanced Oil Recovery*, first edition, Prentice Hall, Engelwood Cliffs, NJ 07632 (1989).

[64] LeBlanc, J.L. and Caudle, B.H.: "A Streamline Model for Secondary Recovery," *Society of Petroleum Journal* (March 1971) 7–12.

[65] Lee, B.: "Potentiometric-model Studies of Fluid Flow in Petroleum Reservoirs," *Trans. AIME* (1948) **174**, 41.

[66] Lee, S-T, Lo, H. and Dharmawardhana, B.T.: "Analysis of Mass Transfer Mechanisms Occurring in Rich Gas Displacement Process," paper SPE 18062

presented at the 1988 SPE Annual Technical Conference and Exhibition, Houston, TX, October 2-5.

[67] LeVeque, R. J.: *Numerical Methods for Conservation Laws*, Birkhaeuser Verlag (1992).

[68] Lin, J.: *An Image Well Method for Bounding Arbitrary Reservoir Shapes in the Streamline Model*, PhD dissertation, U. of Texas , Austin (December 1972).

[69] Liu, P.L-F., Cheng A.H-D., Ligget J.A., and Lee, J.H.: "Boundary Integral Equation Solutions to Moving Interface Between Two Fluids in Porous Media," *Water Resources Research* (October 1981) **17**, No. 5, 1445–1452.

[70] Martin, J.C. and Wegner, R.E.: "Numerical Solution of Multiphase, Two-Dimensional Incompressible Flow Using Streamtube Relationships," *Society of Petroleum Engineers Journal* (October 1979) 313–323.

[71] Martin, J.C., Woo, P.T., and Wegner, R.E.: "Failure of Stream Tube Methods To Predict Waterflood Performance of an Isolated Inverted Five-Spot at Favorable Mobility Ratios," *Journal of Petroleum Technology* (February 1973) 151–153.

[72] Masukawa J. and Horne, R.N.: "Application of the Boundary Integral Method to Immiscible Displacement Problems," *SPE Reservoir Engineering* (August 1988) 1069–1077.

[73] Matanga, G.: "Stream Functions in Three-Dimensional Groundwater Flow," *Water Resources Research* (September 1993) **29**, No. 9, 3125–3133.

[74] Matheron, G. and de Marsily, G.: "Is Transport in Porous Media Always Diffusive? A Counterexample.," *Water Resources Research* (1980) **16**, No. 5, 901–9177.

[75] Mathews, J.L., Emanuel, A.S., and Edwards, K.A.: "Fractal Methods Improve Mitsue Miscible Predictions," *Journal of Petroleum Technology* (November 1989) 1136–1989.

[76] Mishra, S.: *On the Use of Pressure and Tracer Test Data for Reservoir Description*, PhD dissertation, Stanford University, Stanford, CA (1987).

[77] Monroe, W.W.: "The Effects of Dissolved Methane on Composition Paths in Quaternary CO_2-Hydrocarbon Systems," Master's thesis, Stanford University, Stanford, CA (August 1986).

[78] Monroe, W.W., Silva, M.K., Larsen, L.L. and Orr, F.M. Jr.: "Composition Paths in Four-Component Systems: Effect of Dissolved Methane on 1D CO_2 Flood Performance," *Soc. Pet. Eng. Res. Eng.* (August 1990) 423–432.

[79] Morel-Seytoux, H.: "Analytical-Numerical Method in Waterflooding Predictions," *Society of Petroleum Engineers Journal* (September 1965) 247–258.

[80] Muskat, M.: *Flow of Homogeneous Fluids*, International Human Resources Development Corporation, 137 Newbury Street, Boston MA 02116 (1937, 1982).

[81] Muskat, M.: "The Theory of Potentiometric Models," *Trans. AIME* (1948) **179**, 216–221.

[82] Muskat, M. and Wyckoff, R.: "A Theoretical Analysis of Waterflooding Networks," *Trans. AIME* (1934) **107**, 62–77.

[83] Nelson, R.: "Evaluating the Environmental Consequences of Groundwater Contamination 2. Obtaining Location/Arrival Time and Location/Outflow Quantity Distributions for Steady Flow Systems," *Water Resources Research* (March 1978) **14**, 416–428.

[84] Neuman, S.: "Universal Scaling of Hydraulic Conductivities and Dispersivities in Geologic Media," *Water Resources Research* (August 1990) **26**, No. 8, 1749–1758.

[85] Newley, T.M.J. and Merrill R.C. Jr.: "Pseudocomponent Selection for Compositional Simulation," *Soc. Pet. Eng. Res. Eng.* (November 1991) **6**, No. 4, 490–496.

[86] Numbere, D. and Tiab, D.: "An Improved Streamline-Generating Technique That Uses the Boundary (Integral) Element Method," *SPE Reservoir Engineering* (August 1988) 1061–1068.

[87] Orr, F.M., Jr., Johns, R.T. and Dindoruk, B.: "Miscibility in Four-Component Vaporizing Gas Drives," paper SPE 22637 presented at the 1991 SPE Annual Technical Conference and Exhibition, Dallas, TX, October 6–9.

[88] Orr, F.M., Jr., Johns, R.T. and Dindoruk, B.: "Miscibility in Four-Component Vaporizing Gas Drives," *Soc. Pet. Eng. Res. Eng.* (1993) **8**, No. 28, 135–142.

[89] Pande, K.: "Effects of Gravity and Viscous Crossflow on Hydrocarbon Miscible Flood Performance in Heterogeneous Reservoirs," paper SPE SPE 24935 presented at the 1992 67th Annual Technical Conference and Exhibition, Washington, DC, October 4–7.

[90] Pande, K.K. and Orr, F.M., Jr.: "Interaction of Phase Behavior, Reservoir Heterogeneity and and Crossflow in CO_2 Floods," paper SPE 19668 presented at the 1989 SPE Annual Technical Conference and Exhibition, San Antonio, TX, October 8–11.

[91] Parsons, R.W.: "Directional Permeability Effects in Developed and Unconfined Five-Spots," *Journal of Petroleum Technology* (April 1972) 487–494.

[92] Peng, D.Y. and Robinson, D.B.: "A New Two-Constant Equation of State," *Ind. Eng. Chem. Fund.* (1976) **15**, 59–64.

[93] Perkins, T. and Johnston, O.: "A Review of Diffusion and Dispersion in Porous Media," *SPEJ* (March 1963) No. 3, 70–80.

[94] Renard, G.: "A 2D Reservoir Streamtube EOR Model with Periodical Automatic Regeneration of Streamlines," *In Situ* (1990) **14**, No. 2, 175–200.

[95] Sato, K.: *Accelerated Perturbation Boundary Element Model for Flow Problems in Heterogeneous Reservoirs*, PhD dissertation, Stanford University (1992).

[96] Sato, K. and Horne, R.: "Perturbation Boundary Element Method for Heterogeneous Reservoirs: Partt 1 — Steady-State Flow Problems," *SPE Formation Evaluation* (December 1993) 306–314.

[97] Sato, K. and Horne, R.: "Perturbation Boundary Element Method for Heterogeneous Reservoirs: Part 1 — Transient-Flow Problems," *SPE Formation Evaluation* (December 1993) 315–322.

[98] Sato, K. and Abbaszadeh, M.: "Complex Variable Boundary Element Method fo Tracking Streamlines across Fractures," Proc. of the 4th European Conference on the Mathematics of Oil Recovery, Roros, Norway (June 7–10 1994) Topic D.

[99] Sheldon, J. and Dougherty, E.: "A Numerical Method for Computing the Dynamical Behavior of Fluid-Fluid Interfaces in Permeable Media," *Society of Petroleum Engineers Journal* (June 1964) 158–170.

[100] Sorbie, K.S., Feghi, F., Pickup, G.E., Ringrose, P.S., and Jensen J.L.: "Flow Regimes in Miscible Displacement in Heterogeneous Correlated Random Fields," paper SPE 24140 presented at the 1992 SPE/DOE Eighth Symposium on Enhanced Oil Recovery, Tulsa, OK, April.

[101] Stalkup, F.I.: "Miscible Displacement," Monograph 8, Soc. Pet. Eng. of AIME, New York (1983).

[102] Stalkup, F.I.: "Displacement Behavior of the Condensing/Vaporizing Gas Drive Process," paper SPE 16715 presented at the 1987 SPE Annual Technical Conference and Exhibition, Dallas, TX, September.

[103] Strack, O.: *Groundwater Mechanics*, Prentice Hall, Englewood Cliffs (1989).

[104] Tang, R.W., Behrens, R.A., Emanuel, A.S.: "Reservoir Studies Using Geostatistics To Forecast Performance," paper SPE 18432 presented at the 1989 SPE Symposium on Reservoir Simulation, Houston, TX.

[105] Tchelepi, H.: *Viscous Fingering, Gravity Segregation, and Permeability Heterogeneity in Two-Dimensional and Three-Dimensional Flows*, PhD dissertation, Stanford University (March 1994).

[106] Todd, M.R. and Longstaff, W.J.: "The Development, Testing and Application of a Numerical Simulator for Predicting Miscible Flood Performance," *Trans., AIME, 253* (1972) 874–882.

[107] UTCOMP–3.2: *An Equation of State Compositional Simulator*, Center for Petroleum and Geosystems Engineering, University of Texas at Austin, TX 78712 (May 1993).

[108] Waggoner, J.R., Castillo, J.L., and Lake, L.W.: "Simulation of EOR Processes in Stochastically Generated Permeable Media," *Soc. Pet. Eng. Formation Eval.* (June 1992) 173–180.

[109] Walsh, B.W. and Orr, F.M. Jr.: "Prediction of Miscible Flood Performance: The Effect Of Dispersion on Composition Paths in Ternary Systems.," *IN SITU* (1990) **14**, No. 1, 19–47.

[110] Wang, B., Lake, L.W., and Pope, G.A.: "Development and Application of a Streamline Micellar/Polymer Simulator," paper SPE 10290 presented at the 1981 56th Annual Fall Technical Conference and Exhibition, San Antonio, TX.

[111] Wattenbarger, R.: *Simulation of Tracer Flow Through Heterogeneous Porous Media*, PhD dissertation, Stanford University (1993).

[112] Yih, C.: "Stream Functions in Three-Dimensional Flow," *La Houille Blanche* (1957) **3**, 445–450.

[113] Zauderer, E.: *Partial Differential Equations of Applied Mathematics*, second edition, Wiley-Interscience, New York, NY (1989).

[114] Zick, A.A.: "A Combined Condensing/Vaporizing Mechanism in the Displacement of Oil by Enriched Gas," paper SPE 15493 presented at the 1986 SPE Annual Technical Conference and Exhibition, New Orleans, LA, October.

[115] Zijl, W.: "Numerical Simulations Based on Stream Functions and Velocities in Three-Dimensional Groundwater Flow," *J. Hydrol.* (1986) **85**, 349–365.

Appendix A

Generating Permeability Fields

Although many sophisticated techniques exist to generate correlated permeability fields (*Deutsch and Journel, 1992*), a moving window method is used in this thesis because of its simplicity and robustness. The underlying assumption is that the permeability k is log-normally distributed. Thus, the probability that $\ln k$ is less than or equal to some values x is given by

$$P(x) = \frac{1}{\sigma\sqrt{2\pi}} \int_{-\infty}^{x} e^{-\frac{(t-\mu)^2}{2\sigma^2}} dt \quad , \tag{A.1}$$

where μ and σ^2 are the average and variance respectively of the random variable $x = \ln k$. The algorithm is as follows.

1. **Setting up the grid.** If the desired reservoir is to have NX by NY grid blocks, then the actual grid used to find the correlated field must have $(NX + IX)$ by $(NY + IY)$ blocks, where $(IX \times \Delta x)$ and $(IY \times \Delta y)$ are greater than or equal to the radii in the x- and y-directions of the moving window. Δx is and Δy specify the size of each grid block. This will assure that all $(NX \times NY)$ blocks will be assigned an average value calculated from the same number of points.

2. **Generating a spatially random uniform distribution.** The easiest way to accomplish this is to simply draw $(NX + IX) \times (NY + IY)$ random values from the closed interval $[0, 1]$ and assign them sequentially to each grid block. In fact, it is better to generate a uniform distribution by picking $(NX+IX)\times(NY+IY)$

equally spaced values from the open interval $(0, 1)$ and assigning them randomly to the grid blocks. The advantage is that the underlying distribution will always be symmetrical and independent from the random number generator. The random number is only used to pick a random location in space, but the numerical value of the random number is discarded.

3. **Normal transformation.** This step is not strictly necessary, but it does add clarity to the method and is therefore presented here. With all blocks having been assigned a value between zero and one, the underlying uniform distribution is transformed to a standardized normal distribution ($\mu = 0, \sigma = 1$) by using the inverse of the cumulative distribution function. Recall that the standardized cumulative distribution function is defined as

$$\Phi(u) = \frac{1}{\sqrt{2\pi}} \int_{-\infty}^{u} e^{-\frac{t^2}{2}} dt \ . \tag{A.2}$$

Thus, for each point x_i from the uniform distribution a point u_i is found from

$$u_i = \Phi^{-1}(x_i) \ . \tag{A.3}$$

The inversion, of course, is done numerically. A good source for expressions approximating Φ and Φ^{-1} is *Abramovitz and Stegun* (1970).

4. **Moving window.** With the underlying distribution now being normal, but randomly distributed, an ellipse is used as a moving window to find the correlated field. The value for each block ($\bar{u}_i$) is found by simply centering the ellipse on the grid block and averaging all values (u_i) that fall within the ellipse. The resulting spatial correlation will then have a range equal to the diameters of the ellipse. The resulting field is still normally distributed but with a standard deviation less then one ($\sigma' < 1$) and a mean very close to zero ($\mu' \approx 0$).

5. **Transforming to absolute permeability.** Finally, the averaged field is scaled such that it has the desired standard deviation, or order of magnitude variation, and average. If the average field values of part 4 are denoted by $\bar{u}_i$ and have an average and standard deviation given by $\bar{\mu}$ and $\bar{\sigma}$ then the transformation is

given by

$$\frac{\ln k_i - \mu_{\ln k}}{\sigma_{\ln k}} = \frac{\bar{u}_i - \bar{\mu}}{\bar{\sigma}} \quad , \tag{A.4}$$

where $\mu_{\ln k}$ and $\sigma_{\ln k}$ and the desired values for the permeability field. The actual permeability values are therefore found using

$$k_i = \exp\left(\frac{\sigma_{\ln k}}{\bar{\sigma}}(\bar{u}_i - \bar{\mu})\right) + \mu_{\ln k} \quad . \tag{A.5}$$

Appendix B

Summaries of Relevant Papers

Muskat and Wyckoff, 1932: *A Theoretical Analysis of Waterflooding Networks*
In this paper Muskat and Wyckoff investigate the recovery efficiency of well patterns using streamlines. Using an electrical conduction model, they consider a staggered line drive, a direct line drive, a five-spot, and a seven-spot. The reservoir is considered homogeneous and tracer-flow assumptions are used for all calculations (although they discuss their results in terms of multi-phase flow). They conclude that the staggered line drive has 'the most favorable physical features'. It is interesting to note though, that Muskat and Wyckoff conclude their discussion by suggesting that well spacing and arrangement may be of minor importance compared to the channeling caused by 'high permeability zones within the main body of sand'.
Contribution: Quantifying flood efficiencies of four different well patterns using streamtubes.

Higgins and Leighton, 1962 (11/61)[1]: *A Computer Method to Calculate Two-Phase Flow in Any Irregularly Bounded Porous Medium*
This paper is generally considered as being the first to introduce streamtubes to model two-phase flow in porous media. Higgins and Leighton acknowledge that complex well spacing have been studied using 'potentiometric' models before, but point out that these considered single phase flow only. They test their two-phase approach for a five-spot against laboratory waterfloods reported by *Douglas et al.* (1959) as well as their 'long method' for end-point viscosity ratios ranging from 0.083 to 754. They report good matches, though it is important to note that the relative permeability curves they used ('permeability-saturation curves') give rise to rarefaction waves only. The Higgins and Leighton method divides streamtubes into 'sand elements' of equal volume. At the end of each time step, the average mobility (actually referred to as average permeability in the paper) and geometric shape factor are calculated for each sand element. The total resistance along each streamtube ('channel') is then used to find the instantaneous flow rate. The streamtubes are calculated only ones using a single phase formulation and the reservoir is assumed homogeneous.
Contribution: Two-phase flow solution accounting for changing mobility distribution along streamtubes.

Higgins and Leighton, 1962 (4/62): *Computer Predictions of Water Drive of Oil and Gas Mixtures Through Irregularly Bounded Media–Three Phase Flow*

[1]The date in parentheses indicates when the work was first presented.

In this paper, Higgins and Leighton extend their streamtube method to three phase flow. The one-dimensional, three-phase flow solution is constructed by using the water-oil fractional flow to find the two-phase mixed-wave solution and having the displaced oil and gas move ahead of the front by assuming that no oil is displaced by the mobile gas. By considering several non-communicating layer solutions, each of which can have different petrophysical properties, Higgins and Leighton show a good match for a particular field case.
Contribution: Three-phase flow solution along streamtubes.

Hauber, 1964: *Prediction of Waterflood Performance for Arbitrary Well Patterns and Mobility Ratios*
Hauber presents general expressions for determining injectivity, time, and cumulative water injected when the water-oil interface has moved a given distance along a streamtube. He introduces a distortion factor for non-unit mobility ratio displacements to account for changing streamtube geometries as the flood progresses. Although the title of this paper is promising and Hauber indeed presents a rather 'mathematical' approach, it is difficult to follow his derivations, in part due to the confusing notation.
Contribution: Analytical expressions to calculate injectivity, time, and cumulative water injected for an arbitrary streamtube.

Higgins, Boley, and Leighton, 1964 (5/64): *Aids to Forecasting the Performance of Water Floods*
In this paper Higgins et al. extend their method presented in 1962 to a seven-spot, a direct line-drive, and a staggered line-drive. The five-spot results first presented in 1962 are given as well. In all cases the reservoir is considered homogeneous and streamtubes are calculated only once using the single phase assumption. Five streamtubes with 40 cells each were used for each symmetry element in the patterns investigated. In this paper Higgins et al. conclude that phase mobilities (Higgins et al. call them permeabilities) have a greater influence on oil recovery than well spacing patterns. Although never mentioned explicitly, it appears that they used straight line relative permeability curves leading, as in their 1962 paper, to rarefaction waves only. It is interesting to note that they also briefly touch on how an unfavorable vertical permeability profile can be a dominating factor on recovery but do not elaborate.
Contribution: Extension of streamtube approach to different well patterns.

Doyle and Wurl, 1971 (10/69): *Stream Channel Concept Applied to Waterflood Performance Calculations For Multiwell, Multizone, Three-Component Cases*
In this paper Doyle and Wurl extend the Higgins and Leighton streamtube approach to fields that have a non-regular well pattern. Streamtubes ('channels') are generated for the entire field and all necessary information stored for each channel to allow displacement calculations. An example field application is presented. Although Doyle and Wurl do not present any substantially new idea, the paper conveys the simple and straightforward ideas of the streamtube approach though its clear exposition.
Contribution: Application of streamtube solution to non-symmetrical well patterns.

LeBlanc and Caudle, 1971 (5/70): *A Streamline Model for Secondary Recovery*
This paper is, in essence, a rewrite of the original 1962 Higgins and Leighton paper, but improves on the mathematical formulation of the problem. LeBlanc and Caudle generate the streamlines using superposition and explicitly write-out the expressions for the x and y velocity components, something Higgins and Leighton in fact never did. They also mention that each streamtube will see an equal injected volume for the unit mobility case, thus eliminating any need of geometrical information

about the streamtube. LeBlanc and Caudle use the center streamline for all their calculations. But their claim of not having to know the entire streamlines is unsubstantiated . Although true for the limiting unit mobility case, in all other cases they rely on the unit mobility streamlines (and thus on knowledge about the entire flow field) to find the total resistance down each tube.
Contribution: Eliminating Higgins and Leighton geometrical shape factors.

Martin, Woo, and Wegner, 1973 (2/73): *Failure of Stream Tube Methods to Predict Waterflood Performance of an Isolated Five-Spot at Favorable Mobility Ratios*
In this letter to JPT, Martin et al. argue that for favorable mobility ratios the streamtube approach underestimates recovery due the fact that the streamlines in the watered-out region are almost independent of the high-mobility region ahead of the water bank. They show that a better solution is obtained by updating the tubes several times as the flood progresses. A nice graph is presented showing the constant streamlines compared to the streamlines recalculated at some later time. The idea is to recalculate the streamtubes, locate the old saturations onto the new streamtubes, and continue the displacement calculations.
Contribution: Quantifying the error due to the constant streamtube assumption. Show improved recovery prediction by updating streamtube periodically.

Parsons, 1972 (10/71): *Directional Permeability Effects in Developed and Unconfined Five-Spots*
In this paper Parsons investigates the effect of directional permeability on unit mobility displacements using streamlines. Contrary to previous authors, Parsons accumulates a 'time-of-flight' along streamlines, with equal time-of-flight points on different streamlines delineating a flood front. Parsons presents a number of streamline maps for different maximum permeability directions and anisotropy ratios and clearly shows that anisotropy can substantially affect the displacement process. This is particularly true for unconfined patterns.
Contribution: Investigation of the effect of areal anisotropy in permeability on recovery for unit mobility displacements. Use of a time-of-flight coordinate.

Martin and Wegner, 1979 (4/78): *Numerical Solution of Multiphase, Two-Dimensional Incompressible Flow Using Stream-Tube Relationships*
In this paper Martin and Wegner quantify the error caused by the assumption of fixed streamtubes. Although their title contains the word multi-phase, they only consider the two-phase immiscible waterflood problem. By investigating mobility ratios ranging from 0.1 to 1000, they demonstrate that the largest error occurs for favorable mobility ratios. They correctly attribute this to the large mobility decrease across the water bank in the $M = 0.1$ case. It should be noted though, that the relative permeabilities used by Martin and Wegner give rise to pure rarefaction waves in all unfavorable mobility ratio cases. Finally, it is interesting to note that they mention how the problem of numerical diffusion can be overcome using streamtubes. Unfortunately, they never actually quantify this advantage of the streamtube approach.
Contribution: Investigation of the error caused by the fixed streamtube assumption.

Bommer and Schechter, 1979 (10/78): *Mathematical Modeling of In-Situ Uranium Leaching*
This paper is an interesting application of the streamtube method to uranium leaching. In particular, the single phase, unit mobility type displacement involved in this application justifies the constant streamtube assumption. A component balance accounting for chemical reactions and physical diffusion is then solved by finite-differences along each streamtube. The area of interest is bounded through the use of image wells which are placed using an algorithm developed by (*Lin*)1972. This algorithm is not discussed in the paper. A homogeneous areal domain is assumed in this work.

Contribution: One-dimensional finite-difference solution along streamtubes. Application to uranium leaching.

Lake, Johnston, and Stegemeier, 1981 (10/78): *Simulation and Performance Prediction of a Large-Scale Surfactant/Polymer Project*
In this paper Lake et al. apply the streamtube method to surfactant/polymer flooding. Physical data from laboratory experiments along with a layered geological model are used in a cross-sectional finite difference simulation to derive response functions for the displacement. These response functions are then mapped onto streamtubes to capture the areal pattern of the flood as dictated by well positions and rates. In this way the detailed physics describing the surfactant/polymer process are kept intact for a field-scale simulation. Because the mobility is near unity for most cases, the streamtubes are kept constant throughout the study. A homogeneous areal domain is assumed in this work.
Contribution: Mapping of response functions obtained from representative cross-sections by detailed finite-difference simulation onto streamtubes.

Wang, Lake, and Pope, 1981 (10/81): *Development and Application of a Streamline Micellar/Polymer Simulator*
In this paper, Wang et al. solve the concentration equations for a Micellar/Polymer by finite differences along streamlines. This is analogous to the approach used by (*Bommer and Schechter*)1979 to model a uranium leaching process. No vertical effects are included and the streamlines are considered fixed. Wang et al. include areal anisotropy and show that it can have a substantial impact on recovery.
Contribution: Finite-difference solution of a Micellar/Polymer flood along streamlines.

Emanuel, Alameda, Behrens, and Hewett, 1989 (9/87): *Reservoir Performance Prediction Methods Based on Fractal Geostatistics*
In this paper Emanuel et al. show four example applications (three CO_2 floods and one mature waterflood) of the hybrid streamtube technique proposed by *Lake et al.* (1981). The cross-sectional response function is found by detail finite-difference simulation with a fractal description of the porosity/permeability distribution and coreflood data. The areal streamtube solution accounts for non-unit mobility ratios by updating the flow rates according to the total flow resistence, areal permeability trends, and no-flow boundaries. In all cases, Emanuel et al. show excellent agreement with total field response. They include areal distributions of permeability/thickness values to find areal streamtubes in order to improve specific well matches, but point out that the method is best in predicting total field performance.
Contribution: Accounting for areal heterogeneity in the streamtube geometry. Example solutions for four field cases.

Mathews, Emanuel, and Edwards, 1988 (10/88): *A Modeling Study of the Mitsue Stage 1 Miscible Flood Using Fractal Geostatistics*; 1989 (10/88) *Fractal Methods Improve Mitsue Miscible Predictions*
In these papers Mathews et al. present a study of the Mitsue Stage 1 miscible flood using streamtubes. This work follows very closely that of *Emanuel et al.* (1989). Mathews et al. show a comparison of projections based on finite-difference models (areal) and the streamtube method. These projections are also compared to available field performance data.
Contribution: Comparison of finite-difference pattern predictions with hybrid streamtube approach.

Tang, Behrens, and Emanuel, 1989 (2/89): *Reservoir Studies Using Geostatistics To Forecast Performance*

This paper presents two field scale examples (a waterflood and a CO_2 flood) of the streamtube approach. The approach is the same as presented by *Emanuel et al.* (1989). Again, excellent agreement with field data is demonstrated. In determining the cross-sectional response function, Tang et al. varied the width of the cross-section in the finite difference simulation in order to capture the transition from radial flow near the wells to linear flow further away. In the presence of gravity, this may be an important consideration. Furthermore, ten different fractional flow curves where generated in order to account for varying CO_2 slug sizes each streamtube sees because of the nonlinearity of the problem.

Contribution: Multiple fractional flow functions to account for varying slug sizes in unfavorable mobility cases.

Hewett and Behrens, 1991 (6/89): *Scaling Laws in Reservoir Simulation and Their Use in a Hybrid Finite Difference/Streamtube Approach to Simulating the Effects of Permeability Heterogeneity*

In this paper Hewett and Behrens present a detailed discussion on the scaling properties of hyperbolic conservation problems. Their work is clearly motivated by the opportunity of mapping one-dimensional solutions along streamtubes. In particular, Hewett and Behrens show that for single slug injections the solution is scalable by t_D/t_{Ds} and x_D/t_{Ds}, where t_{Ds} is the slug volume. They also discuss alternating slug injections. Since the streamtube method traditionally requires an averaged cross-sectional response, Hewett and Behrens discuss the influence of heterogeneity on scaling laws. They show that, in general, heterogeneity causes scaling laws to fail, though in some cases the permeability correlation length may be used as an additional scaling parameter to give reasonably scaled solutions. Finally, they compare solutions obtained using streamtubes with upscaled cross-sectional response functions and traditional finite difference formulations with pseudofunctions. Unfortunately they show no quantitative data for this comparison.

Contribution: Scaling of slug injections. Upscaling of cross-sections. Review of hyperbolic scaling laws.

Renard, 1990 (2/90): *A 2D Reservoir Streamtube EOR Model with Periodical Automatic Regeneration of Streamlines*

In this paper Renard departs from the assumption of constant streamtubes. Instead, he periodically updates the streamtubes and redistributes the fluids accordingly. Renard presents a micellar/polymer example in which he compares field data with fixed and updated streamtube solutions. The solution with updated streamtubes is closer to the field data then the one using fixed streamtubes. Unfortunately the paper is rather short and many question remain unanswered. For example, it is unclear if the fixed streamtube solution accounts for the changing mobility ratio by distributing the total flow accordingly. By redistributing the fluids, the initial conditions for the next time step are clearly not going to be uniform anymore. Renard never specifies how he determines the one-dimensional solution along the streamtubes. Finally, the areal reservoir is composed of 9 homogeneous zones–an unlikely description for a real reservoir.

Contribution: Solution with periodic updating of streamtubes.

King, Blunt, Mansfield, and Christie, 1993 (2/90): *Rapid Evaluation of the Impact of Heterogeneity on Miscible Gas Injection*

In this paper King et al. use a modified streamline approach to evaluate the impact of heterogeneity on miscible displacements. They introduce a time-of-flight coordinate to map the Todd & Longstaff

model along each streamline, much in the same way as *Parsons* (1972) does to locate the position of a tracer front. To account for the changing mobility field though, King et al. introduce a boost factor which they determine by integrating from the inlet to the isobar of the the fastest finger tip. The streamlines though, are calculated only once. King et al. apply their technique to estimate the uncertainty in recovery.
Contribution: Combining time-of-flight idea with boost factor. Application to assessing uncertainty due to reservoir heterogeneity.